

CURRENT STUDIES IN MATERIALS SCIENCE AND ENGINEERING



EDITORS
Hakan GÖKMEŞE
Şaban BÜLBÜL
Yusuf UZUN

ISRES
Publishing

Current Studies in Materials Science and Engineering

Edited by

Hakan GÖKMEŞE

Assoc. Prof. Dr, Necmettin Erbakan University
Seydisehir Ahmet Cengiz Faculty of Engineering,
Department of Mechanical Engineering, Konya, Türkiye

Şaban BÜLBÜL

Assoc. Prof. Dr., Necmettin Erbakan University
Seydisehir Ahmet Cengiz Faculty of Engineering,
Department of Mechanical Engineering, Konya, Türkiye

Yusuf UZUN

Assist. Prof. Dr., Necmettin Erbakan University
Seydisehir Ahmet Cengiz Faculty of Engineering,
Department of Computer Engineering, Konya, Türkiye

Language Editors

Lecturer Ceren DOĞAN

School of Foreign Languages, Necmettin Erbakan University, Türkiye

Email : cerendogan@erbakan.edu.tr

Özlem YALÇINKAYA

Ministry of National Education,
Directorate General for Innovation and Educational Technologies, Ankara, Türkiye

Email : ozlemyalcinkaya11@gmail.com





Current Studies in Materials Science and Engineering

Editors

Hakan GÖKMEŞE

Şaban BÜLBÜL

Yusuf UZUN

Cover Design & Layout

Resul BÜTÜNER

Ministry of National Education,

Directorate General for Innovation and Educational Technologies, Ankara, Türkiye

Email : resul.butuner@eba.gov.tr

This book was typeset in 10/12 pt. Times New Roman, Italic, Bold and Bold Italic.

Copyright © 2024 by ISRES Publishing

All rights reserved. No part of this book may be reproduced in any form, by photostat, microfilm, retrieval system, or any other means, without prior written permission of the publisher.

Current Studies in Materials Science and Engineering

Published by ISRES Publishing, International Society for Research in Education and Science (ISRES). Includes bibliographical references and index.

ISBN

978-625-6959-41-5

Date of Issue

October, 2024

Contact

Askan Mah. Akinbey Sok. No: 5/A Meram/Konya/Türkiye

isresoffice@gmail.com

www.isres.org

PREFACE

Dear Readers,

Engineering and technology applications are showing progress and innovation day by day. This book, signed by The International Society for Research in Education and Science (ISRES), which has gained great prestige with national and international activities, covers various topics in the field of materials science under the name of “Current Studies in Materials Science and Engineering”. This book consists of thirteen different sections containing many standard and theoretical studies, analyses and evaluations.

The book includes reviews and comprehensive studies on very important topics such as architectural materials and applications, materials used in renewable energy applications, nickel-titanium alloys, antibacterial titanium alloys, metal welding technologies and new generation steel alloys, polymer materials and properties, power plants, active carbon, material recycling, plastic deformation, composite and hybrid techniques, powder metal technology and fiber reinforced composite material properties.

The book, which includes many interesting sections within the scope of national and international engineering applications and materials science, will guide many researchers and academic studies. We believe that these studies will foster progress in academia and industry

We wish you a good reading.

October, 2024

Prof. Dr. Hakan GÖKMEŞE

Necmettin Erbakan University

Seydisehir Ahmet Cengiz Faculty of Engineering

E-mail : hakan1440@gmail.com

ORCID : 0000-0003-0053-8444

Assoc. Prof. Dr. Şaban BÜLBÜL

Necmettin Erbakan University

Seydisehir Ahmet Cengiz Faculty of Engineering

E-mail : sabanbulbul@erbakan.edu.tr

ORCID : 0000-0002-9268-1469

Assist. Prof. Dr. Yusuf UZUN

Necmettin Erbakan University

Seydisehir Ahmet Cengiz Faculty of Engineering

E-mail : yuzun76tr@gmail.com

ORCID : 000-0002-7061-8784

TABLE OF CONTENTS

CHAPTER 1	Research on the Usage Areas of Building Materials with Silica Aerogel Content in Architectural Applications <i>Tuba ARKAN DEMİRÖRS, Kerim ÇINAR</i>
1-30	
CHAPTER 2	Materials Used in Renewable Energy Applications <i>Edip TAŞKESEN, Gökür KAYATAŞ ONGUN</i>
31-52	
CHAPTER 3	Nickel-Titanium (NiTi) Alloys in Dentistry <i>Ahmet Burçin BATIBAY, Muhammed İhsan ÖZGÜN</i>
53-63	
CHAPTER 4	Antibacterial Properties of Titanium Alloys <i>Ahmet Burçin BATIBAY, Fatih ERCİ</i>
64-75	
CHAPTER 5	S700MC Steel Material and Gas Metal Arc Welding Under Difficult Load and Carrying Industrial Application Conditions <i>Fatma Nur ŞAHİN, Hakan GÖKMEŞE</i>
76-88	
CHAPTER 6	Use of Polymers in Soil Erosion Control <i>Vildan ERCİ</i>
89-101	
CHAPTER 7	Investigation of the Color, Glossiness, and Surface Roughness Properties of Particleboards Produced with Activated Carbon Addition <i>Mehmet Emin ERGÜN, Filiz KOYUNCU, Abdullah İSTEK, Ahmet CAN, İsmail ÖZLÜSOYLU</i>
102-112	
CHAPTER 8	Multi-Directional Forging Process as a Severe Plastic Deformation Method <i>Mehmet ŞAHBAZ</i>
113-127	
CHAPTER 9	Wear Performance of Ex-situ NbC and In-situ Al4C3 Reinforced A356 Matrix Hybrid Composites at High Temperatures <i>Doğan ŞİMŞEK, İjlal ŞİMŞEK</i>
128-144	
CHAPTER 10	Microstructure Analysis of Particle Reinforced Aluminum Matrix Composites Produced by Powder Metallurgy Using Image Processing Method <i>Nuri ATİK, Yusuf KARABACAK, İjlal ŞİMŞEK, Doğan ŞİMŞEK</i>
145-156	
CHAPTER 11	Investigation of Mechanical Behaviour of Crimp Effect on Fiber Reinforced Composite Materials <i>Hasan Hüseyin TAŞER, Mehmet KAYRICI</i>
157-168	
CHAPTER 12	Metal Recovery with Calixarene <i>Ümmü ÖZGÜN, Muhammed İhsan ÖZGÜN</i>
169-180	
CHAPTER 13	4E Analyses of the Power Plants <i>Dilek Nur ÖZEN</i>
181-194	

CONTRIBUTORS

Assist. Prof. Dr. Yusuf UZUN
Necmettin Erbakan University,
Seydişehir Ahmet Cengiz Faculty of Engineering,
Department of Computer Engineering, Konya, Türkiye

Prof. Dr. Hakan GÖKMEŞE
Necmettin Erbakan University,
Seydişehir Ahmet Cengiz Faculty of Engineering,
Department of Mechanical Engineering, Konya, Türkiye

Assoc. Prof. Dr. Şaban BÜLBÜL
Necmettin Erbakan University,
Seydişehir Ahmet Cengiz Faculty of Engineering,
Department of Mechanical Engineering, Konya, Türkiye

Dr. Tuba ARKAN DEMİRÖRS
KTO Karatay University,
Faculty of Fine Arts and Design,
Department of Interior Architecture, Konya, Türkiye

Prof. Dr. Kerim ÇINAR
KTO Karatay University,
Faculty of Fine Arts and Design,
Department of Architecture, Konya, Türkiye

Assoc. Prof. Dr. Dilek Nur ÖZEN
Necmettin Erbakan University,
Faculty of Engineering,
Department of Mechanical Engineering, Konya, Türkiye

Dr. Ahmet Burçin BATIBAY
Necmettin Erbakan University,
Faculty of Engineering,
Department of Metallurgical and Materials Engineering, Konya, Türkiye

Dr. Muhammed İhsan ÖZGÜN
Necmettin Erbakan University,
Faculty of Engineering,
Department of Metallurgical and Materials Engineering, Konya, Türkiye

Assoc. Prof. Dr. Fatih ERCİ
Necmettin Erbakan University,
Faculty of Science,
Department of Biotechnology, Konya, Türkiye

Assist. Prof. Dr. Vildan ERCİ

Selçuk University,
Faculty of Agriculture
Department of Soil Science and Plant Nutrition, Konya, Türkiye

Dr. Ümmü ÖZGÜN

Necmettin Erbakan University,
Faculty of Engineering,
Department of Basic Science, Konya, Türkiye

Assoc. Prof. Dr. Mehmet Emin ERGÜN

Alanya Alaaddin Keykubat University,
Akseki Vocational High School,
Department of Forestry, Antalya, Türkiye

Dr. Filiz KOYUNCU

Dicle University,
Institute of Natural and Applied Sciences,
Department of Chemistry, Diyarbakır, Türkiye

Prof. Dr. Abdullah İSTEK

Bartın University,
Faculty of Forestry,
Department of Forest Industry Engineering, Bartın, Türkiye

Assoc. Prof. Dr. Ahmet CAN

Bartın University,
Faculty of Forestry,
Department of Forest Industry Engineering, Bartın, Türkiye

Assoc. Prof. Dr. İsmail ÖZLÜSOYLU

Bartın University,
Faculty of Forestry,
Department of Forest Industry Engineering, Bartın, Türkiye

Assist. Prof. Dr. Mehmet ŞAHBAZ

Karamanoğlu Mehmetbey University,
Faculty of Engineering
Department of Mechanical Engineering, Karaman, Türkiye

Dr. Mehmet KAYRICI

Necmettin Erbakan University,
Seydişehir Ahmet Cengiz Faculty of Engineering,
Department of Mechanical Engineering, Konya, Türkiye

Lecturer, M.Sc. Hasan Hüseyin TAŞER

İstanbul Gelişim University,
Gelişim Vocational School,
Department of Hybrid and Electric Vehicles, İstanbul, Türkiye

MSc. Fatma Nur ŞAHİN

Necmettin Erbakan University,
Institute of Science,
Department of Mechanical Engineering, Konya, Türkiye

Assoc. Prof. Dr. Doğan SIMSEK

National Defence University
Army NCO Vocational HE School
Department of Automotive Technology, Balıkesir, Türkiye

Assoc. Prof. Dr. Ijlal ŞİMŞEK

National Defence University
Army NCO Vocational HE School
Department of Mechatronics Technology, Balıkesir, Türkiye

Managing Editors

Hakan GÖKMEŞE Hakan GÖKMEŞE PhD is a Professor of Mechanical Engineering at Necmettin Erbakan University in Konya, Türkiye. He holds a master's degree in Metallurgy Education from Gazi University. His main areas of interest are casting technology, powder metallurgy, heat treatments and composites-nanocomposites applications.

E-mail: hakan1440@gmail.com , ORCID: 0000-0003-0053-8444

Şaban BÜLBÜL is an Associate Professor at Necmettin Erbakan University Faculty of Mechanical Engineering. Polymeric materials, manufacturing technologies and modern welding techniques are the editor's main interests.

E-mail: sabanbulbul42@hotmail.com, ORCID: 0000-0002-9268-1469

Yusuf UZUN PhD, is an Assistant Professor of Computer Engineering at Necmettin Erbakan University in Konya, Türkiye. He holds a PhD in Mechanical Engineering from Necmettin Erbakan University. His main areas of interest are artificial intelligence, autonomous systems and augmented reality applications. He also works as the Rector's Advisor at Selcuk University.

E-mail: yuzun76tr@gmail.com, ORCID: 000-0002-7061-8784

CHAPTER 1

Research on the Usage Areas of Building Materials with Silica Aerogel Content in Architectural Applications

Tuba ARKAN DEMİRÖRS

KTO Karatay University, Türkiye

Kerim ÇINAR

KTO Karatay University, Türkiye

To Cite This Chapter:

Arkan Demirörs, T. & Çınar, K. (2024). Research on the Usage Areas of Building Materials with Silica Aerogel Content in Architectural Applications. In H. Gokmese, S. Bulbul, & Y. Uzun (Eds.), *Current Studies in Materials Science and Engineering* (pp. 1-30).ISRES Publishing.

Introduction

Materials science is progressing in line with the developments in technology, and this situation manifests itself in the field of building materials and architecture as well as in many fields (Alparslan, 2021; Arı, 2022; Arkan Demirörs, 2023; Yıldız & Seçkin, 2019). The development of technology has had an impact on the production of different building materials, and the materials used in architectural and interior architecture applications have diversified (Güdük & Satıcı; 2022). In addition, thanks to many methods developed via technology, it has been possible to further improve the physical, chemical, and mechanical properties of traditional building materials used in architectural applications or to produce building materials with new properties (Baetens et al., 2011; Bertolini et al., 2010; Çüçen & Altuncı, 2022; Farahmandjou & Khalili, 2013). Silica aerogel materials, which have been used in many sectors such as aerospace, aviation, automotive, chemistry, textile, medicine, and cosmetics since they were produced by Kistler in 1930, have become widely used in the fields of architecture, interior architecture, and construction due to their very light and very insulating properties, and they have become materials that make a high contribution to the construction sector (Buğdaycı, 2008; Cuce et al., 2014; Gurav et al., 2010; Hrubesh 1998; Sebdani et al. 2021; Szczepaniak et al., 2022). Although the discovery of silica aerogels dates back to the 20th century, there is no doubt that the properties of the material have improved with the innovations brought by modern technology and have become responsive to today's needs.

The most important known feature of silica aerogel materials produced with nanotechnology, which is today's technology, is that they have a low thermal conductivity coefficient. Thanks to these properties, silica aerogels are defined as a “*super-insulating*” solid material (Buğdaycı, 2008). Moreover, thanks to their superior thermal insulation capabilities, silica aerogels attract a lot of attention in terms of their use with architectural building materials such as gypsum, cement, and glass (Huang & Niu, 2015; Lakatos, 2019; Szodrai et al., 2016). The combined use of silica aerogels with building materials increases the performance of these materials and makes them more efficient (Alparslan, 2021; Baetensa, 2011; Curto & Cineri, 2020; Gür, 2010). In addition, the porosity and low-density properties of silica aerogels enable them to be characterized as a very light solid material (Buğdaycı, 2008). Other remarkable properties of silica aerogel materials are acoustic and fire insulation. It can be said that thanks to these properties, the areas of their use will start to become more widespread in the following years (Baetens, 2011; Neugebauer, 2014).

On the other hand, the fact that the increasing greenhouse gas concentration due to the use of fossil fuels in recent years has caused global warming has led to the necessity of taking various measures in this regard, and the idea of using energy more effectively and efficiently has gained importance (Bostancıoğlu, 2011). Energy consumption in architectural structures accounts for a large part of the energy consumed all over the world. A significant part of this consumed energy is used for heating purposes in buildings (Köken & Kanık, 2022). Therefore, thermal insulation applications in buildings have gained importance in order to minimize heat losses in architectural structures and increase energy efficiency (Arslan & Aktaş, 2018). Materials used for thermal insulation purposes in architectural applications bring a number of disadvantages such as additional load, additional cost, and additional time to buildings (Özer & Özgünler, 2019). In this context, the development of the heat preservation properties of building materials by using the developing technology in the field of architecture and interior architecture will provide advantages in many ways. The use of building materials that are produced with advanced technology and have high thermal conductivity instead of conventional thermal insulation in buildings is important for energy efficiency and sustainability (Arkan Demirörs, 2023). In this respect, silica aerogel-containing building materials, known as innovative building materials developed with advanced technology, are used in architectural applications as materials that can meet these needs.

The purpose of this study was to investigate the contribution of silica aerogel-containing building materials to architectural design. In this direction, the place and importance of silica aerogel materials in the field of architecture were explained. Through the literature review, the usage areas of silica aerogel with low thermal conductivity coefficients in architectural applications on thermal insulation were investigated, and application examples were examined. In addition, test analyses of silica aerogel-contained structure samples prepared in a laboratory environment were investigated. The numerical data and results obtained in this study can be a reference in the industrial production of silica aerogel materials. Finally, it is expected that this study will be a foundation for other scientific studies to be conducted on this subject.

The Place and Importance of Silica Aerogel Material in the Field of Architecture

In recent years, the increasing interest in new building materials and the fact that products that play a key role in energy saving offer advanced solutions for thermal insulation have brought the importance of the material to the agenda in the field of architecture. Due to the rapid increase in energy consumption in buildings in the construction sector, the use of advanced materials with thermal insulation properties has become a need. In this context, silica aerogels, which are used as a component of many insulation products and have high thermal insulation ability, are added to building materials in different reinforcement ratios and used in architectural applications. Silica aerogel materials with superior properties such as high thermal performance are also porous products with low mass density. In addition to their many unique properties, their use in the field of architecture is widely preferred, especially for the purpose of thermal and sound insulation in buildings (Calisesi, 2017). In this context, many building materials such as silica aerogel-reinforced plasters, concrete, glasses, gypsum boards, wallpapers, and aerogel blankets with low thermal conductivity have been produced in recent years, and for energy saving, materials reinforced with silica aerogel have been used for thermal insulation purposes in buildings (Buratti et al., 2014; Buratti et al., 2016; Cuce et al., 2014, Moretti, 2017).

Research studies conducted on insulation materials containing silica aerogel have aimed to find a solution to this problem by addressing the problem of environmental sustainability. These studies have revealed that the use of building materials containing silica aerogel contributes to sustainable architecture in many ways. Energy demand has gradually increased in the world over the past thirty years due to industrial developments, economic and cultural development, and population growth. Non-renewable energy sources still dominate the energy market, although their reserves are limited. The construction sector is responsible for 42% of the total energy consumption (Curto & Cinieri, 2020). As in the whole world, residences constitute a large part of the architectural structures in Türkiye. In terms of energy consumption, residences use a large part of the energy. 85% of the energy used in residential buildings is consumed for heating. In addition, due to the lack of thermal insulation in 70% of residences in Türkiye and the increase in energy use in residences, insulation applications in architectural structures to ensure thermal insulation and energy efficiency in residences are increasingly important in terms of energy saving (Arslan & Aktaş, 2018). The use of silica aerogels in the field of architecture contributes to the issue of energy saving, ensuring efficiency in energy use and energy sustainability. The issue of sustainability has been an important part of the architecture field for many years. For this reason, the use of innovative silica aerogel-reinforced materials can provide high insulation values in buildings (Pacheco Torgal et al., 2016).

The Use of Silica Aerogel Material in The Field Of Architecture

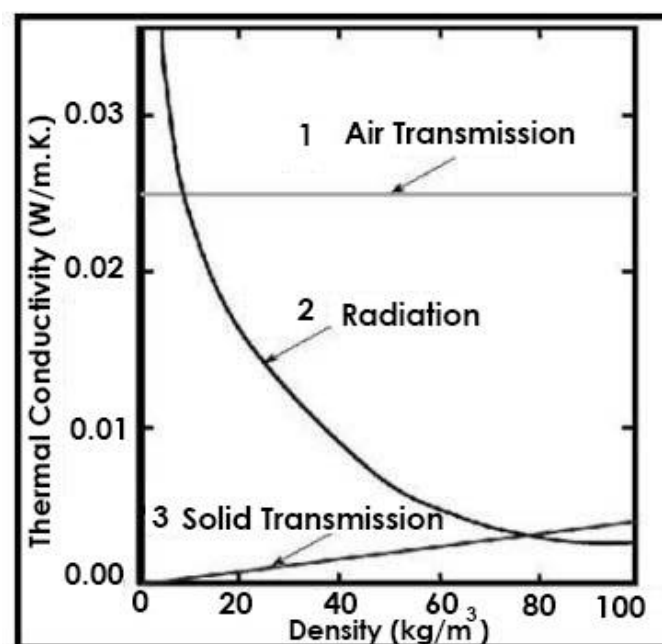
In architecture, building envelopes are composed of different structural and functional components such as interior and exterior walls, doors, windows, ceilings, roofs, flooring, and facades. Since all these parts have an important role in energy efficiency, materials produced with different technologies have been proposed to improve energy performance in buildings (Santos et al., 2014). New high-performance materials produced using advanced technology and offering alternative solutions for thermal insulation in architectural structures by providing the best possible thermal insulation

without increasing the thickness of the building envelopes (TS 825) have been used for heat preservation in building envelopes (Ng et al., 2015). Furthermore, in addition to improving the thermal insulation performance of building materials, many superior features such as sound insulation, water absorption, fire resistance, and durability for applications under load can be provided thanks to the technology. In this context, silica aerogel-containing materials' properties developed with technology and their high thermal performance due to their exceptional physical and chemical structure offer an innovative option to conventional insulation. With these properties, new-generation silica aerogel-containing materials are rapidly gaining a place in architectural applications (Baetens et al., 2011).

In architectural structures, thermal insulation is used on ceilings, floors, interior and exterior walls, exterior facades, windows, and roofs. The hollow structure of the insulation materials used in the building components makes it possible to have a low thermal conductivity, a high thermal resistance, and a low thermal permeability. A good understanding of the heat transfer mechanism of insulating materials, which provide heat preservation, through air gaps is important in terms of developments in energy efficiency and thermal insulation in structures. A study explained that there are three basic components of heat flow of conventional insulating materials (Kistler, 1935, as cited in Bayrakçı et al., 2011). As can be seen in Figure 1, he defined these components as air conduction, radiation, and solid conduction. Heat conduction in insulating materials occurs by displacing a gas with a density lower than the density of the air in the material. During this displacement, the thermal conductivity of the material decreases. In addition, the decrease in air pressure inside the materials that provide thermal conductivity affects the increase in the thermal insulation capacity. According to Kistler, heat preservation is associated with the micro- or macro-porous nature of the material, and thermal conductivity decreases as the pore size decreases (Kistler, 1935, as cited in Bayrakçı et al., 2011).

Figure 1.

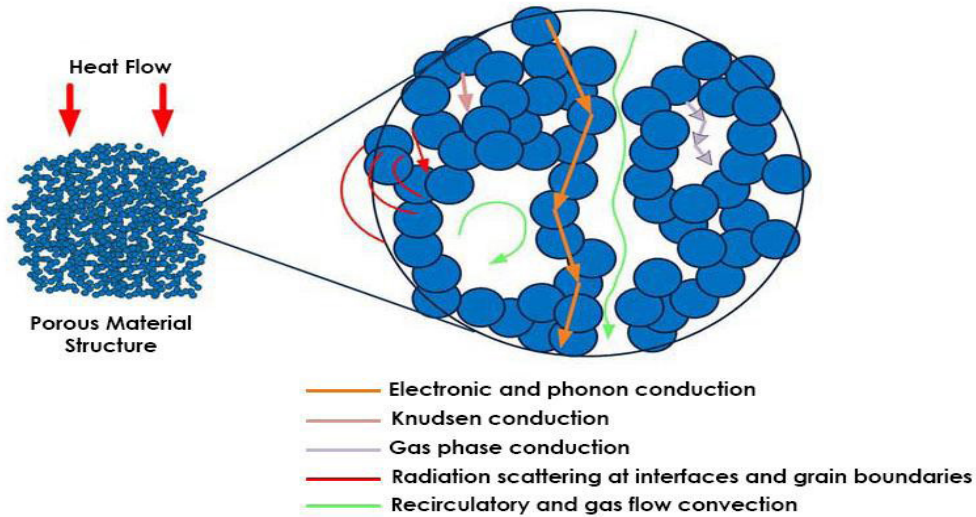
Heat Transfer Mechanisms in Conventional (Fibre and Foam) Insulation (Kistler, 1935, as cited in Bayrakçı et al., 2011)



Understanding how the heat transfer mechanism works in a porous environment is a very important step for the development of thermal insulation materials. Figure 2 shows a schematic representation of the transmission, convection, and radiation mechanisms that occur during the heat transfer in porous materials. During the heat transfer in the transmission mechanism, phoneme transmission of the solid matrix, electronic transmission, and gas phase transmission are provided. The thermal conductivity of porous and insulating material depends on the density and porosity properties of the material since it is directly related to the solid content of the material. As the solid density of porous materials increases, the solid thermal conductivity of the material increases. In addition, depending on decreasing porosity, increasing density leads to a decrease in conductivity that is in the gas phase (Ülker et al., 2014).

Figure 2.

Heat Transfer Mechanisms in Conventional Materials (Ülker et al., 2014)



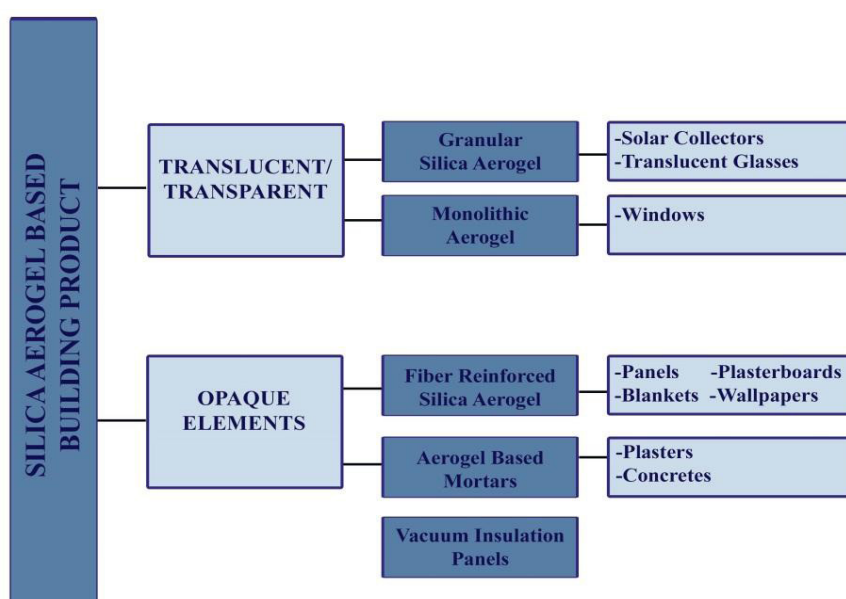
The conventional materials used in building insulation to provide thermal insulation are classified as mineral wool, expanded polystyrene (EPS), extruded polystyrene (XPS), polyurethane (PUR), cork, and cellulose (Huang, 2012). The use of conventional insulation materials is not preferred much due to many disadvantages such as application thickness, floor area limitation, transportation volume limitation, architectural restrictions, health and environmental problems, and economic reasons (Al Zaidi, 2017). For this reason, studies aiming to develop more effective thermal insulation systems in line with technological developments have come to the agenda. The development of thermal insulation systems takes place in two ways. The first is the improvement of the thermal insulation properties of existing materials, while the second is the development of new materials with increased thermal insulation properties (Ülker et al., 2014). Silica aerogel-reinforced insulation materials are an innovative insulation material developed as an alternative to conventional insulation materials and show performance about seven times more than conventional materials (Baetens et al., 2011; Gür, 2010). It has been found that the thermal conductivity coefficients of silica aerogel-reinforced insulation materials are significantly lower than the thermal conductivity coefficients of various conventional materials used for thermal insulation (Ülker et al., 2014). The lower the thermal conductivity coefficient, the higher the insulation property of the material (Bayrakçı et al., 2011). With the applications of silica aerogel-reinforced

insulation materials, which have a low thermal conductivity coefficient, thermal comfort has been provided in buildings, more energy has been saved, and heating costs have been reduced. Thus, silica aerogel-reinforced insulation materials have gained an important place in applications in the field of architecture thanks to the many advantages they provide (Baetens et al., 201; Gür, 2010).

Silica aerogel is currently used as a component for various insulation solutions and building products. In Figure 3, a classification of silica aerogel-based building products used in architectural building components is shown. According to this classification, silica aerogel-based building products are examined in 2 groups: transparent (transparent and translucent) and opaque elements.

Figure 3.

Classification of Silica Aerogel Based Building Products (Curto & Cinieri, 2020)



Transparent and Translucent Silica Aerogel Materials and Applications in Architectural Structures

Silica aerogels are used by architects and designers in buildings as a transparent or translucent insulation material because they combine the characteristics of low thermal conductivity and high daylight and solar energy transmittance. With these superior properties, silica aerogels found application area in building components such as translucent window systems for the first time in 1980 (Berardi, 2015). Subsequently, with the developing technology, studies on the development of granular and monolithic aerogel-based windows and insulation panels have been continuing for the last 10 years (Baetens et al., 2011). As a result of these research studies, silica aerogel-reinforced glass and window systems have found application areas in many architectural structures.

Applications of Silica Aerogel-Reinforced Glasses and Window Systems in Architectural Structures

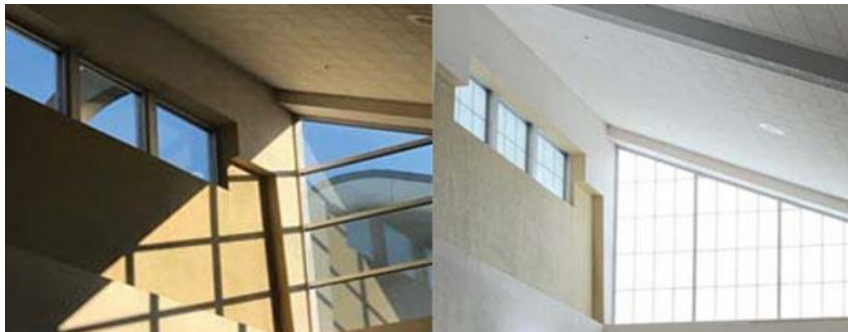
Windows are among the building elements that have an important role in architectural design. Windows contribute to architectural design and structure in many aspects such as

the formation of exterior facades, the illumination of interior spaces, and the connection of the interior to the outside. In recent years, the use and applications of silica aerogel materials in window systems have attracted attention. Silica aerogels are used in glass and window systems in two forms: *granular* and *monolithic*. Granular translucent silica aerogel materials are much easier to use compared to monolithic aerogels. When granular silica aerogels are incorporated into window systems in buildings, they provide thermal insulation to buildings as well as reflect daylight indoors. This shows that the material with silica aerogel content has a good optical permeability property. Thanks to these properties, daylight can easily enter the buildings (Gao, et al., 2016; Garnier, et al., 2015). The main difference between monolithic silica aerogel glasses and granular silica aerogel glasses is that granular silica aerogel materials do not have an optic transparent appearance. These properties cause the image of glass materials consisting of granular silica aerogel to form an optical image that is not transparent, as if it were viewed from a milk cup. It is known that glasses consisting of granular silica aerogel, which is characterized by low transparency, scatter light much more than other glasses. In addition, compared to standard glasses, granular silica aerogel glasses have a softer light transmission and reduced shading (Koebel et al., 2012).

The Cabot Corporation is the first and largest supplier of granular silica aerogel materials with high optical properties. Lumira brand aerogel products developed by this company have been designed to optimize light transmission for use in daylight lighting applications of architectural structures (Koebel et al., 2012). On the other hand, in the application made by Kalwall Corporation, renovation was carried out at Spokane International Airport in Washington through the existing project to provide passenger comfort (Figure 4). The goal here was to create a translucent solution for glass windows that do not need a view from the outside. In addition, since sun rays passing through the glass windows in the atrium area, which allowed direct sunlight, caused glare, and passengers and employees were uncomfortable with this situation, the existing glasses were replaced with translucent sandwich panels containing Lumira aerogel at a thickness of 70mm. In this way, the translucent structure of the sandwich panels produced by Kalwall Corporation with Cabot Lumira aerogel prevents glare by distributing daylight, and thus, visual comfort is provided in the interior. In addition, it has been determined that these panels have a value of 0.05 Wm²K U (Thermal permeability coefficients) (URL-1).

Figure 4.

Kalwall Corporation's Translucent Sandwich Panel Application Produced with Cabot Lumira Aerogel for Spokane International Airport (Washington, USA) (Built By Zeck Butler Architecture) (URL-1)













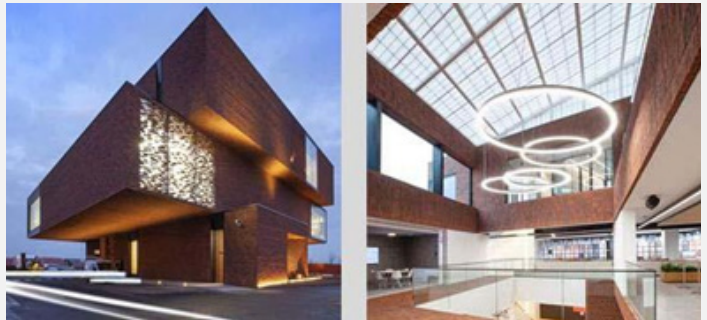



Kalwall’s Cabot Lumira aerogel-filled translucent sandwich panels are innovative materials that provide high thermal insulation, create a bright interior space by improving the quality of the indoor environment, cause minimal damage to the environment by reducing the carbon emission of architectural structures, provide energy conservation, and contribute to sustainable architecture by creating thermal, visual, and acoustic comfort conditions. These products are used in the wall systems of architectural structures, combined curtain walls, facades instead of walls, window systems, and ceiling windows (Altın, 2014; URL-2). Application examples of the use of semi-transparent Kalwall aerogel content panels in many different architectural structures (car showrooms, universities, airports, office, libraries, and hospital) are given in Table 1 (URL-3).

Table 1.

Building Application Examples of Translucent Aerogel Sandwich Panels (Belongs to Kalwall Corporation) (URL-3)

Building Name	Architectural Office	Building Photo	Building Interior Photo
Mercedes Benz Building (Belgium)	Jaspers-Eyers & Partners		
Audi Showroom (London)	Wilkinson Eyre Architecture		
BMW Wolverhampton (London)	MDG Architecture		

<p>Glasgow International Airport (Scotland)</p>	<p>3DReid Architecture</p>	
<p>Raleigh-Durham International Airport (USA)</p>	<p>Clark Nexsen Architecture</p>	
<p>Cornell University (New York)</p>	<p>Gruzen Samton IBI Group</p>	
<p>Deakin University / Gray Puksand (Australia)</p>	<p>Gray Puksand</p>	
<p>Office Buildings (Belgium)</p>	<p>Architectengroep PSK, UAU Collectiv</p>	
<p>Weiner TownHouse (New York)</p>	<p>LOT-EK Architecture & Design</p>	

<p>Angus Glen Community Centre & Library (Canada)</p>	<p>Perkins + Will</p>	
<p>Benenden Hospital (UK)</p>	<p>CA Vaughan Blundell + SR Architects</p>	

One of the first examples of daylight lighting in a building is the skylight of the gymnasium and physical education hall of the Buchwiesen school (Figure 5), designed by the architects V. and A. Amsler and built-in Zurich in 2003. Scobalit, located in Germany, is a leading company that produces aerogel-filled composite panels for translucent daylight applications. Super-insulated Scobatherm products consist of Cabot aerogel granule-filled glass fiber-reinforced polyester resin composite profile (Koebel et al., 2012).

Figure 5.

Roof Construction Application Examples of Granular Aerogel Filled Glass Fibre Composite Panels Produced by Cabot Corporation (Koebel et al., 2012)



Another example of applications in which silica aerogels are used as a translucent insulation material is the use of translucent silica aerogel glass materials instead of external walls in buildings (Curto & Cinieri, 2020). In Figures 6 and 7, examples of translucent silica aerogel-insulated windows in architectural applications are presented. The first of these examples belongs to the translucent aerogel windows used on the outer wall of the Yale University Sculpture Building Gallery. The other example is translucent aerogel insulation material, which can be applied on both the roof and the outer wall to increase the use of daylight in buildings, prevent glare, and ensure homogeneous distribution of light indoors and thermal insulation. Thanks to their thermal insulation

properties, these materials also reduce heating and cooling costs by a significant amount (Baetens et al., 2011).

Figure 6.

Examples of Translucent Aerogel Panels Used in the Exterior Wall of Yale University (New Haven, Connecticut, USA) (Baetens et al., 2011)



Figure 7.

Application Examples of Translucent Aerogel Building Materials Used in Roof and Exterior Walls That Increase The Use of Daylight and Provide Thermal Insulation in Buildings (Baetens et al., 2011)



Another example of granular silica aerogel-based glass applications is a system developed by ISOTEG, an R&D project at ZAE Bayern in Germany. ISOTEG aimed to develop a new glass based on granular silica aerogel. These glasses were created from a double-walled layer filled with granular silica aerogel inside a 16 mm wide polymethyl methacrylate (PMMA) in the middle of two cavities filled with 12 mm krypton or argon gas. Then, these were mounted between two panes of glass. In this study, the optical and thermal properties of granular silica aerogel particles were investigated. In experiments, some parameters such as gas pressure, external pressure load, temperature, and gas filling were changed to determine the effects of silica aerogel powders on heat transfer. Subsequently, the thermal conductivity values calculated for granular silica aerogel-reinforced glass and glass without granular silica aerogel reinforcement were examined comparatively. For the entire glass unit (the thickness of the glass was less than 50 mm), heat transfer coefficients of less than $0.4 \text{ W/m}^2\text{K}$ and a total solar energy transmittance of 35% were obtained (Reim et al., 2005).

Within the scope of the HILIT+ project of the European Union, a monolithic silica aerogel-based window was developed (Figure 8). It was stated that monolithic silica aerogels were more appropriate for window glass construction compared to granular aerogels due to their transparent structure. These windows were developed with vacuum glazing technology by applying a pressure between 1 and 10 mbar. The thermal permeability value of approximately $0.66 \text{ W/m}^2\text{K}$ was measured for monolithic silica aerogel glass with a thickness of 13.5 mm produced together with vacuum glazing technology (Baetens et al., 2011). Aspen Aerogels Company developed reinforced monolithic, translucent aerogel panels for aerogel window applications. The U-value of the monolithic aerogel panel that had a thickness of 2.5 cm and was sandwiched between two glass panels was measured at a level lower than $0.5 \text{ Wm}^{-2}\text{K}^{-1}$. The company's manufacturers emphasized that the biggest challenge in producing monolithic aerogel was to produce one-piece panels with high optical quality, flawless, and without cracks. This is because producing high optical quality, large-area monolithic aerogel panels requires a very precise production process. In addition, it has been stated that due to the high production costs of monolithic silica aerogels, attempts at commercialization are currently not at a sufficient level (Koebel et al., 2012; Ülker et al., 2014).

Figure 8.

Example of Monolithic Silica Aerogel-Based Window Developed within the Scope of HILIT+ Project (Koebel et al., 2012)



The German company Okalux developed a window that had aerogel reinforcement and was named Okagel. By filling the gap in the double glasses with granular silica aerogel, an opaque and highly insulating window element was formed. The product had a thermal permeability value of $0.3 \text{ Wm}^{-2}\text{K}^{-1} \text{ U}$ and was a material with a fairly high thermal insulation. One of the most famous building examples where the company used Okagel window elements is the British Halley VI in Antarctica (Figure 9). It is a Research Station (URL-4). Another building where Okagel window systems are used is the Tengelmann Climate Market building in Mühlheim, Germany (Figure 10). Okagel window systems provide the thermal preservation of the building by keeping the incoming sunlight indoors without glare and without harsh shadows. In addition, the incoming sunlight can also be distributed indoors evenly and in a balanced way (URL-5).

Figure 9.

Okagel Window Used at Halley VI British Antarctic Research Station (URL-6)



Figure 10.

Okagel Glass with High Thermal Insulation Properties Used in the Tengelmann Climate Market Building in Mühlheim, Germany (URL-5)



It is known that architects and designers have been searching for innovative, efficient, sustainable, and environmentally friendly building materials in recent years. In this context, the use of fabric roofing materials, which are innovative materials, have translucent and insulating properties, can provide natural lighting, and important benefits for roofing systems, is gaining interest. The Birdair Company operating in North America is a pioneer in the development of roofing solutions and the production of these innovative materials. Tensotherm brand aerogel content roofing material, manufactured by this company, is produced from lightweight stretchable fabric membrane material with superior thermal and acoustic insulation performance. In addition, Tensotherm, a textile-based roofing material, provides a bright interior and energy saving by allowing non-reflective sunlight to pass through. The roofing material containing silica aerogel has applications in many different areas including industrial buildings, event halls, congress centers, hotels, and sports complexes. Some of the projects where Tensotherm brand roofing material with aerogel content has been used are: Khalifa International Stadium in Doha, Qatar, Mercedes Benz Stadium in Atlanta, USA, Arthur Ashe Stadium in New York, USA, USTA Grandstand Stadium in New York, QingKou Sports Center

in China, National stadium in Brazil, La Plata stadium in Argentina, Dedmon Athletics Center of Radford University in the USA, Kuwait National stadium, and Hamburg HSH Nordbank Arena in Germany. Despite their high costs, being lightweight, simple to install, long-lasting, optical transmission, water vapor permeability, and thermal and acoustic insulation make these transparent aerogel-containing textile roofing materials used in these projects highly preferable (URL-7).

Opaque Silica Aerogel Insulation Materials and Applications in Architectural Structures

Opaque silica aerogel-based insulation materials in architectural structures are boards, panels, blankets, wallpapers, paints, plasters, and concrete reinforced with aerogel (Curto & Cinieri, 2020).

Silica Aerogel Reinforced Gypsum and Concrete Plasters and Their Applications in Architectural Structures

There are a limited number of studies on silica aerogel-based thermal insulation plasters. Barbero et al. (2014) conducted a study related to thermal insulation plasters in the European Market. To this issue, they found innovative solutions for thermal insulation plasters consisting of silica aerogel-reinforced materials with nano-sized pores. In this context, the issue that many alternative methods can make significant contributions to the development of the material came to the fore. The most important decision taken within this framework was to reduce the thickness required for the material and to reach a higher thermal performance level for the material. The authors emphasized that silica aerogel-based plasters could be used in the restoration of both new and existing buildings by using techniques known in today's construction industry and that these innovative silica aerogel-based plasters would provide many advantages both in application and use (Barbero et al., 2014).

According to the researchers (Barbero et al., 2014), thermal insulation plasters have the advantage of being applied in curved, curvilinear areas, and organic forms. Their flexibility makes silica aerogel-based plasters appropriate materials for architectural design and application solutions. In addition, their easy application on the facades makes them preferable for the improvement of existing buildings. When a group of researchers compared the insulation plasters available on the market with aerogel plaster, they revealed that the thermal conductivity of silica aerogel-containing plaster was significantly lower. The research results are very promising, especially in terms of experiments based on both laboratory and field tests (Barbero et al., 2014).

As a result of the Buratti et al. (2014) research studies, silica aerogel-based insulation plasters, determined to have many usage advantages, have been developed and manufactured in recent years, and they have also been used in new renovations of architectural structures. Subsequently, silica aerogel-based insulation plasters have been commercialized within a short time. Silica aerogel-based gypsum plaster mixtures utilized for insulation purposes are used in many applications, including internal and external wall surfaces. In addition, because they show similar content and characteristics to the materials used in historical buildings, they have been applied to the internal and external wall surfaces in the renovation works of historical buildings. Thus, thanks to the innovative structure and thermal conductivity properties of silica aerogel-based gypsum

plasters, thermal insulation, and energy efficiency are provided without changing the external appearance of historical buildings. Figure 11 shows the on-site application of silica aerogel-reinforced plasters. It is stated that the application is made easier by the direct spraying method on complex brick wall geometry. In addition, the hydrophobic structure of silica aerogel powders helps to prevent water absorption by repelling the water in the material. Silica aerogel-based plasters create significantly breathable surfaces compared to conventional plasters and also ensure that the surfaces do not get wet by preventing moisture from entering the medium (Buratti et al., 2014).

Figure 11.

Application of Silica Aerogel Reinforced Plasters (Buratti et al. 2014)



In another study conducted by Buratti et al. (2014), researchers investigated the thermal and acoustic characterization of innovative insulation coatings consisting of hydrophobic granular silica aerogel. Hydrophobic granular aerogel in different reinforcement ratios (approximately by volume %0, %80-90, %91-95, and %96-99) was mixed with the natural plaster manually. The thermal conductivity coefficients of the prepared samples were measured. Table 2 shows the laboratory test results of the study conducted by Buratti et al. (2014). The results of the study revealed that as the amount of silica aerogel increased, the thermal conductivity value and the density of the prepared plaster decreased. In other words, as the amount of silica aerogel increased, the material became a good thermal insulator. It was determined that the thermal conductivity value of the gypsum experimental sample containing hydrophobic granular aerogel of 96-99% by volume decreased compared to natural plaster, an aerogel unadulterated experimental sample. As a result, it was found that the thermal properties of aerogel-reinforced plasters were much superior compared to conventional materials. Thus, it was proven that insulation materials with low thermal conductivity, such as silica aerogel-based mortar mixtures, reduce heat losses in buildings, as well as save energy and costs for air conditioning and heating throughout the building's life. This silica aerogel-based plaster, developed and commercialized by Agosti Nanotherm and Arte & Mestieri under the brand Tillica pasta, is used as a restoration material in historical buildings (Buratti et al., 2014).

Table 2.

Thermal Conductivity Analysis Results of Plasters Containing Aerogel Material at Different Reinforcement Ratios (Buratti et al., 2014)

	Granular Aerogel (%volume)	Thermal Conductivity (W/mK)	
Natural lime plaster	-		0,50
Hydrated lime plaster + aerogel	80-90		0.050-0.045
Hydrated lime plaster + aerogel	91-95		0.021-0.019
Hydrated lime plaster + aerogel	96-99		0.016-0.014

Ibrahim et al. (2015) used insulation plasters containing silica aerogel in exterior thermal insulation applications and conducted investigations for the development of the material. They found that when silica aerogel-based plasters were applied both in the facade applications of new buildings and on the traditional masonry facades of historical buildings, they showed a high insulation performance. In addition, they revealed that insulation materials containing silica aerogel were easily applicable and could be used for thermal reinforcement of existing buildings with known techniques in practice. The purpose of the study was to investigate the hydrothermal performance of external walls and determine the energy performance of these plastered and non-plastered buildings. As a result, it was determined that insulation materials containing silica aerogel significantly reduced wall-induced heat losses and therefore the energy consumption of the house. They also showed that adding silica aerogel-based plaster to the outer surface of walls significantly reduced or eliminated moisture risks. Thus, due to the hydrophobic nature of aerogel, silica aerogel-based plasters reduced water absorption and ensured that the material's volumetric composition and thermal behavior were kept constant (Ibrahim et al., 2015).

In another study, Stahl et al. (2012) focused on a plaster consisting of hydrophobic granular silica aerogel (60-90% by volume). This prepared material was first used in the reinforcement of historically sensitive buildings. This plaster mixture consisted of a binder, which did not contain cement and minarets, and some solid substances. Cement material was not used because it was not compatible with both the physical and chemical structure of the historical walls. When cement material is used in historical buildings, the impermeability of the wall increases, moisture is prevented from moving away, and undesirable situations such as flowering are encountered. It was possible to apply this mixture prepared within the scope of the study both by hand and with plastering machines. However, it was stated that the thermal conductivity value of the samples produced by the plastering machine increased more than that of the plaster produced by hand. The reason for this was that there was more water input in the production by machine. The thermal conductivity value of the produced plaster was measured as approximately 0.025 W/mK on the hot plate device. This value was quite low and showed that the plaster provided thermal insulation. In Figure 12, an image of the produced silica aerogel-based plaster applied to an area of 1 m² is given (Stahl et al., 2012).

Figure 12.

1 m² Test Wall With Low Thickness, Silica Aerogel Based Plaster Application (Stahl vd.,2012)



Together with the Fixit group at Empa, the Swiss Federal Laboratories for Materials Science and Technology has developed insulation plasters containing granular silica aerogel (Figure 13). This plaster contains more than 80% silica aerogel granules by volume and is applied to the walls by spraying with conventional industrial machine-based projection systems. After the application of the silica aerogel content material to the wall by spraying method, the thermal conductivity value was measured and it was found that this value was below 0.025 W/mK. In addition, when the samples obtained after the wall spray test were measured, the thermal conductivity value was measured around 0.08-0.09 W/mK under ambient conditions. Moreover, the measured values showed that the thermal insulation performance of this material was more than twice the thermal insulation performance of standard insulation plaster materials (Koebel et al., 2012).

Figure 13.

Cross-Section of Silica Aerogel Insulating Plaster Material Developed by Empa and Fixit (Koebel et al., 2012)



Parexlanko and MINES ParisTech/AR-MINES/CEP are French companies that produce silica aerogel-reinforced plasters. The objectives of the companies are to obtain good thermo-mechanical compatibility for applications of hydrophobic granular silica aerogels with methods as close as possible to conventional methods (e.g., cement-based

mortars). The thermal conductivity value of the mortars produced by the companies was measured as close to 0.050 W/MK (as measured by the guarded-hot-plate method), and it was determined that the bending strength, which is among the mechanical strength properties of mortars, was greater than 0.5 MPa. Later, the company aimed to industrialize the production of this material. After that, the French FUI project was selected for experimental application, and it was planned that the application would be carried out in old existing buildings located in France (Koebel et al., 2012). In another study conducted by Nanotech Aspen, boards based on silica aerogel technology and combined with polypropylene, glass fiber, and drywall sheets were developed for insulation purposes (Curto & Cinieri, 2020).

In recent years, the fact that granular silica aerogels exhibit high thermal performance compared to conventional materials when they are combined with different building materials and used for thermal insulation purposes has made these materials a focal point. It has been proven that by using these materials, not only plaster and mortar products can be produced, but also ultralight gypsum boards and concrete can be produced by mixing them with many building materials such as sand and cement. Due to the fact that the cement materials containing granular silica aerogel are lightweight, it is possible to build more earthquake-resistant structures with these materials. In another study, opaque gypsum boards and panels based on silica aerogel were developed. With these products with low thermal conductivity, it was possible to insulate the building envelope without increasing the wall thickness. Materials with silica aerogel content are nature-friendly. Therefore, they significantly contribute to the reduction of carbon emissions. It is also known that due to the hydrophobic properties of materials, they provide waterproofing in architectural structures (Curto & Cineri, 2020; Alparslan, 2021).

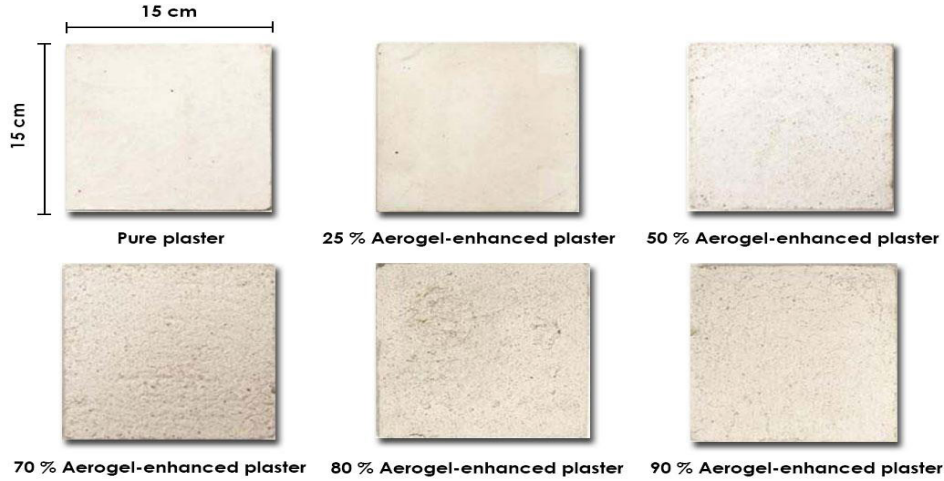
In their study, Mermer and Pişkin (2019) aimed to perform silica aerogel synthesis by ultrasound-assisted sol-gel method from sand and to use silica aerogel in the production of plaster with thermal insulation properties. For this purpose, they realized the production of silica aerogel with hydrophobic properties from commercial sand under ambient pressure. Thermal conductivity measurement analysis was performed on the prepared insulation plaster samples. When thermal conductivity values of the gypsum mixtures produced using different silica aerogel reinforcement ratios (0%, 1%, 5%, and 10%) were examined, it was determined that the gypsum plaster sample containing 10% silica aerogel had a more effective insulation property (at a rate of 26.05%) compared to the plaster without aerogel. It was emphasized that this developed product could be used as a thermal performance-enhancing insulation material on buildings' interior and exterior wall surfaces (Mermer & Pişkin, 2019).

Nosrati and Berardi (2018) developed insulation plasters reinforced with hydrophobic granular silica aerogel. Gypsum powder was mixed with hydrophobic silica aerogel supplied by Cabot Corporation. Then the experimental samples were created in a laboratory environment by pouring the resulting plaster into molds with dimensions of 150x150x200mm. In Figure 14, the thermal conductivity analysis results of gypsum board samples produced at different hydrophobic silica aerogel reinforcement ratios (0%, 25%, 50%, 70%, 80%, and 90% by volume) are shown. Based on these results, it was determined that the experimental sample without silica aerogel reinforcement had a thermal conductivity of 0.140 W/mK, while the experimental sample with the highest reinforcement ratio had a thermal conductivity value of 0.027 W/mk. It was observed that the thermal conductivity value decreased as the amount of silica aerogel increased.

As a result, it was concluded that the gypsum plaster sample containing silica aerogel provided 82.2% more effective thermal insulation than gypsum plaster without silica aerogel (Nosrati & Berardi, 2018).

Figure 14.

Hydrophobic Silica Aerogel Plaster Samples (Nosrati & Berardi, 2018)



In their study, Berardi and Nosrati (2018) produced gypsum board samples. They planned the silica aerogel additive ratios of the samples to be 0%, 25%, 50%, 70%, 80%, and 90% by volume. By applying an accelerated aging process to gypsum board samples prepared at different silica aerogel reinforcement ratios under laboratory conditions, they examined the effects of this aging process on the thermal performance of insulation materials reinforced with silica aerogel. The thermal conductivity coefficients of the prepared samples were measured before and after the aging process. The thermal conductivity results measured before the aging process revealed that the thermal conductivity value decreased as the amount of aerogel increased. The thermal conductivity value of the gypsum board sample containing 90% aerogel by volume decreased by about 80.68% compared to the gypsum board sample without aerogel. This value indicated that the sample with a high aerogel ratio had a more effective insulation property. Subsequently, the thermal conductivity values of the experimental samples were analyzed after the aging process (20 years). Based on the results, it was determined that there was a decrease in the thermal conductivity coefficient as the aerogel reinforcement rate increased under normal conditions, and after aging, the thermal conductivity coefficients in the same aerogel reinforcement ratios increased only by less than 10% compared to the initial values. Finally, this study showed that despite some deterioration due to the aging of the material, the thermal conductivity of aerogel-reinforced materials remains significantly lower after aging compared to the thermal conductivity of conventional insulation materials that were not exposed to the aging process (Berardi & Nosrati, 2018).

Achard et al. (2011) produced and patented an insulating plaster containing hydrophobic silica aerogel including mineral and organic binders. It was stated that the density of the produced insulation plaster with hydrophobic aerogel content was 156 kg/m³, and the thermal conductivity coefficient was 0.0268 W/mK. This plaster, which has a highly developed thermal insulation property, is applied by spraying on the wall surface of the structure (Achard et al., 2011).

Bostancı (2021) conducted a research study on the evaluation of the thermal conductivity properties of hybrid silica fume mortar mixtures with silica aerogel reinforcement. For this purpose, he obtained cement mortar mixtures with low silica aerogel reinforcement ratios (0%, 0.25%, and 0.5% by weight of cement), and added low sodium carbonate (Na_2CO_3) for alkaline activation of mortar mixtures. Experiments were carried out after curing periods of 2, 7, and 28 days of the obtained mortar mixtures. The experimental results revealed that the thermal conductivity value of the experimental samples decreased as the amount of silica aerogel increased due to the silica aerogel added to the mortar mixtures. It was reported that the thermal conductivity value of the experiment sample without silica aerogel reinforcement improved by 28% compared to the thermal conductivity value of the experiment sample with 0.25% silica aerogel reinforcement (Bostancı, 2021).

Üstündağ and Sola (2022) investigated the effect of silica aerogel and silica fume on the thermal conductivity properties of cement-based mortars. For this purpose, they determined the reinforcement ratios of silica aerogel in low amounts (0%, 0.25%, and 0.5% by weight of cement). Cement, silica fume, and standard sand were used together with silica aerogel in the preparation of mortar samples. The prepared mortar samples were subjected to curing, wetting-drying effect, and MgSO_4 effect in water for 16 weeks. As a result of the experiments, the highest thermal conductivity reduction (31.2%) was obtained from a water-curing sample with the addition of silica fume at an aerogel content of 0.25%. On the other hand, the lowest thermal conductivity coefficient (1.458 W/mK) was measured in the sample that contained 0.25% silica fume and aerogel and completed the curing process under the influence of MgSO_4 (Üstündağ & Sola, 2022).

Silica Aerogel Reinforced Boards, Panels, Blankets, and Their Applications in Architectural Structures

Silica aerogel materials have the desired thermal properties for insulation applications. But to improve some of the properties of silica aerogel materials and eliminate the weaknesses of the material (such as brittleness), effective methods have been considered. Some endeavors have been made to prepare silica aerogel in different physical forms while maintaining their properties, to strengthen them by adding a second component, or to obtain stronger materials with the desired thermal performance by doing both. In this context, boards, panels, and blankets containing silica aerogel have been developed, and innovative solutions have been obtained with these innovative materials in architectural applications.

The insulation blanket produced by Aspen Aerogel, one of the largest silica aerogel material manufacturers, under the name Spaceloft, has widespread use in the construction sector. A sample project supported by the Swiss Federal Office of Energy (SFOE) was carried out for the application of a silica aerogel blanket. A multi-family townhouse built in the early 20th century in Zurich was chosen as the scope of the project, and Aspen Spaceloft blanket insulation was applied to the facade by preserving the original style and shape of the house unchanged. In the first stage, the cladding of the original wall on the exterior was removed and two 10 mm-thick Spaceloft blankets were attached. Then, a standard insulation plaster with a thickness of 30 mm was applied to the material. After the application, it was found that the thermal insulation value of the reinforced wall was less than one-third of the original thermal insulation value. In Figures 15 and 16, application images of the installation of Spaceloft blankets on the

exterior of the building are shown (Koebel et al., 2012).

Figure 15.

Renovation of an Early 20th Century Townhouse in Zurich, Switzerland. (a) Exterior View of The House Before Renovation (b) Exterior Appearance of The House After Renovation (Koebel et al., 2012)

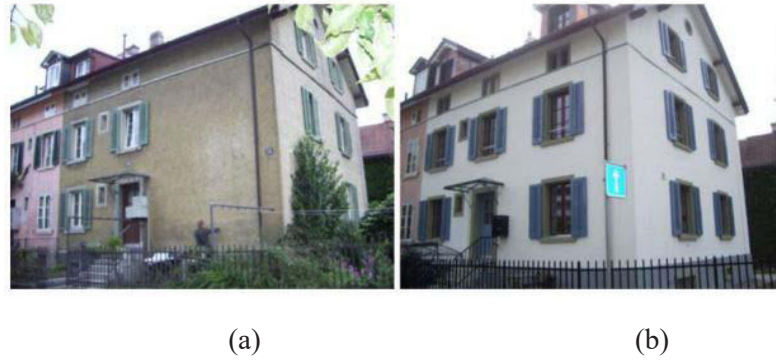


Figure 16.

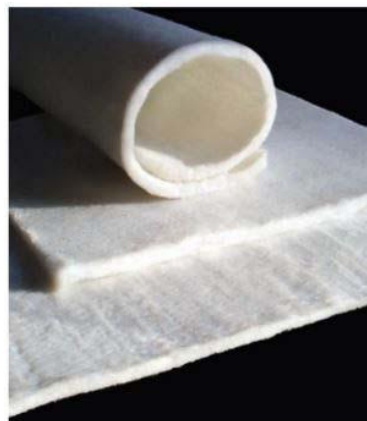
Exterior Wall Insulation Installation Application With Spaceloft Blankets (Koebel et al., 2012)



Another product developed by Aspen Aerogel is fiber composite cover, which is a flexible aerogel for thermal insulation. This product, which has low thermal conductivity, also has a fairly good load-bearing ability (Figure 17).

Figure 17.

Aerogel Fibre Composite Cover Developed by Aspen Aerogel (Ryu, 2000)

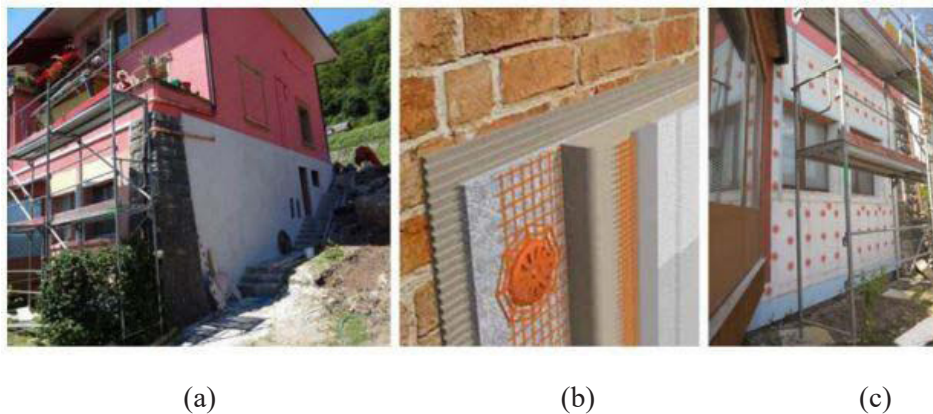


Another example of materials containing silica aerogel is the StoTherm in Aevero product. This product is a composite sheet, but it is produced from silica granule aerogel

by combining it with polymeric binders. From the application point of view, the ease of installation of the material ensures that the renovation of the building is completed quickly and provides a great advantage in the construction industry. Another example of silica aerogel-containing blankets is the ‘AeroCalce’ construction product. An example of the exterior facade application of a house is given in Figure 18. With this material, the basement floor insulation of the house was strengthened (Koebel et al., 2012).

Figure 18.

Insulation Applications Used in Architectural Structures with AeroCalce Brand Aerogel-Containing Insulation Blanket (a) Front And Side View of the Building (b) Photo of the Nine-Section of the AeroCalce Brand Insulation Blanket (c) Wall and Window Details on the Ground Floor (Koebel et al., 2012)



Aerogips gypsum panel produced by the company ‘‘Ama Aerogel’’ is a product that is combined with a high-density gypsum-coated board and provides thermal and acoustic performance based on silica aerogel (Figure 19). This product plays a significant role in the energy saving of buildings by providing maximum thermal insulation in the area. Aerogips insulation board, which provides thermal insulation, is used on horizontal and vertical surfaces, walls, floors, and ceilings, in all structures where lightweight walls are used, and in the design of new non-load-bearing walls. Gypsum boards are used for interior interventions of existing buildings, residential and commercial applications, interior renovations, and restoration processes of historical buildings. The building material has a thermal conductivity coefficient close to 0.015 W/mK. In addition, it has a waterproof property with a water-repellent structure (URL-8).

Figure 19.

Thermal Insulation Application of Aerogips Gypsum Board on Interior Wall (URL-9)



Silica Aerogel-Reinforced Paints and Wallpapers, and Their Applications in Architectural Structures

In this section, application examples of silica aerogel-containing paints, wallpapers, and wall coverings developed for thermal insulation purposes are presented. Building materials containing silica aerogel are used on the interior and exterior wall surfaces of buildings. The “*Thermogel Paint*” produced using the new technology by the “AMA Aerogel” company is a product with the consistency of paint. Unlike standard paints, it minimizes the formation of thermal bridges by preventing the spread of energy to the wall and reflects heat. Because Thermogel Paint reduces thermal bridges on surfaces, it creates breathable surfaces by preventing the formation of condensation and moisture on the wall. Thus, it prevents the risk of mold formation on the wall by reducing it to a minimum. This product creates an insulating barrier effect on the surface where it is applied and provides energy savings. Compared to standard paints, the resistance of paints with silica aerogel content to heat transfer is at least four times higher. This product, which has a low coefficient of thermal conductivity, prevents the transmission of heated air to the interior in summer and allows it to stay inside the building longer by preventing the transmission of inside heat to the outside in winter (Figure 20). The usage area of Thermogel paint is quite wide. This high-quality paint is applied on plastic and glass surfaces, interior and exterior walls, prefabricated concrete elements, and roofs (URL-10).

Figure 20.

Application of Thermogel Paint Product Produced by Ama Aerogel Company (URL-11)



Nguyen et al. (2020) obtained a thermal insulation paint by adding the hydrophobic silica aerogel powder they synthesized to water-based acrylic paint at low reinforcement rates (3-7%) and examined the thermal insulation performance of this paint. As a result of the experiments, it was found that the thermal performance improved significantly in the innovative paint obtained with hydrophobic silica aerogel reinforced at a rate of 6 wt% (Nguyen et al., 2020).

On the other hand, strengthening the residential building stock is of great importance for the European construction sector in the coming years. To achieve the 2050 decarbonization targets set by the EU Energy Roadmap, the EASEE research project funded by the European Commission has addressed this issue by developing a holistic approach to the thermal reinforcement of buildings. Within the scope of this project, they have initiated studies on the development of super-insulated and silica aerogel-based textile wallpaper for “*indoor energy adaptation*” in existing residential buildings. They have aimed to create an insulation layer by applying the developed textile wallpaper to the interior walls of existing structures. For the textile wallpaper with silica aerogel

content to show high thermal performance (reaching a value of 0.2 W/m²K U in colder climates) and provide water vapor permeability, characterization studies have been carried out, and it was tested at the laboratory scale. The fabric finishing system of textile wallpaper has been designed in a way that cleaning and installation will be easy and that it provides convenient stretching and disassembly. In addition, they are materials that provide ease of transportation and storage. To apply the textile wallpaper, a residence in Milan was selected as a study area. Later, the inner wall of the residence was reinforced with silica aerogel-based textile wallpaper application (Figure 21). The purpose of this application was to test the applicability of textile wallpaper in a real space. It was stated that within the scope of the project, implementation of application simulation is very useful for determining a number of standards to determine the issues that need to be taken into account during installation and to test possible problems that may arise in a realistic situation (Masera et al., 2017).

Figure 21.

Aerogel-Based Textile Wallpaper Application (Masera et al., 2017)



Industrial Nanotech Inc. has developed a new type of paint by adding silica aerogel particles to paints. Company researchers note that this patented material, called Nansulate, can provide an important thermal insulation performance. This material consists of highly porous particles. This material with silica aerogel content is applied in a thin layer, and in this way, it limits the heat transfer. This product can also be used in interior and exterior wall applications by mixing with water-based paints. In addition, it has been stated in the literature that it can be used for insulation purposes in attics, windows that do not require full opening, plastic or wooden shutters, and water heaters. Another research study that attracts attention in this regard is the HIPIN (High-Performance Insulation Based on Nanostructured Encapsulation of Air) project. The HIPIN project aims to develop silica aerogel particles that can be added to insulation materials and that have more flexible, durable, and robust properties. In addition, in the project, it has been emphasized that the development of more robust silica aerogels will reduce the cost of aerogel production. Within the scope of the project, it is targeted that the developed products will be able to be integrated into plasters, paints, and even thick coatings and be applied (Ülker et al., 2014).

Conclusion

In this study, the use of silica aerogel-containing building materials in architecture, interior architecture, and the construction sector was investigated within the framework of exemplary applications. As a result of the investigations, it was seen that building materials containing silica aerogel were applied in architectural applications in the fields of construction and design. It was found that silica aerogel materials had superior

properties such as high thermal performance, improved the thermal conductivity properties of the traditional building materials they were reinforced with, and had a positive effect on heat preservation and energy efficiency in architectural structures. In addition, it was observed that many features such as energy, performance, environmental friendliness, and sustainability were included in these innovative silica aerogel-based materials thanks to technology, and thus, the performance and productivity levels of building materials were improved and increased.

On the other hand, in line with the literature review, it was determined that building materials containing silica aerogel were used to restore old structures as well as to increase the energy efficiency of existing buildings. It was observed that in the interior of buildings, by using transparent and translucent products containing silica aerogel, lighting with daylight, which is a renewable energy source, providing thermal, visual, and acoustic comfort, and contributing to achieving sustainable structures were ensured. Moreover, it was seen that in the construction of sustainable architectural structures, in addition to providing energy savings, materials containing silica aerogel made a great contribution to minimizing the damage caused to the environment thanks to their environmentally friendly properties. Finally, it is thought that this study will contribute to the development of production methods of silica aerogel materials in the light of technological developments and their widespread use in the construction sector and will create a new perspective in terms of the use of silica aerogel materials in the architectural design process of the future.

References

- Achard, P., Arnaud, R., Echantillac, T., Bellet, A., Aulagnier, M., Daubresse, A. (2011). Insulating silica xerogel plaster. Patent.
- Al Zaidi, I. K. A. (2017). Nano SiO₂ – The Production of Concrete Blocks With Thermal Super Insulation Property By Addition of Nano SiO₂-Aerogel. Master Thesis, Erciyes University, Institute of Science and Technology, Kayseri.
- Alparslan, G. (2021). Use of aerogel in cement. *Journal of Sustainable Engineering Applications and Technological Developments*, 4(2), 53-58.
- Altın, M. (2014). Aerogel Use in Sustainable Buildings. *Insulation Journal*, (123).
- Arslan, M. A. & Aktaş, M. (2018). Evaluation of insulation materials used in construction sector based on heat and sound insulation. *Polytechnic Journal*, 21(2), 299-320.
- Arı, A. C. (2022). Investigation of the use of building materials produced by nanotechnological methods in the construction sector. *Uluborlu Journal of Vocational Sciences*, 5(1), 14-27.
- Arkan Demirörs, T. (2023). Synthesising Silica Aerogel By Sol-Gel Method And Developing The Performance Of Architectural Building Material. Ph. D. Thesis, KTO Karatay University, Institute of Graduate Education, Konya.
- Baetens, R., Jelle, B.P. & Gustavsen, A. (2011). Aerogel Insulation for Building Applications: A State-of-the-Art Review. *Energy and Buildings*, 43, 761–769.

- Barbero S., Marco D., Ferrua C., and Pereno A. (2014). Analysis on existent thermal insulating plasters towards innovative applications: Evaluation methodology for a real cost-performance comparison. *Energy and Buildings*, 77, 40-47.
- Bayrakçı, H. C., DAVRAZ, M., Başpınar, E. (2011). New Generation Of Thermal Insulation Material: Vacuum Insulation Panel. *SDU Journal of Technical Sciences*, 1(2), 1-12.
- Berardi, U. (2015). Development of glazing systems with silica aerogel. *Energy Procedia*, 78 394-399.
- Berardi U. & Nosrati R. H. (2018). Long-term thermal conductivity of aerogel-enhanced insulating materials under different laboratory aging conditions. *Energy*, 147, 1188- 1202.
- Bertolini, C., Crivellaro, A., Marciniak, M., Marzi, T., & Socha, M. (2010). Nanostructured materials for durability and restoration of wooden surfaces in architecture and civil engineering. *In the World Conference on Timber Engineering-WCTE* (31).
- Bostancı, L., (2021). Mechanical, Pore Structure, Thermal Conductivity and Microstructure Properties of Silica Aerogel-Incorporated Hybrid Silica Fume Mortars. *Dicle University Journal of Engineering*, 12(1), 147-163.
- Bostancıoğlu, E. (2011). Mevcut binalarda yapılan ekolojik iyileştirmelerin enerji kazancı. *The Turkish Online Journal of Design, Art and Communication-TOJDAC*, 1, 2.
- Buğdaycı, İ. (2008). The World's Best Solid Aerogel, *Journal of Science and Technology*.
- Buratti, C., Moretti, E., Belloni, E., Agosti, F. (2014). Development of Innovative Aerogel Based Plasters: Preliminary Thermal and Acoustic Performance Evaluation. *Sustainability*, 6(9), 5839-5852.
- Buratti, C., Moretti, E., Belloni, E. (2016). Aerogel plasters for energy building efficiency: Nano and Biotech Based Materials for Energy Building Efficiency (Pacheco, vd., Ed.). *Springer International Publishing*, 17-40.
- Calisesi, M. (2017). Aerogel Incorporated Plasters and Mortars: the case study of precast panels. Tesi di laurea in. *Alma Mater Studiorum Universita Di Bologna*, Italia.
- Cuce, E., Cuce, P. M., Wood, C. J., Riffat, S. B. (2014). Toward aerogel based thermal superinsulation in buildings: A comprehensive review. *Renewable and Sustainable Energy Reviews*, 34, 273–299.
- Curto, D., D. & Cinieri, V. (2020). Aerogel-Based Plasters and Energy Efficiency of Historic Buildings. Literature Review and Guidelines for Manufacturing Specimens Destined for Thermal Tests. *Sustainability*, 12, 9457.
- Çüçen, A., & Altuncı, Y. T. (2022). Investigating the opportunities to use nanotechnological building materials in architecture. *Journal of Technical Sciences*, 12(1), 17- 23.
- Farahmandjou, M., & Khalili, P. (2013). Study of nano SiO₂/TiO₂ superhydrophobic

- self-cleaning surface produced by sol-gel. *Australian Journal of Basic and Applied Sciences*, 7(6), 462-465.
- Garnier, C., Muneer, T., McCauley, L. (2015). Super Insulated Aerogel Windows: Impact on Daylighting and thermal performance. *Building and Environment*, 94, 231-238.
- Gao, T., Jelle, B. P., Gustavsen, A. (2016). Building integration of aerogel glazings. *Procedia Engineering*, 145, 723-728.
- Gurav, J. L., Jung, I. K., Park, H. H., Kang, E. S., Nadargi, D.Y. (2010). Silica Aerogel: Synthesis and Applications. *Journal of Nanomaterials*, 11.
- Güdük, M. B., & Satıcı, B. (2022). Effect of Technological Developments On Architecture and Materials. *Journal of Technology and Applied Sciences* 4(2), 77-86.
- Gür, M. (2010). Nanomaterials in the Context of Nanoarchitecture. *Uludağ University Journal of The Faculty of Engineering and Architecture*, Cilt 15, Sayı 2
- Hrubesh, L., W. (1998). Aerogel Applications. *Journal of Non-Crystalline Solids*. 225, 335-342.
- Huang, L. (2012). Feasibility of using silica aerogel as insulation for buildings. Master of Science Thesis, KTH School of Industrial Engineering and Management, Stockholm.
- Huang, Y., Niu, J. L. (2015). Energy and visual performance of the silica aerogel glazing system in commercial buildings of Hong Kong. *Construction and Building Materials*, 94, 57-72.
- Ibrahim, M., Biwole, P. H., Achard, P., Wurtz, E., & Ansart, G. (2015). Building envelope with a new aerogel-based insulating rendering: Experimental and numerical study, cost analysis, and thickness optimization. *Applied Energy*, 159, 490–501.
- Koebel, M., Rigacci, A., Achard, P. (2012). Aerogel-based thermal superinsulation: an overview. *Journal of Sol-gel Science and Technology*, 63, 315-339.
- Köken, A., & Kanık, M. (2022). Thermal Insulation And Textile Applications with Aerogels. *Journal of Textiles and Engineering*, 29(128), 249-260.
- Lakatos, Á. (2019). Stability investigations of the thermal insulating performance of aerogel blanket, *Energy and Buildings*, 185, 103–111.
- Masera, G., Ghazi Wakili, K., Stahl, T., Brunner, S., Galliano, R., Monticelli, C., Aliprandia, S., Zanelli, A., Elesawye, A. (2017). Development of a super-insulating, aerogel-based textile wallpaper for the indoor energy retrofit of existing residential buildings. *Procedia Engineering*, 180, 1139-1149.
- Mermer, N.K., Pişkin, S. (2019). Synthesis of aerogel usage of sand by ultrasonically assisted sol-gel method, characterization and thermal insulation plaster application. *Journal of the Faculty of Engineering and Architecture of Gazi University*, 34(3), 1253-1263.
- Moretti, E., Merli, F., Cuce, E., Buratti, C. (2017). Thermal and acoustic properties of aerogels: preliminary investigation of the influence of granule size. *Energy*

- Procedia*, 111, 472-480.
- Neugebauer, A., Chen, K., Tang, A., Allgeier, A., Glicksman, LR., Gibson, L. J. (2014). Thermal conductivity and characterization of compacted, granular silica aerogel. *Energy and Buildings*, 79, 47-57.
- Nguyen, T. H., Mai, N. T., Reddy, V. R. M., Jung, J. H., Truong, N. T. N. (2020). Synthesis of silica aerogel particles and its application to thermal insulation paint. *Korean Journal of Chemical Engineering*, 37(10), 1803-1809.
- Ng, S., Jelle, B., P., Sandberg, L. I. C., Gao, T., Wallevik, Ó. H. (2015). Experimental investigations of aerogel-incorporated ultra-high performance concrete. *Construction and Building Materials*, 77, 307-316.
- Nosrati, R. H. ve Berardi, U. (2018). Hygrothermal characteristics of aerogel-enhanced insulating materials under different humidity and temperature conditions. *Energy and Buildings*, 158, 698-711.
- Özer, N. & Özgünler, S. A. (2019). Evaluation of performance on the wall sections of insulation materials used in construction. *Journal of Uludag University Faculty of Engineering*, 24(2), 25-48.
- Pacheco Torgal, F., Buratti, C., Kalaiselvam, S., Granqvist, C.-G., Ivanov, V. (Eds.) (2016). Nano and Biotech Based Materials for Energy Building Efficiency. *Springer: Cham, Switzerland*.
- Reim, M., Körner, W., Manara, J., Korder, S., Arduini-Schuster, M., Ebert, H.P., Fricke, J. (2005). Silica aerogel granulate material for highly thermal insulation and daylighting. *Solar Energy*, 79(2), 131–139.
- Ryu J. (2000). Flexible aerogel superinsulation and its manufacture. U.S. Patent No 6,068,882, 2000.
- Santos, P., Martins, C., Silva, L. S. (2014). Thermal performance of lightweight steel-framed construction systems. *Metallurgical Research & Technology*, 111, 329-338.
- Sebdani, Z. M., Begum, H., Schoenwald, S., Horoshenkov, K. V., Malfait, W. J. (2021). A review on silica aerogel-based materials for acoustic applications. *Journal of NonCrystalline Solids*, 562, 120770.
- Stahl, T., Brunner, S., Zimmermann, M., Ghazi Wakili, K. (2012). Thermo-hygric properties of a newly developed aerogel based insulation rendering for both exterior and interior applications. *Energy Building*, 44, 114-117.
- Szczepaniak, R., Komórek, A., Przybyłek, P., Krzyżak, A., Rośkowicz, M., Godzimirski, J., Pinkiewicz, E., Jaszczak, W., Kosicka, E. (2022). Research into mechanical properties of an ablative composite on a polymer matrix base with aerogel particles. *Composite Structures*, 280, 114855.
- Szodrai, F., Lakatos, Á., Kalmár, F. (2016). Analysis of the change of the specific heat loss coefficient of buildings resulted by the variation of the geometry and the moisture load, *Energy*, 115, 820–829.
- Ülker, Z., Şanlı, D., Erkey, C. (2014). Applications of Aerogels and Their Composites in Energy-Related Technologies. *Supercritical Fluid Technology for Energy and Environmental Applications*, 157-180.

Üstündağ, Ö., Sola, O. Ç. (2022). Effect of aerogel/silica fume under curing methods on properties of cement-based mortars. *Journal of Construction*, 21(2), 368-386.

Yıldız, B. & Seçkin, N. P. (2019). Evaluation of perceptual differences of materials in architecture. *Istanbul Sabahattin Zaim University Journal of Institute of Science and Technology*, 1(2), 6-14.

Azuma, R., Baillot, Y., Behringer, R., Feiner, S., Julier, S. & MacIntyre, B.(2001). Recent advances in augmented reality, *Computer Graphics and Applications*, IEEE, 21(6), 34-47.

Electronic References

URL-1:<https://www.kalwall.com/wp-content/uploads/2022/04/spokaneprojectreport-2.pdf>
(Date of Access:02.Mar.2024).

URL-2:<https://www.kalwall.com/wp-content/uploads/2022/03/Product-Overview.pdf>
(Date of Access:02.Mar.2024).

URL-3: <https://www.kalwall.com/portfolio/>
(Date of Access:02.Mar.2024).

URL-4:<https://www.glastroesch.com/de/de/ueber-uns/geschaeftsbereiche/okalux>
(Date of Access:02.Mar.2024).

URL-5:<https://www.glastroesch.com/en/about-us/media-center/news/post/tengelmann-climate-market>
(Date of Access:02.Mar.2024).

URL-6:<https://hbarchitects.co.uk/halley-vi-british-antarctic-research-station/>
(Date of Access:02.Mar.2024).

URL-7: <https://www.birdair.com/membrane/insulated-translucent-membrane/>
(Date of Access: 03.Mar.2024).

URL-8:<http://amaaerogel.com/wp-content/uploads/2019/06/AEROPAN-TRVERSIYON.jpg>
(Date of Access:03.Mar.2024)

URL-9:https://www.archiproducts.com/en/products/ama-composites/aerogel-thermal-insulation-panel-aerogips_137878
(Date of Access:03.Mar.2024).

URL-10: <https://amaaerogel.com/thermogel-paint/>
(Date of Access:03.Mar.2024).

URL-11: <https://amaaerogel.com/galeri/>
(Date of Access:03.Mar.2024).

Acknowledgments

This study is derived from the doctoral thesis titled “ Synthesising Silica Aerogel by Sol-Gel Method and Developing The Performance of Architectural Building Material ” completed at KTO Karatay University Graduate Institute, Department of Architecture.

About The Authors

Tuba ARKAN DEMİRÖRS holds an integrated PhD degree in Architecture in 2023. She is a guest instructor, in the Department of Interior Architecture at KTO Karatay University in Konya, Türkiye. Her main areas of interest are materials and technology in architecture and interior architecture, building materials and interior architecture design.

E-mail: tuba_arkan@hotmail.com, **ORCID:** 0000-0003-3278-9045

Kerim ÇINAR is a Professor of Architecture at KTO Karatay University in Konya, Türkiye. He is a Professor of Architecture at KTO Karatay University. His main areas of interest are architectural design, design in architectural settlements and materials and technology in architecture.

E-mail: kerim.cinar@karatay.edu.tr, **ORCID:** 0000-0003-4318-7736

Similarity Index

The similarity index obtained from the plagiarism software for this book chapter is 10%.

CHAPTER 2

Material Use in Renewable Energy Applications

Edip TAŞKESEN

Şırnak University, Türkiye

Göknur KAYATAŞ ONGUN

Bolu Abant İzzet Baysal University, Türkiye

To Cite This Chapter:

Taskesen, E. & Kayatas Ongun, G. (2024). Material Use in Renewable Energy Applications. In H. Gokmese, S. Bulbul, & Y. Uzun (Eds.), *Current Studies in Materials Science and Engineering* (pp. 31-52). ISRES Publishing.

Introduction

Energy is essential for sustaining life, utilized in various sectors such as heating, lighting, transportation, and industry. Renewable energy resources, including solar, wind, geothermal, biomass, hydroelectric, and marine energies, are readily available in nature, offering sustainable alternatives. These resources are harnessed through active and passive systems. While active systems employ technical means, passive systems utilize natural decisions like site selection (Gülay, 2008).

Renewable energy sources are defined by their ability to replenish at a rate equal to or faster than their depletion (Akıncı & Kök, 2017). The International Energy Agency underscores renewables as energy replenished more than consumed, with global potential and dispersal (International Energy Agency, 2015). Such resources play a pivotal role in combating the waste crisis, aligning with material efficiency practices in cities. Material efficiency, integral to the circular economy, entails strategies like waste reduction, recycling, and sustainable material usage.

Industries, transportation, and buildings, being high-energy and material consumption sectors, significantly impact urban sustainability (UN-Habitat, 2023). Efficient buildings, lighting, and heating systems coupled with renewable integration can curtail energy consumption and emissions. For instance, aluminum usage in buildings ensures durability and low maintenance.

In sustainable cities, renewables like wind, hydro, and geothermal energy offer clean alternatives, reducing carbon footprint and enhancing air quality. They also foster energy independence, contributing to urban resilience. Consequently, strategies promoting energy and material efficiency are imperative for urban sustainability.

Renewable energy applications heavily rely on material choices. This section delves into key materials used in solar panels, heat pumps, wind turbines, biomass boilers, and geothermal systems, elucidating their properties and significance in advancing towards a sustainable future.

Material Selection in Solar Energy Applications

The Sun is one of the most significant stars in our universe. It formed approximately 5 billion years ago and is expected to continue its existence for about another 6 billion years. The Sun is the source of life for the Earth and is also one of the most important factors influencing the climate on the Earth's surface. The distance of the Sun from the Earth is 150 million kilometers, with an approximate weight of 109 quadrillion tons and a diameter of about 1.5 million kilometers. Its emitted light reaches the Earth after approximately 8 minutes. The Sun has a temperature of about 15 million degrees Celsius and continuously generates energy by converting hydrogen into helium through nuclear fusion. This nuclear fusion process occurs due to the intense pressure and temperature inside the Sun. Therefore, the Sun is of vital importance for the continuation of life on the Earth (Alahmad et al., 2023).

Solar energy, derived from the sun's radiant energy, is a vital and abundant renewable resource, serving as the cornerstone of various energy applications (Yıldırım & Teke, 2013). With an average of 173 billion MW of energy received annually, it surpasses the total fossil energy resources by 160-fold (Toprak & Küçük, 2018). Utilized in electricity generation and heat production, solar energy offers inexhaustible potential (Sayın, 2006).

Photovoltaic (PV) panels, predominantly composed of silicon-based materials, efficiently convert sunlight into electricity, while materials like aluminum, known for high thermal conductivity, find utility in solar collectors (Kaynak & Kaya, 2018). As of 2010, solar energy accounted for only 3.3% of global electricity generation, a figure expected to rise to 11.8% by 2035 (Mevka, World Key Statistics 2011).

Solar energy applications span low-, medium-, and high-temperature domains. Low-temperature applications, such as water and residential heating, employ plane collectors, while medium-temperature applications utilize focused collectors for industrial purposes (Kaynak & Kaya, 2018). Photovoltaic applications directly convert solar radiation into electrical energy, originally developed for space missions and now deployed in remote locations (Kaynak & Kaya, 2018). Optimal utilization of solar energy requires positioning within the "Sun Belt," roughly between 45° north and south latitudes.

Solar Cells

Solar cells, or photovoltaic diodes, directly convert solar energy into electrical energy using the photovoltaic phenomenon. Typically, they have square, rectangular, or circular surfaces, around 100 cm² in area and 0.2-0.4 mm thick. Solar cells generate electrical voltage when exposed to light. Maximum irradiance at sea level on a clear day is about 1000 W/m², and annual solar energy per 1m² ranges from 800 to 2600 kWh, with conversion efficiencies between 5% and 70% depending on the cell structure (Özel, 2003).

To increase power output, solar cells are connected in parallel or series, forming solar cell modules or photovoltaic modules. Semiconductor diodes within the PV element

convert sunlight directly into electrical energy through the internal photoelectric effect (Özel, 2003).

Semiconductors have valence and conduction bands separated by a forbidden energy gap. When a photon with sufficient energy is absorbed, it creates an electron-vacancy pair, separated by the electric field at the PN junction in solar cells. This separation creates useful power output. Solar cells also create electron-vacancy pairs internally but without an electric field, they recombine (Kutlu, 2002).

During production, an electrostatic zone is formed near the battery's front surface, freeing electrons when exposed to light. Other elements in the silicon crystal destabilize it, sweeping free electrons to the surface for collection (Kutlu, 2002).

With the solar industry's rapid growth, solar cells are crucial for converting solar energy into electricity, especially in energy-efficient building design. They're durable, low maintenance, and can be connected modularly to meet various power needs, even functioning as small power plants.

Working Principles of Solar Cells

Most solar cells, including those made of silicon, operate on the principle of converting sunlight into electricity. When sunlight hits the solar cell, it excites the electrons in the silicon atoms, causing them to become negatively charged. These excited electrons create an electrical current, which can be harnessed to power various devices. Silicon crystals in the solar cell contain additional elements that create an electrostatic zone near the surface, allowing the free electrons to move freely. As photons bombard the solar cell, electrons gain energy and flow through the electrostatic zone, generating electric current.

Structure of Solar Cells

A monocrystalline silicon solar cell is dark blue in color and weighs less than 10 grams. On the top surface, there are front contacts, usually copper, which collect the current. Underneath is a 150 nm thick, non-reflective coating layer to prevent reflection. The front surface is designed in pyramids and cones to capture light. The electric current is generated in two layers: the N-layer with phosphorus atoms added, and the P-layer with boron atoms added, separated by a P-N junction. The rear contact acts as a positive contact (Sick & Erge, 1996).

The structure formed by combining modules is called a panel, used to increase power. Output power can be 12, 24, 48 V or higher. Panels can be connected to the controller or battery group together or each panel can be connected individually for easier maintenance. All photovoltaic generators used in the system form a grid, which can be divided into sub-mesh groups for easier placement and output control.

System Elements of Solar Electricity

Photovoltaic Panel: It is a panel formed by the combination of small cells, where electric current is created for the effect of sun rays.

Solar Regulator: An automation system that ensures that the current generated in the panel is properly transferred to the battery system or direct use, and prevents damage to the panel and battery.

Battery Group: It is the equipment where the electricity generated by the panels is stored for later use.

Inverter: Direct current is produced in solar panels and this current is stored in the battery. In daily life, the current needs to be changed as alternating-current electronic devices are generally used. The device that performs this process is called an inverter.

Photovoltaic (PV) Panel

PV, photovoltaic, converts sunlight into electricity through solar cells, generating megawatts of electricity even with minimal light, without additional energy sources or pollution (Altın, 2005). Semiconductor elements move atoms in the last orbit, creating electric current by moving electrons. PV batteries, typically 0.2-0.4 mm thick, produce direct current and can be interconnected in series or parallel. Panels are dark-colored for better light absorption, with durable, power-free construction (Altın, 2005).

Solar energy tech is divided into heat and Direct Electricity (Solar Cells/PV Batteries/PV). Solar power plants generate electricity from sunlight, while photovoltaic systems use light energy to create voltage and electric current (Sick & Erge, 1996). These systems consist of a solar panel, charging unit, batteries, and inverter. The inverter converts stored DC into usable AC (Sick & Erge, 1996).

Figure 1.

Systems used for solar electricity generation and their classification (Anonymous, 2011d)



SPP (Solar Power Plants) consists of solar panels, charge regulators, batteries, inverters, and meter units. Direct current electrical energy is generated from solar panels. Batteries are charged with the direct current produced with the help of charge regulators. Batteries are connected to the inverter. Inverters convert direct current into alternating current. Thus, the electrical energy we can use is produced. If the power plant is connected to the grid, meters are used to determine the amount of energy transferred to the grid. If the power plant is not connected to the grid, there is no need for a meter (Roberts & Guariento, 2009).

Photovoltaic systems are installed with different system structures such as grid-connected and grid-free, with and without energy storage. For this reason, the components in the systems vary such as photovoltaic panels, inverters, battery groups, cables, charging units, and generators.

Materials Used in Photovoltaic Panels

They are generally categorized into 2 main groups: silicon and compound semiconductors. Photovoltaic cells can be divided into three categories;

First Generation: Crystalline silicon solar cells (c-Si and mc-Si)

Second Generation: Thin film solar cells (a-Si, CdTe, CIS or CIGS)

Third Generation: Solar cells based on nanotechnology (Tandem, Supertandem, Intermediate Band Solar Cells, etc.) (Anonymous, 2011s).

Photovoltaic Cells and Panels PV panels are a complete unit. A panel consists of a PV cell, top layer, capsule protecting the cell, back layer, fiberglass, and frame.

The elements that make up a typical photovoltaic system are;

- Photovoltaic modules,
- Power conditioners (inverters and other converters, control elements),
- Batteries,
- Power cables, measures taken to protect people and the system from electrical hazards (fuses, etc.)

Inverters

Inverters convert DC into AC by rhythmically changing the DC polarity to a desired AC frequency. They are crucial in grid-connected systems, transforming solar panel electricity into single-phase or three-phase AC to match the grid. These inverters, tailored for specific phases, work in tandem with solar panel and grid power, ensuring continuous supply during panel power drops. Solar energy can be harnessed in two ways: through heat using concentrators, or directly into electricity using solar cells (Figure 2).

Figure 2.

Basic equipment that makes up the solar panel system(Anonymous, 2011d)



Unit on Determining the Position of the Sun

Optical Sensors

“Sensors” are elements that detect a physical quantity such as light, temperature, humidity, pressure, magnetic field, and position and convert it into an electrical signal. Temperature and light are the most commonly measured physical parameters. All sensors are required to have a linear connection between their input and output. Such a linear characteristic simplifies both the analysis and the handling of the signal. The concept of EM (electromagnetic) radiation is used in industrial control for measuring, i.e. sensing, at visible or infrared wavelengths. The application techniques are called

“optics” (Messenger & Ventre, 2004).

PhotoResistors

Photoresistances, based on semiconductor conductivity change with light intensity, are also known as photoconductive sensors. When light is absorbed, electrons move from valence to conduction bands, decreasing resistance. Commonly using Cadmium Sulfide (CdS) and Cadmium Selenide (CdSe) in the visible spectrum, they have energy band gaps of 2.42 eV and 1.74 eV respectively (Messenger & Ventre, 2004).

Charge Control Devices

The main task of a charge controller is to ensure that the storage element operates under safe conditions (preventing overcharging and over-discharging of the battery). In PV systems, charging power and energy are limited and dependent on varying solar irradiance and load demand. There are known charging techniques such as constant current-constant voltage charging (cc/cv) or more complex charging techniques.

Monocrystalline and Polycrystalline Solar Panels

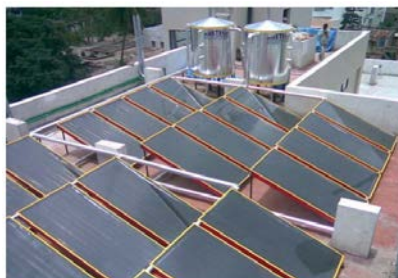
Since the 1950s, silicon solar cells have been efficient and stable. Recent technologies have boosted photovoltaic conversion efficiencies. Monocrystalline panels dominate the market with their high efficiency. However, their production cost is a drawback, leading to interest in other types. Lab efficiency reaches 24%, while commercial modules range from 15% to 18%. They're great for long-term investments with a payback period of 4-6 years and only a 7% efficiency loss over 20 years. These batteries are thin, dark blue, and weigh less than 10 grams, with front contacts made of copper.

Monocrystalline solar cells have front contacts made of copper on the top surface. They collect current and have a conical, pyramidal shape for optimal light capture. A non-reflective coating layer about 150 nm thick sits beneath the contacts to absorb most light. The lack of this coating affects efficiency negatively (Eruz, 2015).

Planar solar collectors are the most common solar thermal technology. These collectors, part of hot water systems, gather solar energy. Components include a tank for heated water, insulated pipes, pumps, and controllers (Figure 3).

Figure 3.

Solar collector hot water system (Anonymous, 2011d)



Solar collector systems are divided into two natural circulation and pumped. Both systems are also designed as open and closed systems. These are natural circulation systems, pumped systems, open systems, and closed systems.

Solar Wall System

Solarwall is an air heating system with solar energy. It allows the air to be heated without

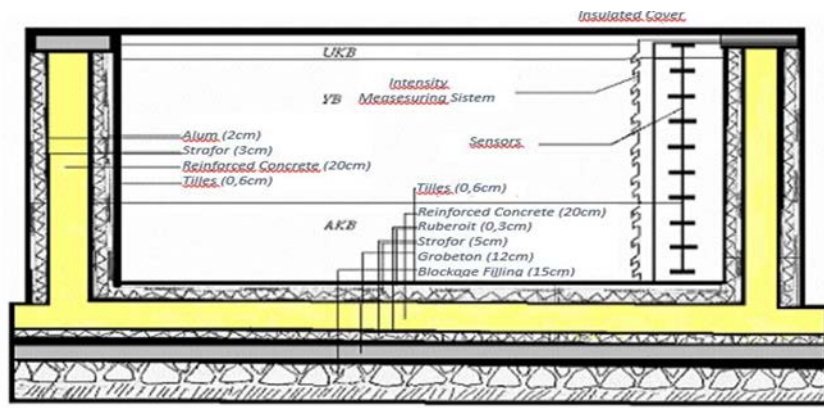
consuming energy by absorbing solar energy with perforated metal panels that can be installed on building facades. The air passing through these panels is fed to the ventilation system and used for pre-heating the building ventilation. The benefit of the solar wall application and its contribution to the annual fuel consumption were estimated with the analysis and the system was designed accordingly.

Solar Ponds

The pool floor, 5 to 6 meters deep, absorbs solar radiation, heating water to 90°C. Heat distribution is regulated by salt concentration, increasing from top to bottom. The lower part maintains a high temperature due to saturated salt concentration. Hot water can be used for heating or electricity generation in the Rankine cycle.

Figure 4.

Schematic representation of a solar pond (Anonymous, 2011d)



Solar Chimneys

In this method, electricity is generated by utilizing the air movement caused by the heat effect of the sun. The soil and air inside a structure covered with transparent material exposed to the sun will heat up more than the ambient temperature. Since the heated air will rise if the roof is sloped and the airflow is directed to a very high chimney, an air flow-wind at a speed of 15 m/sec will occur inside the chimney. A horizontal wind turbine placed at the entrance of the chimney will convert this wind into electricity (Figure 5). The power of a plant can be between 30-100 MW. There is no application except for a few experimental systems.

Figure 5.

Solar chimney (Anonymous, 2011d)

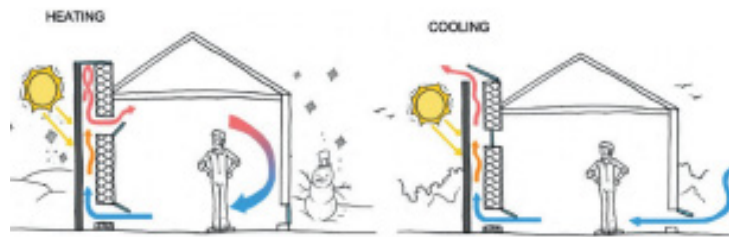


Solar chimneys and solar energy can be used for ventilation and cooling purposes.

These chimneys are designed on the south side of the building and do not exceed the roof height. The outer surface of the chimney is covered with transparent glass and the inner surface is covered with dark metal material to absorb sunlight. The air inside the chimney rises under the influence of the Sun and exits the chimney. When the wind speed is low, the expulsion process is accelerated by a rotating wind cone placed on top of the chimney. The cold air entering the lower point of the chimney creates circulation and natural ventilation is provided. The heating and cooling principle of solar chimneys is explained in Figure 6.

Figure 6.

Heating-cooling principle of solar chimneys (Anonymous, 2011d)



Stirling Engines

Stirling engines are external combustion engines and heat must be supplied to the heat sink from a heat source. To use Stirling engines in systems where electricity is generated from solar energy, the Sun's rays must be concentrated on the heat sink of the Stirling engine.

Materials Used in Wind Turbine Blades

Wind energy, a renewable and clean energy source, originates from the Sun, leading to airflow between pressure differentials (MoENR, 2019). Wind energy derives from solar radiation, accounting for 2% of solar energy transformed into wind energy, driven by temperature and pressure differentials (MoENR, 2019). Wind results from the displacement of air masses due to heating, with warmer air rising, forming low pressure, and cooler air descending, forming high pressure (Öztürk, 2013).

Wind turbines convert wind energy into mechanical energy, utilizing lightweight and durable materials like carbon fiber and fiberglass for their blades (Statista, 2021). Wind variability is influenced by geographical features like hills, valleys, and bodies of water (Statista, 2021). Valleys can channel and accelerate wind flow, while ridges increase wind speed by compressing air masses (Yang, Lin & Zhang, 2020). Land-sea temperature differentials generate sea or lake breezes affecting wind patterns (Yang, Lin & Zhang, 2020).

Electricity production from wind generators is directly linked to wind speed, with Betz's theorem stating energy yield varies with the cube of wind speed (İlkılıç, 2016).

Wind Turbines

Wind turbines convert wind kinetic energy into electricity or motion. They're categorized as grid-connected or battery-powered, storing energy or delivering it directly. Components include a generator, gearbox, tower, electronics, and blades, with a 20-year lifespan and 120,000-hour operational capacity.

Horizontal axis turbines have blades perpendicular to wind direction, with rotation parallel to it. Fewer blades increase rotor speed, with an average efficiency of 45%. Ideally, they're positioned 20-30m high and 10m above obstacles. The blade tip speed ratio (λ) is the ratio of wind speed to the rotor tip speed.

If;

$\lambda = 1/5$ Multi-blade rotor,

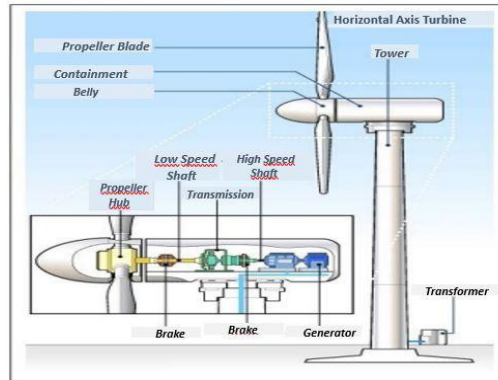
$\lambda = 6/8$ Three-bladed rotor,

$\lambda = 9/15$ Two-bladed rotor,

$\lambda > 15$ Single-blade rotors used.

Figure 7.

Wind turbine (Url-2)

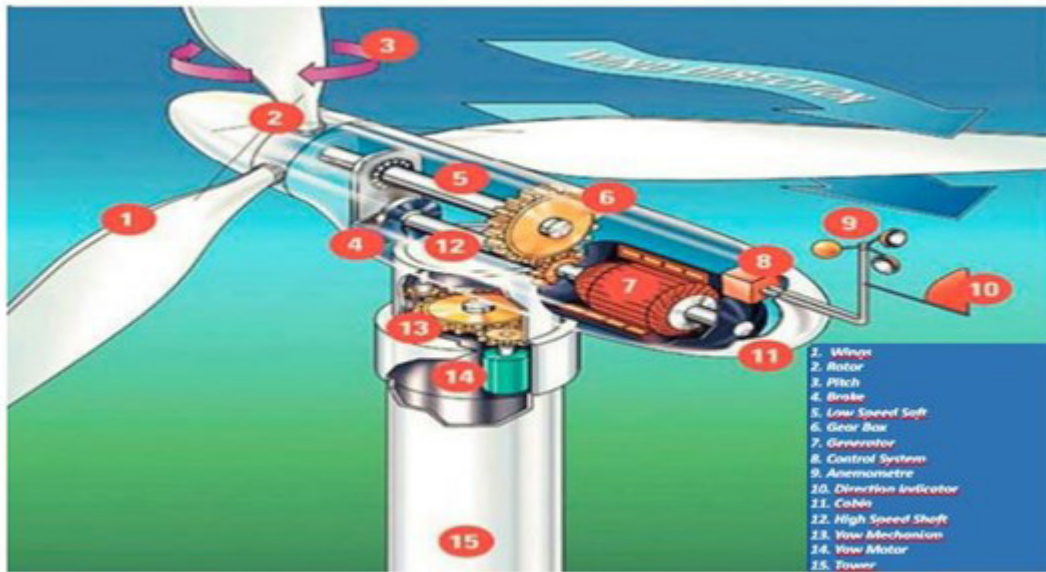


A wind turbine usually consists of a tower, a generator, speed converters (gearboxes), electrical-electronic elements, and a propeller. The electrical energy generated from the generator is stored in batteries or delivered directly to the receivers (Elibüyük & Üçgöl, 2014). The lifetime of wind turbines varies according to turbine quality and local climate characteristics. The average lifetime is 20-25 years (General Directorate of Electrical Power Resources Survey and Development Administration, 2016). Wind turbines are classified according to their axes of rotation, speed, power, number of blades, wind effect, gear characteristics, and mounting positions.

Basic Elements of Wind Turbines

Turbines may consist of different elements according to their design and construction. However, each turbine has similar components that perform the same function, albeit with different characteristics. The system parts of a turbine are shown in Figure 8. In general, it can be analyzed under parts: tower, blades, and in-cabin equipment (Demir, 2007).

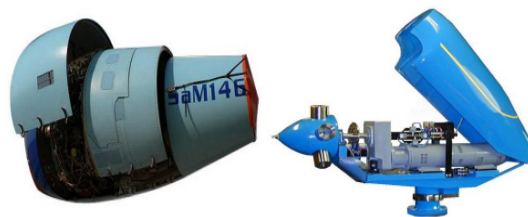
Figure 8.
Wind Turbine System Parts (Mevka, World Key Statistics 2011)



Nacelle (Cabin)

The Nacelle is a type of cabin that contains all mechanical parts except the wing. It is made of a stainless steel sheet. According to its capacity, it has enough free space for a technician to make repairs inside. It needs an internal frame to carry and evenly distribute the weight of the components it carries. Power components include a generator to convert mechanical energy into electrical energy, a rotating bearing (yaw drive) on the tower to turn the turbine into the wind, and electronic systems for process control and monitoring.

Figure 9.
Nacelle for Large and Small Capacity Turbines (Mevka, World Key Statistics 2011)

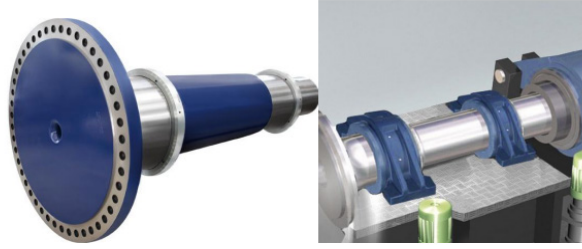


Low-Speed and High-Speed Shaft

The rotary motion coming from the turbine blades is transferred to the gearbox and then to the generator. Low-speed and high-speed shafts perform this transmission task. The low-speed shaft is the shaft to which the blades are connected and rotates at 30-60 revolutions per minute. The high-speed shaft is the shaft that drives the generator and is located between the gearbox and the generator. The high-speed shaft is smaller in diameter and higher in operating speed.

Figure 10.

Low-speed and High-Speed shafts (Mevka, World Key Statistics 2011)



Gearbox

Gearboxes mount low- and high-speed shafts for generator electricity generation, rotating at 1,200-1,550 rpm. Some models use belt or chain pulleys. They increase rotational load from low to high shafts, from 20-60 rpm to 1200-3000 rpm, converting high torque to low. Rotation speed adjusts for optimal electricity generation. Wind turbine gearboxes have fixed tongue ratios, three types: planetary, helical, and worm.

Planetary gearboxes are common in wind turbines, offering flexible design and high efficiency. They're compact, reducing gearbox weight, a significant part of turbine weight (Deghanian & Maerefat, 2021).

Coupling

Coupling is the element that transfers the rotational motion and therefore the moment generated in a power source to another system (machine, pump, reducer, conveyor, etc.). In wind turbines, the coupling provides the connection between the gearbox and the generator. Flexible rubber materials can also be used as couplings. This ensures the matching between the gearbox and the generator during the first movement. The use of flexible rubber-like materials prevents possible damage (Repp, 2004).

Figure 11.

Coupling(Mevka, World Key Statistics 2011)



Mechanical Brake

Extreme wind speeds can sometimes be very dangerous for turbines. High speeds of the blades can damage both the blades and the internal parts. For this reason, turbines are equipped with 2 fail-safe systems. The steel disc brake is a disc-type brake placed on the high-speed shaft between the gearbox and the generator. On some turbines, the brakes can also be connected to the low-speed shaft. This disc brake is provided using two fail-safe hydraulic brake calipers.

Generator

Wind turbine generators convert mechanical energy into electrical energy. The generators used in wind power plants can be alternating current or direct current generators. Even if the electric current obtained here is of insufficient quality alternating current or direct current, it can be made suitable for the grid with various power electronics devices. Direct current generators are currently only used in small wind power plants to store energy in batteries. This is because they require frequent maintenance and are more expensive than alternating current generators.

Figure 12.

Wind Turbine Generators (Mevka, World Key Statistics 2011)



Large turbine (over 1000kW) generators typically produce 3-phase voltage at 690 V, which is then stepped up to 10-30 kV using transformers before being fed into the distribution or interconnected network. Small power generators utilize small blades, while large blades are only efficient in strong winds, where they can generate power close to the generator's capacity, minimizing waste. However, large generators struggle to operate at low wind speeds.

Cooling Unit

Like many machinery systems, medium and large-capacity wind turbines require a cooling system. The cooling unit is used to remove the heat generated by the gearbox, generator, and hydraulic brake systems during operation. It is vital for turbine efficiency and safety. Generator and gearbox efficiencies decrease with increasing temperature. There are two types used by manufacturers: air and liquid-cooled. It consists of units such as a fan, coolant, and engine filter.

Figure 13.

Gearbox and Generator Cooling Units (Mevka, World Key Statistics 2011)



Slewing Bearing (Yaw-Shift System)

The rotating bearing is the system that ensures that the wind is constantly directed towards the rotor in turbines. Thus, it ensures that maximum power is obtained from the wind. Servomotors are used to rotate the nacelle against the wind together with

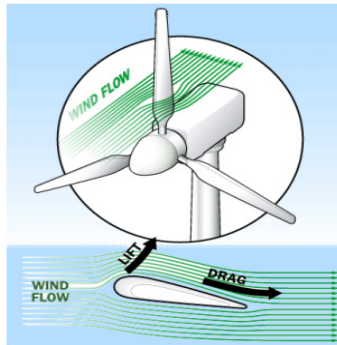
the propeller. In large-capacity wind turbines, 4 motors are generally used. The yaw mechanism is operated by an electronic control unit that senses the wind direction. The yaw system, which is also the element that connects the nacelle to the tower, reduces the stress on the turbine blades and nacelle by making them ninety degrees perpendicular to the wind according to the signal from the control mechanism at high speeds. Thus, it protects the system.

Blades

Blades are the most important part of turbines in terms of both cost and manufacturing technology. This is why this section is emphasized in more detail. Most turbines are designed with two or three blades. The wind hitting the blades lifts and rotates the blades. The blade structure varies depending on whether the turbine receives wind from the front or the back. In this section, 3-bladed wind turbine blades, which are the type of almost all commercially produced wind turbines, are evaluated. The forces acting on the wind turbine according to the blade diameter are shown in Figure 14.

Figure 14.

Forces acting on the wind turbine blade (Mevka, World Key Statistics 2011)



Hub

In a wind turbine, the part to which the blades are connected is called the hub. The turbine hub transmits the power received from the blades to the generator through the transmission shaft. As seen in Figure 15, it can be in different geometric shapes such as plate, pipe, and sphere.

Figure 15.

Wind Turbine Hub Examples (Mevka, World Key Statistics 2011)



Tower

They are tubular or lattice-shaped poles, made of steel, which allow the turbine body to

be placed on the top plane. It is an advantage for the tower to be high as wind speeds increase as it rises above the ground. Towers can be tubular and lattice-shaped. Rope-supported mast-type towers are generally used in small turbine applications. Tubular towers have an internal staircase to reach the turbine casing. The foundation on which the turbine tower sits is reinforced concrete construction and a 120 circular foundation is laid to carry the 40-50 m tower. With the help of large cranes, the towers are placed on the construction foundation (Figure 16).

Figure 16.

Tubular and Lattice Tower (Mevka, World Key Statistics 2011)



Charge Regulator

Charge regulators work as a control mechanism in wind, solar, or hybrid systems. They are intelligent electronic circuits that perform and manage the energy distribution process according to the system status and automatically select the most ideal operating mode. The main functions of the control units can be summarized as charging and discharging the batteries under the most appropriate conditions, temperature settings and suitability, lightning control, different protection/insurance systems, sending different alarms to the center, recording all data from wind turbines and solar panels or sending them to the desired location via modem.

Accumulators

A wind turbine only generates electricity when there is wind. However, energy may be needed at other times when there is no generation, or more electricity may be needed than is generated instantaneously. This is why most small-capacity wind turbines are used in combination with batteries that can store electrical energy. Electrochemical batteries are best suited for energy storage in hybrid systems. The energy in batteries is converted from chemical energy to electrical energy during discharge. The opposite happens during charging. Batteries can consist of one or more cells according to the output voltage they will provide and the current capacity they will carry. Generally, the terminal voltage of a one-cell battery varies between 1.2 and 2 volts.

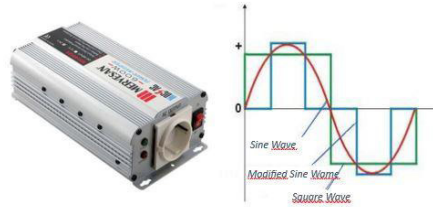
Inverter

Inverters are DC-AC converters that convert direct current to alternating current. The task of an inverter is to convert a direct voltage at its input into a symmetrical alternating voltage at its output with the desired amplitude and frequency. The voltage and frequency values obtained at the output can be constant or variable. By changing the DC voltage at the input and keeping the inverter gain constant, a variable output voltage can be obtained. Inverters have different names according to the waveform of the current they convert; 'square waveform, modified sine wave, pure sine wave. While the inverter is

converting, it also provides an increase in electrical voltage. Wind turbines produce at 12-24 volt values. This value reaches 220 Volt household voltage with the help of inverters. Inverters are also divided into various groups in terms of the power they provide. It is possible to find inverters from 600 W capacity up to 8000W in the market.

Figure 17.

Basic Inverter Structure and Wave Types (Mevka, World Key Statistics 2011)



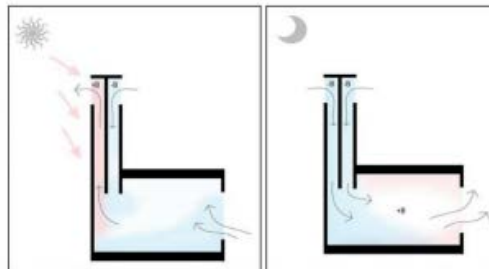
Wind Towers

Wind towers use solar and wind energy together. Wind towers provide natural ventilation of the interior space and provide thermal comfort with the necessary humidity regulations.

Wind towers take cool air indoors and discharge the heated and rising indoor air. During the day, cool air entering through the north opening of the wind tower ventilates the interior, and heated air is exhausted from the south side. At night, the wind tower provides indoor air circulation (Figure 18).

Figure 18.

Day and night operation principles of wind towers (Erkinay, 2012)



Basic Materials Used in Wind Turbine Blade Production

Polymer Matrix: The main tasks performed by the polymer matrix in the composite structure are as follows;

- To ensure that the fiber structure stays together,
- Protecting the fiber structure against external factors,
- To ensure that the stress on the structure is transferred homogeneously between the fibers.

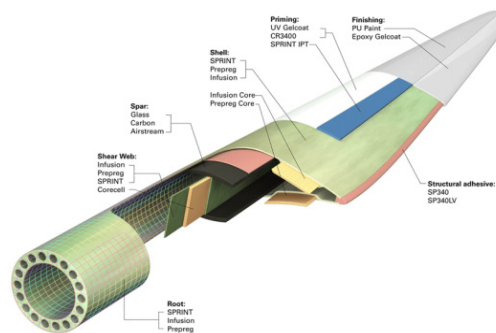
For this purpose, epoxy resin is generally used in wing construction. Since the volumetric shrinkage (between 1-3%) and dimensional stability values of epoxy resins are better than other thermoset resins, they are preferred in the production of large-scale wind turbine blades together with amine (strength enhancing) based hardener systems.

Fiber Reinforcement Materials: They are the basic load-carrying elements in the composite structure. The effectiveness of the fibers used in a fiber-reinforced polymeric

composite structure depends on the type of fiber used, the length of the fiber structure, the fiber volume, and the fiber orientation. Glass fiber, carbon fiber, and aramid fiber are used as reinforcement materials in polymeric composite applications. The choice of reinforcement material is determined by the intended use, production method, and cost of the end product. In the production of wind turbine blades, versatile fabrics woven with glass fibers made of epoxy glass are mostly preferred. The mechanical properties of a fabric are greatly affected by the way it is woven. For this reason, in the design of wind turbine blades, the force distribution on the aerodynamic structure is first calculated and then fabrics containing the appropriate weaving are selected (Sevim, 2009). The image of the sandwich structures in the blade section is given in Figure 19.

Figure 19.

Image of Sandwich Structures in Wing Section (Sevim, 2009)



Intermediate (Core) Materials: Intermediate materials are filling materials used in composite products with sandwich structures. Especially increasing the flexural strength has led to an increase in the use of composite products. Due to the use of intermediate materials, it is possible to increase the flexural strength by 3.5 times and rigidity by 7 times with a weight increase of approximately 3%. In wind turbine blades, PVC (Polyvinyl chloride), PET (Polyethylene terephthalate) foam, and balsa wood sheets with a variety of thickness options (between 5-50 mm) are widely used as intermediate materials (Immerkjaer, 2003).

Materials Used in Bioenergy Production

Bioenergy production involves converting organic materials like biomass or biogas into energy using biodegradable materials like agricultural waste, wood residues, and fertilizers, with specially designed tanks and pipes for methane storage.

Biomass energy comes from living or non-living biological substances, including animal, plant, and urban wastes, used to generate energy by releasing hydrogen and carbon energy. Resources vary based on climate, vegetation, and geography, generally having low density and calorific value, negatively affecting fuel quality (Bayraç & Özarslan, 2018).

Biomass resources encompass wood, agricultural crops and by-products, municipal solid waste, animal waste, food processing waste, aquatic plants, and algae, offering a renewable energy alternative to fossil fuels (Çukurçayır & Sağır, 2008).

Materials in Hydroelectric Energy Applications

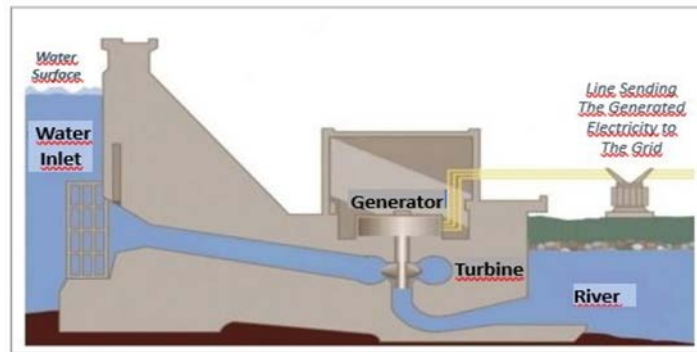
Hydroelectric power plants (HPPs) are crucial for the national economy and environmental protection, being the most eco-friendly among power plants (Görez & Alkan, 2005). They harness hydraulic energy, one of the oldest sources, from water, necessitating their location near water sources. Advancements in electricity transmission technology have boosted the utilization of hydraulic energy. These plants convert flowing water's energy into electricity through turbines, driven by the water's speed or height drop (MoNE, 2012).

HPPs, vital for energy production, determine energy from water flow and waterfall rates, offering benefits like emission reduction, local construction, job creation, and rural economic empowerment (MoENR, 2019). They commonly employ sturdy materials like concrete and steel, with special alloys for turbine durability due to water pressure variations.

Water from reservoirs formed along water courses feeds turbines through tunnels, converting into kinetic energy, which, when the turbine rotates, generates mechanical energy further converted into electricity by generators (Öztürk, 2013). See Figure 20 for an HPP's operational illustration.

Figure 20.

The Operational System of Hydroelectric Power Plant (Url-2)

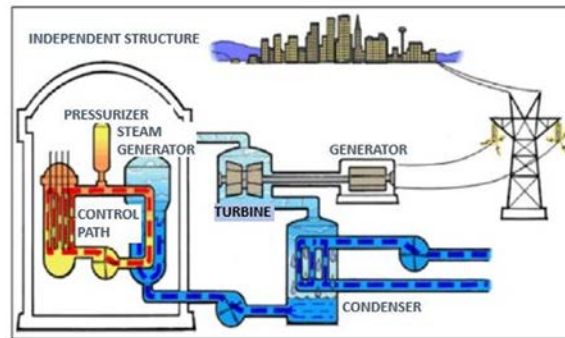


Hydraulic energy is formed indirectly from solar radiation. It is an energy source that constantly renews itself. It is the most important renewable source in world electricity generation. In developing countries such as India and China, hydroelectric power plants constitute the majority of energy production from renewable sources.

Materials in Geothermal Energy Applications

Geothermal energy is defined as hot water, steam, and gases containing chemicals formed by the heat accumulated in various depths of the earth's crust. It is a renewable, sustainable, reliable, environmentally friendly primary energy source. The heat energy in the depths of the Earth's crust is obtained by bringing the charged rainwater to the surface of the Earth by drilling and making it useful to people. There are many geothermal resources in Türkiye, so heating, cooling, and electricity generation in buildings are provided by these resources (Kayataş, 2016).

Figure 21.
Advanced geothermal systems (Url-4)



Geothermal Heat Pumps

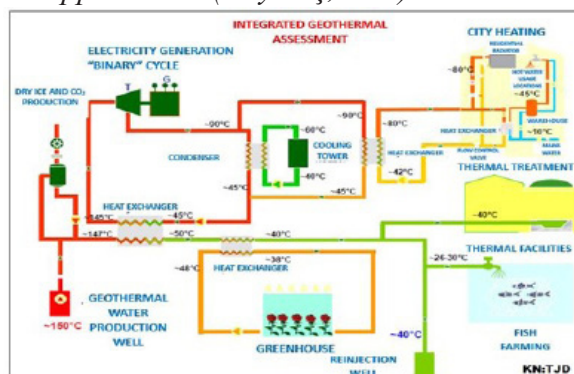
Geothermal energy can be defined as hot water and vapor formed by the heat accumulated in various depths of the Earth’s crust, which has a continuous temperature of more than 200°C and may contain more dissolved minerals, various salts, and gases than the normal ground and surface waters around it. This hot fluid reaches the earth’s surface through fractures and forms thermal resources, or it is extracted by drilling and converted into economic use.

Ground Source Heat Pumps

A heat pump is an electrically powered system that transfers heat energy between mediums, named for its ability to move heat. Ground source heat pumps utilize the Earth’s constant temperature underground, serving as a heat source in winter and a heat well in summer. They’re favored for their dual heating and cooling functions, energy efficiency, and integration with advanced technology (Develioğlu, 2012).

Closed Systems employ heat exchangers, circuits, and buried polyethylene pipes to circulate liquid continuously under pressure. Geothermal systems are dynamic, open, and variable, situated in the Earth’s upper crust where heat flux is high. They rely on permeable zones for groundwater movement, trapping geothermal fluids to form convection cells and store heat.

Figure 22.
Integrated geothermal applications (Kayataş,2016)



Turbine

Turbines are where thermal energy is converted into mechanical energy. In general, high-speed, multistage, radial, or mixed-flow units provide high turbine efficiency. The organic fluid is released from the evaporator as superheated steam hits the turbine blades

and mechanical work is obtained (ICMM, 2023).

Recirculation Pumps

Recirculation pumps used in the extraction of resources from geothermal energy have very large dimensions. Large casting workshops are needed to produce these parts. In addition, due to the temperature of the geothermal fluid and the mineralized substances in it, cavitation and temperature-resistant materials must be used and processed.

Steam - Water Separators

Separators are systems that separate the water-steam mixture coming out of the source and adjust it to a constant steam pressure. They ensure continuity in steam turbines by providing constant pressure balance.

Filters

As geothermal resources are known to come out of the ground, there are many foreign particles (soil, sand, etc.) in the steam water mixture during production from the source. They are used to prevent these particles from causing blockages on the turbine blades and system line.

Hydrogen Energy

Hydrogen, abundant in compounds like water, serves as a promising energy carrier, derived from primary energy sources through various conversion processes. While it can be directly employed in internal combustion engines and flameless combustion, recent focus has shifted towards fuel cell technology, offering clean and efficient energy conversion without traditional steam boilers or turbines. Despite its novelty, global hydrogen production already reaches 500 billion cubic meters annually, primarily utilized in the chemical and petrochemical sectors. Its carbon-free nature distinguishes it from fossil fuels, promising environmental benefits, and its versatility spans from heating to electricity generation, facilitated by its easy transportation over long distances without significant losses.

Conclusion

Renewable energy applications can be greatly enhanced by selecting appropriate materials, which significantly impact their efficiency, durability, and sustainability. The examples cited herein underscore the importance and diversity of materials crucial for renewable energy technologies. Material selection plays a critical role in ensuring the efficiency, durability, and longevity of renewable energy systems, supporting the advancement and proliferation of technologies such as solar, wind, bioenergy, and hydropower. The array of materials discussed in this chapter underscores their significance in the renewable energy sector. As more environmentally friendly, efficient, and cost-effective materials are developed, renewable energy applications will likely become more widespread, laying the groundwork for a sustainable energy future.

Key Findings:

- The choice of materials profoundly influences the effectiveness, resilience, and sustainability of renewable energy applications.
- Specialized materials tailored to different energy sources, including solar, wind, bioenergy, and hydropower, are crucial for advancing these technologies.

- Material efficiency is pivotal in combating global warming and climate change, making it imperative for countries to prioritize.
- Türkiye has seen a significant rise in energy and material consumption, leading to heightened greenhouse gas emissions, and necessitating urgent steps toward energy and material efficiency.
- While Türkiye has made strides in enhancing resource efficiency, material efficiency remains relatively underexplored, warranting focused attention and action.
- Türkiye's commitment to achieving net-zero emissions by 2053, coupled with its late ratification of the Paris Agreement, underscores the urgency for accelerated energy and material efficiency efforts both domestically and internationally.

References

- Akıncı, Z.D. & Kök, M. (2007). Renewable Energy and Public Health. *Journal of Istanbul University Vocational School of Health Services*, 5(1), pp:43-55.
- Alahmad, H., Taşkesen, E., & Bilen, E. N. (2023). Overview of Space-Based Solar Energy. *Researcher*, 03(02), 53–75. <https://dergipark.org.tr/tr/pub/researcher/issue/79270/1332802>
- Altın, M.(2005). Research on The Architectural Use of Photovoltaic (PV) Components in Turkey From the View Point of Building Shape, 37. pp, İzmir.
- Anonymous, 2011d, <http://www.eie.gov.tr/turkce/YEK/gunes/guneskollektor.html>.
- Anonymous, 2011s, www.gunessistemleri.com.
- Bayraç, H. & Özarslan, B. (2018). An Empirical Analysis of the Relationship between Biomass Energy and Economic Growth: The Case of Turkey". *Yalova Journal of Social Sciences*, 8/17 (October 2018): 1-17.
- Çukurçayır & Sağır, (2008). Energy Problem, Environment and Alternative Energy Sources.
- Dehghanian, P. & Maerefat, M. (2021). Energy efficiency in buildings: A review of the latest technologies and future prospects. *Energy Reports*, 7, 1756-1774.
- Demir, F. N. (2007). Wind Turbines. Dokuz Eylül University, Faculty of Engineering, Department of Mechanical Engineering, Izmir, 6-18.
- Develioğlu, M. (2012). Technological Development of Ground Source Heat Pumps and Applicability in Turkey. Master Thesis, Hacettepe University, Ankara.
- Ministry of Energy and Natural Resources (2019). National Energy Balance Table. Access address: 01.06.2024.
- Erkinay, P. U. (2012). A Review on the Use of Wind Energy from Renewable Energy Sources in Buildings in Turkey. Master's Thesis, Çukurova University, Adana.
- Eruz,Ü.(2015).EfficiencyComparison of Polycrystalline,Monocrystalline and Thin Film Panels from Solar Panel Types in Karabük Conditions. Karabuk University Institute of Science and Technology, Master's Thesis, Karabuk.
- Görez, T. & Alkan, A. (2005). Turkey's Renewable Energy Resources and Hydroelectric Energy Potential. Yeksem 2005 III. Renewable Energy Resources Symposium, Mersin, pp.123-127.

- Gülay, A. N. (2008). The Future of Turkey in terms of Renewable Energy Resources and Comparison with the European Union. (Master's Thesis), Dokuz Eylül University, Institute of Science and Technology, Izmir.
- https://enerjiapi.enerji.gov.tr/Media/Dizin/EIGM/Raporlar/Ulusal_Enerji_Denge_Tablolari/2019%20Y%C4%B1%20Genel%20Enerji%20Denge%20Tablosu.xlsx.
- ICMM, (2023). https://twitter.com/ICMM_com/status/1679471595352465408 (Date of Access: 15. 07. 2023).
- Immerkjaer, N. (2003). Optimising of Reliability Large Wind Turbine Blades. LM Wind Power.
- International Energy Agency. (2015). Energy outlook report. Access address: <https://www.iea.org/reports/world-energy-outlook-2015>
- İlkılıç, Z. (2016). Development of Wind Energy and Wind Energy Systems in Turkey. Batman University Life Sciences Journal, 6/2/2: 1-13.
- Kayataş, G. (2016). Experimental Investigation of Alternative Fluid Utilization in Geothermal Energy Supported Organic Rankine Cycle. Karabuk University, Institute of Science and Technology, Department of Energy Systems Engineering, Master's Thesis, Karabuk.
- Kaynak, T. & Kaya, F. (2018). The impact of sustainable architectural design on energy efficiency. Journal of Energy and Power Engineering, 12 (2), 98-107.
- Kutlu, S. (2002). Electric Power Generation with Solar Farm and an Application Analysis in SDU Campus Area. Süleyman Demirel University Institute of Science and Technology, Department of Mechanical Education, Isparta.
- MEB, (2012). Renewable Energy Sources and Importance.
- Messenger, R.A. & Ventre, J. (2004). Photovoltaic Systems Engineering 2nd ed. CRC Pres, New York, 21-25, 31-35, 415-431.
- Mevka, World Key Statistics (2011). Renewable Energy Resources in Konya. Material Producibility Research, Konya Chamber of Industry Reports.
- Özel, S. (2003). Photovoltaic Solar Energy and Its Utilization in Lighting Systems. <http://elektrikci.hypermart.net/pv/pv.htm>
- Öztürk, H. (2013). Renewable energy sources. Istanbul: Birsen Publishing House, pp. 44-176.
- REPP, (2004). Wind Energy Development Location of Wind Manufacturing.
- Roberts, S. & Guariento, N. (2009). Building integrated photovoltaics: a handbook. Berlin: Birkhäuser, s.45.
- Sayın, S. (2006). The Importance of the Use of Renewable Energy in the Building Sector of Our Country and the Possibilities of Utilizing Solar Energy in Buildings. Selçuk University, Master's Thesis, Konya.
- Sevim, C. (2009). Characterization of Alternative Polymeric Structures for Wind Turbine Blades. Ege University, Institute of Science and Technology, Department of Energy Technology, PhD Thesis.
- Sick, F. & Erge, T. (1996). Photovoltaics in Buildings: A Design Handbook for Architects

and Engineers. Paris, XYZ Publishing.

- Statista. (2021). Distribution of carbon dioxide emissions produced by the transportation sector worldwide in 2021, by subsector.” (<https://www.statista.com/statistics/1185535/transport-carbon-dioxide-emissions-breakdown/> Access Date: 18.05.2023).
- Toprak, M. E. & Küçük, Y. (2018). Sustainable energy sources and energy performance of buildings. *Journal of Energy Technologies and Policy*, 6 (1), 56-63.
- UN-HABITAT. Urban Energy. <https://unhabitat.org/topic/urban-energy> (Access Date: 16.07.2023).
- Url-2, <http://www.thesisat.org/ruzgar-enerjisi-ve-ruzgarin-gucu.html> Access Date:: 27.05.2023
- Yang, Y., Lin, B., & Zhang, W. (2020). A review of life cycle assessment of building energy efficiency technologies. *Renewable and Sustainable Energy Reviews*, 119, 109584.
- Yıldırım, H.B. & Teke, A. (2013). Solar energy and usage areas. *New Energy Magazine*, Issue:35.

About The Authors

Edip TAŞKESEN, PhD, graduated from Fırat University, Faculty of Arts and Sciences, Department of Chemistry in 2005. In 2008, he completed his master’s degree at Harran University, Institute of Science and Technology, Department of Chemistry with the thesis titled “Synthesis, Characterization and Use of Polyacrylonitrile Macrophoto Initiator in Block Copolymer Preparation by Redox Method”. In 2015, he was accepted to the PhD program at Karabuk University, Department of Energy Systems Engineering. In 2021, he completed his PhD with the thesis titled “Experimental and Numerical Investigation of the Flow and Heat Transfer Characteristics of Ferro Nanofluid Flowing in a Circular Cross-Section Channel Under the Effect of Constant Magnetic Field”. As of 2021, he continues to work as a Dr. Faculty Member in the Department of Energy Systems Engineering at Şırnak University. Edip Taşkesen’s articles have been published in various academic journals.

E-mail: ediptaskesen@gmail.com, **ORCID:** 0000-0002-3052-9883

Göknur KAYATAŞ ONGUN, PhD, completed her undergraduate education in Geological Engineering and Environmental Engineering, and her master’s and doctoral degrees in Energy Systems Engineering. She is currently working as a lecturer at Bolu Abant İzzet Baysal University, Vocational School of Technical Sciences, Department of Electricity and Energy. She has worked on renewable energy sources, geothermal energy, environment and drying.

E-mail: goknur.kayatasongun@ibu.edu.tr, **ORCID:** 0000-0003-1811-1975

Similarity Index

The similarity index obtained from the plagiarism software for this book chapter is 10%.

CHAPTER 3***Nickel-Titanium (NiTi) Alloys in Dentistry******Ahmet Burçin BATIBAY****Necmettin Erbakan University, Türkiye****Muhammed İhsan ÖZGÜN****Necmettin Erbakan University, Türkiye***To Cite This Chapter:**

Batibay, A.B. & Ozgun, M. I. (2024). Nickel-Titanium (NiTi) Alloys in Dentistry. In H. Gokmese, S. Bulbul, & Y. Uzun (Eds.), *Current Studies in Materials Science and Engineering* (pp. 53-63). ISRES Publishing.

Introduction

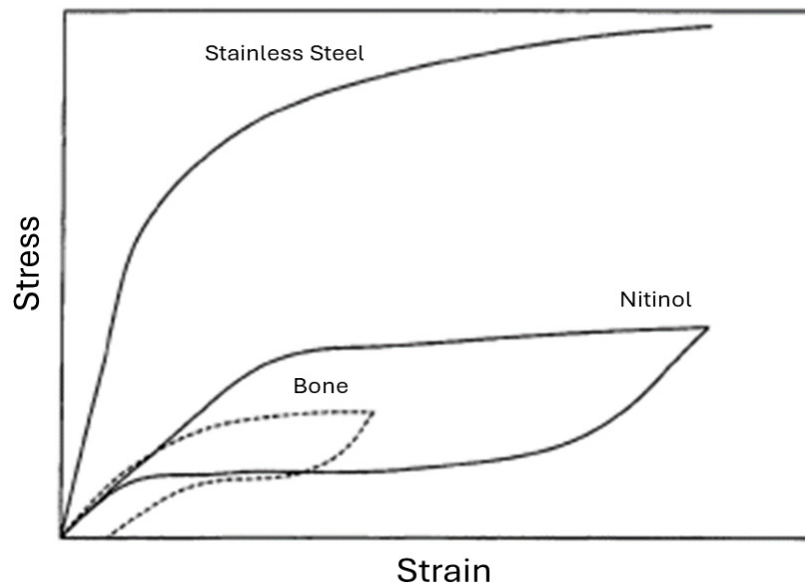
NiTi alloys are well known for their exceptional shape memory effect (SME), superelasticity, robust strength, good ductility, and corrosion resistance, rendering them as highly adaptable materials suitable for a wide range of applications in different sectors (Lu et al., 2017). NiTi alloys demonstrate a reduced Young's modulus and increased toughness in contrast to conventional biomedical metallic materials, offering benefits in minimizing stress shielding effects and averting brittle failure during implantation (Liu et al., 2013). The remarkable characteristics of NiTi alloys have led to their extensive utilization in various applications like dental implants, stents, robotics, and actuators (Novák et al., 2017).

Given that Fig. 1 NiTi alloys have biomimetic properties with the human body. For this reason, it is very common to use it as an implant in bone tissue in the human body. As NiTi alloys exhibit mechanical behavior close to bone tissue in terms of hardness, deformation, and wear are at the minimum level in their use as an implant (Krishna et al., 2007).

The austenite-martensite phase transformation (Fig. 2) that occurs in NiTi alloys at low temperatures offers significant advantages for the use of this alloy. The martensite phase is soft and easily deformable. The austenite phase, however, is hard. With heating, the martensite phase can easily transform into the austenite phase at a temperature of 100 °C. Thus, the metal, which is deformed and shaped at low temperatures, can be converted into a hard phase by heating, and a strength increase can be achieved (Thompson, 2000).

Figure 1

Schematic stress-strain curve of stainless steel, Ni-Ti alloys and human bone (Krishna et al., 2007)

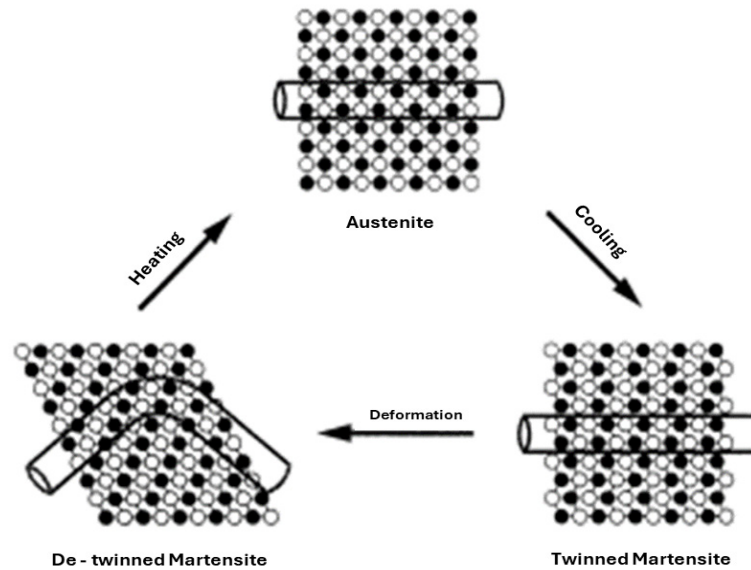


The characteristics of NiTi alloys are notably shaped by the techniques used in their processing. For instance, procedures like cold drawing and low-temperature annealing can influence the sensing attributes of NiTi alloys, leading to alterations in peak shifts and phase transitions (Li, 2023). The implementation of electropulsing during rolling has been identified as a method to enhance the malleability of NiTi alloys, which are commonly susceptible to rapid hardening and complex processing (Zhu & Tang, 2017). Additionally, the use of composite coatings such as hydroxyapatite-titanium-MWCNTs through electrophoretic deposition has been proven to enhance both the corrosion resistance and cellular response of NiTi alloys (Maleki-Ghaleh & Khalil-Allafi, 2019).

Surface coatings are crucial in altering the characteristics of NiTi alloys. Research has indicated that TiN coatings can improve the biocompatibility of untreated NiTi alloys, suggesting possibilities for enhanced biomedical uses (Lifeng et al., 2011). Likewise, TiO₂ coatings generated via microarc oxidation have exhibited improved anti-corrosion features and bonding durability for NiTi alloys (H. R. Wang et al., 2012). Furthermore, the use of Al₂O₃ nanopowders has proven effective in boosting the wear resistance of NiTi shape memory alloys, emphasizing the importance of surface adjustments in optimizing alloy functionality (Şahin & Öksüz, 2014).

Figure 2

Austenitic-Martensitic phase transformation of Ni-Ti alloys (Thompson, 2000)



In summary, NiTi alloys are outstanding materials with distinct characteristics that render them extremely sought-after for a diverse range of uses. The manipulation of processing methods, coatings, and surface alterations is essential in customizing the attributes of these alloys to fulfill precise application needs, especially within the realms of biomedical and tribological applications.

NiTi Alloys in Dentistry

NiTi alloys have made a substantial contribution to the dental field as a result of their distinctive characteristics and uses. These alloys are widely employed in endodontic tools, like rotary files, owing to their exceptional superelasticity and low elastic modulus, which improve the process of root canal preparation (Pereira et al., 2012). The application of thermomechanical treatment to NiTi instruments has notably enhanced their resistance to cyclic fatigue and transformation temperatures, thereby increasing their durability for clinical applications (Zupanc et al., 2018).

NiTi alloys offer enhanced strength and a reduced modulus of elasticity compared to stainless steel alloys, rendering them well-suited for a range of dental uses (Thompson, 2000). Extensive research has confirmed the biocompatibility of NiTi shape memory alloys, which exhibit superior corrosion resistance in comparison to traditional materials like stainless steel (Es-Souni et al., 2005). The utilization of NiTi rotary instruments has significantly improved the precision and effectiveness of root canal procedures in recent years (Kuzekanani, 2018). Moreover, the shape memory capability of NiTi alloys has been recognized in dental practices, underscoring their adaptability and efficiency (Guillory & Vall, 2022).

In summary, NiTi alloys provide a blend of mechanical characteristics, biocompatibility, and corrosion resistance, establishing them as essential materials for a variety of dental treatments and tools, thereby playing a significant role in advancing the field of dentistry.

NiTi Alloys in Orthodontics

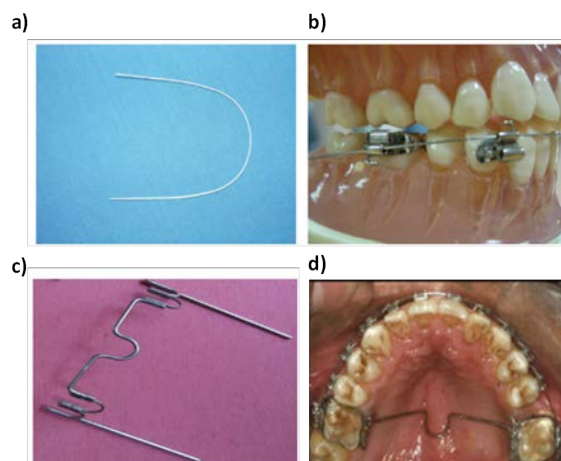
NiTi alloys play a crucial role in orthodontics owing to their distinct characteristics and uses. These alloys are renowned for their shape memory and pseudoelasticity, which are highly beneficial in orthodontic procedures (Primožic et al., 2022). Nevertheless, challenges have been identified with NiTi alloys in orthodontics, such as concerns regarding the loss of superelasticity and the potential for sudden fractures (Elkhal Letaief et al., 2018).

Research on the biocompatibility of NiTi shape memory alloys has shown improved resistance to corrosion when compared to conventional materials such as stainless steel (Oh et al., 2006). The incorporation of NiTi alloys in orthodontic devices has notably improved the standard of orthodontic care (Garrec et al., 2005). The utilization of the shape memory properties of NiTi alloys has been successfully applied in orthodontic practices, highlighting their versatility and effectiveness (Belasic et al., 2021).

In orthodontic applications, NiTi alloys have started to be used in braces and straighteners, palate expander apparatus as seen Fig. 3. In these applications, besides being biocompatible and biomimetic, its memory feature with phase transformation at low temperatures is used. In these orthodontic applications, the material, which is deformed in the martensitic phase at room temperature, turns into an austenite phase with body temperature after being placed in the body and applies a stress to the area where it is located. In the use of stainless steel material, the process time is prolonged since the stretching process is performed externally mechanically (Auricchio et al., 2021; Petrini & Migliavacca, 2011; T W Duerig et al., 1990).

Figure 3

Orthodontic uses of NiTi alloys a) NiTi orthodontic wire b) orthodontic wire utilization c) palatal expander (Petrini & Migliavacca, 2011) d) palatal expander utilization (Katti et al., 2013)



In conclusion, NiTi alloys are essential in orthodontics, providing a distinctive array of mechanical characteristics, biocompatibility, and resistance to corrosion that significantly influence the orthodontic field.

NiTi Alloys in Endodontic

NiTi alloys have a significant impact on endodontics, playing a crucial role in various procedures within this dental specialty. Their shape memory and superelasticity properties make them highly valuable in endodontic applications. However, challenges like potential superelasticity loss and the risk of sudden fractures have been noted with NiTi alloys in endodontics. Research on the biocompatibility of NiTi shape memory alloys has shown superior corrosion resistance compared to conventional materials like stainless steel. The incorporation of NiTi alloys in endodontic instruments has substantially enhanced the quality of endodontic care. Additionally, the effective utilization of the shape memory effect of NiTi alloys in endodontic practices underscores their versatility and efficacy in improving patient outcomes (Sezgin & Gündoğar, 2020).

NiTi alloy dental files are used in endodontics for dental root canal treatment. As can be seen in Fig.4, it can bend by the shape of the canal and can show super elasticity enough to take its old shape again. Although NiTi-based alloys have a low elastic modulus, they have a hardness in the range of 300 - 350 HV, which can abrade in the canal folds of the tooth. The hardness of the dentin is 70 HV and this value decreases to 30-35 HV in the vicinity of the tooth canal (Dilibal, 2005).

Figure 4

Use of Ni-Ti alloy channel files (Orozco-Ocampo et al., 2022)



NiTi Alloys in Maxillofacial Surgery

The NiTi alloy, well-known for its shape memory characteristics and compatibility with living tissues, has found extensive use across diverse medical domains, with a notable presence in maxillofacial surgery. NiTi-based osteosynthesis materials have been integrated into minimally invasive surgical techniques within the realms of oral and maxillofacial surgery (Naujokat et al., 2022). The unique attributes of NiTi shape memory alloys have enabled their utilization not only in orthodontics and aerospace engineering but also prominently in medical specialties like maxillofacial surgery (Treadway et al., 2015).

In mandibular surgery, NiTi alloy is used to restore the maxilla with the help of distractors. To open the maxilla in the desired direction, the bone tissue is cut and bridged, and the bone tissue is allowed to complete itself. After the completion of the bone in the cut area, NiTi alloy distractors are removed. Since NiTi alloy distractors exhibit superelastic behavior, the force on them is adjusted according to the growth rate and removed. Figure 5 shows the use of the distractor and its condition in vitro (Lekston

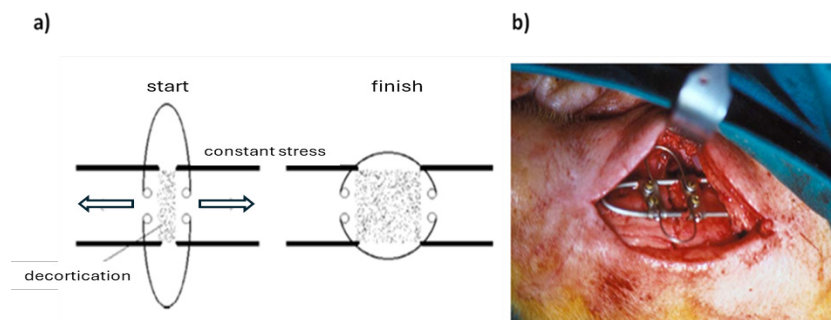
et al., 2004).

The utilization of NiTi alloys in maxillofacial surgery represents a significant aspect of dentistry, extending to orthodontic wire uses. Apart from their application in maxillofacial surgery, NiTi alloys find diverse uses in various areas of dentistry as well (Acar, 2018).

NiTi alloys have been effectively utilized in maxillofacial surgery due to their reduced stiffness, shape memory capabilities, and effectiveness in managing diverse medical conditions (Korkmaz & Sağlam, 2022). Porous NiTi shape memory alloys have been explored as a promising alternative in orthopedic surgeries, including those in maxillofacial procedures, showcasing improved biocompatibility and favorable treatment outcomes (Li et al., 2011). Furthermore, NiTi staples have been devised for internal osteosynthesis in maxillofacial surgery, operating as shape memory staples triggered by the patient's body temperature (Lekston et al., 2012). The adaptability of NiTi alloy has resulted in its widespread application in various medical fields, encompassing orthodontics, cardiovascular surgery, orthopedic interventions, and reconstructive procedures like maxillofacial surgeries (Stambolić et al., 2016).

Figure 5

a) Distractor sketch b) In vitro usage on maxilla bone (Lekston et al., 2004)



In cases of significant bone defects in maxillofacial surgeries, reconstructive methodologies incorporating NiTi implants, such as endoprotheses, have been utilized in conjunction with procedures like bone fragment reimplantation (Medvedev et al., 2016). The Department of Maxillofacial Surgery at University Hospital Rijeka has been prominently engaged in the care of tissues and the execution of surgical interventions associated with maxillofacial surgeries (Avirović et al., 2016). Moreover, research findings have presented information on the reattachment of the mandible head in instances of traumatic injuries, emphasizing the importance of such interventions within the domain of maxillofacial surgery (Medvedev & Adygezalov, 2017).

In summary, the distinctive characteristics and compatibility with living tissues of NiTi alloys have made them indispensable in different aspects of maxillofacial surgery, including osteosynthesis materials, staples, and implants employed in reconstructive surgeries.

Conclusions

Nickel-titanium (NiTi) alloys are extensively employed in dentistry because of their outstanding mechanical characteristics, compatibility with biological systems, and corrosion resistance. These alloys have greatly enhanced a variety of dental processes, notably in the preparation, shaping, and instrumentation of root canals, resulting in

improved clinical results and patient welfare in the dental field. The mechanical attributes of NiTi tools play a crucial role in the effectiveness of root canal preparation, particularly in dealing with curved or flattened canals (Gavini et al., 2018).

Manufacturers have adopted sophisticated manufacturing techniques to improve the mechanical characteristics of NiTi alloys, enhancing their resilience to breakage and boosting their flexibility (Zupanc et al., 2018). The utilization of controlled memory wires such as M-Wire or R-phase wire in the production of NiTi instruments signifies a novel era of NiTi alloys with enhanced flexibility and resistance to fatigue (Shen et al., 2013). The exceptional biocompatibility of NiTi alloys renders them highly advantageous for diverse dental uses, such as bone implants and orthodontic archwires (Bansiddhi et al., 2008; Huang, 2005). NiTi alloys find extensive application in dentistry, orthopedics, and vascular surgery owing to their remarkable biocompatibility and resistance to corrosion (Wang et al., 2023; Widantha et al., 2021). Furthermore, NiTi shape memory alloys have gained significance across various sectors, including dentistry, due to their distinctive attributes like shape memory, pseudoelasticity, and corrosion resistance (Maletta et al., 2014). The incorporation of NiTi alloys in dentistry has transformed the process of root canal preparation, with the introduction of NiTi instruments bringing about substantial changes in the field of endodontics. The utilization of NiTi alloys in endodontics has spurred progress in canal-shaping methodologies, enhancing the outcomes of treatments (Arias & Peters, 2022). Grasping the attributes of NiTi files is crucial for dentists conducting root canal procedures, underscoring the critical significance of expertise in effectively employing these tools (Kwak et al., 2021).

References

- Acar, E. (2018). Şekil hafızalı alaşımların biyomedikal uygulamaları. *European Journal of Science and Technology*. <https://doi.org/10.31590/ejosat.429048>
- Arias, A., & Peters, O. A. (2022). Present status and future directions: Canal shaping. *International Endodontic Journal*, 55(S3), 637–655. <https://doi.org/10.1111/iej.13698>
- Auricchio, F., Boatti, E., Conti, M., & Marconi, S. (2021). SMA biomedical applications. In *Shape Memory Alloy Engineering* (pp. 627–658). Elsevier. <https://doi.org/10.1016/B978-0-12-819264-1.00019-4>
- Avirović, M., Matušan-Ilijaš, K., Juretić, M., Cerović, R., Jonjić, N., & Lučin, K. (2016). Prognostic value of invasive tumor front grading in squamous cell carcinoma of oral cavity. *Medicina Fluminensis*, 52(3), 408–414. https://doi.org/10.21860/52;3_408
- Bansiddhi, A., Sargeant, T. D., Stupp, S. I., & Dunand, D. C. (2008). Porous NiTi for bone implants: A review. *Acta Biomaterialia*, 4(4), 773–782. <https://doi.org/10.1016/j.actbio.2008.02.009>
- Belasic, T. Z., Pejova, B., Curkovic, H. O., Kamenar, E., Cetenovic, B., & Spalj, S. (2021). Influence of intraoral application of antiseptics and fluorides during orthodontic treatment on corrosion and mechanical characteristics of nickel-titanium alloy in orthodontic appliances. *The Angle Orthodontist*, 91(4), 528–537. <https://doi.org/10.2319/052620-480.1>
- Dilibal, S. (2005). Nikel-titanyum şekil bellekli alaşım üretimi ve şekil bellek eğitimi. *Yıldız Technical University, Graduate School of Science and Engineering, PhD Thesis, Istanbul*.

- Elkhal Letaief, W., Fathallah, A., Hassine, T., & Gamaoun, F. (2018). Finite element analysis of hydrogen effects on superelastic NiTi shape memory alloys: Orthodontic application. *Journal of Intelligent Material Systems and Structures*, 29(16), 3188–3198. <https://doi.org/10.1177/1045389X18754356>
- Es-Souni, M., Es-Souni, M., & Fischer-Brandies, H. (2005). Assessing the biocompatibility of NiTi shape memory alloys used for medical applications. *Analytical and Bioanalytical Chemistry*, 381(3), 557–567. <https://doi.org/10.1007/s00216-004-2888-3>
- Garrec, P., Tavernier, B., & Jordan, L. (2005). Evolution of flexural rigidity according to the cross-sectional dimension of a superelastic nickel titanium orthodontic wire. *European Journal of Orthodontics*, 27(4), 402–407. <https://doi.org/10.1093/ejo/cji014>
- Gavini, G., Santos, M. dos, Caldeira, C. L., Machado, M. E. de L., Freire, L. G., Iglecias, E. F., Peters, O. A., & Candeiro, G. T. de M. (2018). Nickel–titanium instruments in endodontics: a concise review of the state of the art. *Brazilian Oral Research*, 32(suppl 1). <https://doi.org/10.1590/1807-3107bor-2018.vol32.0067>
- Guillory, M., & Vall, P. (2022). Past, Present, and Future Trends of Nickel Titanium Rotary Instrumentation. *Journal of Veterinary Dentistry*, 39(3), 257–268. <https://doi.org/10.1177/08987564221098566>
- Huang, H. (2005). Surface characterizations and corrosion resistance of nickel–titanium orthodontic archwires in artificial saliva of various degrees of acidity. *Journal of Biomedical Materials Research Part A*, 74A(4), 629–639. <https://doi.org/10.1002/jbm.a.30340>
- Katti, C. G., Katti, G., Kallur, R., & Ghali, S. R. (2013). Magical NiTi expander. *BMJ Case Reports*, bcr2013009140. <https://doi.org/10.1136/bcr-2013-009140>
- Korkmaz, İ. H., & Sağlam, M. (2022). Determination of the Effect of TiN Coating on Self-Fitting Properties of Dental Implants Made of NiTi Alloy. *ACS Biomaterials Science & Engineering*, 8(10), 4586–4595. <https://doi.org/10.1021/acsbiomaterials.2c00550>
- Krishna, B. V., Bose, S., & Bandyopadhyay, A. (2007). Laser Processing of Net-Shape NiTi Shape Memory Alloy. *Metallurgical and Materials Transactions A*, 38(5), 1096–1103. <https://doi.org/10.1007/s11661-007-9127-4>
- Kuzekanani, M. (2018). Nickel–Titanium rotary instruments: Development of the single-file systems. *Journal of International Society of Preventive and Community Dentistry*, 8(5), 386. https://doi.org/10.4103/jispcd.JISPCD_225_18
- Kwak, S. W., Shen, Y., Liu, H., Wang, Z., Kim, H.-C., & Haapasalo, M. (2021). Heat Treatment and Surface Treatment of Nickel–Titanium Endodontic Instruments. *Frontiers in Dental Medicine*, 2. <https://doi.org/10.3389/fdmed.2021.769977>
- Lekston, Z., Drugacz, J., & Morawiec, H. (2004). Application of superelastic NiTi wires for mandibular distraction. *Materials Science and Engineering: A*, 378(1–2), 537–541. <https://doi.org/10.1016/j.msea.2003.12.061>
- Lekston, Z., Stróż, D., & Jędrusik-Pawłowska, M. (2012). Preparation and Characterization of Nitinol Bone Staples for Cranio-Maxillofacial Surgery. *Journal of Materials Engineering and Performance*, 21(12), 2650–2656. <https://doi.org/10.1007/s11665-012-0372-3>
- Li, H., Yuan, B., Gao, Y., Chung, C. Y., & Zhu, M. (2011). Remarkable biocompatibility enhancement of porous NiTi alloys by a new surface modification approach: *In-*

- situ* nitriding and *in vitro* and *in vivo* evaluation. *Journal of Biomedical Materials Research Part A*, 99A(4), 544–553. <https://doi.org/10.1002/jbm.a.33198>
- Li, Y., Lin, J., Xiao, Y., & Min, J. (2023). Effects of cold-drawing and low-temperature annealing on the sensing properties of NiTi alloys. *Material Research Proceeding*, 429–436. <https://doi.org/10.21741/9781644902479-47>
- Lifeng, Z., Yan, H., Dayun, Y., Xiaoying, L., Tingfei, X., Deyuan, Z., ... & Jinfeng, Y. (2011). The underlying biological mechanisms of biocompatibility differences between bare and TiN-coated NiTi alloys. *Biomedical materials*, 6(2), 025012.
- Liu, F., Qiu, W., Wang, H. R., Song, Y., & Wang, F. P. (2013). Biomimetic deposition of apatite coatings on biomedical NiTi alloy coated with amorphous titanium oxide by microarc oxidation. *Materials Science and Technology*, 29(6), 749–753. <https://doi.org/10.1179/1743284712Y.0000000196>
- Lu, X., Li, G., Liu, L., Zhu, X., & Tu, S.-T. (2017). Effect of ambient temperature on compressibility and recovery of NiTi shape memory alloys as static seals. *Advances in Mechanical Engineering*, 9(2), 168781401769228. <https://doi.org/10.1177/1687814017692287>
- Maleki-Ghaleh, H., & Khalil-Allafi, J. (2019). Effect of hydroxyapatite-titanium-MWCNTs composite coating fabricated by electrophoretic deposition on corrosion and cellular behavior of NiTi alloy. *Materials and Corrosion*, 70(11), 2128–2138. <https://doi.org/10.1002/maco.201910940>
- Maletta, C., Sgambitterra, E., Furgiuele, F., Casati, R., & Tuissi, A. (2014). Fatigue properties of a pseudoelastic NiTi alloy: Strain ratcheting and hysteresis under cyclic tensile loading. *International Journal of Fatigue*, 66, 78–85. <https://doi.org/10.1016/j.ijfatigue.2014.03.011>
- Medvedev, Yu. A., & Adygezalov, O. N. Ogly. (2017). Replantation of the head of the mandible in traumatic injuries. *Russian Journal of Dentistry*, 21(1), 33–36. [https://doi.org/10.18821/1728-28022017;21\(1\):33-36](https://doi.org/10.18821/1728-28022017;21(1):33-36)
- Medvedev, Yu. A., Petruk, P. S., Shamanaeva, L. S., Volkova, V. A., & Davidov, A. R. (2016). The use of Foley catheter in reconstructive procedures involving the middle third of the facial skeleton. *Stomatologiya*, 95(3), 31. <https://doi.org/10.17116/stomat201695331-37>
- Naujokat, H., Gökkaya, A. I., Açil, Y., Loger, K., Klüter, T., Fuchs, S., & Wiltfang, J. (2022). In vivo biocompatibility evaluation of 3D-printed nickel–titanium fabricated by selective laser melting. *Journal of Materials Science: Materials in Medicine*, 33(2), 13. <https://doi.org/10.1007/s10856-022-06641-y>
- Novák, P., Moravec, H., Vojtech, V., Knaislová, A., Školáková, A., Kubatík, T. F., & Kopeček, J. (2017). Powder-metallurgy preparation of NiTi shape-memory alloy using mechanical alloying and spark-plasma sintering. *Materiali in Tehnologije*, 51(1), 141–144. <https://doi.org/10.17222/mit.2016.011>
- Oh, K., Joo, U., Park, G., Hwang, C., & Kim, K. (2006). Effect of silver addition on the properties of nickel–titanium alloys for dental application. *Journal of Biomedical Materials Research Part B: Applied Biomaterials*, 76B(2), 306–314. <https://doi.org/10.1002/jbm.b.30369>
- Orozco-Ocampo, Y. M., Álvarez-Vargas, C. A., Jiménez-García, F. N., Escobar-Rincón, D., & Jaramillo-Gil, P. X. (2022). Fatigue failure of NiTi endodontic files: scoping review. *Revista Facultad de Odontología Universidad de Antioquia*, 34(1), 14–30.

- Pereira, E. S. J., Peixoto, I. F. C., Viana, A. C. D., Oliveira, I. I., Gonzalez, B. M., Buono, V. T. L., & Bahia, M. G. A. (2012). Physical and mechanical properties of a thermomechanically treated NiTi wire used in the manufacture of rotary endodontic instruments. *International Endodontic Journal*, 45(5), 469–474. <https://doi.org/10.1111/j.1365-2591.2011.01998.x>
- Petrini, L., & Migliavacca, F. (2011). Biomedical Applications of Shape Memory Alloys. *Journal of Metallurgy*, 2011, 1–15. <https://doi.org/10.1155/2011/501483>
- Primožic, J., Hren, M., Mezeg, U., & Legat, A. (2022). Tribocorrosion Susceptibility and Mechanical Characteristics of As-Received and Long-Term In-Vivo Aged Nickel-Titanium and Stainless-Steel Archwires. *Materials*, 15(4), 1427. <https://doi.org/10.3390/ma15041427>
- Sezgin, G. P., & Gündoğar, M. (2020). Comparison of Torsional Resistance of Reciproc®, WaveOne® and One Shape® Nickel-Titanium Instruments. *Turkiye Klinikleri Journal of Dental Sciences*, 26(1), 26–30. <https://doi.org/10.5336/dentalsci.2019-66077>
- Shen, Y., Zhou, H., Zheng, Y., Peng, B., & Haapasalo, M. (2013). Current Challenges and Concepts of the Thermomechanical Treatment of Nickel-Titanium Instruments. *Journal of Endodontics*, 39(2), 163–172. <https://doi.org/10.1016/j.joen.2012.11.005>
- Stambolič, A., Anžel, I., Lojen, G., Kocijan, A., Jenko, M., & Rudolf, R. (2016). Continuous vertical casting of a NiTi alloy. *Materiali in Tehnologije*, 50(6), 981–988. <https://doi.org/10.17222/mit.2016.111>
- Şahin, Y., & Öksüz, K. E. (2014). Effects of Al₂O₃ Nanopowders on the Wear Behavior of NiTi Shape Memory Alloys. *JOM*, 66, 61–65.
- T W Duerig, K N Melton, D Stöckel, & C M Wayman. (1990). *Engineering Aspects of Shape Memory Alloys*. Elsevier. <https://doi.org/10.1016/C2013-0-04566-5>
- Thompson, S. A. (2000). An overview of nickel–titanium alloys used in dentistry. *International Endodontic Journal*, 33(4), 297–310. <https://doi.org/10.1046/j.1365-2591.2000.00339.x>
- Treadway, J., Abolmaali, A., Lu, F., & Aswath, P. (2015). Tensile and fatigue behavior of superelastic shape memory rods. *Materials & Design*, 86, 105–113. <https://doi.org/10.1016/j.matdes.2015.07.024>
- Wang, H. R., Liu, F., Song, Y., & Wang, F. P. (2012). Structure and properties of TiO₂ coatings on biomedical NiTi alloy by microarc oxidation. *Materials Science and Technology*, 28(8), 1000–1005.
- Wang, X., Xie, D., Wei, L., You, D., Hou, M., & Leng, Y. (2023). DFT investigation of the dissolution trends of NiTi alloys with the B₂ and B19' phases during the initial oxidation stage. *Physical Chemistry Chemical Physics*, 25(29), 19804–19814. <https://doi.org/10.1039/D3CP01024D>
- Widantha, K. W., Basuki, E. A., Martides, E., & Prawara, B. (2021). Effect of hydroxyapatite/alumina composite coatings using HVOF on immersion behavior of NiTi alloys. *Journal of Biomaterials Applications*, 36(3), 375–384. <https://doi.org/10.1177/08853282211022531>
- Zhu, R., & Tang, G. (2017). The improved plasticity of NiTi alloy via electropulsing in rolling. *Materials Science and Technology*, 33(5), 546–551. <https://doi.org/10.1080/02670836.2016.1231745>

Zupanc, J., Vahdat-Pajouh, N., & Schäfer, E. (2018). New thermomechanically treated NiTi alloys – a review. *International Endodontic Journal*, 51(10), 1088–1103. <https://doi.org/10.1111/iej.12924>

About The Authors

Ahmet Burçin BATIBAY, PhD, is a Doctor at Necmettin Erbakan University, Department of Metallurgical and Materials Engineering in Konya, Türkiye. He holds a PhD in Materials Science and Engineering from Afyon Kocatepe University. His main areas of interest are powder metallurgy, biomaterials and materials characterizations.

E-mail: abbatibay@erbakan.edu.tr, **ORCID:** 0000-0002-2606-5115.

Muhammed İhsan ÖZGÜN, is a research assistant of Metallurgy and Materials Engineering at Necmettin Erbakan University in Konya, Türkiye. He holds a PhD in Mechanical Engineering at Necmettin Erbakan University. His main areas of interest are material characterization, metal casting, recycling of metals.

E-mail: miozgun@erbakan.edu.tr, **ORCID:** 0000-0003-0048-3439.

Similarity Index

The similarity index obtained from the plagiarism software for this book chapter is 11%.

CHAPTER 4

Antibacterial Properties of Titanium Alloys

Ahmet Burçin BATIBAY

Necmettin Erbakan University, Türkiye

Fatih ERCİ

Necmettin Erbakan University, Türkiye

To Cite This Chapter:

Batibay, A.B. & Erci, F. (2024). Antibacterial Properties of Titanium Alloys. In H. Gokmese, S. Bulbul, & Y. Uzun (Eds.), *Current Studies in Materials Science and Engineering* (pp. 64-75). ISRES Publishing.

Introduction

Titanium is a multifaceted substance recognized for its outstanding characteristics that render it immensely beneficial across a range of sectors. Its widespread application in medical settings is due to its compatibility with living tissues and its ability to withstand corrosion, establishing it as the preferred material for use within bones (Goutam et al., 2014). The characteristics of titanium, including its elevated specific strength, reduced density, resistance to corrosion, lack of magnetism, ease of welding, and ability to withstand impacts, have positioned it as a favored option for marine pipelines transporting seawater (Liu et al., 2023). Titanium and its alloys are preferred in the dental and orthopedic sectors due to their biocompatibility, corrosion resistance, and exceptional mechanical characteristics (Prasad et al., 2015).

In metallurgy, titanium alloys have been engineered to possess Young's moduli similar to that of cortical bone, improving their biological and mechanical attributes, thus rendering them appropriate for use in biomedical applications (Niinomi et al., 2016). Moreover, incorporating titanium into steel has demonstrated enhancements in its particular tensile strength and ductility, surpassing even the most lightweight and robust metallic materials on record (Kim et al., 2015). The addition of titanium to aluminum matrix composite materials has been discovered to substantially enhance their hardness, rendering them appropriate for a multitude of applications (Mikheev & Kalashnikov, 2023).

The distinctive characteristics of titanium, including its corrosion resistance, exceptional mechanical robustness, and lightweight nature, have resulted in its heightened utilization across diverse sectors, encompassing aerospace components, chemical facilities, and nuclear applications (Setoyama et al., 2004). The spontaneous creation of a protective titanium dioxide film on titanium contributes to its exceptional corrosion resistance and minimal toxicity in contrast to other biometals (Sarraf et al., 2022).

Furthermore, by modifying its thickness, the mechanical characteristics of titanium mesh can be enhanced, rendering it appropriate for clinical applications in treating bone defects (Bai et al., 2019).

In summary, the remarkable attributes of titanium, such as its biocompatibility, resistance to corrosion, mechanical robustness, and lightweight nature, have solidified its status as a crucial material across a broad spectrum of uses, spanning from biomedical to industrial domains.

Properties of Titanium Alloys

Titanium alloys have attracted considerable interest in multiple sectors owing to their outstanding attributes and broad range of applications. Extensive research and development efforts have been dedicated to improving the mechanical and biological features of these alloys, rendering them appropriate for diverse applications, including those in the biomedical field (Rosa et al., 2019). Integrating titanium into diverse materials has been demonstrated to improve their structural and mechanical characteristics, including hardness and strength, consequently broadening their effectiveness across a variety of applications (Khrustalyov et al., 2019). In the aerospace sector, titanium alloys are greatly appreciated for their ability to resist corrosion and their remarkable strength-to-weight ratio, establishing them as the preferred option for essential components (Ben Boubaker et al., 2020).

The incorporation of titanium and its alloys has significantly transformed sectors like aviation, aerospace, sports gear, and healthcare, where their exceptional mechanical robustness and compatibility with living tissues have been pivotal in the progress of technology and medical practices (Bhattacharya et al., 2017). The exploration of cost-effective titanium alloys has involved the addition of elements such as iron to stabilize the alloy compositions, especially in powder metallurgy applications (Yu et al., 2017). Since their introduction in the 1950s, titanium and its alloys have evolved into essential materials in the aerospace sector, showcasing swift acceptance and extensive utilization (Li et al., 2004).

Titanium alloys have been utilized in the medical domain as well, with the incorporation of nickel-titanium alloys improving the functionality of endodontic tools, streamlining processes, and enhancing patient outcomes (Sung et al., 2010). The distinctive characteristics of titanium alloys, including their resistance to corrosion, robust mechanical properties, and lightweight nature, have established them as vital materials in a variety of sectors, encompassing biomedical and industrial fields (Polishetty & Littlefair, 2020). Despite the benefits they offer, integrating titanium alloys into composite materials may present difficulties in terms of machinability, emphasizing the need for additional research and development in this domain (Xu et al., 2021).

In summary, the incorporation of titanium alloys has had a substantial influence on various sectors, providing a blend of exceptional characteristics that have resulted in their extensive acceptance in crucial uses, spanning from aerospace components to medical implants.

The Use of Ti Alloys as Biomaterials

Metals and their alloys, such as titanium, cobalt, and stainless steel, are widely used in clinical settings to create hip and knee prostheses, bone plates, screws, and other medical tools because of their mechanical qualities, resistance to corrosion, and good

biocompatibility. Up to 2.5 million dollars has been quoted as the price of medical equipment composed of metals and alloys (Zhang et al., 2021).

Titanium (Ti) is widely used in orthopedic and dental implant materials, such as artificial joint prostheses, fracture fixation plates, nails, rods, screws, wires, and dental and cardiovascular implants. In orthopedic implants, such as hip and knee replacements, titanium's high strength and corrosion resistance make it an ideal choice, especially for load-bearing implants. Dental implants benefit from titanium's biocompatibility and strength, providing a sturdy foundation for replacement teeth. These materials are made possible by Ti's excellent biocompatibility, superior corrosion resistance, lightweight nature, high tensile strength, and compatibility with magnetic resonance imaging (Kaur & Singh, 2019). Despite being intended to be biocompatible, biomedical materials have the potential to elicit immune responses because they are not native to the body. Therefore, improving biocompatibility is necessary to stop rejection reactions and localized inflammation. The development of biomaterials focuses on methods to lessen the reaction of foreign bodies and enhance the integration of the material with the host tissues (Karakullukcu et al., 2023).

Commercially pure Ti (grade 4) and Ti6Al4V alloys are currently the most widely used alloys. However, low fatigue strength, poor wear resistance, and comparatively high cost are the main disadvantages of Ti alloys. Due to the high elastic modulus, major clinical concerns include stress shielding and implant loosening, which can result in Implant-Associated Infections (IAI) and problems with stress protection. Furthermore, Ti6Al4V alloys containing trace amounts of aluminum and vanadium ions may result in reduced cell adaptation and potential harm to human health. Research on the design of new Ti alloys is still in progress, with particular attention paid to Ti-Mo, Ti-Nb-Ta-Zr, and Ti-Al-Sr-Zr alloys (Jiao et al., 2021). Two important factors in the development of biocompatible Ti-alloys are low elastic modulus and biotoxicity. Alloys based on Ti, Al, and V have a low modulus, but they also contain harmful elements like Mn and V. Because of their mechanical compatibility and biocompatibility, β -type Ti-alloys containing non-toxic elements like Nb, Ta, Zr, Mo, and Hf have been effectively employed in bone implants as a solution (Verma, 2020). The biocompatibility and biocorrosion properties of the Ti alloys are unaffected by the addition of Ag/Cu (Liu & Zhang, 2015). Even so, the antibacterial titanium alloys about 110 GPa have a high modulus. This means that creating a new Ti alloy with low Young's modulus and strong antibacterial properties is essential. Incorporating Ag/Cu elements into β -type or nearly β -type Ti alloys could be one of the possible measurements to realize these alloys (Cai et al., 2021).

Antibacterial Properties

Antibacterial characteristics play a crucial role in diverse uses, prompting the advancement of materials with built-in antimicrobial features. The integration of various antibacterial substances into dental restoration materials has enabled the formulation of compounds with antimicrobial attributes (Enan et al., 2021). Research has explored the use of cerium and cerium oxide-based materials for antibacterial purposes, offering valuable insights into potential mechanisms and strategies for antibacterial effects (Qi et al., 2020). Metal nanoparticles or their oxides have been intentionally selected to impart distinctive capabilities, including antibacterial and photocatalytic attributes, in polymeric membranes incorporating nanometals (Rabajczyk et al., 2021).

In the healthcare sector, the addition of graphene oxide and chitosan to acrylic bone cement has shown promise in enhancing osseointegration and providing antibacterial

properties (Zapata et al., 2020). Films possessing antibacterial characteristics are produced by directly incorporating biologically active compounds into the polymer matrix, as exemplified by the impact of birch tar on altering the physical, chemical, and biocidal attributes of polylactide-based films (Richert et al., 2021). Phenolic acids have been introduced into cationic waterborne polyurethanes to boost the antibacterial efficacy against a range of bacteria (Zhang et al., 2020).

Hydrogel formulations for wound care have been enhanced by incorporating antibacterial agents such as chitosan and silver ions to reduce bacterial infections. The antibacterial capability of hydrogels has been achieved through the introduction of silver nanowires (Zou et al., 2022). Tea tree essential oil and poly(ethylene glycol) were introduced into polylactide-based films to enhance their antibacterial and physicochemical characteristics (Tarach et al., 2020). Mussel-mimicking adhesive hydrogels with antibacterial attributes have been created for use in wound dressing applications (Chen et al., 2023).

Furthermore, the addition of zinc oxide-decorated graphene into poly(butylene adipate-co-terephthalate) has shown remarkable antibacterial effectiveness (Tsou et al., 2023). The synergistic effect of silver nanoparticles and oxygen plasma treatment has been investigated to improve the antibacterial characteristics of polyglycolic acid and PLGA (Fortunati et al., 2013). Fluorinated antimicrobial lysine-based peptidomimetics have demonstrated improved antimicrobial efficacy against bacteria (Molchanova et al., 2018). The incorporation of silver nanoparticles in dental alloys has been investigated to boost antibacterial characteristics (Ionita et al., 2018). Furthermore, bio-phenol MQ silicone resin has been developed with self-regulating antibacterial properties (Ji et al., 2019). In summary, the integration of diverse antibacterial substances into materials across various sectors has led to the creation of advanced solutions with enhanced antimicrobial properties, paving the way for potential applications in wound healing, dental treatments, and medical implants.

Antibacterial Properties of Ti Alloys

Implant-related bacterial infections may cause implants to become loose or perhaps fail. Metallic implants are susceptible to prosthetic bacterial infections during surgery. This issue has become increasingly problematic, with clinical studies reporting infection incidences ranging from 10% to 50%, highlighting bacterial infection as a significant cause of implant failure (Seebach & Kubatzky, 2019).

In addition to administering antibiotics during surgical procedures, another strategy to mitigate bacterial infections involves the utilization of implants endowed with antibacterial properties. Antimicrobial surfaces can be classified as passive or active, with passive surfaces having an anti-adhesive effect that hinders bacterial adherence and accumulation, while active surfaces release biocides to combat bacteria. Surfaces that are contact-active or non-adhesive pose a lower risk of resistance development (Hornschuh et al., 2020). Non-adhesive surfaces prevent bacterial accumulation and biofilm formation, making it difficult for bacteria to adhere and grow into host tissues. In combating device-associated infections, it is essential to address biofilm-producing bacteria, commonly isolated from infected orthopedic implants like *Staphylococci* (Arciola et al., 2012).

The two primary methods used to evaluate the antibacterial activity of alloys are agar diffusion experiments and plate counting. The antimicrobial efficacy of an alloy can be greatly influenced by the technique used for antimicrobial testing (Zhang et al., 2013).

all. Studies have shown discrepancies in results between agar diffusion tests, where an alloy may not exhibit antibacterial properties, and plate counting methods, where the alloy can eliminate over 99% of bacterial colonies. Various parameters such as incubation conditions, culture medium, alloy size, bacterial count, and bacterial species can influence the outcomes of antibacterial measurements (Mahmoudi et al., 2022). For instance, the antibacterial activity of a Ti-Cu alloy was reported to increase from 90% to 100% when the incubation time was extended from 7 to 24 hours (Liu et al., 2014). The antibacterial activity of alloys is a complex interplay of material composition, surface modifications, and testing methodologies.

The antimicrobial characteristics of titanium alloys have garnered considerable attention across diverse sectors owing to their possible uses. The integration of antibacterial elements into titanium alloys has demonstrated the potential to improve their ability to combat microbes. Research has investigated the utilization of different antibacterial agents, including copper, silver, and chitosan, to give antibacterial attributes to titanium alloys (Gilbert-Chirivella et al., 2017; Liu et al., 2016; Ma et al., 2022). Furthermore, researchers have explored surface alterations, such as the incorporation of nano-coatings and nano-tubes, to improve the antibacterial properties of titanium alloys (Gunpath et al., 2018; Xie et al., 2022). The advancement of titanium alloys with antibacterial attributes presents significant promise for use in wound healing, dental treatments, and medical implants, providing sophisticated solutions with enhanced antimicrobial effectiveness (Alqattan et al., 2021; Niinomi et al., 2016; Yang et al., 2022).

The antimicrobial characteristics of titanium alloys have attracted considerable research attention. Several investigations have focused on integrating antibacterial elements such as copper, silver, and nanomaterials into titanium alloys to amplify their ability to kill bacteria (Liu et al., 2020; Ma et al., 2022; Zhang et al., 2016; Zhao et al., 2009). Copper-containing titanium alloys have exhibited strong antibacterial properties alongside favorable biocompatibility, rendering them a viable option for medical use (Liu et al., 2016). Likewise, titanium alloys with varying copper levels have displayed antibacterial effects against prevalent pathogens such as *Staphylococcus aureus* and *Escherichia coli* (Pandey et al., 2022; Zhang et al., 2016). Furthermore, the incorporation of copper and silver into titanium alloys has been shown to enhance their antibacterial traits (Mao et al., 2022).

Surface alterations, such as creating textured surfaces with submicron particles or applying antibacterial coatings, have been studied to improve the antibacterial characteristics of titanium alloys (Xie et al., 2022; Xue et al., 2020; Zhang et al., 2013). Moreover, methods like incorporating antibacterial medications or introducing inorganic antibacterial components onto the surface have been examined to enhance the antibacterial efficacy of titanium implants (Ren et al., 2021). Additionally, the advancement of innovative titanium alloys with heightened antibacterial properties and reduced elastic modulus has been documented, underscoring a persistent endeavor to enhance the antibacterial performance of these materials (Cai et al., 2021). Research has also investigated the mechanisms behind the antibacterial properties of titanium alloys, including the production of reactive oxygen species triggered by micro-area potential variances on the alloy surface (Fu et al., 2022). Additionally, employing sophisticated methods like the anodization of titanium alloys to generate titanium dioxide layers has been demonstrated to boost antibacterial efficacy through photocatalytic processes (Mori et al., 2022). Furthermore, the utilization of laser-based surface treatments has

been examined to fabricate antibacterial surfaces on titanium alloys (Shaikh et al., 2019).

In summary, investigations on antibacterial titanium alloys involve diverse strategies, including the integration of antibacterial substances, surface alterations, and elucidation of the mechanisms governing their antibacterial efficacy. These endeavors are directed towards augmenting the antibacterial characteristics of titanium alloys, to enhance their effectiveness in averting infections associated with implants and enhancing overall biocompatibility.

Antibacterial Alloying Elements

To create antibacterial metal alloys, antibacterial alloying elements must be carefully chosen. The three main categories of antibacterial agents are usually organic, inorganic, and natural. It is commonly known that copper (Cu) and silver (Ag) are common alloying elements used in the creation of antibacterial metal alloys. Silver, renowned for its bactericidal properties, has a long history of intentional use in surgical settings (Zhu et al., 2022).

According to recent studies, adding copper to titanium alloys strengthens their antibacterial qualities, which makes Ti-Cu alloys a viable choice for lowering infections linked to devices (Wang et al., 2019; Zhang et al., 2013). The Ti-Cu alloys that are created when copper is added to titanium show potent antibacterial activity against a variety of bacteria, including *Staphylococcus aureus* and *Escherichia coli*, while still retaining good biocompatibility, indicating that they may find use as implant materials (Liu et al., 2014). Studies have demonstrated that Ti-Cu alloys with a copper content of 5 wt. % or higher exhibit noteworthy antibacterial rates against bacteria, demonstrating how copper can effectively boost titanium alloys' antibacterial qualities (Yi et al., 2020). The metal ion-killing mechanism and the contact antibacterial mechanism are the two main hypotheses that make up the antibacterial mechanism (Mahmoudi et al., 2022; Ning et al., 2015). Strongly antibacterial metal elements like Cu, Ag, and Zn are frequently used as alloying elements in materials, contributing to the metal ion-killing mechanism. To attain a high level of antibacterial efficacy, metals or alloys must release a sufficient concentration of metal ions (Xie et al., 2024). For instance, studies have indicated that the concentration of Cu ions released from titanium alloys should exceed 0.34 mg/L to achieve significant antibacterial effectiveness (Zhang et al., 2013). Current studies have looked into the use of copper (Cu) or silver (Ag) in photosensitive or photothermal materials; these studies have shown that these materials have antibacterial qualities against bacteria and produce large amounts of radical oxygen species (ROS). Metal ions, such as Ag ions, are thought to be the mechanism underlying this antibacterial effect. They are thought to disrupt cell walls, damage cell membranes, cause protein degradation, interfere with cell respiration, and ultimately cause microbial death (Feng et al., 2000; Fu et al., 2021).

References

- Alqattan, M., Peters, L., Alshammari, Y., Yang, F., & Bolzoni, L. (2021). Antibacterial Ti-Mn-Cu alloys for biomedical applications. *Regenerative Biomaterials*, 8(1). <https://doi.org/10.1093/rb/rbaa050>
- Arciola, C. R., Campoccia, D., Speziale, P., Montanaro, L., & Costerton, J. W. (2012). Biofilm formation in Staphylococcus implant infections. A review of molecular mechanisms and implications for biofilm-resistant materials. *Biomaterials*, 33(26), 5967–5982. <https://doi.org/10.1016/j.biomaterials.2012.05.031>
- Bai, L., Ji, P., Li, X., Gao, H., Li, L., & Wang, C. (2019). Mechanical Characterization

- of 3D-Printed Individualized Ti-Mesh (Membrane) for Alveolar Bone Defects. *Journal of Healthcare Engineering*, 2019, 1–13. <https://doi.org/10.1155/2019/4231872>
- Ben Boubaker, H., Mareau, C., Ayed, Y., Germain, G., & Tidu, A. (2020). Impact of the initial microstructure and the loading conditions on the deformation behavior of the Ti17 titanium alloy. *Journal of Materials Science*, 55(4), 1765–1778. <https://doi.org/10.1007/s10853-019-04014-5>
- Bhattacharya, S. Kr., Sahara, R., Kitashima, T., Ueda, K., & Narushima, T. (2017). First principles study of oxidation of Si-segregated α -Ti(0001) surfaces. *Japanese Journal of Applied Physics*, 56(12), 125701. <https://doi.org/10.7567/JJAP.56.125701>
- Cai, D., Zhao, X., Yang, L., Wang, R., Qin, G., Chen, D., & Zhang, E. (2021). A novel biomedical titanium alloy with high antibacterial property and low elastic modulus. *Journal of Materials Science & Technology*, 81, 13–25. <https://doi.org/10.1016/j.jmst.2021.01.015>
- Chen, Y., Fan, X., Lu, J., Liu, X., Chen, J., & Chen, Y. (2023). Mussel-Inspired Adhesive, Antibacterial, and Stretchable Composite Hydrogel for Wound Dressing. *Macromolecular Bioscience*, 23(1). <https://doi.org/10.1002/mabi.202200370>
- Enan, E. T., Ashour, A. A., Basha, S., Felemban, N. H., & Gad El-Rab, S. M. F. (2021). Antimicrobial activity of biosynthesized silver nanoparticles, amoxicillin, and glass-ionomer cement against *Streptococcus mutans* and *Staphylococcus aureus*. *Nanotechnology*, 32(21), 215101. <https://doi.org/10.1088/1361-6528/abe577>
- Feng, Q. L., Wu, J., Chen, G. Q., Cui, F. Z., Kim, T. N., & Kim, J. O. (2000). A mechanistic study of the antibacterial effect of silver ions on *Escherichia coli* and *Staphylococcus aureus*. *Journal of Biomedical Materials Research*, 52(4), 662–668. [https://doi.org/10.1002/1097-4636\(20001215\)52:4<662::AID-JBM10>3.0.CO;2-3](https://doi.org/10.1002/1097-4636(20001215)52:4<662::AID-JBM10>3.0.CO;2-3)
- Fortunati, E., Mattioli, S., Visai, L., Imbriani, M., Fierro, J. L. G., Kenny, J. M., & Armentano, I. (2013). Combined Effects of Ag Nanoparticles and Oxygen Plasma Treatment on PLGA Morphological, Chemical, and Antibacterial Properties. *Biomacromolecules*, 14(3), 626–636. <https://doi.org/10.1021/bm301524e>
- Fu, S., Zhang, Y., Qin, G., & Zhang, E. (2021). Antibacterial effect of Ti Ag alloy motivated by Ag-containing phases. *Materials Science and Engineering: C*, 128, 112266. <https://doi.org/10.1016/j.msec.2021.112266>
- Fu, S., Zhang, Y., Yang, Y., Liu, X., Zhang, X., Yang, L., Xu, D., Wang, F., Qin, G., & Zhang, E. (2022). An antibacterial mechanism of titanium alloy based on micro-area potential difference induced reactive oxygen species. *Journal of Materials Science & Technology*, 119, 75–86. <https://doi.org/10.1016/j.jmst.2021.12.031>
- Gilabert-Chirivella, E., Pérez-Feito, R., Ribeiro, C., Ribeiro, S., Correia, D. M., González-Martín, M. L., Manero, J. M., Lanceros-Méndez, S., Ferrer, G. G., & Gómez-Ribelles, J. L. (2017). Chitosan patterning on titanium implants. *Progress in Organic Coatings*, 111, 23–28. <https://doi.org/10.1016/j.porgcoat.2017.04.027>
- Goutam, M., Giriya pura, C., Mishra, S., & Gupta, S. (2014). Titanium allergy: A literature review. *Indian Journal of Dermatology*, 59(6), 630. <https://doi.org/10.4103/0019-5154.143526>
- Gunpath, U. F., Le, H., Handy, R. D., & Tredwin, C. (2018). Anodised TiO₂ nanotubes as a scaffold for antibacterial silver nanoparticles on titanium implants. *Materials Science and Engineering: C*, 91, 638–644. <https://doi.org/10.1016/j.jmst.2018.05.015>

msec.2018.05.074

- Hornschuh, M., Zwicker, P., Schmidt, T., Kramer, A., & Müller, G. (2020). In vitro evaluation of contact-active antibacterial efficacy of Ti-Al-V alloys coated with the antimicrobial agent PHMB. *Acta Biomaterialia*, *106*, 376–386. <https://doi.org/10.1016/j.actbio.2020.02.016>
- Ionita, D., Golgovici, F., Mazare, A., Badulescu, M., Demetrescu, I., & Pandelea-Dobrovicescu, G. (2018). Corrosion and antibacterial characterization of Ag-DLC coating on a new CoCrNbMoZr dental alloy. *Materials and Corrosion*, *69*(10), 1403–1411. <https://doi.org/10.1002/maco.201810147>
- Ji, J., Ge, X., Liang, W., Liang, R., Pang, X., Liu, R., Wen, S., Sun, J., Chen, X., & Ge, J. (2019). A Simple Preparation Route for Bio-Phenol MQ Silicone Resin via the Hydrosilylation Method and its Autonomic Antibacterial Property. *Polymers*, *11*(9), 1389. <https://doi.org/10.3390/polym11091389>
- Jiao, J., Zhang, S., Qu, X., & Yue, B. (2021). Recent Advances in Research on Antibacterial Metals and Alloys as Implant Materials. *Frontiers in Cellular and Infection Microbiology*, *11*. <https://doi.org/10.3389/fcimb.2021.693939>
- Karakullukcu, A. B., Taban, E., & Ojo, O. O. (2023). Biocompatibility of biomaterials and test methods: a review. *Materials Testing*, *65*(4), 545–559. <https://doi.org/10.1515/mt-2022-0195>
- Kaur, M., & Singh, K. (2019). Review on titanium and titanium based alloys as biomaterials for orthopaedic applications. *Materials Science and Engineering: C*, *102*, 844–862. <https://doi.org/10.1016/j.msec.2019.04.064>
- Khrustalyov, A. P., Kozulin, A. A., Zhukov, I. A., Khmeleva, M. G., Vorozhtsov, A. B., Eskin, D., Chankitmongk, S., Platov, V. V., & Vasilyev, S. V. (2019). Influence of Titanium Diboride Particle Size on Structure and Mechanical Properties of an Al-Mg Alloy. *Metals*, *9*(10), 1030. <https://doi.org/10.3390/met9101030>
- Kim, S.-H., Kim, H., & Kim, N. J. (2015). Brittle intermetallic compound makes ultrastrong low-density steel with large ductility. *Nature*, *518*(7537), 77–79. <https://doi.org/10.1038/nature14144>
- Li, J., Guan, Q., Shi, Y. W., & Guo, D. L. (2004). Stress and distortion mitigation technique for welding titanium alloy thin sheet. *Science and Technology of Welding and Joining*, *9*(5), 451–458. <https://doi.org/10.1179/136217104225021643>
- Liu, C., & Zhang, E. (2015). Biocorrosion properties of antibacterial Ti–10Cu sintered alloy in several simulated biological solutions. *Journal of Materials Science: Materials in Medicine*, *26*(3), 142. <https://doi.org/10.1007/s10856-015-5459-6>
- Liu, J., Liu, J., Attarilar, S., Wang, C., Tamaddon, M., Yang, C., Xie, K., Yao, J., Wang, L., Liu, C., & Tang, Y. (2020). Nano-Modified Titanium Implant Materials: A Way Toward Improved Antibacterial Properties. *Frontiers in Bioengineering and Biotechnology*, *8*. <https://doi.org/10.3389/fbioe.2020.576969>
- Liu, J., Zhang, X., Wang, H., Li, F., Li, M., Yang, K., & Zhang, E. (2014). The antibacterial properties and biocompatibility of a Ti–Cu sintered alloy for biomedical application. *Biomedical Materials*, *9*(2), 025013. <https://doi.org/10.1088/1748-6041/9/2/025013>
- Liu, R., Memarzadeh, K., Chang, B., Zhang, Y., Ma, Z., Allaker, R. P., Ren, L., & Yang, K. (2016). Antibacterial effect of copper-bearing titanium alloy (Ti-Cu) against *Streptococcus mutans* and *Porphyromonas gingivalis*. *Scientific Reports*, *6*(1), 29985. <https://doi.org/10.1038/srep29985>

- Liu, X., Gu, X., Zhou, Y., Pan, W., Liu, J., & Song, J. (2023). Antifouling Slippery Surface against Marine Biofouling. *Langmuir*, 39(38), 13441–13448. <https://doi.org/10.1021/acs.langmuir.3c00986>
- Ma, Y., Yan, J., Yan, T., Wang, Q., Bao, Z., & Yi, Z. (2022). Biological properties of Cu-bearing and Ag-bearing titanium-based alloys and their surface modifications: A review of antibacterial aspect. *Frontiers in Materials*, 9. <https://doi.org/10.3389/fmats.2022.999794>
- Mahmoudi, P., Akbarpour, M. R., Lakeh, H. B., Jing, F., Hadidi, M. R., & Akhavan, B. (2022). Antibacterial Ti–Cu implants: A critical review on mechanisms of action. *Materials Today Bio*, 17, 100447. <https://doi.org/10.1016/j.mtbio.2022.100447>
- Mao, X., Shi, A., Wang, R., Nie, J., Qin, G., Chen, D., & Zhang, E. (2022). The Influence of Copper Content on the Elastic Modulus and Antibacterial Properties of Ti-13Nb-13Zr-xCu Alloy. *Metals*, 12(7), 1132. <https://doi.org/10.3390/met12071132>
- Mikheev, R., & Kalashnikov, I. (2023). Aluminium matrix hybrid composite materials reinforced with carbides and intermetallics. *E3S Web of Conferences*, 376, 01011. <https://doi.org/10.1051/e3sconf/202337601011>
- Molchanova, N., Hansen, P. R., Damborg, P., & Franzyk, H. (2018). Fluorinated antimicrobial lysine-based peptidomimetics with activity against methicillin-resistant *Staphylococcus pseudintermedius*. *Journal of Peptide Science*, 24(7). <https://doi.org/10.1002/psc.3098>
- Mori, Y., Masahashi, N., & Aizawa, T. (2022). A Review of Anodized TiNbSn Alloys for Improvement in Layer Quality and Application to Orthopedic Implants. *Materials*, 15(15), 5116. <https://doi.org/10.3390/ma15155116>
- Niinomi, M., Liu, Y., Nakai, M., Liu, H., & Li, H. (2016). Biomedical titanium alloys with Young's moduli close to that of cortical bone. *Regenerative Biomaterials*, 3(3), 173–185. <https://doi.org/10.1093/rb/rbw016>
- Ning, C., Wang, X., Li, L., Zhu, Y., Li, M., Yu, P., Zhou, L., Zhou, Z., Chen, J., Tan, G., Zhang, Y., Wang, Y., & Mao, C. (2015). Concentration Ranges of Antibacterial Cations for Showing the Highest Antibacterial Efficacy but the Least Cytotoxicity against Mammalian Cells: Implications for a New Antibacterial Mechanism. *Chemical Research in Toxicology*, 28(9), 1815–1822. <https://doi.org/10.1021/acs.chemrestox.5b00258>
- Pandey, A. K., Gautam, R. K., & Behera, C. K. (2022). Microstructure, mechanical strength, chemical resistance, and antibacterial behavior of Ti–5Cu–x%Nb biomedical alloy. *Biomedical Materials*, 17(4), 045022. <https://doi.org/10.1088/1748-605X/ac7763>
- Polishetty, A., & Littlefair, G. (2020, September 1). Comparative Study of Machinability of Additive Manufactured and Wrought Titanium Alloy using Abrasive Waterjet Machining. *Progress in Canadian Mechanical Engineering. Volume 3*. <https://doi.org/10.32393/csme.2020.1267>
- Prasad, S., Ehrensberger, M., Gibson, M. P., Kim, H., & Monaco, E. A. (2015). Biomaterial properties of titanium in dentistry. *Journal of Oral Biosciences*, 57(4), 192–199. <https://doi.org/10.1016/j.job.2015.08.001>
- Qi, M., Li, W., Zheng, X., Li, X., Sun, Y., Wang, Y., Li, C., & Wang, L. (2020). Cerium and Its Oxidant-Based Nanomaterials for Antibacterial Applications: A State-of-the-Art Review. *Frontiers in Materials*, 7. <https://doi.org/10.3389/fmats.2020.00213>
- Rabajczyk, A., Zielecka, M., Cygańczuk, K., Pastuszka, Ł., & Jurecki, L. (2021).

- Nanometals-Containing Polymeric Membranes for Purification Processes. *Materials*, 14(3), 513. <https://doi.org/10.3390/ma14030513>
- Ren, Y., Qin, X., Barbeck, M., Hou, Y., Xu, H., Liu, L., & Liu, C. (2021). Mussel-Inspired Carboxymethyl Chitosan Hydrogel Coating of Titanium Alloy with Antibacterial and Bioactive Properties. *Materials*, 14(22), 6901. <https://doi.org/10.3390/ma14226901>
- Richert, A., Olewnik-Kruszkowska, E., Dąbrowska, G. B., & Dąbrowski, H. P. (2021). The Role of Birch Tar in Changing the Physicochemical and Biocidal Properties of Polylactide-Based Films. *International Journal of Molecular Sciences*, 23(1), 268. <https://doi.org/10.3390/ijms23010268>
- Rosa, N., Marta, M., Vaz, M., Tavares, S. M. O., Simoes, R., Magalhães, F. D., & Marques, A. T. (2019). Intramedullary nailing biomechanics: Evolution and challenges. *Proceedings of the Institution of Mechanical Engineers, Part H: Journal of Engineering in Medicine*, 233(3), 295–308. <https://doi.org/10.1177/0954411919827044>
- Sarraf, M., Rezvani Ghomi, E., Alipour, S., Ramakrishna, S., & Liana Sukiman, N. (2022). A state-of-the-art review of the fabrication and characteristics of titanium and its alloys for biomedical applications. *Bio-Design and Manufacturing*, 5(2), 371–395. <https://doi.org/10.1007/s42242-021-00170-3>
- Seebach, E., & Kubatzky, K. F. (2019). Chronic Implant-Related Bone Infections—Can Immune Modulation be a Therapeutic Strategy? *Frontiers in Immunology*, 10. <https://doi.org/10.3389/fimmu.2019.01724>
- Setoyama, D., Matsunaga, J., Muta, H., Uno, M., & Yamanaka, S. (2004). Characteristics of titanium–hydrogen solid solution. *Journal of Alloys and Compounds*, 385(1–2), 156–159. <https://doi.org/10.1016/j.jallcom.2004.04.132>
- Shaikh, S., Kedia, S., Singh, D., Subramanian, M., & Sinha, S. (2019). Surface texturing of Ti6Al4V alloy using femtosecond laser for superior antibacterial performance. *Journal of Laser Applications*, 31(2). <https://doi.org/10.2351/1.5081106>
- Sung, H.-J., Ha, J.-H., & Kim, S.-K. (2010). Influence of taper on the screw-in effect of nickel-titanium rotary files in simulated resin root canal. *Journal of Korean Academy of Conservative Dentistry*, 35(5), 380. <https://doi.org/10.5395/JKACD.2010.35.5.380>
- Tarach, I., Olewnik-Kruszkowska, E., Richert, A., Gierszewska, M., & Rudawska, A. (2020). Influence of Tea Tree Essential Oil and Poly(ethylene glycol) on Antibacterial and Physicochemical Properties of Polylactide-Based Films. *Materials*, 13(21), 4953. <https://doi.org/10.3390/ma13214953>
- Tsou, C.-H., Ge, F., Lin, L., Yuan, S., De Guzman, M. R., & Potiyaraj, P. (2023). Barrier and Biodegradable Properties of Poly(butylene adipate-*co*-terephthalate) Reinforced with ZnO-Decorated Graphene Rendering it Antibacterial. *ACS Applied Polymer Materials*, 5(3), 1681–1695. <https://doi.org/10.1021/acsapm.2c01507>
- Verma, R. P. (2020). Titanium based biomaterial for bone implants: A mini review. *Materials Today: Proceedings*, 26, 3148–3151. <https://doi.org/10.1016/j.matpr.2020.02.649>
- Wang, X., Dong, H., Liu, J., Qin, G., Chen, D., & Zhang, E. (2019). In vivo antibacterial property of Ti-Cu sintered alloy implant. *Materials Science and Engineering: C*, 100, 38–47. <https://doi.org/10.1016/j.msec.2019.02.084>
- Xie, Y., Cui, S., Hu, J., Yu, H., Xuan, A., Wei, Y., Lian, Y., Wu, J., Du, W., & Zhang,

- E. (2024). Design and preparation of Ti-xFe antibacterial titanium alloys based on micro-area potential difference. *BioMetals*, 37(2), 337–355. <https://doi.org/10.1007/s10534-023-00551-4>
- Xie, Y., Lu, M., Cui, S., Yu, H., Wang, L., Ke, H., & Zhang, E. (2022). Construction of a Rough Surface with Submicron Ti₂Cu Particle on Ti-Cu Alloy and Its Effect on the Antibacterial Properties and Cell Biocompatibility. *Metals*, 12(6), 1008. <https://doi.org/10.3390/met12061008>
- Xu, J., Chen, M., Paulo Davim, J., & El Mansori, M. (2021). A Review on the Machinability of Aerospace-Grade CFRP/Titanium Stacks. *Advanced Materials Letters*, 12(1), 1–7. <https://doi.org/10.5185/amlett.2021.011591>
- Xue, T., Attarilar, S., Liu, S., Liu, J., Song, X., Li, L., Zhao, B., & Tang, Y. (2020). Surface Modification Techniques of Titanium and its Alloys to Functionally Optimize Their Biomedical Properties: Thematic Review. *Frontiers in Bioengineering and Biotechnology*, 8. <https://doi.org/10.3389/fbioe.2020.603072>
- Yang, F., Zhang, Z., Li, Y., Xiao, C., Zhang, H., Li, W., Zhan, L., Liang, G., Chang, Y., Ning, C., Zhai, J., Zhou, Z., & Yu, P. (2022). In Situ Construction of Black Titanium Oxide with a Multilevel Structure on a Titanium Alloy for Photothermal Antibacterial Therapy. *ACS Biomaterials Science & Engineering*, 8(6), 2419–2427. <https://doi.org/10.1021/acsbiomaterials.2c00256>
- Yi, C., Ke, Z., Zhang, L., Tan, J., Jiang, Y., & He, Z. (2020). Antibacterial Ti-Cu alloy with enhanced mechanical properties as implant applications. *Materials Research Express*, 7(10), 105404. <https://doi.org/10.1088/2053-1591/abc371>
- Yu, C., Cao, P., & Jones, M. (2017). Microstructural Evolution during Pressureless Sintering of Blended Elemental Ti-Al-V-Fe Titanium Alloys from Fine Hydrogenated-Dehydrogenated Titanium Powder. *Metals*, 7(8), 285. <https://doi.org/10.3390/met7080285>
- Zapata, M. E. V., Hernandez, J. H. M., Grande Tovar, C. D., Valencia Llano, C. H., Vázquez-Lasa, B., San Román, J., & Rojo, L. (2020). Osseointegration of Antimicrobial Acrylic Bone Cements Modified with Graphene Oxide and Chitosan. *Applied Sciences*, 10(18), 6528. <https://doi.org/10.3390/app10186528>
- Zhang, E., Li, F., Wang, H., Liu, J., Wang, C., Li, M., & Yang, K. (2013). A new antibacterial titanium-copper sintered alloy: Preparation and antibacterial property. *Materials Science and Engineering: C*, 33(7), 4280–4287. <https://doi.org/10.1016/j.msec.2013.06.016>
- Zhang, E., Ren, J., Li, S., Yang, L., & Qin, G. (2016). Optimization of mechanical properties, biocorrosion properties and antibacterial properties of as-cast Ti-Cu alloys. *Biomedical Materials*, 11(6), 065001. <https://doi.org/10.1088/1748-6041/11/6/065001>
- Zhang, E., Zhao, X., Hu, J., Wang, R., Fu, S., & Qin, G. (2021). Antibacterial metals and alloys for potential biomedical implants. *Bioactive Materials*, 6(8), 2569–2612. <https://doi.org/10.1016/j.bioactmat.2021.01.030>
- Zhang, Y., Zhang, W., Deng, H., Zhang, W., Kang, J., & Zhang, C. (2020). Enhanced Mechanical Properties and Functional Performances of Cationic Waterborne Polyurethanes Enabled by Different Natural Phenolic Acids. *ACS Sustainable Chemistry & Engineering*, 8(47), 17447–17457. <https://doi.org/10.1021/acssuschemeng.0c05883>
- Zhao, L., Chu, P. K., Zhang, Y., & Wu, Z. (2009). Antibacterial coatings on titanium implants. *Journal of Biomedical Materials Research Part B: Applied Biomaterials*,

91B(1), 470–480. <https://doi.org/10.1002/jbm.b.31463>

Zhu, B., Zhang, Y., Chen, Y., Yuan, P., Wang, W., Duan, H., & Wang, Z. (2022). Synthesis, Characterization and Antimicrobial Studies of Ti-40Nb-10Ag Implant Biomaterials. *Metals*, 12(8), 1391. <https://doi.org/10.3390/met12081391>

Zou, L., Chang, B., Liu, H., Zhang, X., Shi, H., Liu, X., Euchler, E., & Liu, C. (2022). Multiple Physical Bonds Cross-Linked Strong and Tough Hydrogel with Antibacterial Ability for Wearable Strain Sensor. *ACS Applied Polymer Materials*, 4(12), 9194–9205. <https://doi.org/10.1021/acsapm.2c01494>

About The Authors

Ahmet Burçin BATIBAY, PhD, is a Doctor at Necmettin Erbakan University, Department of Metallurgical and Materials Engineering in Konya, Türkiye. He holds a PhD in Materials Science and Engineering from Afyon Kocatepe University. His main areas of interest are powder metallurgy, biomaterials and materials characterization.

E-mail: abbatibay@erbakan.edu.tr, **ORCID:** 0000-0002-2606-5115

Fatih ERCİ, PhD, is an Associate Professor at Necmettin Erbakan University, Department of Biotechnology in Konya, Türkiye. He holds a PhD in Bioengineering from Yıldız Technical University. His main areas of interest are biomaterials, nanomaterials and antibacterial and cytotoxic properties of materials.

E-mail: ferce@erbakan.edu.tr, **ORCID:** 0000-0002-3044-7343

Similarity Index

The similarity index obtained from the plagiarism software for this book chapter is 16%.

CHAPTER 5

S700mc Steel Material and Gas Metal Arc Welding Under Difficult Load and Carrying Industrial Application Conditions

Fatma Nur ŞAHİN

Necmettin Erbakan University, Türkiye

Hakan GÖKMEŞE

Necmettin Erbakan University, Türkiye

To Cite This Chapter:

Gokmese, H. & Sahin, F. (2024). S700MC Steel Material and Gas Metal Arc Welding Under Difficult Load and Carrying Industrial Application Conditions. In H. Gokmese, S. Bulbul, & Y. Uzun (Eds.), *Current Studies in Materials Science and Engineering* (pp. 76-88). ISRES Publishing.

Introduction

MIG/MAG welding, also known as gas metal arc welding (GMAW), has a wide range of applications because of the widespread use of alloyed and unalloyed steel as raw materials in the industry. The GMAW method is especially preferred in the automotive, aviation, transportation, construction, and transportation/crane sectors due to the structure of the steel material used, well-welded connections in terms of mechanical and chemical properties, and cost. Structural steels are used in many areas of industry, especially in bridge and building construction, ship, railway, and crane production. MIG (Metal Inert Gas)/ MAG (Metal Active Gas) welding is the most commonly used method of joining these structural steels. It has become one of the most preferred welding methods today due to its advantages in terms of speed, efficiency, high melting power, quality weld seam, and cost compared to other welding methods. For this reason, consumables such as equipment, electrodes, and shielding gas have been the subject of much research and are improving as technology advances (Şık, 2007). With this welding method, the importance of shielding gases that affect the mechanical and chemical properties of the weld metal has increased and many studies have been carried out on them. Particularly in MAG welding, which has a wide application area, argon-based carbon dioxide, and oxygen additive gases are highly preferred in terms of both good quality weld seams, economy, and availability. The biggest reason for this superiority over MIG welding is the high cost of inert shielding gases. In addition to the structural steels that are frequently preferred in the industry, the use of high-strength S700 structural steel, specially produced by SSAB, which provides strength by reducing grain sizes with the developing technology, has also

become widespread. It is especially preferred in the automotive industry due to its higher load-carrying capacity at the same weight compared to other steels.

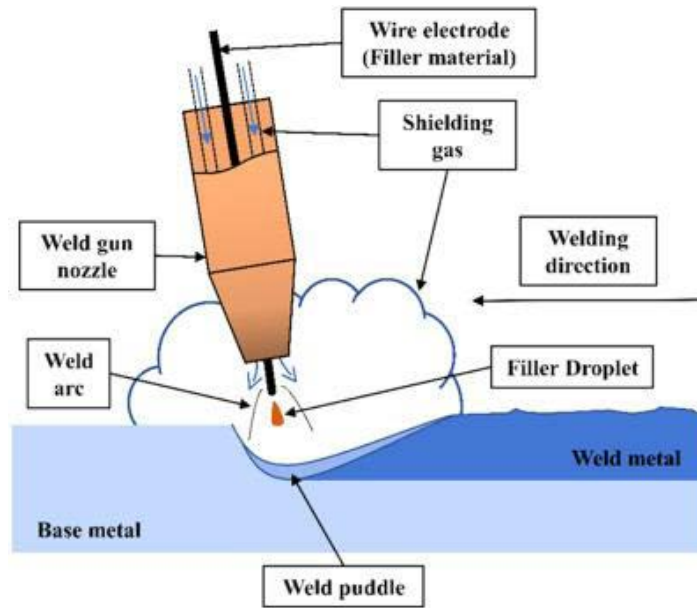
This chapter aims to shed light on the working principle, application methods, and parameters of GMAW. In addition, it is expected that the mechanical and structural properties of S700 steel will be understood by examining the experimental results obtained in MAG welding applications.

Gas Metal Arc Welding (GMAW)

Although gas metal arc welding (GMAW) emerged as an idea in the 1920s, its commercial use began in 1948. In the early days, welding operations were carried out under inert gas protection with thin melting electrodes at high currents, and this method was used in welding aluminum. Later, it became a method applied to various metals using carbon dioxide and gas mixtures as shielding gases with low and pulsed currents. The method performed with an electrode melting under the protection of inert gas is called MIG (Metal Inert Gas) welding, and the method performed with an electrode melting under the protection of active or mixed gases such as carbon dioxide is called MAG (Metal Active Gas) welding. As can be understood from here, the historical process that started with MIG welding continued with MAG welding. This method, which is called MIG/MAG welding in Germany and the UK, is referred to as GMAW (Gas Metal Arc Welding) in the USA. (Eryürek et al., 2007).

GMAW is preferred in many areas such as railway and shipbuilding, automotive industry, pipe welding, and construction industry due to its high metal deposition rate and the ability to optimize weld quality with multiple parameters. The working principle is basically based on the electric arc formed by the effect of heat between the material to be welded and a melting electrode (Rubino et al., 2023). In the GMAW method, a melting electrode is used, which is automatically fed continuously with a protective gas. In this welding method, the working principle of which is given in Figure 1, when the electrode starts to be fed through the torch, melting occurs with the heat of the arc formed between the electrode and the workpiece. The arc starts when the electrode touches the workpiece. The electric arc passes through an ionized gas using an electric current. For the shielding gas to become an ion, it must reach a certain voltage value and each gas has an ionization value. Atoms moving rapidly from cathode to anode lose electrons and the atom becomes ionized. With the energy generated as a result of this, heat is released and the material begins to melt in the heated area. In this way, melting progresses continuously.

Approximately 95% of the heat is carried by electrons and the rest by ions. The surface of the welded metal and the electrode melt with the heat created by this heat. The melting electrode fills the welding pool as filler metal. The welding area of the molten metal and the electrode are protected from the negative effects of the atmosphere by the protective gas coming from the welding torch. After the arc is stopped in the junction area, the weld metal solidifies and the welding process is completed (Şık, 2002).

Figure 1*Principle of Gas Metal Arc Welding (Dinbandhua et al., 2021)*

As a result of the arc formed by the effect of heat, metal transfer occurs in the form of molten droplets from the electrode to the workpiece. The superior properties of GMAW in terms of efficiency are based on this metal transfer mechanism. To keep the weld quality at the best levels and to obtain a weld seam with superior mechanical properties, the drop transfer mechanism plays an active role due to its direct transmission to the molten pool. This drop transmission mechanism varies depending on the welding current intensity, the composition of the shielding gas, and the chemical structure and diameter of the electrode. (Sato et al., 2024).

Parameters Affecting Welding Quality in GMAW

Welding parameters are the most important criteria that affect the quality of the welding process and the weld seam. Appropriate parameters must be selected to obtain a weld connection with the desired mechanical properties and to weld more easily under suitable conditions. In the selection of these parameters, in addition to the expected mechanical properties; Factors such as the material type and thickness of the weld metal and the welding position to be applied are taken into consideration (Demirci, 2010). The most important welding parameters in gas metal arc welding with melting electrode; welding current intensity, arc voltage, welding current type and polarization, welding speed, electrode type and diameter, wire feeding speed, free electrode length, type and flow rate of shielding gas, nozzle distance, angle of the torch. Before starting the welding process, the type and diameter of the electrode, the type of shielding gas, and the welding current type are variables that need to be adjusted and it is not possible to change them throughout the welding process. Torch angle and free electrode length are secondary adjustable parameters that can only be determined during welding. Apart from these, other variables such as current intensity, arc voltage, wire feed speed, and welding speed are primary adjustable welding parameters (Geçmen, 2006).

Welding Current Intensity

One of the important parameters affecting the penetration, width, and height of the weld

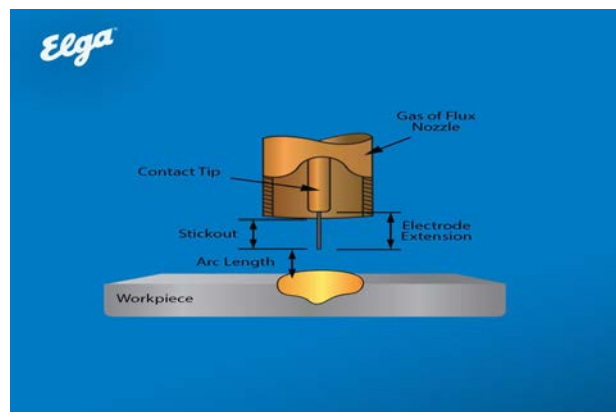
seam is the current intensity. In gas metal arc welding, when all parameters are constant and the current intensity is increased, the depth, width, and height of the weld seam also increase. When the current intensity is reduced, the amount of melted metal decreases, and the depth of the seam decreases. When the current intensity is very low, there is not sufficient melting in the workpiece and there is not sufficient bonding in the welded area (Demirci, 2010). At very high current intensities, there is a wide weld pool and very deep penetration, which causes perforation in thin metals (Geçmen, 2006).

Arc Voltage (Arc Length)

The distance between the molten weld pool and the tip of the electrode is the arc length and is the most important variable affecting the arc voltage. In gas metal arc welding, a sufficient increase in arc voltage allows a wide weld seam to be obtained. While penetration increases with increasing voltage, penetration decreases after a certain value. To benefit from this lack of penetration, very high voltage values can be used in some widely spaced root passes. Thus, a connection is provided between two passes with a wide welding seam. When the arc voltage is very low, the weld seam is quite narrow and high. When the voltage is reduced further, it causes porosity, which is an undesirable condition in the weld seam (Demirci, 2010).

Figure 2

Image of free electrode length and arc length in GMAW (Elga Welding, 2024)



Free Electrode Length

One of the most important variables in GMAW is the free electrode length (Figure 2). The free electrode length is the distance between the extreme point of the nozzle inside the torch and the extreme outside part of the electrode. As this distance increases, the resistance of the electrode increases and its temperature rises. As a result, the current intensity decreases and the amount of melting at the tip of the electrode decreases. This causes the depth to decrease and the weld seam height to increase. This situation, which is undesirable in joint welding, is suitable for filler welding due to the increase in the amount of accumulated metal. A more stable and constant arc is obtained by keeping the free electrode length short (Demirci, 2010).

Welding Speed

In gas metal arc welding, as the welding speed increases, the seam width decreases. At very high welding speeds, the form of the seam is distorted. However, in some applications, it is better to weld quickly in several passes instead of welding slowly in a single pass. When welding is done slower than the optimum welding speed, low

penetration and faulty joints may occur due to the arc falling in front of the weld pool (Karakoç, 2012). However, welding speed is not a single parameter. To reduce costs in industrial applications, the fastest source without exceeding optimum levels is preferred (Demirci, 2010).

Welding Current Type and Polarity

The welding current provided by the power unit is of two types: direct current and alternating current. Direct current welding machines are preferred when welding at constant current values is desired; In some cases, welding machines that provide alternating (variable) current are preferred depending on the desired weld seam. The type of welding current also affects polarization. While welding is done in a fixed polarity in alternating current welding machines, the poles can be changed in constant current direct current welding machines. The polarity variable is an important factor on weld seam geometry, depth, and height. Appropriate polarization is selected for the material used and the welding method. Polarity affects the amount of heat going to the base metal.

There are two types of polarization methods used in the welding method. The connection of the electrode to the cathode (negative pole) and the workpiece to the anode (positive pole) is straight polarization and electrons flow from the electrode to the work piece. The polarization method in which the electrode is connected to the anode and the workpiece to the cathode is the reverse polarization method, and electrons flow from the workpiece to the electrode (Demirci, 2010). Direct current welding machines are used in GMAW. In these welding machines, the electrode is connected to the positive pole, and the workpiece is connected to the negative pole. That is, the reverse polarization method is used. If the polarization is changed, the spatter will increase due to irregular arcing. In addition, as the heat zone changes, the amount of melting in the electrode will increase, and penetration in the welding area will decrease (Geçmen, 2006).

Electrode Speed

There is a direct proportion between the melting speed and the electrode speed. As the electrode speed increases, the current intensity increases; This increases penetration. Electrode speed is a variable related to current intensity and voltage parameters. In constant voltage gas metal arc welding machines, the current intensity is adjusted together with the electrode speed (Karakoç, 2012).

Type and Diameter of Electrode

The composition of the electrode that carries the electric current to the workpiece has a huge impact on the weld seam. For this reason, it is very important to choose electrodes suitable for the desired mechanical properties in the welded area, depending on the type and thickness of the material to be welded and the composition of the gas to be used.

In GMAW, it is used with high current strengths and large diameter electrodes. These electrodes, which are used in the welding of thick metals, provide complete melting at the welding mouth and welding is done in a shorter time. Larger drops fall into the weld pool from larger diameter electrodes and wider weld seams are obtained. Although lower currents are used with small-diameter electrodes, the current density of small-diameter electrodes is higher. Thus, weld seams with deeper penetration are obtained with small-diameter electrodes (Demirci, 2010).

Type and Flow Rate of Shielding Gas

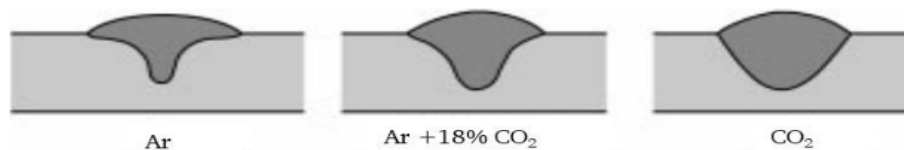
Gases that protect the weld pool in GMAW from the negative nitrogen and oxygen components of the air; It is one of the most important parameters affecting the weld quality, penetration, form, mechanical, and chemical properties of the weld seam. For this reason, the most appropriate shielding gas should be selected by taking into account the physical and chemical properties of the base metal, the type of electrode to be used, and the welding method (Geçmen, 2006).

In the welding of ferrous metals using the MAG method, pure carbon dioxide or mixed gases obtained by mixing carbon dioxide, oxygen, and argon in various combinations and ratios are used. Due to the high heat input in welding with pure carbon dioxide, welding can be done faster than other gases used at the same current intensities.

Additionally, greater melting amounts and deeper penetration are achieved. However, excessive splashing and intense welding fumes are its biggest disadvantages. Argon-oxygen mixed gases are the mixed gases with the lowest melting power. In the weld seam, penetration is low and height is high. However, unlike carbon dioxide, welding is done with minimal smoke and spatter. Argon-carbon dioxide mixture gases provide a depth midway between the penetration provided by pure carbon dioxide and argon-oxygen (Figure 3) (Demirci, 2010). A more linear metal transfer is achieved in mixtures of high amounts of argon, carbon dioxide, and oxygen; It is possible to obtain a quality weld seam by balancing the negative effects of gases alone (Geçmen, 2006). In the MIG welding method, argon, helium, and argon-helium mixture shielding gases are used to join light metals. Among these gases, argon has the least melting amount and the narrowest seam and penetration; In addition, it is the most costly and least spattering protective gas. When helium is used, a wider and deeper welded seam is obtained with its high melting power. However, it has a higher arc voltage at the same arc length as argon and is more costly due to more gas consumption (Demirci, 2010).

Figure 3

Effect of Shielding Gas Types on Welding Seam Form (Eleman, 2022)



Gas flow rate, as well as the type of shielding gas, affects the welding quality, and a flow rate adjustment is made according to the electrode diameter used. When the gas flow rate is too low, there will be pores (foaming) in the weld seam because there will be insufficient protection. In addition, since the ionized gas environment is not sufficiently formed, spattering occurs due to unstable arc formation. If the gas flow rate is too high, molten metal drops are dispersed by the turbulence that occurs, causing excessive splashing. This again creates excess pores. (Geçmen, 2006).

Torch Angle and Welding Direction

Gas flow rate, as well as the type of shielding gas, affects the welding quality, and a flow rate adjustment is made according to the electrode diameter used. When the gas flow rate is too low, there will be pores (foaming) in the weld seam because there will be insufficient protection. In addition, since the ionized gas environment is not sufficiently formed, spattering occurs due to unstable arc formation. If the gas flow rate is too high, molten

metal drops are dispersed by the turbulence that occurs, causing excessive splashing. This again creates excess pores. In the right-hand welding method, the torch is tilted towards the welding direction. Thus, the pressure of the arc pushes the molten metal against the welding direction, allowing the base metal to melt deeper and penetration increases. Additionally, a higher and narrower weld seam is obtained. In the left welding method, the torch is tilted in the opposite direction of the welding direction. Arc pressure pushes some of the molten metal towards the weld, causing the weld pool to become larger, and a wide seam is obtained. However, the base metal cannot melt deeply, and a flat weld seam with low penetration results. For this reason, the left welding method is used in joining thin parts and root pass welding (Geçmen, 2006). In gas metal arc welding of steels, the right welding method, which has less spatter, is generally preferred (Demirci, 2010).

Metal Active Gas Arc Welding (MAGAW) and S700MC Steel Material

Metal active gas welding is an efficient welding method that provides a quality welded connection when joining two similar or different metals. While shielding gases protect the weld metal from the negative effects of air, they ensure that the arc formed between the filler metal (electrode) and the workpiece continues (Singh et al., 2022). In welding processes of steels, MAG (Metal Active Gas) arc welding is the most preferred method in terms of arc stability and weld quality. The different physical properties of the shielding gases used affect the behavior of the arc and therefore the types of metal conduction. For this reason, the effect of the shielding gas in the MAG welding method is one of the important issues to be examined. In this method, high amounts of argon and some mixtures of oxygen and carbon dioxide are generally preferred as protective gases. As a result of experimental studies, it has been observed that metal conduction increases with the mixture of argon and low amounts of carbon dioxide. It has been determined that a more stable arc is obtained in welding processes with shielding gases containing argon, carbon dioxide, and oxygen, compared to a mixture of argon and carbon dioxide (Zhao et al., 2018).

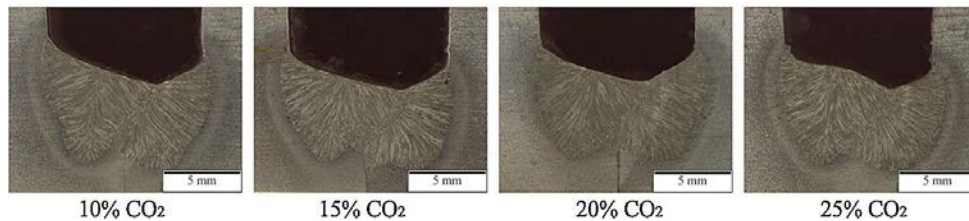
As a result of their experimental studies, Liao and Chen obtained a stable arc in 98%Ar+2%CO₂ and 98%Ar+2%O₂ mixtures, and the least spattering occurred compared to other mixtures. It has been observed that in argon and carbon dioxide mixtures, splatter rates increase with increasing carbon dioxide. At the same time, as the oxidizing effect increases with the addition of oxygen, as in carbon dioxide, the splash rate also increases. In addition, studies show that protective gases also affect the microstructure. It has been observed that as the amount of carbon dioxide increases in argon and carbon dioxide mixtures, the number of ferrites decreases as the carbon content in the metal increases. Since there is no carbon dioxide in the 98%Ar+2%O₂ mixture, the carbon content does not increase and the ferrite number is highest. It is thought that the reason why ferrite numbers are observed almost the same in the 93%Ar + 2% O₂ + 5% CO₂ mixture is that the decomposition of CO is delayed by oxygen (Liao & Chen, 1998).

Katherasan et al., examined shielding gas mixtures, effects and mechanical, metallurgical properties of flux-cored arc welding with 100%Ar, 95%Ar+5%CO₂, 90%Ar+10%CO₂, 80%Ar+20%CO₂, 75%Ar+23%CO₂+2%O₂, 70%Ar+25%CO₂+5%O₂ and 100%CO₂. It was observed that while there was a ductile rupture on the fracture surface at room temperature, a ductile rupture consisting of several splits occurred at lower temperatures. As the amount of carbon dioxide in the shielding gas increased,

the toughness of the weld metal and ferrite percentages decreased (Katherasan et al., 2013). Şık, in his experimental study, examined the mechanical properties of the weld metal by combining 4 mm thick S355JR structural steel with MAG welding method with SG2 and SG3 electrodes under 80%Ar+%18CO₂+%2O₂, 88%Ar+10%CO₂+%2O₂ and 93Ar+%5CO₂+%2O₂ protective gas. He found that the mechanical properties of the weld seam obtained by using 88%Ar+10%CO₂+2%O₂ gas and SG3 electrode were higher (Şık, 2007).

Figure 4

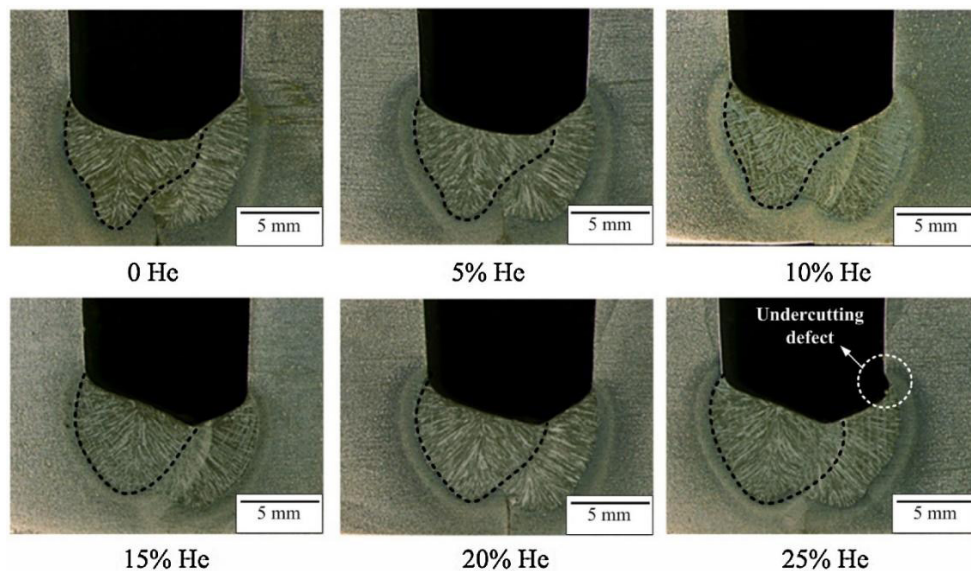
Welding Seams at Different CO₂ Rates (Cai et al., 2017)



In another experimental study conducted with MAG welding on steels, it was observed that when the carbon dioxide ratio in the shielding gas exceeded 15%, the arc length decreased, the metal drop came into contact with the molten pool without leaving the electrode, and accordingly, it caused a lot of spatters. In MAG welding, it has been observed that the arc length decreases when the content of helium, another gas in the mixed gases, is increased above 20%. However, compared to argon gas, which is commonly used in MAG welding, it has been determined that helium transfers more heat to the environment due to its high thermal conductivity and increases the cross-sectional area through which heat can pass. This enabled a larger arc core to be obtained. In addition, the high ionization energy of helium increases the arc voltage as the amount of helium increases at constant current and constant arc length. At constant welding voltage, the welding current decreased as the amount of helium and carbon dioxide increased. Figure 4 shows the weld seams obtained with different carbon dioxide ratios, and Figure 5 shows the weld seams obtained with different helium ratios. As shown in Figure 5, as the helium content increases, the depth of the weld seam increases, but it has been observed that at high rates this causes undercut defects.

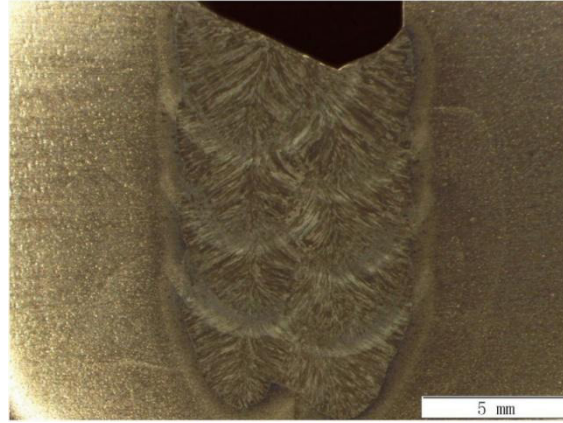
Figure 5

Welding Seams with Different Helium Ratios (Cai et al., 2017)



In MAG welding, it is possible to obtain a quality weld seam with some helium added to argon. In the experimental study, it was determined that a multi-layered and solid welded connection was obtained by using 80%Ar+10%CO₂ and 10%He, as shown in Figure 6 (Cai et al., 2017).

Figure 6
Multilayer Weld Seam (Cai et al., 2017)



High-strength steels (HSS) are frequently preferred in the construction industry, especially for high and long-span structures, due to their superiority over mild steels with their high strength at low weights (Zhong & Zhao, 2022). S700MC, HSS steel, is called heat-treated rolled fine-grained structural steel according to EN 10025-4 standard. It has been preferred in many sectors in recent years due to its high strength, light structure, and good weldability properties. More stress can be applied to S700MC steel, whose grain size is reduced with alloying elements in its structure, in thinner sections compared to S355JR steel with similar properties. This makes it more efficient in terms of production performance, load capacity, and cost. Thanks to the vanadium, titanium, and niobium elements added to its structure, the grain size is reduced. A high-strength structure is obtained with its small-grained structure and heat-treated rolling used in the production method (Gür, 2022).

S700MC steel is also known as Strenx steel produced by SSAB Company. High efficiency can be achieved from this steel if it is produced according to SSAB's standards. In addition, it is possible to achieve faster and higher quality production with the data provided by the company regarding mechanical properties, tolerances, application designs, and correct material selection. Due to its light structure and load-carrying capacity, S700MC steel is widely used in the ship, crane, and trailer sectors where transportation and lifting are high (Ünlütürk, 2023).

Table 1
Chemical Composition of S700MC Steel(%) (SSAB, 2023)

C	Si	Mn	P	S	Al	Nb	V	Ti
0,12	0,21	2,1	0,02	0,01	0,015	0,09	0,2	0,15

The yield strength of S700 steel in the high-strength steels (HSS) class, which is produced by various methods and has different chemical compositions (Table 1), is 700 N/mm² (Shakil et al., 2020). Table 2 gives the yield and tensile strengths and % elongation values of S700 steel at different thicknesses.

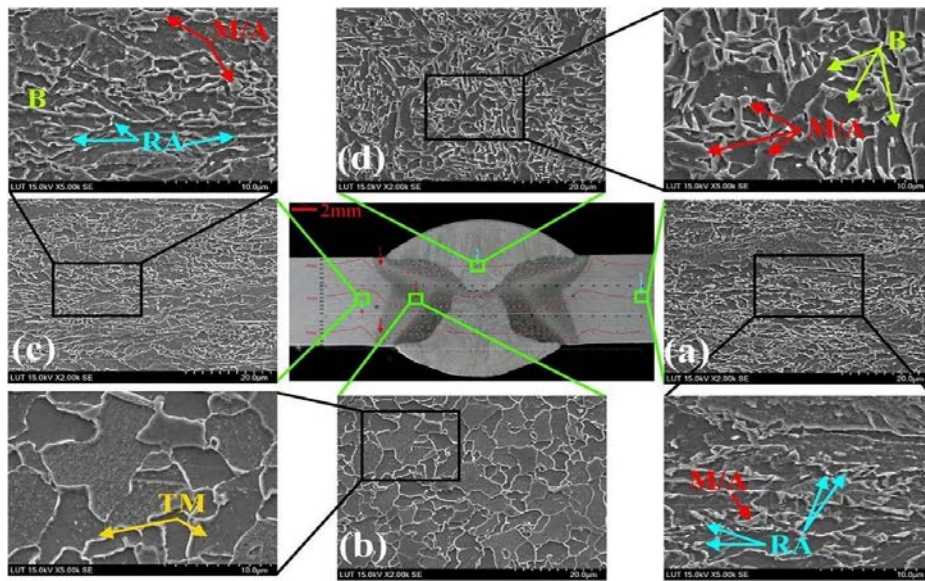
Table 2
Mechanical Properties of S700MC Steel (SSAB, 2023)

Thickness (mm)	Yield Strength (MPa)	Tensile Strength (MPa)	Elongation A_{80} (%)	Elongation A_5 (%)
2-3	700	750-950	10	12
3.01-6	700	750-950	-	12
6.01-10	700	750-950	-	12

Shakil et al., who conducted experimental studies on hot-rolled S700MC steel for cold forming, examined the mechanical properties of the steel. They cut with a water jet to obtain samples from 4 mm thick steel sheet without the effect of heat on the metal. The mechanical properties of the tensile samples obtained by the size and shape specified in the EN ISO 6892-2 standard were examined at different temperatures in the tensile device by heating them up to 800 °C. They found that there was no decrease in the yield strength of steel up to 400 °C. While the elastic modulus was stable at low temperatures, it started to break down above 400 °C. According to researchers, the reason for this is related to the microstructure of the steel. According to the data they obtained as a result of their experimental studies, researchers predicted that more tests should be carried out with different chemical compositions and different production methods to obtain more accurate results on HSSs (Shakil et al., 2020).

Amraei et al. carried out experimental studies to examine the structural and mechanical properties of S700 steel after gas metal arc welding. They combined 8 mm S700 steel with the MAG welding method by opening a 60 ° double groove V welding joint with a 1 mm gap and using a 1 mm Union Ni 2.5 electrode with a yield strength of 510 MPa and a carbon content of 0.08%. When the tensile test results were examined, it was seen that there was a slight decrease in the yield strength of the butt-welded samples. It has been determined that the welding process reduces the ductility of the material and the elongation values decrease. However, no weld porosity was found in the samples applied to the GMAW method. It was determined that the hardness value in the heated affected area of the samples for which microhardness analysis was performed decreased by 26-34% compared to the base metal. Researchers examining the microstructure results shown in Figure 7 found that the base metal consists of bainite, martensite-austenite islands, and small austenite blocks; softened HAZ consists of tempered martensite and granular bainite, which causes a decrease in hardness; They found that the HAZ and weld metal consist of bainite structure (Amraei et al., 2019).

Figure 7
S700 Microstructure Images (Amraei et al., 2019)



(a) Base metal (b) Softened HAZ (c) HAZ (d) Weld metal

Conclusion

In this section, research has been conducted on the working principle, equipment requirements, and welding parameters of gas metal arc welding, which is widely used in the industry, and the structure and weldability of high-strength S700 steel. By researching the experimental studies in the literature, the mechanical and structural changes caused by heat input and MAG welding method applications on the S700 structural steel were examined. As a result of the studies, it was seen that heat input to S700 steel had a negative effect in terms of strength. In the joining of S700 steel with the MAG welding method, microstructural changes in the HAZ and weld area caused a decrease in hardness in the HAZ and weld metal of the material. Additionally, there was a slight decrease in yield strength. Apart from the studies given as examples in this section, when the welded structures of all high-strength steels such as S700 in the literature are examined, it is seen that there are negative effects on their structural and mechanical properties due to their fine-grained structure and special chemical composition. Therefore, there is a need for more research and the development of different application methods compared to other structural steels. The positive results obtained from applications with appropriate parameters support this prediction. As a result, it is thought that S700 steel will be more preferred in the future due to its light and high-strength structure and many advantages in the transportation and construction sectors, and therefore more research will be required accordingly.

References

- Amraei, M., Ahola, A., Afkhami, S., Björk, T., Heidarpour, A., & Zhao, X. L. (2019). Effects of heat input on the mechanical properties of butt-welded high and ultra-high strength steels. *Engineering Structures*, 198, 109460. <https://doi.org/10.1016/J.ENGSTRUCT.2019.109460>
- Cai, X., Fan, C., Lin, S., Ji, X., Yang, C., & Guo, W. (2017). Effects of shielding gas composition on arc properties and wire melting characteristics in narrow gap MAG welding. *Journal of Materials Processing Technology*, 244, 225–230. <https://doi.org/10.1016/J.JMATPROTEC.2017.01.036>

- Demirci, D. (2010). *Investigation of the effects of polarization on seam form by DC welding in different welding processes* [Master's Thesis]. Dokuz Eylül University Institute of Science and Technology.
- Dinbandhua, Prajapati, V., Vora, J. J., & Abhishek, K. (2021). Advances in gas metal arc welding process: modifications in short-circuiting transfer mode. *Advanced Welding and Deforming*, 67–104. <https://doi.org/10.1016/B978-0-12-822049-8.00003-7>
- Eleman, B. (2022). *Comparison of macrostructure and mechanical properties of welding seams as a result of S355 quality steel welded by new generation (inverter) and traditional MIG / MAG welding machines* [Master's Thesis]. Yıldız Technical University Institute of Science and Technology.
- Elga Welding. (2024, 5 May). What are stickout electrode extension and contact tip to work distance- 5 May 2024. <https://elgawelding.com/what-are-stickout-electrode-extension-and-contact-tip-to-work-distance---05-may-2024>
- Eryürek, B., Sevük, A., & Odabaş, A. (2007). *Welding technology* (2nd ed.). Askaynak, 56-120.
- Geçmen, İ. (2006). *The application of gas metal arc welding for steels* [Master's Thesis]. Marmara University Institute of Science and Technology.
- Gür, Y. (2022). *Investigation of the microstructural and mechanical properties of S700 MC high strength construction steel combined with MIG/MAG welding* [Master's Thesis]. Gazi University Institute of Science and Technology.
- Karakoç, S. (2012). *Application of gas metal arc welding to steel and the parameters* [Master's Thesis]. Mustafa Kemal University Institute of Science and Technology.
- Katherasan, D., Sathiya, P., & Raja, A. (2013). Shielding gas effects on flux cored arc welding of AISI 316L (N) austenitic stainless-steel joints. *Materials & Design*, 45, 43–51. <https://doi.org/10.1016/J.MATDES.2012.09.012>
- Liao, M. T., & Chen, W. J. (1998). The effect of shielding-gas compositions on the microstructure and mechanical properties of stainless-steel weldments. *Materials Chemistry and Physics*, 55(2), 145–151. [https://doi.org/10.1016/S0254-0584\(98\)00134-5](https://doi.org/10.1016/S0254-0584(98)00134-5)
- Rubino, F., Tucci, F., Caruso, S., Umbrello, D., & Carlone, P. (2023). An integrated numerical approach to simulate the filler deposition and the shape distortions in gas metal arc welding. *CIRP Journal of Manufacturing Science and Technology*, 45, 26–34. <https://doi.org/10.1016/J.CIRPJ.2023.05.010>
- Sato, Y., Ogino, Y., & Sano, T. (2024). Role of material properties on metal transfer dynamics in gas metal arc welding. *Journal of Materials Processing Technology*, 326, 118347. <https://doi.org/10.1016/J.JMATPROTEC.2024.118347>
- Shakil, S., Lu, W., & Puttonen, J. (2020). Experimental studies on mechanical properties of S700 MC steel at elevated temperatures. *Fire Safety Journal*, 116, 103157. <https://doi.org/10.1016/J.FIRESAF.2020.103157>
- Singh, L., Singh, A., & Singh, B. (2022). MAG shield gas influence study on impact strength of Al-5052 joint. *Materials Today: Proceedings*, 68, 1057–1062. <https://doi.org/10.1016/J.MATPR.2022.08.338>
- Şık, A. (2002). *Effects of gas compositions on mechanical properties of MIG/MAG welded automobile body sheets* [PhD Thesis]. Gazi University Institute of Science and Technology.

- Şık, A. (2007). Investigation of the effect of shielding gas mixtures on the mechanical properties of steel constructions that are applied MIG/MAG welding. *Tujs Trakya Univ J Sci*, 8(1), 55–60. <http://fbe.trakya.edu.tr/>
- Şık, A. (2007). A research into the effect of additional electrode types and protective mixture gases on the bending fatigue life of steel material that is welded with MIG/MAG welding method. *J. Fac. Eng. Arch. Gazi Univ.*, 22(4), 769–777.
- SSAB. (2024, 5 May). Urun teklifi 700 mc-d-e- 5 May 2024. <https://www.ssab.com/tr-tr/markalar-ve-urunler/strenx/urun-teklifi/700/mc-d-e---5-may-2024>
- Toprak Şenol, H. (2020). *Investigation of welding parameters in the arc welding electrodes with intelligent systems* [Master's Thesis]. Muğla Sıtkı Koçman University Institute of Science and Technology.
- Ünlütürk, G. F. (2023). *Calculating the suitable heat input of S700 MC steel with robotic welding systems and investigation of its effect on mechanical properties and application to automation* [Master's Thesis]. Zonguldak Bülent Ecevit University Institute of Science and Technology.
- Zhao, Y., Shi, X., Yan, K., Wang, G., Jia, Z., & He, Y. (2018). Effect of shielding gas on the metal transfer and weld morphology in pulsed current MAG welding of carbon steel. *Journal of Materials Processing Technology*, 262, 382–391. <https://doi.org/10.1016/J.JMATPROTEC.2018.07.003>
- Zhong, Y., & Zhao, O. (2022). Experimental and numerical studies on post-fire behaviour of S700 high strength steel circular hollow sections under combined compression and bending. *Thin-Walled Structures*, 181, 110004. <https://doi.org/10.1016/J.TWS.2022.110004>

About The Authors

Hakan GÖKMEŞE, PhD is an Associate Professor of Mechanical Engineering at Necmettin Erbakan University in Konya, Türkiye. He has a master's degree in Metallurgy Education from Gazi University. His main areas of interest are casting technology, powder metallurgy, heat treatments and composites-nanocomposites applications.

E-mail: hakan1440@gmail.com, **ORCID:** 0000-0003-0053-8444

Fatma Nur ŞAHİN, MSc, graduated from Necmettin Erbakan University, Institute of Science, Department of Mechanical Engineering. She worked as a quality and production manager in the forklift and trailer industry. She has worked in the supervision and management of welded manufacturing applications, which is her main area of expertise.

E-mail: fnursahin7@gmail.com **ORCID:** 0000-0001-6071-0168

Similarity Index

The similarity index obtained from the plagiarism software for this book chapter is %9.

CHAPTER 6

Use of Polymers in Soil Erosion Control

Vildan ERCİ

Selcuk University, Türkiye

To Cite This Chapter:

Erci, V. (2024). Use of Polymers in Soil Erosion Control. In H. Gokmese, S. Bulbul, & Y. Uzun (Eds.), *Current Studies in Materials Science and Engineering* (pp. 89-101). ISRES Publishing.

Introduction

Soil is an important resource for human survival, sustaining food security, and protecting ecosystems (Wuepper et al., 2019). Globally, soil erosion is a major factor in land degradation, affecting millions of hectares in tropical regions. Reduced productivity, a decline in biodiversity, weakened ecosystem resilience and increased vulnerability to climate change are the consequences of this phenomenon (Vågen & Winowiecki, 2019). Soil erosion affects the cycling of soil materials and energy, reduces the fertility of grassland soil, and jeopardizes the stability of terrestrial ecosystems and ecosystem services (Cui et al., 2024). Soil erosion is worsened by factors such as water erosion, resulting in decreased nutrient availability, lower soil water retention capacity, and negatively impacting ecosystem productivity and the carbon balance in ecosystems (Yue et al., 2016). Beyond just decreasing agricultural productivity, soil erosion also has an impact on water bodies downstream by deteriorating aquatic habitats, lowering water storage capacity in reservoirs used to generate hydroelectric power, and decreasing water transparency (Durán Zuazo & Rodríguez Pleguezuelo, 2008). Soil erosion not only has direct effects on the environment but also can cause thinning of the soil layer, deterioration of soil structure, and decreased soil nutrient levels (Zhang et al., 2003).

Considering the type of soil and putting appropriate preventative measures in place that are suited to its qualities are crucial for successfully preventing soil erosion. Preventing soil erosion is essential for protecting soil used for growing food, preserving ecosystem functions, and minimizing the financial costs of off-site impacts (Hamanaka et al., 2019). An ideal soil stabilizer should be inexpensive, easy to produce and use, capable of forming a crust that is highly resistant to erosion, and safe for the environment without adding to existing pollution. (Dong et al., 2008). Soil properties like strength, water stability, and hardness have significantly improved as a result of the effective stabilization of soil using a variety of inorganic additives, including fly ash, slag, cement, and lime. It has been discovered that these additives give stabilized soil a dense structure, improving its properties. Even though these additions improve the properties of the soil, they can occasionally prevent vegetation growth in the stabilized soil (Bai et al., 2023).

The potential of polymers as soil conditioners to improve soil properties such as ductility, strength, and water stability has made them increasingly popular in soil stabilization applications. Both natural and synthetic polymers have been widely investigated for their ability to improve soil cementation. Studies have shown that the

application of polymers can lead to notable enhancements in soil structure stability, water-holding capacity, and hydraulic conductivity (Ayeldeen et al., 2017; Liu et al., 2018). Polymers are effective tools for reducing soil erosion rates and boosting soil fertility, even at low application doses. They also improve soil aggregates and structural stability (Yakupoglu et al., 2019). Using polymers has been associated with better stability of soil structure, resulting in less soil sealing, increased infiltration rates, and lower runoff and soil erosion (Ben-Hur, 2006). Polymers such as polyacrylamide (PAM) and polysaccharides can reduce soil erosion by stabilizing soil aggregates and increasing resistance to erosion. Since the 1950s, polyvinyl alcohol (PVA) and PAM have been used in studies on erosion (Yakupoglu et al., 2019).

Biopolymers are eco-friendly materials utilized in various geoenvironmental applications, including the removal of heavy metals from polluted soils, soil hydraulic conductivity reduction, erosion prevention, and soil enhancement (Lee et al., 2022). Biopolymers, organic polymers derived from diverse biological organisms, have attracted considerable interest in the field of soil remediation owing to their environmentally benign and biodegradable characteristics (Chang et al., 2016). An eco-friendly and sustainable way to enhance the mechanical properties of soil is using biopolymers. Studies reveal that biopolymers, even in small amounts, can considerably increase soil strength—often at much lower levels than traditional binders (Chang & Cho, 2019; Fatehi et al., 2023; Joga & Varaprasad, 2019). Additionally, the investigation of biopolymers for soil stabilization has improved the establishment of vegetative cover, decreased the transport of suspended solids in surface water runoff, and reduced soil erosion (Larson et al., 2010). Through direct interactions with soil particles, biopolymers form strong matrices that significantly improve the mechanical properties of soil. The strong biopolymer-soil matrices that result from these interactions are made possible by the high specific surfaces and electrical charges of biopolymers (Vishweshwaran et al., 2021).

Soil Erosion

Soil erosion is a common worldwide problem that is causing significant worry in numerous nations. It occurs when soil is deteriorated by a combination of natural factors as well as human actions like intensive agriculture (Nasir Ahmad et al., 2020). The loss of the top layer of soil due to wind and water is known as soil erosion, and it is a serious problem that jeopardizes environmental sustainability and agricultural productivity (Borrelli et al., 2017). The fertility, productivity, and general biodiversity of the soil are all seriously threatened by soil erosion (Alewell et al., 2019). In addition to the obvious elements of wind and rain, erosion is a complex phenomenon that is influenced greatly by slope, vegetation cover, soil erodibility, and conservation efforts (Ikhsan et al., 2021). Soil erosion is influenced by a wide range of human activities, such as land cover changes, agricultural practices, and climate change. The two main mechanisms through which erosion can negatively impact an area are soil degradation and soil transportation to different locations (Belay & Mengistu, 2021; Hikmah, 2019; Susanti et al., 2019). Transportation-related soil degradation has been demonstrated to be largely caused by erosion, which has detrimental effects on the environment, water resources, and agricultural areas. Even though the extent of erosion differs from location to location, it always has a detrimental effect on the environment because it alters the characteristics of soil particles and results in a large loss of soil nutrients (İmamoglu et al., 2018; Saygin et al., 2019).

Reduced agricultural productivity and soil degradation can result from soil erosion, a serious environmental problem. Soil erosion is a multifaceted process that

involves different types of erosion, including surface, gully, stream, and raindrop erosion (Hamanaka et al., 2019; Verma et al., 2021). Wind and water erosion are recognized as the primary agents responsible for soil and nutrient losses (Tuo et al., 2018). Surface runoff is the primary cause of water-induced accelerated soil erosion. Depletion of important soil resources, increased pollution, and sediment buildup in water bodies are all consequences of water erosion, a serious environmental problem. Significant regions of topsoil are lost because of this process, and sediment accumulates there, leading to negative environmental effects like contaminated water supplies and deteriorated soil (Costa et al., 2018; Silva et al., 2024; Wysocka-Czubaszek & Czubaszek, 2015). In addition to carrying soil particles, surface runoff also carries bacterial communities and organic carbon, which has an impact on the dynamics of ecosystems and soil health (Le et al., 2020). Wind transports both fine and coarse particles across landscapes, which is a significant process known as wind erosion (Jarrah et al., 2020). A complex process influenced by many different factors is wind erosion. In certain areas, long-term wind erosion may contribute to soil salinization by causing soil to become coarser, have less organic matter in the soil, and have a higher pH (Mo et al., 2023). Wind erosion harms ecosystems and poses a serious threat to the environment, much like water erosion does. Sandier soil types are more susceptible to wind erosion, which can damage plants, reduce agricultural output, and hasten the process of desertification (Riksen & de Graaff, 2001). One powerful illustration of the seriousness of this environmental problem is the severe drought and wind erosion that hit the Great Plains in the 1930s (Hansen & Libecap, 2003). The health of humans and the ecosystem are greatly impacted by air pollution, which is a serious problem caused by dust and other particles eroded by wind. Many situations have been investigated when it comes to the relationship between wind erosion and air pollution. According to studies, downwind air quality can be impacted by wind erosion and the dust emissions that result from agricultural lands (Güneş, 2011; Lackóová et al., 2021).

Evaluation of the soil's erodibility is a crucial first step in preventing erosion, since environmental and human factors are known to have a major impact on erosion processes (Dede et al., 2022). The erodibility of soil is influenced by several key factors, such as its organic matter content, texture, permeability, and structure. These elements draw attention to the intricate relationship between soil properties and susceptibility to erosion (Udumoh et al., 2018). Applying erosion control measures effectively requires an understanding of the causes and effects of erosion. It is possible to calculate soil erosion susceptibility parameters by considering the different physicochemical properties of the soil. These factors are essential for assessing how vulnerable soils are to erosion. Soil erosion and deterioration are largely determined by factors such as extrinsic conditions and inherent properties of the soil (Le Bissonnais et al., 1993; Mamedov et al., 2015). A thorough plan that considers soil erosion's effects both on and off-site is required to effectively control erosion. To manage erosion, this entails emphasizing the necessity of improving the control measures that are currently in place, and introducing new adaptive strategies (Majoro et al., 2020). Altogether, soil properties, land cover, and climate are just a few of the many variables that affect the complex process of erosion. Degradation of soil and damage to the environment can result from various types of erosion. For landscapes and ecosystems to be less negatively impacted by erosion, it is essential to implement efficient erosion control techniques.

Soil erosion prevention using polyacrylamide (PAM) and its derivatives

Polyacrylamide is a water-soluble polymer made up of carbon chains with amide

groups, consisting of repeating units of acrylamide (AM). Under high temperature or alkaline conditions, polyacrylamide undergoes thermal or basic hydrolysis, respectively, converting amide groups into anionic carboxylate groups, resulting in the formation of Partially Hydrolyzed Polyacrylamide (PHPA) (Ma et al., 2015). The versatile polymer polyacrylamide (PAM) is widely used as a binder in many different sectors, including soil modification, and has attracted a lot of interest from researchers. This polymer has a wide range of uses in agriculture, the environment, and industry. PAM is an efficient way to address problems in agriculture like runoff, infiltration, and soil erosion (Choi et al., 2016; Weston et al., 2009). At specific application rates, PAM has been demonstrated in studies to effectively reduce erosion and enhance water infiltration. With increased porosity and water infiltration rates, PAM application enhances the properties of the soil and enhances aggregate stability. Charge density, concentration, and molecular weight of polyacrylamide (PAM) are some of the properties that affect how well it stabilizes soil (Chen et al., 2016, 2018).

Polyacrylamide (PAM), either alone or in combination with other substances, has been demonstrated in numerous studies to improve soil properties. The application of PAM on soil physical characteristics has been found to increase soil porosity and water infiltration rates, ultimately enhancing aggregate stability within the soil profile (J. Zhang et al., 2022). The study by Lu et al. (2018) investigated the effectiveness and durability of polyacrylamide (PAM) and polysaccharide (Jag C 162) in reducing soil erosion under simulated rainfall conditions. The research found that both PAM and Jag C 162 were successful in reducing surface runoff, controlling sheet erosion, and enhancing soil aggregates by binding and stabilizing soil particles (Lu et al., 2018). Recent research has been dedicated to exploring the impact of polymer blends on stabilizing and reducing erosion on silty sand slopes. The study specifically focused on assessing the efficacy of modified carboxymethylcellulose (M-CMC), a unique soil stabilizer that combines polyacrylamide (PAM) with carboxymethylcellulose (CMC) to target the stabilization of silty sand. The investigation aimed to evaluate the effects of different concentrations of the M-CMC stabilizer on microstructure, permeability, shear strength, and water sensitivity. The findings revealed that as the concentration of M-CMC increased, there was an improvement in water sensitivity and shear strength, although the infiltration rate decreased. Moreover, the results from rainfall simulations demonstrated that plots treated with M-CMC exhibited enhanced infiltration rates, reduced soil loss, and increased erosion resistance during periods of heavy rainfall (Yang et al., 2019). Lu et al., (2018), explored the efficacy of polyacrylamide (PAM) and polysaccharide in mitigating soil erosion under simulated rainfall conditions. Both polymers, PAM and polysaccharide, were found to decrease surface runoff, control soil erosion, and enhance soil aggregates by binding and stabilizing soil particles (Lu et al., 2018).

Poly (Vinyl Alcohol) Based Polymers

Poly (vinyl alcohol) (PVA) is a synthetic polymer that is semi-crystalline and has the chemical formula $[\text{CH}_2\text{CH}(\text{OH})]_n$. serves as an environmentally friendly soil stabilizer. (Kukul & Sarkar, 2010; Mok et al., 2020). Polyvinyl alcohol (PVA) is a water-soluble synthetic polymer that differs from polyvinyl acetate (PVAc) in the presence of hydroxyl groups, making it hydrophilic. PVA is produced due to the sensitivity of the ester groups in PVAc.

PVA is known for its high polarity and capability to create hydrogen bonds with hydroxyl groups in soil minerals, leading to improved characteristics in soft clays.

Research shows that adding PVA can significantly enhance the properties of soft clays, highlighting its potential for use in soil improvement applications (Mirzababaei et al., 2017). One potential soil conditioner that is effective at lowering soil erodibility is polyvinyl alcohol (PVA). Research indicates that the utilization of PVA synthetic soil conditioners can mitigate the depletion of available soil moisture in sandy soil, thereby leading to a noteworthy enhancement in crop yield, water use efficiency, and macronutrient uptake (Aly, 2020). The study by Kukal et al. (2007) examined how the application of polyvinyl alcohol (PVA) affected the stability of soil aggregates from various land uses when exposed to water droplets from a raindrop simulator.

According to the results, soils that have been eroded have the least water drop stability, which is followed by soils from farms, forests, and grasslands. Additionally, the study showed that smaller aggregates showed better stability than larger ones. Crucially, PVA application improved water drop stability significantly across a range of aggregate sizes and land uses (Kukal et al., 2007). In the semi-arid tropical regions, Kukal and Sarkar (2010) examined the effects of mulching and polyvinyl alcohol (PVA) application on splash erosion and infiltration in sandy loam and silty loam soils. The goal of the study was to investigate problems caused by structural instability, such as splash erosion and soil crust formation, and the impact on soil infiltration rates and seed germination. Results showed that covering with straw mulch significantly reduced spatter erosion, although the effects on infiltration rates varied depending on PVA application. Remarkably, in sandy loam soils as opposed to silty loam soils, mulching and PVA were more effective at lowering splash erosion and enhancing soil infiltration (Kukal & Sarkar, 2010). The effects of polyvinyl alcohol (PVA) and polyacrylamide (PAM) as soil conditioners on runoff and splash erosion were examined in a different study using a rainfall simulator in a lab setting. Significant reductions in splash and runoff erosion were found to occur with increasing doses of PVA and PAM. The study emphasized the role that PVA and PAM play in enhancing soil stability and lowering the risk of erosion in laboratory settings, as well as their capacity to mitigate erosion processes (Yonter, 2010).

The ability of soil to retain water is a crucial element that impacts the growth of vegetation, and polyvinyl alcohol (PVA) has a notable impact on this due to its molecular structure. Zhou et al. (2021) emphasized the distinct molecular structure of PVA, which permits efficient interaction with water molecules and, as a result, makes it easier to absorb and store a significant amount of water along the lengthy polymer chain (Zhou et al., 2021). All in all, the importance of PVA's ability to combine with water molecules makes it a valuable material for applications where water retention is crucial, such as in agriculture, horticulture, and environmental engineering.

Biopolymers in controlling soil erosion

Biopolymers have gained considerable attention in the field of soil stabilization due to their potential to improve geotechnical properties (Huang et al., 2021). The advantageous qualities of biopolymers in soil stabilization are consistent with their natural rhizosphere functions, which include surface adhesion, cell self-adhesion to biofilms, formation of protective barriers, water retention around roots, and nutrient accumulation. Because of these advantages over other methods of improving soil quality and their ability to promote plant growth, biopolymers are an adaptable and sustainable way to improve soil characteristics (Larson et al., 2012).

The beneficial effects of polymers like β -glucan, guar gum, and xanthan gum on soil properties and plant growth have been the subject of extensive research. In a variety of soil types and harsh environmental circumstances, these biopolymers have

demonstrated great promise for improving soil stability, water retention, erosion resistance, and vegetation growth (Kumar et al., 2022).

For soil applications, especially in soil improvement for engineering purposes, xanthan gum has proven to be a useful and affordable biopolymer. Bagheri et al. (2023) conducted a study on the impact of xanthan gum biopolymer on soil mechanical properties, which included tests such as Atterberg limits, unconfined compression, and triaxial tests. For soil applications, especially in soil improvement for engineering purposes, xanthan gum has proven to be a useful and affordable biopolymer. Furthermore, the study evaluated the biopolymer-treated soil's resilience to cycles of wetting and drying, demonstrating its increased strength in comparison to the untreated soil. These results highlight the potential of xanthan gum biopolymer as an environmentally friendly way to improve soil for engineering applications (Bagheri et al., 2023).

Ayeldeen et al. (2018) investigated various biopolymers such as xanthan gum, guar gum, carrageenan, and modified starches. The findings indicated that these biopolymers can reduce wind erosion to varying degrees, depending on the type of biopolymer and concentration utilized. The resistance to erosion even after numerous wet and dry cycles was especially noteworthy for modified starches and guar gum. The research additionally presented a neural network model for estimating soil loss mass in various cycles and concentrations, offering a novel method for calculating the effect of biopolymers on erosion control (Ayeldeen et al., 2018). Biopolymers like guar gum, xanthan gum, and chitosan are beneficial for increasing soil stability, decreasing hydraulic conductivity, and improving erosion control during rainfall (Shariatmadari et al., 2020; Tran Thi Phuong et al., 2022). The study by Lemboye (2021) aimed to improve the resistance of dune sand to wind erosion by using biopolymers of agricultural origin, specifically acacia gum, sodium alginate, and pectin. The study involved wind tunnel experiments and penetration tests, which demonstrated that using biopolymers significantly enhanced the sand's ability to resist erosion caused by wind compared to sand that was untreated or treated with water. Images from scanning electron microscopy showed that the biopolymers formed a robust bond between sand particles, leading to improved resistance against cracking and erosion (Lemboye et al., 2021).

Among various types of biopolymers, gel-type biopolymers have been found to exhibit superior interparticle interactions with clay particles compared to coarse particles like sand. These interactions are attributed to direct ionic or hydrogen bonding and matrix formation, which are more pronounced in clay particles than in neutral sand particles. Specifically, gellan gum biopolymer has been identified as a significant contributor to strengthening gellan gum-sand blends through the densification and aggregation effects of highly strained gellan gum hydrogels between sand particles (Chang et al., 2015; Chang & Cho, 2019).

Biopolymers, like those from microbes, can improve soil erosion resistance by forming connections between soil particles, thereby limiting water infiltration and absorption into the soil (Josifovski & Nikolovska Atanasovska, 2022). Exopolysaccharides (EPS) are essential components in soil, contributing significantly to soil structure and moisture retention. These complex polymers, produced by various microorganisms play a crucial role in soil aggregation and moisture levels (Barthès & Roose, 2002; Cania et al., 2019). *Rhizobium tropici*, a symbiotic nodulator of legume plants, has been studied for its potential application in reducing soil erosion and improving soil stability. Research has shown that the biopolymer produced by *Rhizobium tropici*, known for its gel-like EPS, can considerably lower the transportation of sediment, heavy metals in leachate, and erosion caused by surface runoff (Larson et al., 2016). Higher cation

exchange capacity, higher water retention, and higher enzyme activity are all associated with EPS presence in soil, and these factors all support soil fertility and health (Valarini et al., 2003).

Conclusions

The stability of ecosystems and sustainable agriculture is threatened by soil erosion, a major worldwide problem. Wind and water are the main natural forces that cause soil erosion, which degrades the environment and reduces soil fertility. Several preventative strategies, such as using polymers as soil conditioners, have been developed to help stop soil erosion. Hydrophilic polymers, such as polyvinyl alcohol (PVA) and polyacrylamide (PAM), have been shown to help improve soil fertility and lower rates of erosion. Factors like the properties of the polymer and the features of the soil affect how polymers are applied to soil. The potential of biopolymers to increase soil durability, strengthen soil, decrease permeability, and increase erosion resistance has drawn attention. Soils treated with biopolymers have better mechanical characteristics, such as more aggregate stability and structural integrity. Additionally, the blending of biopolymers with other substances, like plant fibers, has demonstrated the ability to strengthen soil and improve its resistance to erosion. Finally, applying polymeric soil amendments offers a practical and efficient way to address non-point source pollution issues and mitigate soil erosion. Biopolymers provide a sustainable response to the problems caused by soil erosion in agriculture and environmental conservation initiatives by increasing soil stability, lowering erosion rates, and increasing soil fertility.

References

- Alewell, C., Borrelli, P., Meusburger, K., & Panagos, P. (2019). Using the USLE: Chances, challenges and limitations of soil erosion modelling. *International Soil and Water Conservation Research*, 7(3), 203–225. <https://doi.org/10.1016/j.iswcr.2019.05.004>
- Aly, E. (2020). Effect of Water Regimes and Polyvinyl Alcohol on Faba Bean Yield, Chemical Composition and Water Use Efficiency. *Journal of Soil Sciences and Agricultural Engineering*, 11(12), 769–777. <https://doi.org/10.21608/jssae.2020.160915>
- Ayeldeen, M., Negm, A., El Sawwaf, M., & Gädda, T. (2018). Laboratory study of using biopolymer to reduce wind erosion. *International Journal of Geotechnical Engineering*, 12(3), 228–240. <https://doi.org/10.1080/19386362.2016.1264692>
- Ayeldeen, M., Negm, A., El-Sawwaf, M., & Kitazume, M. (2017). Enhancing mechanical behaviors of collapsible soil using two biopolymers. *Journal of Rock Mechanics and Geotechnical Engineering*, 9(2), 329–339. <https://doi.org/10.1016/j.jrmge.2016.11.007>
- Bagheri, P., Gratchev, I., & Rybachuk, M. (2023). Effects of Xanthan Gum Biopolymer on Soil Mechanical Properties. *Applied Sciences*, 13(2), 887. <https://doi.org/10.3390/app13020887>
- Bai, Y., Liu, J., Xiao, H., Song, Z., Ma, K., & Deng, Y. (2023). Soil stabilization using synthetic polymer for soil slope ecological protection. *Engineering Geology*, 321, 107155. <https://doi.org/10.1016/j.enggeo.2023.107155>
- Barthès, B., & Roose, E. (2002). Aggregate stability as an indicator of soil susceptibility to runoff and erosion; validation at several levels. *CATENA*, 47(2), 133–149. [https://doi.org/10.1016/S0341-8162\(01\)00180-1](https://doi.org/10.1016/S0341-8162(01)00180-1)

- Belay, T., & Mengistu, D. A. (2021). Impacts of land use/land cover and climate changes on soil erosion in Muga watershed, Upper Blue Nile basin (Abay), Ethiopia. *Ecological Processes*, *10*(1), 68. <https://doi.org/10.1186/s13717-021-00339-9>
- Ben-Hur, M. (2006). Using synthetic polymers as soil conditioners to control runoff and soil loss in arid and semi-arid regions—a review. *Soil Research*, *44*(3), 191. <https://doi.org/10.1071/SR05175>
- Borrelli, P., Robinson, D. A., Fleischer, L. R., Lugato, E., Ballabio, C., Alewell, C., Meusburger, K., Modugno, S., Schütt, B., Ferro, V., Bagarello, V., Oost, K. Van, Montanarella, L., & Panagos, P. (2017). An assessment of the global impact of 21st century land use change on soil erosion. *Nature Communications*, *8*(1), 2013. <https://doi.org/10.1038/s41467-017-02142-7>
- Cania, B., Vestergaard, G., Krauss, M., Fließbach, A., Schloter, M., & Schulz, S. (2019). A long-term field experiment demonstrates the influence of tillage on the bacterial potential to produce soil structure-stabilizing agents such as exopolysaccharides and lipopolysaccharides. *Environmental Microbiome*, *14*(1), 1. <https://doi.org/10.1186/s40793-019-0341-7>
- Chang, I., & Cho, G.-C. (2019). Shear strength behavior and parameters of microbial gellan gum-treated soils: from sand to clay. *Acta Geotechnica*, *14*(2), 361–375. <https://doi.org/10.1007/s11440-018-0641-x>
- Chang, I., Im, J., & Cho, G.-C. (2016). Introduction of Microbial Biopolymers in Soil Treatment for Future Environmentally-Friendly and Sustainable Geotechnical Engineering. *Sustainability*, *8*(3), 251. <https://doi.org/10.3390/su8030251>
- Chang, I., Jeon, M., & Cho, G.-C. (2015). Application of Microbial Biopolymers as an Alternative Construction Binder for Earth Buildings in Underdeveloped Countries. *International Journal of Polymer Science*, *2015*, 1–9. <https://doi.org/10.1155/2015/326745>
- Chen, Z., Chen, W., Li, C., Pu, Y., & Sun, H. (2016). Effects of polyacrylamide on soil erosion and nutrient losses from substrate material in steep rocky slope stabilization projects. *Science of The Total Environment*, *554–555*, 26–33. <https://doi.org/10.1016/j.scitotenv.2016.02.173>
- Chen, Z., Wang, R., Han, P., Sun, H., Sun, H., Li, C., & Yang, L. (2018). Soil water repellency of the artificial soil and natural soil in rocky slopes as affected by the drought stress and polyacrylamide. *Science of The Total Environment*, *619–620*, 401–409. <https://doi.org/10.1016/j.scitotenv.2017.11.146>
- Choi, Y., Kim, M., Kim, Y., Jeon, J., & Seo, M. (2016). Implementation of Polyacrylamide in the Agricultural Environment and its Recent Review. *Korean Journal of Soil Science and Fertilizer*, *49*(5), 440–448. <https://doi.org/10.7745/KJSSF.2016.49.5.440>
- Costa, C. W., Lorandi, R., de Lollo, J. A., Imani, M., & Dupas, F. A. (2018). Surface runoff and accelerated erosion in a peri-urban wellhead area in southeastern Brazil. *Environmental Earth Sciences*, *77*(5), 160. <https://doi.org/10.1007/s12665-018-7366-x>
- Cui, M., Bao, B., Wu, Y., Hui, N., Li, M.-H., Wan, S., Han, S., Ren, F., & Zheng, J. (2024). Light grazing alleviates aeolian erosion–deposition effects on microbial communities in a semi-arid grassland. *Ecological Processes*, *13*(1), 31. <https://doi.org/10.1186/s13717-024-00510-y>
- Dede, V., Turan, İ. D., Dengiz, O., Serin, S., & Pacci, S. (2022). Effects of Periglacial Landforms on Soil Erosion Sensitivity Factors and Predicted by Artificial

- Intelligence Approach in Mount Cin, NE Turkey. *Eurasian Soil Science*, 55(12), 1857–1870. <https://doi.org/10.1134/S106422932260138X>
- Dong, Z., Wang, L., & Zhao, S. (2008). A potential compound for sand fixation synthesized from the effluent of pulp and paper mills. *Journal of Arid Environments*, 72(7), 1388–1393. <https://doi.org/10.1016/j.jaridenv.2008.02.008>
- Durán Zuazo, V. H., & Rodríguez Pleguezuelo, C. R. (2008). Soil-erosion and runoff prevention by plant covers. A review. *Agronomy for Sustainable Development*, 28(1), 65–86. <https://doi.org/10.1051/agro:2007062>
- Fatehi, H., Ong, D. E. L., Yu, J., & Chang, I. (2023). The Effects of Particle Size Distribution and Moisture Variation on Mechanical Strength of Biopolymer-Treated Soil. *Polymers*, 15(6), 1549. <https://doi.org/10.3390/polym15061549>
- Güneş, F. (2011). Çölleşme, Toplumsal-Ekonomik Boyut ve Sürdürülebilir Geçim Paradoksu: Konya-Karapınar Örneği. *Çalışma ve Toplum*, 1(28), 19–38. <https://dergipark.org.tr/pub/ct/issue/71795/1155169>
- Hamanaka, A., Sasaoka, T., Shimada, H., & Matsumoto, S. (2019). Experimental study on soil erosion under different soil composition using rainfall simulator. *Plant, Soil and Environment*, 65(4), 181–188. <https://doi.org/10.17221/68/2019-PSE>
- Hansen, Z. K., & Libecap, G. D. (2003). Small Farms, Externalities, and the Dust Bowl of the 1930s. *SSRN Electronic Journal*. <https://doi.org/10.2139/ssrn.460622>
- Hikmah, N. ‘Izzatul. (2019). Local Wisdom Of Farmers On The Northern Slopes Of Ungaran Mountain To Reduce Erosion On Agricultural Land (Case Study in Persen Hamlet, Sekaran Village). *Proceedings of the International Conference on Rural Studies in Asia (ICoRSIA 2018)*. <https://doi.org/10.2991/icorsia-18.2019.70>
- Huang, J., Kogbara, R. B., Hariharan, N., Masad, E. A., & Little, D. N. (2021). A state-of-the-art review of polymers used in soil stabilization. *Construction and Building Materials*, 305, 124685. <https://doi.org/10.1016/j.conbuildmat.2021.124685>
- Ikhsan, M., Safriani, M., Silvia, C. S., & Dari, R. (2021). Prediction of Land Erosion Events in the Down Stream Kreung Meureubo Watershed West Aceh District. *International Journal of Engineering, Science and Information Technology*, 1(4), 70–76. <https://doi.org/10.52088/ijesty.v1i4.173>
- İmamoglu, A., Eraslan, S., Coşkun, A., Saygın, F., & Dengiz, O. (2018). Farklı toprak özelliklerine bağlı toprak kabuk oluşumu. *Türk Coğrafya Dergisi*, 71, 47–52. <https://doi.org/10.17211/tcd.411983>
- Jarrah, M., Mayel, S., Tatarko, J., Funk, R., & Kuka, K. (2020). A review of wind erosion models: Data requirements, processes, and validity. *CATENA*, 187, 104388. <https://doi.org/10.1016/j.catena.2019.104388>
- Joga, J. R., & Varaprasad, B. J. S. (2019). Sustainable Improvement of Expansive Clays Using Xanthan Gum as a Biopolymer. *Civil Engineering Journal*, 5(9), 1893–1903. <https://doi.org/10.28991/cej-2019-03091380>
- Josifovski, J., & Nikolovska Atanasovska, A. (2022). Biopolymer soil stabilization as protection from slope erosion and shallow sliding. *EGU General Assembly Conference Abstracts*, EGU22-4236.
- Kukal, S. S., Kaur, M., Bawa, S. S., & Gupta, N. (2007). Water-drop stability of PVA-treated natural soil aggregates from different land uses. *CATENA*, 70(3), 475–479. <https://doi.org/10.1016/j.catena.2006.11.013>
- Kukal, S. S., & Sarkar, M. (2010). Splash erosion and infiltration in relation to mulching

- and polyvinyl alcohol application in semi-arid tropics. *Archives of Agronomy and Soil Science*, 56(6), 697–705. <https://doi.org/10.1080/03650340903208871>
- Kumar, S. A., Kannan, G., Vishweswaran, M., & Sujatha, E. R. (2022). *Review on Biopolymer Stabilization—A Natural Alternative for Erosion Control* (pp. 185–200). https://doi.org/10.1007/978-981-16-9744-9_12
- Lackóová, L., Pokrývková, J., Kozlovsky Dufková, J., Policht-Latawiec, A., Michałowska, K., & Dąbrowska, J. (2021). Long-Term Impact of Wind Erosion on the Particle Size Distribution of Soils in the Eastern Part of the European Union. *Entropy*, 23(8), 935. <https://doi.org/10.3390/e23080935>
- Larson, S., Ballard, J., Griggs, C., Newman, J. K., & Nestler, C. (2010). An Innovative Non-Petroleum Rhizobium Tropici Biopolymer Salt for Soil Stabilization. *Volume 5: Energy Systems Analysis, Thermodynamics and Sustainability; NanoEngineering for Energy; Engineering to Address Climate Change, Parts A and B*, 1279–1284. <https://doi.org/10.1115/IMECE2010-38933>
- Larson, S. L., Newman, J. K., Griggs, C. S., Beverly, M., & Nestler, C. C. (2012). *Biopolymers as an Alternative to Petroleum-Based Polymers for Soil Modification, ESTCP ER-0920: Treatability Studies*. <https://doi.org/10.21236/ADA569577>
- Larson, S. L., Nijak Jr, G., Corcoran, M., Lord, E., & Nestler, C. (2016). *Evaluation of Rhizobium tropiciderived biopolymer for erosion control of protective berms*. ERDC TR-16-5. US Army Corps of Engineers, Engineer Research and Development
- Le Bissonnais, Y., Singer, M. J., & Bradford, J. M. (1993). Assessment of soil erodibility : the relationship between soil properties, erosion processes and susceptibility to erosion. In *Farm Land Erosion* (pp. 87–96). Elsevier. <https://doi.org/10.1016/B978-0-444-81466-1.50012-5>
- Le, H. T., Rochelle-Newall, E., Ribolzi, O., Janeau, J. L., Huon, S., Latsachack, K., & Pommier, T. (2020). Land use strongly influences soil organic carbon and bacterial community export in runoff in tropical uplands-. *Land Degradation & Development*, 31(1), 118–132. <https://doi.org/10.1002/ldr.3433>
- Lee, M., Kwon, Y.-M., Park, D.-Y., Chang, I., & Cho, G.-C. (2022). Durability and strength degradation of xanthan gum based biopolymer treated soil subjected to severe weathering cycles. *Scientific Reports*, 12(1), 19453. <https://doi.org/10.1038/s41598-022-23823-4>
- Lemboye, K., Almajed, A., Alnuaim, A., Arab, M., & Alshibli, K. (2021). Improving sand wind erosion resistance using renewable agriculturally derived biopolymers. *Aeolian Research*, 49, 100663. <https://doi.org/10.1016/j.aeolia.2020.100663>
- Liu, J., Bai, Y., Li, D., Wang, Q., Qian, W., Wang, Y., Kanungo, D., & Wei, J. (2018). An Experimental Study on the Shear Behaviors of Polymer-Sand Composite Materials after Immersion. *Polymers*, 10(8), 924. <https://doi.org/10.3390/polym10080924>
- Lu, S., Wang, Z., Hu, Y., Liu, B., & Liu, J. (2018). Effectiveness and Durability of Polyacrylamide (PAM) and Polysaccharide (Jag C 162) in Reducing Soil Erosion under Simulated Rainfalls. *Water*, 10(3), 257. <https://doi.org/10.3390/w10030257>
- Ma, Q., Shuler, P. J., Aften, C. W., & Tang, Y. (2015). Theoretical studies of hydrolysis and stability of polyacrylamide polymers. *Polymer Degradation and Stability*, 121, 69–77. <https://doi.org/10.1016/j.polymdegradstab.2015.08.012>
- Majoro, F., Wali, U. G., Munyaneza, O., Naramabuye, F.-X., & Mukamwambali, C.

- (2020). On-site and Off-site Effects of Soil Erosion: Causal Analysis and Remedial Measures in Agricultural Land - a Review. *Rwanda Journal of Engineering, Science, Technology and Environment*, 3(2). <https://doi.org/10.4314/rjeste.v3i2.1>
- Mamedov, A. I., Levy, G. J., & Huang, C. (2015). Evolutionary Semantics of Anthropogenesis and Bioethics of Nbc-Technologies. *Biogeosystem Technique*, 5(3), 232–242. <https://doi.org/10.13187/bgt.2015.5.232>
- Mirzababaei, M., Arulrajah, A., & Ouston, M. (2017). Polymers for Stabilization of Soft Clay Soils. *Procedia Engineering*, 189, 25–32. <https://doi.org/10.1016/j.proeng.2017.05.005>
- Mo, J., Li, J., Wang, Z., Song, Z., Feng, J., Che, Y., Rong, J., & Gu, S. (2023). Spatiotemporal Evolution of Wind Erosion and Ecological Service Assessments in Northern Songnen Plain, China. *Sustainability*, 15(7), 5829. <https://doi.org/10.3390/su15075829>
- Mok, C. F., Ching, Y. C., Muhamad, F., Abu Osman, N. A., Hai, N. D., & Che Hassan, C. R. (2020). Adsorption of Dyes Using Poly(vinyl alcohol) (PVA) and PVA-Based Polymer Composite Adsorbents: A Review. *Journal of Polymers and the Environment*, 28(3), 775–793. <https://doi.org/10.1007/s10924-020-01656-4>
- Nasir Ahmad, N. S. B., Mustafa, F. B., Muhammad Yusoff, S. @ Y., & Didams, G. (2020). A systematic review of soil erosion control practices on the agricultural land in Asia. *International Soil and Water Conservation Research*, 8(2), 103–115. <https://doi.org/10.1016/j.iswcr.2020.04.001>
- Riksen, M. J. P. M., & de Graaff, J. (2001). On-site and off-site effects of wind erosion on European light soils. *Land Degradation & Development*, 12(1), 1–11. <https://doi.org/10.1002/ldr.423>
- Saygın, F., Dengiz, O., & İç, S. (2019). Mikro Havza Ölçeğinde Erozyona Duyarlılık Parametreleri İle Bazı Toprak Özellikleri Arasındaki İlişkilerin Belirlenmesi. *Toprak Su Dergisi*. <https://doi.org/10.21657/topraksu.654768>
- Shariatmadari, N., Reza, M., Tasuji, A., Ghadir, P., & Javadi, A. A. (2020). Experimental study on the effect of chitosan biopolymer on sandy soil stabilization. *E3S Web of Conferences*, 195, 06007. <https://doi.org/10.1051/e3sconf/202019506007>
- Silva, C. M. da, Brito, L. G. de, Silva, M. M. A. da, Carvalho, A. E. F. B. de, Almeida Júnior, J. P. de, Silva, M. F. da, Silva, W. A. da, & Pereira Filho, J. (2024). Quantification of water, soil and nutrient losses in the Farinha river basin, Carolina - MA, in the Cerrado biome. *Caderno Pedagógico*, 21(5), e4078. <https://doi.org/10.54033/cadpedv21n5-009>
- Susanti, Y., Syafrudin, S., & Helmi, M. (2019). Soil Erosion Modelling at Watershed Level in Indonesia: a Review. *E3S Web of Conferences*, 125, 01008. <https://doi.org/10.1051/e3sconf/201912501008>
- Tran Thi Phuong, A., Ilhan, C., Tran Thanh, N., & Gye-Chun, C. (2022). Numerical modelling of slope stabilization with xathan gum-treated soil. *Vietnam Journal of Earth Sciences*. <https://doi.org/10.15625/2615-9783/17924>
- Tuo, D., Xu, M., & Gao, G. (2018). Relative contributions of wind and water erosion to total soil loss and its effect on soil properties in sloping croplands of the Chinese Loess Plateau. *Science of The Total Environment*, 633, 1032–1040. <https://doi.org/10.1016/j.scitotenv.2018.03.237>
- Udumoh, U., Manuel, I. F., Ehiomogue, P., Ekpo, A., & Unyime, A. (2018). Estimating Erodibility Factor in Soils of Uyo, South-South Nigeria. *International Journal of*

- Current Research and Academic Review*, 6(11), 23–38. <https://doi.org/10.20546/ijcrar.2018.611.004>
- Vågen, & Winowiecki. (2019). Predicting the Spatial Distribution and Severity of Soil Erosion in the Global Tropics using Satellite Remote Sensing. *Remote Sensing*, 11(15), 1800. <https://doi.org/10.3390/rs11151800>
- Valarini, P. J., Díaz Alvarez, M. C., Gascó, J. M., Guerrero, F., & Tokeshi, H. (2003). Assessment of soil properties by organic matter and EM-microorganism incorporation. *Revista Brasileira de Ciência Do Solo*, 27(3), 519–525. <https://doi.org/10.1590/S0100-06832003000300013>
- Verma, S., Midha, V. K., & Choudhary, A. K. (2021). Effect of Parameters on the Runoff Erosion Control Performance of Structurally Modified Jute and Coir Geomeshes over Loamy Sand. *Tekstilec*, 64(2), 149–158. <https://doi.org/10.14502/Tekstilec2021.64.149-158>
- Vishweshwaran, M., Sujatha, E. R., Harshith, N., & Umesh, C. (2021). *Geotechnical Properties of β -Glucan-Treated Clayey Sand* (pp. 63–73). https://doi.org/10.1007/978-981-15-5101-7_6
- Weston, D. P., Lentz, R. D., Cahn, M. D., Ogle, R. S., Rothert, A. K., & Lydy, M. J. (2009). Toxicity of Anionic Polyacrylamide Formulations when Used for Erosion Control in Agriculture. *Journal of Environmental Quality*, 38(1), 238–247. <https://doi.org/10.2134/jeq2008.0109>
- Wuepper, D., Borrelli, P., & Finger, R. (2019). Countries and the global rate of soil erosion. *Nature Sustainability*, 3(1), 51–55. <https://doi.org/10.1038/s41893-019-0438-4>
- Wysocka-Czubaszek, A., & Czubaszek, R. (2015). Quantification of Water Erosion Rates on the Narew River Valley-Sides Using Universal Soil Loss Equation. *Polish Journal of Soil Science*, 47(1), 1. <https://doi.org/10.17951/pjss.2014.47.1.1>
- Yakupoglu, T., Rodrigo-Comino, J., & Cerdà, A. (2019). Potential Benefits of Polymers in Soil Erosion Control for Agronomical Plans: A Laboratory Experiment. *Agronomy*, 9(6), 276. <https://doi.org/10.3390/agronomy9060276>
- Yang, Q., Pei, X., & Huang, R. (2019). Impact of polymer mixtures on the stabilization and erosion control of silty sand slope. *Journal of Mountain Science*, 16(2), 470–485. <https://doi.org/10.1007/s11629-018-4905-6>
- Yonter, G. (2010). Effects of Polyvinylalcohol (PVA) and Polyacrylamide (PAM) as Soil Conditioners on Erosion by Runoff and by Splash Under Laboratory Conditions. *Ekoloji*, 19(77), 35–41. <https://doi.org/10.5053/ekoloji.2010.776>
- Yue, Y., Ni, J., Ciais, P., Piao, S., Wang, T., Huang, M., Borthwick, A. G. L., Li, T., Wang, Y., Chappell, A., & Van Oost, K. (2016). Lateral transport of soil carbon and land–atmosphere CO₂ flux induced by water erosion in China. *Proceedings of the National Academy of Sciences*, 113(24), 6617–6622. <https://doi.org/10.1073/pnas.1523358113>
- Zhang, J., Wang, Q., Mu, W., Wei, K., Guo, Y., & Sun, Y. (2022). Experimental Investigation of the Different Polyacrylamide Dosages on Soil Water Movement under Brackish Water Infiltration. *Polymers*, 14(12), 2495. <https://doi.org/10.3390/polym14122495>
- Zhang, Y., Zhang, H., Peng, B., & Yang, H. (2003). Soil erosion and its impacts on environment in Yixing tea plantation of Jiangsu Province. *Chinese Geographical Science*, 13(2), 142–148. <https://doi.org/10.1007/s11769-003-0008-5>

Zhou, C., Huang, W., Qiu, S., & Liu, Z. (2021). A quantitative study on the amount of water-retaining agent based on adhesive-modified red bed weathered soil. *Bulletin of Engineering Geology and the Environment*, 80(4), 3139–3150. <https://doi.org/10.1007/s10064-021-02113-9>

About The Authors

Vildan ERCİ, PhD, is an assistant professor in the Department of Soil Science and Nutrition, Faculty of Agriculture, Selçuk University, Konya, Türkiye. She holds two PhDs: in Soil Science from Selcuk University and Bioengineering from Yıldız Technical University respectively. Her main areas of interest are soil erosion, soil stabilizers and applications.

E-mail: vildanerci@selcuk.edu.tr, **ORCID:** 0000-0002-0373-024X

Similarity Index

The similarity index obtained from the plagiarism software for this book chapter is 8%.

CHAPTER 7

Investigation of the Color, Glossiness, and Surface Roughness Properties of Particleboards Produced with Activated Carbon Addition

Mehmet Emin ERGÜN

Alanya Alaaddin Keykubat University, Türkiye

Filiz KOYUNCU

Dicle University, Türkiye

Abdullah İSTEK

Bartın University, Türkiye

Ahmet CAN

Bartın University, Türkiye

İsmail ÖZLÜSOYU

Bartın University, Türkiye

To Cite This Chapter:

Ergun, M.E., Koyuncu, F., Istek, A., Can, A. & Ozlusoylu, I. (2024). Investigation of the Color, Glossiness, and Surface Roughness Properties of Particleboards Produced with Activated Carbon Addition. In H. Gokmese, S. Bulbul, & Y. Uzun (Eds.), *Current Studies in Materials Science and Engineering* (pp. 102-112). ISRES Publishing.

Introduction

The significance of wood waste has emerged as a primary area of interest in the realm of sustainable materials engineering, offering a pathway for the development of environmentally conscious products and the optimization of resources. Particleboards are manufactured by combining wood particles or chips with a binder and subjecting them to high pressure and temperature (Kurt, 2022). The other one, the manufacturing of activated carbon-added particleboards is a revolutionary method for fabricating composite materials, among the many applications in this field (Zamani et al., 2022). This novel methodology effectively addresses environmental concerns related to waste

accumulation and advances the development of high-performance materials with improved aesthetic and functional properties by utilizing Scots pine wood waste as a primary feedstock and incorporating zinc chloride as an activation agent.

The utilization of Scots pine (*Pinus sylvestris*) wood waste as a raw material for particleboard production signifies a departure from conventional practices towards a more sustainable and circular economy-driven approach. Scots pine, a prevalent softwood species renowned for its abundance and versatility, contributes significantly to the global pool of wood waste generated by forestry and timber industries (Schubert et al., 2022). By repurposing this abundant yet underutilized resource, researchers and manufacturers endeavor to mitigate the environmental impact of waste accumulation while simultaneously creating value-added products with diverse applications (Nayak and Bhushan, 2019).

At the core of this innovative approach lies the incorporation of zinc chloride as an activation agent, which catalyzes the conversion of lignocellulosic precursors into activated carbon matrices within the wood-based panel structure (Gandini and Lacerda, 2015). Zinc chloride, a versatile chemical compound renowned for its catalytic properties, plays a pivotal role in facilitating the carbonization process, thereby enhancing the structural integrity and performance of the wood-based panel. Through a series of complex chemical reactions, zinc chloride acts as a catalyst, promoting the formation of carbonaceous structures that imbue the wood-based panel with unique properties such as improved thermal stability, mechanical strength, and chemical resistance (Zamani et al., 2022).

The integration of activated carbon into the particleboard matrix introduces a host of beneficial characteristics, chief among them being changed surface properties such as glossiness, color, and surface roughness. These attributes not only contribute to the aesthetic appeal of the particleboards but also play a crucial role in determining their functional suitability across various end-use applications (Dai, and Fan, 2014).

Glossiness, a key indicator of surface quality and visual perception, is profoundly influenced by the scattering and reflection of incident light on the particleboard surface. (Csanády et al., 2015) The incorporation of activated carbon and zinc chloride activation introduces subtle changes in surface microstructure and chemical composition, thereby influencing the overall glossiness of the materials (Dujearic-Stephane et al., 2021). By optimizing activation protocols and fine-tuning processing parameters, manufacturers can achieve desired levels of glossiness, enhancing the visual appeal and marketability of the final product.

The sensitivity of the human eye to various wavelengths of light is not constant and varies from person to person. Thanks to the devices developed to date, color measurements can provide more precise results compared to those made based on human visual judgments. Today, color measurements are conducted using spectrophotometers (Gençer and Kurt, 2023; Kurt and Can, 2021) Color, another critical aspect of surface appearance, serves as a tangible expression of material quality and visual appeal (Sivrikaya et al., 2019). The colorimetric properties of activated carbon-added particleboards are influenced by the intricate interplay between light absorption, reflection, and transmission within the carbonaceous matrix. Through selection of activation agents and control of processing conditions, manufacturers can tailor the color characteristics of particleboards to meet diverse aesthetic preferences and market trends, thereby expanding the range of potential applications for these innovative materials.

Surface roughness, a fundamental determinant of tactile perception and functional performance, embodies the topographical intricacies of particleboard surfaces (Krystofiak et al., 2022). The surface roughness of activated carbon-added particleboards, influenced by factors such as particle size distribution, compaction pressure, and activation duration, directly impacts their mechanical properties and surface functionality. By optimizing activation parameters and refining manufacturing techniques, researchers and manufacturers can achieve desired levels of surface roughness, enhancing the usability and applicability of particleboards across diverse end-use scenarios.

In this research, 1%, 5%, and 9% of the single-layer particleboard manufacturing process was modified to add activated carbon made from pine wood waste and zinc chloride as the activating agent. The glossiness, color change, and surface roughness values of the produced particleboards were investigated.

Material and Method

Materials

Waste wood from a Scots pine (*Pinus sylvestris*) woodworking factory in Seydişehir, Konya, was provided free of charge for this investigation. The manufacturing of activated carbon included the use of the chemical activation process. Zinc chloride ($ZnCl_2$) served as the chemical activator. Particleboards were made using chips that came from broadleaf (*Fagus orientalis/Carpinus betulus/Populus nigra*) and coniferous (*Pinus nigra*) trees. The urea-formaldehyde (UF) adhesive used in this experiment has the following properties: a density between 1265 and 1285 kg/m³, a viscosity between 250 and 310 mPa•s at 22 °C, and a solid content 65%. To cure the adhesive, a solution containing 20% ammonium chloride was applied. The ratio of this solution to the weight of the adhesive was 1.5%. All the chemicals used in this experiment were of analytical purity and were provided by Fluka (Buch, Switzerland) and Merck (Darmstadt, Germany).

Production of single-layer particleboard

The chips obtained from the particleboard plant resulted in the production of single-layer particleboards. The chips were dried to get their moisture level down to 1% to 3% before the adhesive was applied. They were then sealed in plastic bags to keep the air from getting to them. Ultrafiltration (UF) with a solid concentration of 65% was employed in the investigation. Depending on the dry matter content, different amounts of activated carbon 1%, 5%, and 9% were added to the adhesive. After that, the mixture was aggressively agitated for 30 minutes at a speed of 600 revolutions per minute. Adhesive cannon inside a revolving drum mixer (ECOMIX, 42,750 Saint-Denis de Cabanne) was used to apply the adhesive. After manually distributing the board with a wooden mold, it was put in a hot press measuring 400 × 400 × 12 mm. The experimental boards were then created using a hot press (SSP180 Cemil Usta, Türkiye) with a specific pressure of 4.0 N/mm², a temperature of 175°C, and a 5 min duration. Following the hot press, the boards were allowed to cool before being readied for testing. Each group created three particleboards. After pressing, the boards were cooled and conditioned at 65 ± 5% relative humidity and 20 ± 2°C temperature to reach equilibrium moisture content.

Characterization

TESCAN, Brno, Czech Republic, used a scanning electron microscope (SEM) to analyze the particleboard morphologies (Maia3 Xmu model). A thin coating of 5 nm thick gold

was put to the samples to improve the conductivity of the particleboards. The SEM microscope was used to analyze microstructure pictures at a voltage of 20.0 kV.

An oxygen-filled atmosphere was used to conduct proximate analysis on a 2-3 mg sample using the Hitachi STA 7300 thermal gravimetric (TG/DTG) analyzer. In their proximate analysis, Cai et al. (2017) used the TGA method and the equations' parameters to calculate moisture (M), fixed carbon (FC), ash (A), and volatile matter (VM).

$$M = \frac{W - B}{W} \quad (1)$$

$$VM = \frac{B - C}{W} \quad (2)$$

$$A = \frac{D}{W} \quad (3)$$

$$FC = 1 - (M + A + VM) \quad (4)$$

A Konica Minolta spectrophotometer was used to test the particleboards' colors (Osaka, Japan). As per ISO 7724-2 (1984), the data obtained from randomly selected regions were analyzed to derive the L^* , a^* , and b^* values. The CIE Lab system was utilized to evaluate the color coordinates. The L^* , a^* , and b^* color coordinates of the experimental boards were established for each alteration, for particleboards with and without activated carbon. The black-white axis is represented by the L^* axis, where black is represented by $L^* = 0$ and white by $L^* = 100$. The red-green color spectrum is represented by the a^* axis, where positive values indicate red and negative ones denote green. The yellow-blue color spectrum is represented by the b^* axis, where positive values denote yellow and negative ones, blue. The difference between the results acquired by the particleboard, which contained varying ratios of activated carbon, and the control group (0% activated carbon) was used to determine changes in the color coordinates (ΔL^* , Δa^* , and Δb^*). Using Equation (5), the total color differences (ΔE^*) were determined.

$$\Delta E^* = [(\Delta a^*)^2 + (\Delta b^*)^2 + (\Delta L^*)^2]^{1/2} \quad (5)$$

where the variables ΔL^* , Δa^* , and Δb^* denote the change in L^* , a^* , and b^* , respectively. The whole color shift is represented by ΔE^* .

A Konica Minolta Multi gloss 268 plus was used to test the gloss. According to ISO 2813.1994, the radiation's angle of incidence was 20°, 60° and 80. In every test sample, six measurements were taken.

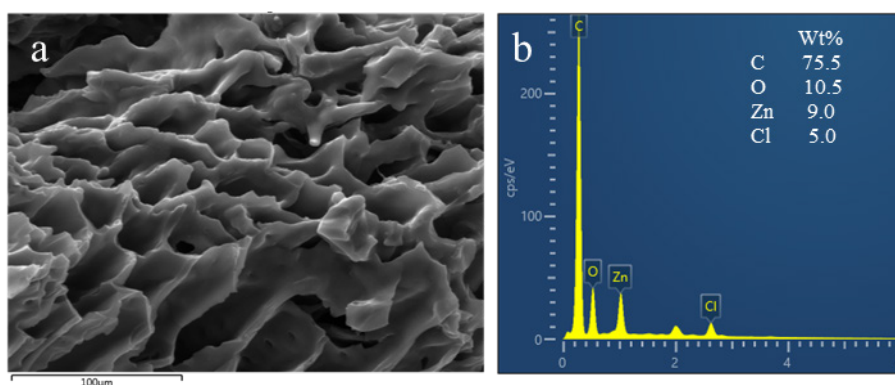
Measurements of surface roughness were conducted using the Mitutoyo SurfTest SJ-301. The test materials were assessed for mean surface roughness (R_a) and maximum height (R_z). By ISO 4287, side measurements were taken on the surfaces of the test and control samples. The measurements were applied to a boundary wavelength of 8 mm, a scanning length of 12 mm, and a velocity of 0.5 mm/s. To assess each group's surface roughness, ten measurements were taken.

Results and Discussion

Characterization of activated carbon

In our previous study (Ergün et al., 2024), the TGA, BET, XRD, FTIR, and particle size measurements of activated carbon obtained from Scots pine wood waste treated with ZnCl_2 activation agents were examined. In this study, the SEM and EDS analysis of the activated carbon obtained from Scots pine wood waste treated with ZnCl_2 activation agents are presented in Figure 1.

Figure 1
SEM (A) and EDS (B) Analyses of Activated Carbon

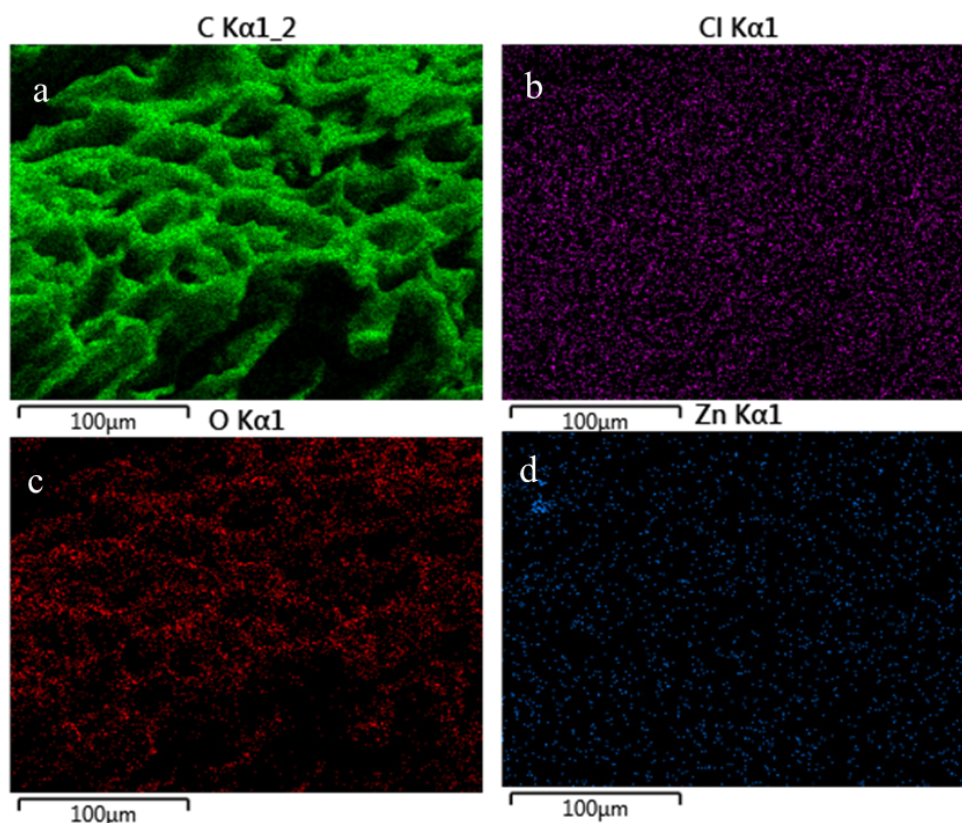


When the SEM image of the activated carbon was examined (Figure 1a), the density and distribution of pores on the surface were evident. The pore sizes appear quite homogeneous, which suggests a high adsorption capacity of the material. This regularity in surface morphology indicates that the activated carbon can selectively adsorb molecules of specific sizes. The presence of micropores is particularly significant for the ability to capture small molecules, making the activated carbon ideal for gas phase applications. On the other hand, the observation of mesopores indicates suitability for the adsorption of larger molecules in liquid-phase applications. The thickness and robustness of the pore walls can affect the mechanical durability and long-term usage of the activated carbon. The SEM image shows that the pore walls are smooth and sturdy, indicating that the material can maintain its form even under high pressure and temperature conditions. Previous studies have observed similar microstructures in activated carbon produced using ZnCl_2 activation agents (Bülbül and Ergün, 2024; Ergün and Ergün, 2024).

As shown in Figure 1b, the elemental analysis of the activated carbon produced from Scots pine wood waste using ZnCl_2 activation agents revealed the presence of 75.5% carbon (C), 10.5% oxygen (O), 9% zinc (Zn), and 5% chlorine (Cl). Elemental analysis of scot pine wood indicates that it contains approximately 50% C and 46% O (Piernik et al., 2022). The reduction of O in the activated carbon structure is due to the removal of oxygen present in the wood waste during activation. In a study by Ergün and Bülbül (2022), the EDS analysis of activated carbon produced with ZnCl_2 activation agents detected 79% C, 10% O, 7.5% Zn, and 3% Cl.

The elemental distributions of activated carbons obtained from Scots pine wood waste treated with ZnCl_2 activation agents were analyzed using Mapping analysis and are presented in Figure 2.

Figure 2
Mapping Analyses of Activated Carbon



The SEM Mapping images have demonstrated that all elements are homogeneously distributed in the produced activated carbon (Figure 2). Additionally, Figures 2c and 2d demonstrate the presence of Zn and Cl elements as a result of using ZnCl₂ as the activation agent. Similar results can be achieved by producing activated carbons from various raw materials using ZnCl₂ activation agents (Ergün and Bülbül, 2022; Özdemir et al., 2023).

Table 1
Proximate analysis results of the activated carbon

	Moisture	Volatile matter	Ash	Fixed carbon
Activated carbon	3.96	26.64	7.26	62.14

The analysis results of the activated carbon indicate a high fixed carbon content of 62.14%, suggesting that the activated carbon has undergone extensive carbonization, thereby possessing a high adsorption capacity. The moisture content of 3.96% shows that the material is relatively dry, minimizing the adsorption of unwanted adsorbates such as water vapor. The volatile matter content of 26.64% indicates the presence of a significant combustible component, which should be considered during thermal processing. The ash content of 7.26% indicates that the activated carbon contains relatively low inorganic matter, typically signifying a purer material.

The high fixed carbon content provides a large surface area for adsorption processes, which is crucial for effectively removing harmful substances from air or liquids, particularly in industrial applications (Singh et al., 2020). The low moisture

content helps maintain the performance of the activated carbon during storage and use. The presence of volatile matter requires careful management of gases that may form during the activation process (Pui et al., 2019). The ash content indicates the purity of the activated carbon and potential contamination sources; therefore, low ash content is preferred for applications in the food and pharmaceutical industries (Vunain et al., 2017).

These analysis results provide an essential basis for assessing the suitability of activated carbon for various applications. For instance, the high fixed carbon content and low ash content suggest that the activated carbon can be effectively used in water purification systems (Jjagwe et al., 2021). The volatile matter content can influence the behavior of activated carbon during thermal processes such as pyrolysis and gasification (Braghiroli et al., 2020). Other studies have found that fixed carbon content varies between 58% and 91% (Güzel et al., 2015; Koyuncu et al., 2022; Inal et al., 2023).

Characterization of Particleboards

This study aims to investigate the effects of activated carbon addition on the color, gloss, and surface roughness properties of particleboards. Activated carbon was produced from Scots pine wood residues using zinc chloride. The activated carbon was characterized using various techniques. Subsequently, the produced activated carbon was added to single-layer particleboards at ratios of 1%, 5%, and 9%. The chipboards produced were named E1, E2, and E3, respectively, according to the addition rates of 1%, 5%, and 9%. The gloss properties of the particleboards are examined in Table 2.

Table 2

Glossiness values of activated carbon reinforced particleboards

	20°	60°	80°
Control	0.5	2.2	1.9
E1	0.5	2.2	1.7
E2	0.5	2.1	1.7
E3	0.5	1.9	1.6

The gloss values were measured at different angles (20°, 60°, 80°). When compared to the control sample, it is observed that samples E1, E2, and E3 have lower values at a 60° angle. This indicates that activated carbon reduces the surface's ability to reflect light. Similarly, a decrease in gloss values is observed in samples E1, E2, and E3 at an 80° angle.

The color changes of particleboards reinforced with 1%, 5%, and 9% activated carbon are presented in Table 3.

Table 3

Color changes of activated carbon reinforced particleboards

	L*	a*	b*	ΔE
Control	58.92	7.89	23.16	-
E1	59.41	8.29	25.49	2.93
E2	57.82	6.72	23.14	3.50
E3	54.43	5.93	20.41	6.66

The color measurements were conducted based on the L*, a*, and b* values.

The L* value represents the gloss level of the samples; the a* value indicates the color tone from green to red, and the b* value represents the color tone from blue to yellow. Compared to the control sample, an increase in L* values and varying changes in a* and b* values were observed in samples E1, E2, and E3. The delta E value expresses the color difference, and the values of 2.93, 3.50, and 6.66 in samples E1, E2, and E3, respectively, indicate a visually noticeable color change. The addition of activated carbon, with its black color, leads to a darkening of the color when added in particleboard production. Previous studies have also found that adding activated carbon up to 7.5% increases the total color change (Ergun et al., 2023), similar results to the current study.

Table 4 displays the surface roughness values Ra and Rmax for particleboards with varying amounts of activated carbon.

Table 4

Surface roughness values of activated carbon reinforced particleboards

	Ra	Rmax
Control	23.13	200.07
E1	22.66	187.38
E2	21.36	189.49
E3	20.25	192.65

The values of Ra and Rmax were used to quantify surface roughness. Sample E1 showed a drop in both values when compared to the control sample, suggesting a smoother surface. Ra and Rmax values increased and decreased, respectively, in sample E2. When comparing sample E3 to the control sample, a decline in both values was seen. These findings imply that the amount of activated carbon added might have varying effects on surface roughness. It was shown that a smoother surface results from carbon fiber reinforcing (Durmaz et al., 2020). These results indicate that the addition of activated carbon can affect and potentially improve the aesthetic properties of particleboards, enhancing their potential for use in furniture and interior design.

Conclusion

In conclusion, the utilization of Scots pine wood waste as a raw material for particleboard production, coupled with the incorporation of zinc chloride as an activation agent, offers a promising avenue for the development of sustainable and high-performance composite materials. By repurposing abundant yet underutilized wood waste, researchers and manufacturers can address environmental concerns related to waste accumulation while creating value-added products with enhanced aesthetic and functional properties.

The integration of activated carbon into the particleboard matrix introduces changes in surface properties such as glossiness, color, and surface roughness. These attributes not only contribute to the visual appeal of the particleboards but also play a crucial role in determining their functional suitability across various end-use applications. Through optimized activation protocols and fine-tuning of processing parameters, manufacturers can achieve desired levels of glossiness, color, and surface roughness, thereby enhancing the marketability and usability of the final product.

The characterization of the particleboards, including morphological analysis using scanning electron microscopy and proximate analysis using thermogravimetric analysis, provides valuable insights into the structural and chemical properties of the materials. Additionally, color measurements using spectrophotometers and surface roughness measurements using profilometers offer quantitative assessments of the

particleboards' color and tactile characteristics. Overall, this study demonstrates the potential of incorporating activated carbon from pine wood waste with zinc chloride as an activating agent in single-layer particleboard production. Further research can explore the optimization of activation parameters and explore additional applications for these innovative materials in various industries. By harnessing the potential of wood waste and adopting sustainable manufacturing practices, the development of environmentally conscious products can be realized, contributing to the advancement of sustainable materials engineering and resource optimization.

Funding

This research was funded by the Scientific and Technological Research Council of Türkiye (TUBITAK) (Project No: 121C429).

References

- Braghiroli, F. L., Bouaffif, H., Neculita, C. M., & Koubaa, A. (2020). Influence of pyro-gasification and activation conditions on the porosity of activated biochars: a literature review. *Waste and Biomass Valorization*, *11*, 5079-5098.
- Bülbül, Ş., & Ergün, H. (2024). Investigation of the usability of activated carbon as a filling material in nitrile butadiene rubber/natural rubber components and modeling by regression analysis. *Journal of Elastomers & Plastics*, *56*(1), 53-73.
- Cai, J., He, Y., Yu, X., Banks, S. W., Yang, Y., Zhang, X., & Bridgwater, A. V. (2017). Review of physicochemical properties and analytical characterization of lignocellulosic biomass. *Renewable and sustainable energy reviews*, *76*, 309-322.
- Csanády, E., Magoss, E., Tolvaj, L., Csanády, E., Magoss, E., & Tolvaj, L. (2015). Wood Surface Stability. *Quality of Machined Wood Surfaces*, 13-108.
- Dai, D., & Fan, M. (2014). Wood fibres as reinforcements in natural fibre composites: structure, properties, processing and applications. In *Natural Fibre Composites* (pp. 3-65). Woodhead publishing.
- Dujearic-Stephane, K., Gupta, M., Kumar, A., Sharma, V., Pandit, S., Bocchetta, P., & Kumar, Y. (2021). The effect of modifications of activated carbon materials on the capacitive performance: surface, microstructure, and wettability. *Journal of Composites Science*, *5*(3), 66.
- Durmaz, S., Erdil, Y. Z., & Avcı, E. (2020). Screw withdrawal resistance and surface roughness of woven carbon and glass fiber-reinforced wood-plastic composites. *BioResources*, *15*(1), 1894-1903.
- Ergün, M. E., & Bulbul, S. (2022). Production and characterization of activated carbon from Black Poplar (*Populus Nigra*) wood waste with different chemical activation methods. *International Advanced Researches and Engineering Journal*, *6*(3), 167-175.
- Ergun, M. E., & Ergun, H. (2024). Influence of activated carbon concentration on foam material properties: Design and optimization. *Arabian Journal for Science and Engineering*, *49*(4), 4877-4888.
- Ergün, M. E., İstek, A., Özlüsoylu, İ., Koyuncu, F., & Bülbül, Ş. (2024). Low formaldehyde-emission particleboards with the addition of Scots pine wood waste derived activated carbon. *Wood Material Science & Engineering*, 1-11.
- Ergun, M. E., Özlüsoylu, İ., İstek, A., & Can, A. (2023). Analysis and impact of activated carbon incorporation into urea-formaldehyde adhesive on the properties of

- particleboard. *Coatings*, 13(9), 1476.
- Gandini, A., & Lacerda, T. M. (2015). From monomers to polymers from renewable resources: Recent advances. *Progress in Polymer Science*, 48, 1-39.
- Gençer, A., & Kurt, R. (2023). Buğday saplarından KOH yöntemiyle elde edilen kağıt hamurlarının parlaklık ve opaklık değerlerinin incelenmesi ve modellenmesi. *Journal of Bartın Faculty of Forestry*, 25(1), 1-8.
- Güzel, F., Saygılı, H., Saygılı, G. A., & Koyuncu, F. (2015). New low-cost nanoporous carbonaceous adsorbent developed from carob (*Ceratonia siliqua*) processing industry waste for the adsorption of anionic textile dye: Characterization, equilibrium and kinetic modeling. *Journal of Molecular Liquids*, 206, 244-255.
- Inal, I. I. G., Koyuncu, F., & Güzel, F. (2023). Investigating the surface properties of red pepper industrial waste-based activated carbons for use as reversible supercapacitor electrodes. *Diamond and Related Materials*, 138, 110212.
- Jjagwe, J., Olupot, P. W., Menya, E., & Kalibbala, H. M. (2021). Synthesis and application of granular activated carbon from biomass waste materials for water treatment: A review. *Journal of Bioresources and Bioproducts*, 6(4), 292-322.
- Koyuncu, F., Güzel, F., & Inal, İ. I. G. (2022). High surface area and supermicroporous activated carbon from capsicum (*Capsicum annum* L.) industrial processing pulp via single-step KOH-catalyzed pyrolysis: Production optimization, characterization and its some water pollutants removal and supercapacitor performance. *Diamond and Related Materials*, 124, 108920.
- Krystofiak, T., Can, A., & Lis, B. (2022). Investigation of roughness and adhesion strength properties of pine and poplar wood heat treated in air and under vacuum after artificial aging. *Coatings*, 12(12), 1910.
- Kurt, R. (2022). Control of system parameters by estimating screw withdrawal strength values of particleboards using artificial neural network-based statistical control charts. *Journal of Wood Science*, 68(1), 64.
- Kurt, R., & Can, A. (2021). Optimization of the effect of accelerated weathering conditions on wood surfaces via the Taguchi method. *BioResources*, 16(1), 1642.
- Nayak, A., & Bhushan, B. (2019). An overview of the recent trends on the waste valorization techniques for food wastes. *Journal of environmental management*, 233, 352-370.
- Özdemir, D., Bulbul, S., & Ergün, M. E. (2023). Production of activated carbon from the waste paper by chemical activation method. *International Advanced Researches and Engineering Journal*, 7(1), 52-61.
- Piernik, M., Woźniak, M., Pinkowski, G., Szentner, K., Ratajczak, I., & Krauss, A. (2022). Impact of the heat treatment duration on color and selected mechanical and chemical properties of Scots pine wood. *Materials*, 15(15), 5425.
- Pui, W. K., Yusoff, R., & Aroua, M. K. (2019). A review on activated carbon adsorption for volatile organic compounds (VOCs). *Reviews in Chemical Engineering*, 35(5), 649-668.
- Schubert, M., Panzarasa, G., & Burgert, I. (2022). Sustainability in wood products: a new perspective for handling natural diversity. *Chemical Reviews*, 123(5), 1889-1924.
- Singh, R. K., Mishra, S. K., Velramar, B., & Kumar, P. R. (2020). Development of biologically-based activated carbon for advanced water and wastewater treatment process. In *Bioremediation of Pollutants* (pp. 215-225). Elsevier.
- Sivrikaya, H., Tesařová, D., Jeřábková, E., & Can, A. (2019). Color change and emission

of volatile organic compounds from Scots pine exposed to heat and vacuum-heat treatment. *Journal of Building Engineering*, 26, 100918.

Vunain, E., Kenneth, D., & Biswick, T. (2017). Synthesis and characterization of low-cost activated carbon prepared from Malawian baobab fruit shells by H₃PO₄ activation for removal of Cu (II) ions: equilibrium and kinetics studies. *Applied Water Science*, 7, 4301-4319.

Zamani, R., Kazemi Najafi, S., & Younesi, H. (2022). Utilization of activated carbon as an additive for urea-formaldehyde resin in medium density fiberboard (MDF) manufacturing. *Journal of Adhesion Science and Technology*, 36(21), 2285-2296.

About The Authors

Mehmet Emin ERGÜN is an associate professor at Forestry and Forest Products, Akseki Vocational Schools, Alanya Alaaddin Keykubat University. His research topics focus on biomass conversion, renewable materials and green chemistry.

E-mail: mehmet.ergun@alanya.edu.tr, **ORCID:** 0000-0002-9938-7561

Filiz KOYUNCU is a PHD in the Institute of Natural and Applied Sciences, Department of Chemistry, Dicle University. Her research topics are biomass conversion, activated carbon production and related materials.

E-mail: flkync@gmail.com, **ORCID:** 0000-0002-9879-8801

Abdullah İSTEK is a professor in the Department of Forest Industry Engineering at Bartın University, Türkiye. His research interests are wood-based composites, forest products chemistry, and polymer composites.

E-mail: aistek@bartin.edu.tr, **ORCID:** 0000-0002-3357-9245

Ahmet CAN is an associate professor in the Department of Forest Industry Engineering at Bartın University, Türkiye. His research interests are wood protection, surface treatments, Energy storage, and polymer composites.

E-mail: acan@bartin.edu.tr, **ORCID:** 0000-0001-5926-6039

İsmail ÖZLÜSOYLU is an associate professor in the Department of Forest Industry Engineering at Bartın University, Türkiye. His research interests include wood-based composite, heat and sound insulation, wood bark board and wood chemistry.

E-mail: iozlusoylu@bartin.edu.tr, **ORCID:** 0000-0002-0391-4794

Similarity Index

The similarity index obtained from the plagiarism software for this book chapter is 18%.

CHAPTER 8

Multi-Directional Forging Process as a Severe Plastic Deformation Method

Mehmet ŞAHBAZ

Karamanoğlu Mehmetbey University, Türkiye

To Cite This Chapter:

Sahbaz, M. (2024). Multi-Directional Forging Process as a Severe Plastic Deformation Method. In H. Gokmese, S. Bulbul, & Y. Uzun (Eds.), *Current Studies in Materials Science and Engineering* (pp. 113-127). ISRES Publishing.

Introduction

In recent years, researchers have discovered that it is possible to make significant structural changes to metals by using ‘severe plastic deformation’ (SPD) techniques. It has been reported that numerous microstructural phenomena, such as the reduction of material grain size to the nanolevel, increased dislocation density, the formation of twins, and the precipitation of secondary phases, occur as a result of SPD (Ruslan Z. Valiev et al., 2013; Ruslan Z. Valiev & Langdon, 2006). The considerable improvement in the mechanical properties of materials due to these microstructural changes has attracted the attention of researchers. Unlike traditional methods, SPD increases the strength of the material without increasing its brittleness; in some cases, it even reduces brittleness. The simultaneous enhancement of material strength and toughness has been a significant finding for material developers, making SPD methods and related studies a focal point of interest worldwide (Bagherpour et al., 2018; V. Segal, 2018). Developing nanomaterials using SPD methods has proven to be both economically and efficiently advantageous compared to other methods. Consequently, the variety of SPD methods is expanding, and the number of studies in this field is steadily increasing.

One of the well-known SPD methods is “multi-directional forging” (MDF), that frequently applied to ferrous metals and, particularly in recent years, to non-ferrous metals. It is used in the development of magnesium, aluminum, titanium alloys, etc., which are notable for their low specific gravity and other important properties. These materials are often preferred in fields such as aerospace and automotive due to their lightness, and improvements in these materials can make significant contributions to these sectors (Bahmani et al., 2019).

In this study, the widely used MDF among SPD methods is explained in detail. Additionally, examples of its application to commonly used industrial metal materials are provided, along with their results. This section will first provide general information about the MDF method, the materials it is applied to (such as aluminum, magnesium, titanium, copper, and certain types of steel), and their importance. Following this, a

literature review will briefly present some studies conducted in these areas.

History and Methods of SPD

The significance of Severe Plastic Deformation (SPD) in metalworking dates back to the Bronze to Iron Age transition for crafting weapons like sword production by repetitive hammering and folding. The foundational principles of SPD techniques originated from P.W. Bridgman's research at Harvard University in the 1930s. His study on the impact of high hydrostatic pressure and shear deformation on solids earned him the Nobel Prize in Physics in 1946 for groundbreaking work (Bridgman, 1935; Percy Williams Bridgman, 1995; Edalati & Horita, 2016b). The successful early applications of these principles included "equal channel angular pressing" (ECAP), developed by Segal et al., in Minsk in the 1970s (Bagherpour et al., 2018; Segal, 2018; Segal, 1977), and "high-pressure torsion" (HPT), derived from Bridgman's work but not widely developed until the 1980s at the Russian Institute of Metal Physics. Severe plastic deformation has emerged as an alternative to traditional technologies. This method focuses on plastically deforming the material to the desired thickness without changing its overall dimensions. For instance, the ECAP method was designed to subject cylindrical or rectangular cross-section billets to severe plastic deformation while maintaining the same cross-sectional area.

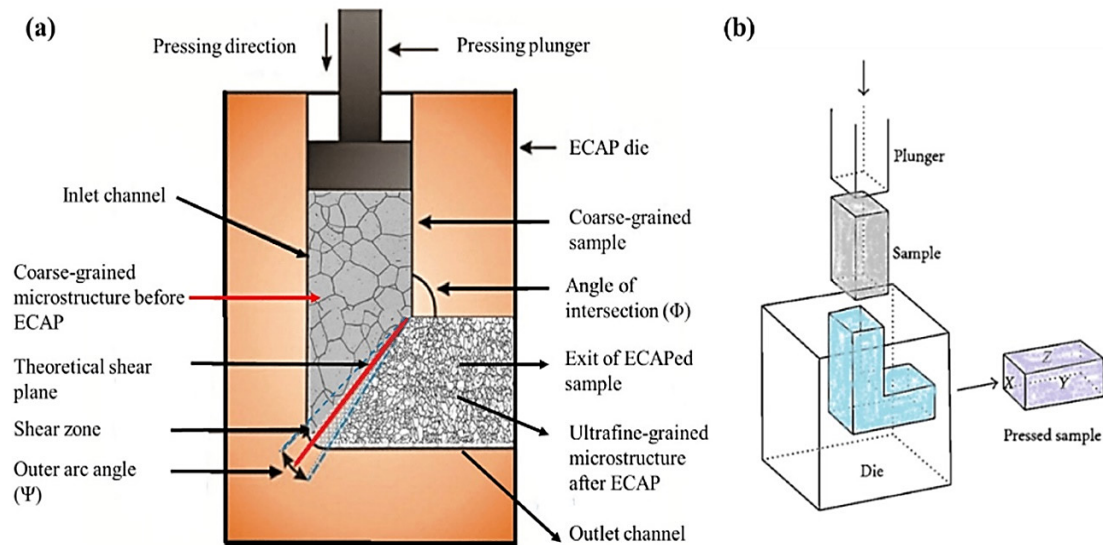
SPD refers to metalworking techniques that involve high stresses, leading to a high dislocation density and ultrafine grain or nanocrystalline structure. It is described as applying stress without significant dimensional changes, resulting in hydrostatic pressure. The process is similar to mechanical alloying, which the researchers described in 1983 as "severe plastic deformation". The mentioned two important SPD methods (ECAP, and HPT) are briefly described below.

Equal Channel Angular Pressing (ECAP)

ECAP is a technique used to apply severe plastic deformation to metallic materials to reduce grain size and improve mechanical properties. Segal designed this method to enhance the plastic deformation capacity of materials and alter their microstructure. During the 1980s and 1990s, ECAP gained interest among researchers worldwide and was applied to various metals, particularly aluminum alloys, to improve their mechanical properties (Iwahashi et al., 1996; Segal et al., 1981). Nowadays, ECAP is widely used to produce high-strength, fine-grained, and nanostructured materials. The method finds extensive applications in industries such as aerospace, automotive, and biomedical sectors. The ECAP process involves pressing the material through a special die that allows it to undergo significant plastic deformation without changing its cross-sectional area. During this process, the material is forced through sharp-angled channels, resulting in substantial improvements in its internal structure (Öğüt et al., 2021; Şahbaz et al., 2019a, 2019b). The application process of ECAP and the grain refinement that occurs in the microstructure of the material during this process are described in detail with the schematic representation below in Figure 1 (Ebrahimi et al., 2023).

Figure 1

Schematic Description of the ECAP Process: (a) The ECAP Die with the Different Parts of, Channels, Angles, and Shear Zone; and (b) The Workpiece Passing Through the ECAP Channels. (Ebrahimi et al., 2023)



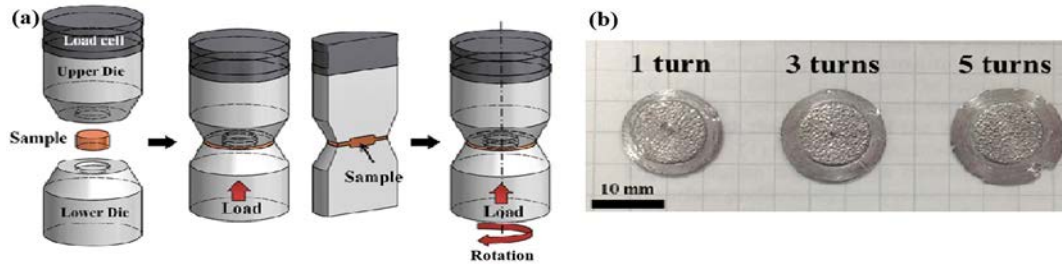
High Pressure Torsion (HPT)

HPT is a well-known severe plastic deformation technique used to refine the grain size of materials to the nanometer scale, significantly improving their mechanical properties. This method involves applying a high compressive force to a disk-shaped sample while simultaneously twisting it. The combination of high pressure and torsional strain results in intense plastic deformation, leading to the formation of ultrafine-grained or nanocrystalline structures (Edalati & Horita, 2016a).

The sample is subjected to pressures typically in the range of several gigapascals (GPa), which helps to maintain structural integrity during severe deformation. Then, the sample is twisted through several rotations, imposing a large shear strain that refines the grain structure. So, the intense deformation leads to the formation of ultrafine grains (less than 100 nm), significantly enhancing the material's mechanical properties such as strength, hardness, and ductility. The figure below shows a schematic representation of an HPT system and HPT-treated specimens (Fig. 2). In this cited study, a pressure of about 6 GPa was applied to a disc specimen with a diameter of 10 mm and a thickness of 1.5 mm, and then the die was rotated once, three times, and five times to deform the specimen (Lee et al., 2016).

Figure 2

Schematic Diagram of the High-Pressure Torsion (HPT) Process (a) and the Specimens After the HPT Process (b) (Lee et al., 2016)



Bridgman studied the effects of high pressure combined with shear deformation on solid materials in the 1930s. The method was further developed and refined in the latter half of the 20th century and has since been extensively used in materials science research to produce nanostructured materials. HPT has been applied to a variety of metals and alloys, including aluminum, titanium, and magnesium, to enhance their mechanical properties. It is widely used in the fields of aerospace, automotive, and biomedical engineering (Bridgman, 1935; Valiev et al., 2014).

HPT has some advantages, such as improving the mechanical properties of a wide range of materials by producing uniform ultrafine grains in the microstructure. However, HPT has some disadvantages, such as the need for specialized equipment capable of applying high pressures and the nature of the process, which requires relatively small sample sizes (Edalati, 2019).

Multi-Directional (or Axial) Forging

Multi-Directional Forging (MDF), also known as Multi-Axial Forging (MAF), is a SPD method used to enhance the mechanical properties of metals by improving their microstructure and refining the grain size. This method involves deforming the material through repeated compressive forces applied along different directions, which induce substantial plastic strain and refine the grain structure to ultrafine or even nanometer scales.

MDF is a simple and cost-effective SPD technique that is often overlooked in literature compared to other techniques like HPT and ECAP. It is easy to use in any plant and can be applied on an industrial scale with various sample sizes. The process involves compressing a cube-shaped specimen along three perpendicular axes, promoting grain refinement and microstructure changes that enhance material strength and thermal stability. Additionally, the low strain amplitude MDF (LSA-MDF) variation helps in recovering work hardness of treated materials post-SPD treatment. Overall, MDF shows great potential for industrial applications. (da Silva et al., 2024).

Historical Background of MDF and Literature Review

If the historical development of MDF is briefly summarized; the concept of multi-directional forging dates back to the early developments in metal forming technologies. However, its systematic application and study for microstructure improvement and mechanical property enhancement are more recent. In recent years, MDF has attracted

attention due to its effectiveness in producing high-strength materials with excellent mechanical properties. Researchers have achieved significant grain refinement and property enhancement by applying MDF to numerous materials specially to metals and alloys. MDF-treated materials with developed microstructures and mechanical properties can be used in many fields. MDF has been used in the development of lightweight metals such as magnesium, aluminum, and titanium alloys, which are very important in aerospace, automotive, and biomedical applications. The method's ability to improve material properties without increasing brittleness makes it particularly valuable in these industries.

A wide range of metals and alloys can be used in the MDF process, transforming their microstructure into uniform and refined grain structures, and improving the material's mechanical properties such as strength, ductility, and toughness. Also, equipment and process setup can be simpler and cheaper compared to other SPD methods. However, it requires precise control of deformation rates and forces when applying MDF, and also, due to the nature of the forging process, it is limited to smaller workpieces. Some of the studies in this field are given below as a summary of the literature review.

A 1988 patent mentions that an MDF method can be used to impart a very fine grain size to aluminum alloys, such as plate-shaped alloys or wrought billets. The alloy was first aged to form precipitates and then deformed along its three major axes in successive operations until it reached a cumulative true strain of at least 8. As a result of the studies tested on different alloys, it has been shown that the mechanical properties of the material increase while the grain size of the material decreases (Ghosh, 1988).

Almeida et al. (2020), conducted a study on severe plastic deformation (SPD), which leads to the refinement and strengthening of metal particles. Among many SPD processing methods, multi-directional forging (MDF) is the only method that can obtain in-situ material stress-strain curves. However, post-processing was necessary to avoid sample shape distortions. A new processing method, called multi-directional constrained forging (MDCF), was proposed to eliminate post-processing by incorporating limited compressive strain. Different strains in MDF result in different material hardening effects, with lower strains resulting in less hardening and increased work hardening capacity for previously deformed materials. High strain levels in MDF after SPD led to improved uniform elongation in materials. The study showed that aluminum's low strain amplitude multi-directional constrained forging (LSA-MDCF) produced microstructures similar to those obtained with free compression, making it a more practical MDF route for reprocessed samples (Almeida et al., 2020).

In their study, Manjunath et al., (2021) demonstrated various characteristic properties of aluminum and its alloys commonly used in materials science and manufacturing processes. These aluminum-based alloys have numerous applications due to their mechanical and interfacial properties such as strength-to-weight ratio, fatigue, hardness, density, equivalent strain, and toughness. The study focused on the multiaxial forging (MAF) or multidirectional forging (MDF) processes to obtain finely equiaxed grains in aluminum alloys. The research aimed to highlight the multidirectional forging technique and explore further directions for ongoing research (Manjunath et al., 2021).

De Faria et al., (2021) found that severe plastic deformation (SPD) significantly strengthened ductile metals, but eliminated further work hardening during monotonous

deformation. Low strain amplitude multi-axial forging (LSA-MDF) after Equal-Channel Angular Pressing (ECAP) caused limited softening and restored work hardening capacity in aluminum. The research analyzed the application of LSA-MDF to aluminum after 4 ECAP passes, observing a renewal in material hardening capacity and changes in microstructures (de Faria et al., 2021).

Akdoğan and Şahbaz (2022) investigated the application of the multidirectional forging (MDF) process on the AA5083 aluminum alloy at room conditions. The MDF process was applied for 4 cycles on cube-shaped specimens homogenized by annealing heat treatment. In the study, a strain rate of 10% was applied for each press applied along three axes. Mechanical properties were evaluated using hardness and compression tests after MDF treatments. The results showed that each MDF cycle increased the hardness and compressive strength properties of the material. In the study, more strength and stiffness increases were observed compared to similar studies, probably due to plastic deformation applied at room conditions (Akdoğan & Şahbaz, 2022).

Deb et al., (2023), used a severe plastic deformation (SPD) technique called multi-axis forging (MAF) to improve grain structure and increase material strength significantly. The advantages of MAF lie in its simple tool design and the ability to process bulk materials, while its main limitation is the non-uniform microstructure created along the cross-section in initial passes. By proposing a production strategy using fewer MAF passes, they achieved a homogeneous microstructure with uniform grain refinement, leading to significant improvements in ductility and isotropic properties. This was confirmed through finite element analysis (FEA) simulations on commercial pure Al and experimental validation. The study highlights the importance of the process-structure-property correlation in material science (Deb et al., 2023).

In the study carried out by Zhang et al., (2024), the effects of multidirectional forging (MDF) and aging treatments on the wear properties of ZK61 magnesium alloy were investigated. Researchers analyzed the microstructure by scanning electron microscopy (SEM) analysis and the mechanical properties by hardness, tensile, and wear tests. Samples were used for three different conditions: homogenized, MDF, and aged samples. ZK61 magnesium alloy from MDF showed higher strength, hardness, and sliding wear properties. It was observed that the wear resistance of the material increased due to grain refinement, hardness, and tensile strength increased with the aging effect, and wear resistance decreased (Zhang et al., 2024).

Application Procedures of MDF

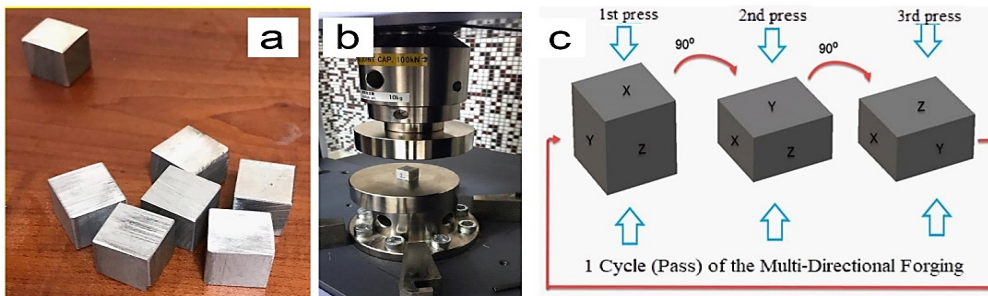
MDF is usually applied with three different die types. The first is called open-die MDF and the process takes place between two flat platens. Here, the flow of the material is not controlled from the sides and convexity may occur on the side surfaces at high strains. the second is a one-axis restricted die, where the material flows only on the axis left open and takes shape. The third is a two axis restricted die, in this system, the material flows in both axes until the die is filled and then takes the shape of the die.

The application of MDF and the subsequent change in the material can be summarized as follows; first, MDF is applied to a cubic or rectangular prism-shaped workpiece (Fig.3a). The material is forged (or pressed) multiple times, typically along three orthogonal axes, respectively (Fig. 3b-c). This multi-directional approach ensures uniform stress distribution throughout the material. Repeated and varied deformation leads to significant grain size reduction, producing ultra-fine grain or nanostructured

materials with improved mechanical properties. The refined microstructure resulting from MDF increases the strength, ductility, and toughness of the material. The MDF specimens used in a study (Nalkıran & Şahbaz, 2023), the actual MDF experimental setup, and the schematic representation of the MDF process are shown in the figure below (Nalkıran & Şahbaz, 2023).

Figure 3

MDF Specimens: (a) Before the MDF Process, (b) Between the Compression Test Plates, (c) Schematic Description of the MDF Process (Nalkıran & Şahbaz, 2023)

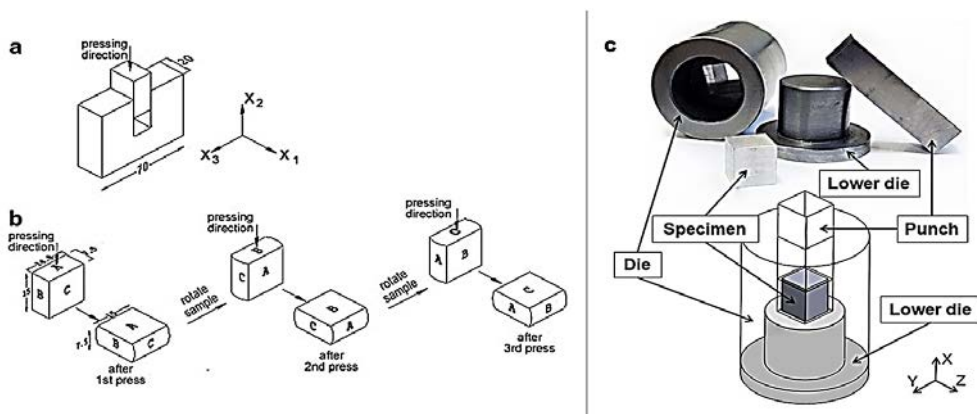


The MDF process is carried out using open molds (between two compression plates) (Nalkıran & Şahbaz, 2023), and in some studies, molds with confining walls were used (Almeida et al., 2020). These restrictive walls are sometimes on one axis (Kundu et al., 2008) and sometimes on two axes (N.G.S. Almeida et al., 2020) and direct the flow of the material. In some studies, the use of confining molds has been reported to affect the microstructural and mechanical properties of the material in the MDF process (Almeida et al., 2020; Almeida et al., 2020).

The following figure shows a schematic representation of an MDF die confined by one axis. The orientation of the sample is the same as the die orientation in Figure 4a. Sample parts are marked A, B, and C. Shown here are three pressings, after which the sequence repeats in Figure 4b. A schematic representation and photographs of the orientation of a biaxially confined MDF die are also shown in Figure 4c.

Figure 4

(a) Orientation of a One-Axis Confined MDF Die, (b) Scheme of Multiple Compression in a Channel Die (Rezaee-Bazzaz & Ahmadian, 2012); (c) Schematic Illustration and Photographs of Orientation of a Two-Axis Confined MDF Die (N.G.S. Almeida et al., 2020)



Results and Discussion

When the studies on MDF in the literature are reviewed, it is seen that some researchers have investigated some materials (Akdoğan & Şahbaz, 2022; Miura et al., 2011; Zhang et al., 2024), while others have prepared review articles (Sharath, 2021) on this subject. This research presents the results of some of them as figures, and explanations. When the studies in the literature are examined, it is noteworthy that the most commonly applied materials in MDF are aluminum (Al), magnesium (Mg), copper (Cu), titanium (Ti), pure forms, and alloys. In addition to these, some zinc (Zn) and nickel (Ni) alloys, iron (Fe), and some steels are also applied to MDF (Manjunath et al., 2021; Sharath, 2021). In these studies, the changes in the microstructure of the material with the effect of MDF are explained by microscopic examinations, and the changes in the mechanical properties are presented accordingly. It was reported that nano-level grain sizes were reached in MDF applications at room temperature or cryogenic environments and in materials with high strain. However, in MDF processes above room temperature, the grain size decreased but did not reach nano levels. In addition, the strength and hardness values of the material increased in proportion to the decrease in grain size. The results of some of these studies are compiled in mechanical, microstructural, and numerical analysis under the subheadings below.

Mechanical Test Results

MDF has a different position from other SPD methods in the detection of mechanical properties. Many MDF application systems (such as compression test devices) can record the force and compression strength that occur when forging the material. When SPD is applied to such material, an increase in the compression strength of the material can be detected (Almeida et al., 2020; Stemler et al., 2019). Figure 5a gives a compressive strength-strain graph for up to 4 cycles for each compression. After 4 cycles, the compressive yield strength (more than twice) and maximum strength values in the material have significantly increased. Figure 5b shows a tensile strength-strain graph up to 4 cycles. After the fourth cycle, the yield strength (over three times) and the ultimate tensile strength (more than twice) of the material have increased significantly.

Figure 5

(a) Compressive Strength-Strain Curves Up to 4 MDF Cycles, with Each Compression Phase (Almeida et al., 2020), (b) Representative Room Temperature Tensile Curves of Titanium in Annealed and Deformed Condition (Photographs of Tensile Tested Samples in Inset) (Kumar et al., 2016)

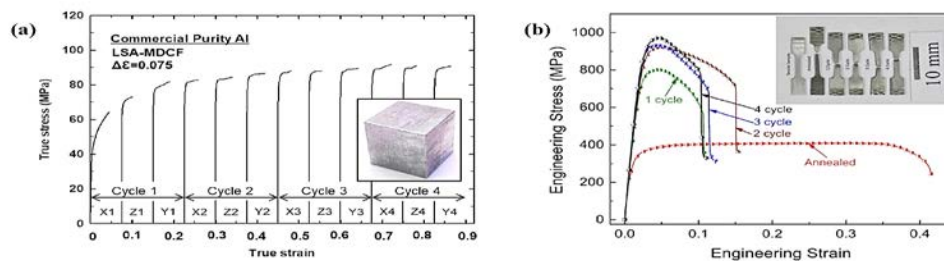
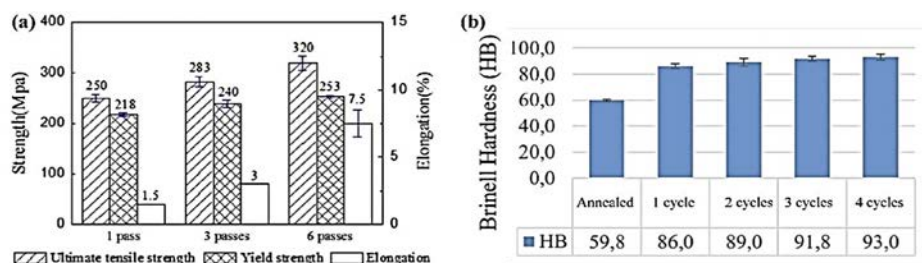


Figure 6a shows the yield strength, ultimate tensile strength, and elongation values for the Mg-Gd-Y-Nd-Zr alloy as a result of 1, 3, and 6 cycles of MDF. It is seen that there is an increase in both strength values and an increase in elongation values, which is the most interesting feature of SPD methods (Xia et al., 2015). Figure 6b shows the increase in hardness in the material as a result of MDF from 1 to 4 cycles for the alloy AA 5083.

As shown in the figure, in each test, the strain increased by 10%, and the post-4 cycles hardness value reached 59.8 to 93 HB (Akdoğan & Şahbaz, 2022).

Figure 6

(a) Tensile Properties for the Mg–Gd–Y–Nd–Zr Alloy After Different Multi-Directional Forging Passes (Xia et al., 2015), (b) Brinell Hardness Values of AA5083 up to 4 Cycles (Akdoğan & Şahbaz, 2022)

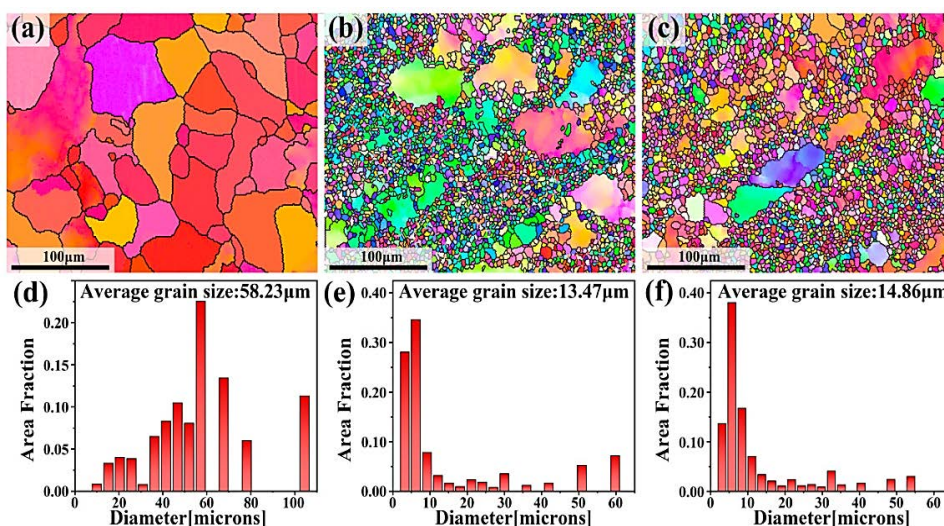


Microstructural Analysis Results

In a study presented below, microstructures (EBSD map) and grain size distribution graphs are given for three different conditions: homogenized, MDF, and MDF + aged samples on ZK61 magnesium alloy. The EBSD maps of homogenized, MDF, and aged samples show significant differences in grain size. Homogenized samples had finer grains after MDF passes. Aging had little effect on grain size due to the low temperature. Grain size distribution maps show average grain sizes of 58.23 μm , 13.47 μm , and 14.86 μm for homogenized, MDF, and aged samples. Maximum grain size decreased from 104.48 μm to 60.51 μm after MDF, with an average of 6.25 μm for fine grains. Overall, the average grain size of homogenized samples decreased by 23% after MDF (Zhang et al., 2024).

Figure 7

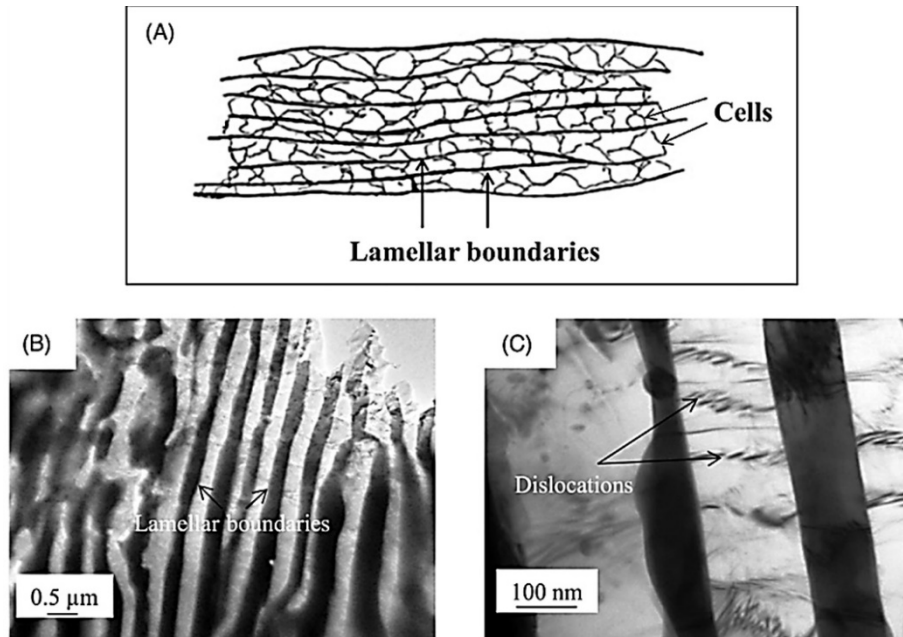
EBSD Maps and Corresponding Grain Size Maps: (a, d) Homogenized Sample, (b, e) MDF Sample, and (c, f) Aged Sample (Zhang et al., 2024).



In a research paper, nano-level developments in the lattice structure of Zn-Al alloys after MDF application were investigated with the help of TEM. In the TEM images obtained, grain subdivision and dislocations in the Zn-Al alloy can be seen in Figure 8.

Figure 8

(a) Schematic Depiction of Lamellar Boundaries, (b) TEM Micrograph After 6 Passes at 200°C, and (c) Enlarged Image of (b) Exhibiting Grain Subdivision and Dislocations in Zn-Al Alloy Processed Under MDF (Sharath, 2021).



The mechanical properties of Zn and its alloy in bearing applications deteriorate over time due to natural aging. Zn-Al alloy undergoes an MDF process at 100°C and 200°C to a cumulative strain of 1.2, resulting in phase transformation and enhancing diffusion. Samples processed at higher temperatures exhibit equiaxed grains and agglomerates of alpha and beta phases. The Cu-rich phase hinders lamellae movement, increasing strain hardening exponent values in high-temperature samples. After processing to a higher strain, lamellar boundaries with interior cells become visible. Impression creep behavior is studied on MDF-processed Zn-Al alloys, showing four phase transformations (Fig.8). Creep properties are more sensitive to temperature changes, with lattice diffusion controlled by dislocation climb as the dominant creep mechanism (Sharath, 2021).

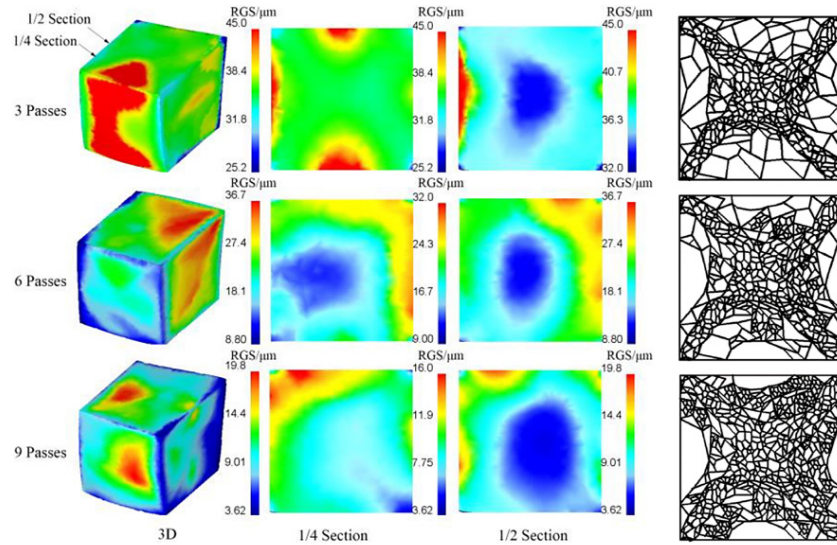
Numerical Analysis Results

Finite element analysis (FEA), or numerical analysis, is very important in terms of predicting the results that may be encountered before the experimental study. With the increase in research in the field of SPD, FEA applications for these methods have also increased. In FEA applications for SPD methods, it is possible to determine how much load the molds will be exposed to during the experiment and design the mold accordingly. In addition, the strain value that will occur in the material is determined by these methods, and predictions can be made about hardness and strength. Numerical analysis results from some studies are given below as an example.

Finite element analyses were conducted to study the hot deformation of superalloy GH4169, using a constitutive equation and dynamic recrystallization model. Three multidirectional forging processes were compared: closed MDF (CMDF), single open MDF, and double open MDF. Results showed that double open MDF had the highest degree of recrystallization, followed by CMDF and single open MDF. CMDF achieved 99.5% recrystallization at 1000 °C and 9 passes, with an average recrystallized grain size of 8.1 μm (Jin et al., 2020).

Figure 9

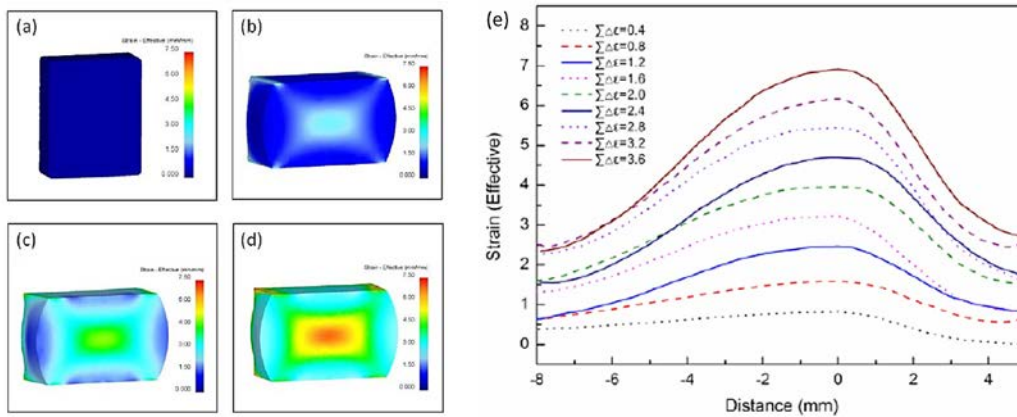
Cloud Diagram for Different Grain Size Distributions for Double-Open MDF at 800 °C (Left 3-Column), Internal Grain Size Change of Double-Open MDF: 3, 6, 9 Passes (Right-Column) (Jin et al., 2020).



In a study, the deformation flow behavior of 2A14 aluminum alloys during MDF was examined under different cumulative strains. Forging was done at 450°C with a deformation rate of 0.15 mms-1 and a transitional strain of 0.4. Numerical simulations using DEFORM-3D revealed that vortex, cross-flow, and folding defects did not occur during deformation. The bending and inhomogeneity of flow lines increased with cumulative strain. FEM analysis aligned with experimental results, showing increased effective strain in various regions of the forgings during MDF. Dynamic recovery was the dominant process, with recrystallized grains and fragmented second phases increasing with effective strain.

Figure 10

Distribution of Effective Strain in the Cross Section of 2A14 Aluminum Alloys Processed by MDF with Various Cumulative Strains: (a) $\Sigma\delta\epsilon=0$; (b) $\Sigma\delta\epsilon=1.2$; (c) $\Sigma\delta\epsilon=2.4$; (d) $\Sigma\delta\epsilon=3.6$, (e) Relationship Between Effective Strain and the Distance from the Edge of the Drum Shape (Wang et al., 2017)



Conclusion

In this study, MDF, an APD method, is examined. In the study, APD methods and their historical development are given first, and then MDF is discussed in detail. A brief

literature review of studies using MDF is given, followed by information on mold designs, application procedures, and parameters. Afterward, the tests and analyses performed to determine the changes in the materials after MDF are given with examples. It is seen that tensile, compression, and hardness tests are generally used to determine mechanical properties, and it is seen that MDF treatment increases these properties. Optical (OM) and electron (SEM, TEM, EBSD, etc.) microscopes were used for microstructural investigations, and image analysis was performed. Thus, the effect of MDF processing on the microstructure of the material was examined, and many phenomena such as grain size refinement, an increase in dislocation density, twin formation, and secondary phase precipitation were observed. The production of nano-sized materials, especially under room temperature or with high-strain applications, has increased interest in MDF.

As a result, it has been observed that MDF, which has ease of application compared to other SPD methods, can make great improvements in the mechanical properties of the material by intervening in the microstructure of the material. The improvement of materials with a high strength-to-weight ratio (Al, Mg, Ti, etc.) with this method is expected to make a significant contribution to many fields, especially in critical sectors such as aviation, automotive, and defense industries.

References

- Akdoğan, E., & Şahbaz, M. (2022). Çok yönlü dövme işleminin aa5083 alüminyum alaşımının mekanik özellikleri üzerindeki etkisi. *European Journal of Science and Technology*, 34, 739–744. <http://dx.doi.org/10.31590/ejosat.1084992>
- Almeida, N.G.S., Pereira, P. H. R., De Faria, C. G., Aguilar, M. T. P., & Cetlin, P. R. (2020). Mechanical behavior and microstructures of aluminum processed by low strain amplitude multi-directional confined forging. *Journal of Materials Research and Technology*, 9(3), 3190–3197. <https://doi.org/10.1016/j.jmrt.2020.01.065>
- Almeida, Natanael Geraldo Silva, Stemler, P. M. A., Faria, C. G. de, Pereira, P. H. R., Aguilar, M. T. P., & Cetlin, P. R. (2020). Hardness, microstructure and strain distributions in commercial purity aluminum processed by multi directional forging (MDF). *Materials Research*, 23(4). <https://doi.org/10.1590/1980-5373-mr-2020-0262>
- Bagherpour, E., Reihanian, M., Pardis, N., Ebrahimi, R., & Langdon, T. G. (2018). Ten years of severe plastic deformation (SPD) in Iran, part I: equal channel angular pressing (ECAP). *Iranian Journal of Materials Forming*, 5(1), 71–113. <https://doi.org/10.22099/IJMF.2018.28756.1101>
- Bahmani, A., Arthanari, S., & Shin, K. S. (2019). Improved corrosion resistant and strength of a magnesium alloy using multi-directional forging (MDF). *The International Journal of Advanced Manufacturing Technology*, 1–13. <https://doi.org/10.1007/s00170-019-04176-1>
- Bridgman, P W. (1935). Effects of high shearing stress combined with high hydrostatic pressure. *Physical Review*, 48(10), 825–847. <https://doi.org/10.1103/PhysRev.48.825>
- Bridgman, Percy Williams. (1995). Nobel Lectures; Physics 1946, General survey of certain results in the field of high-pressure physics, December 11, 1946. *Nobel Lectures*, 1(2).
- da Silva, N. A. N., Flausino, P. C. A., Aguilar, M. T. P., & Cetlin, P. R. (2024). Multi-directional forging. In *Comprehensive Materials Processing* (pp. 130–156). Elsevier. <https://doi.org/10.1016/B978-0-323-96020-5.00033-9>
- de Faria, C. G., Almeida, N. G. S., Balzuweit, K., Aguilar, M. T. P., & Cetlin, P. R.

- (2021). The effect of initial strain in the severe plastic deformation of aluminum on the subsequent work hardening regeneration through low strain amplitude multi-directional forging. *Materials Letters*, 290. <https://doi.org/10.1016/j.matlet.2021.129462>
- Deb, S., Abhilash, M. B., Immanuel, R. J., & Panigrahi, S. K. (2023). Improved structural uniformity and specific strength of commercially pure aluminum through variable temperature multi axial forging: Finite element analysis and experimental study. *International Journal of Lightweight Materials and Manufacture*, 6(3), 434–449. <https://doi.org/10.1016/j.ijlmm.2023.02.001>
- Ebrahimi, M., Attarilar, S., Gode, C., Kandavalli, S. R., Shamsborhan, M., & Wang, Q. (2023). Conceptual analysis on severe plastic deformation processes of shape memory alloys: mechanical properties and microstructure characterization. In *Metals* (Vol. 13, Issue 3). <https://doi.org/10.3390/met13030447>
- Edalati, K. (2019). Review on recent advancements in severe plastic deformation of oxides by high-pressure torsion (HPT). In *Advanced Engineering Materials* (Vol. 21, Issue 1, p. 1800272). John Wiley & Sons, Ltd. <https://doi.org/10.1002/adem.201800272>
- Edalati, K., & Horita, Z. (2016a). A review on high-pressure torsion (HPT) from 1935 to 1988. *Materials Science and Engineering A*, 652, 325–352. <https://doi.org/10.1016/j.msea.2015.11.074>
- Edalati, K., & Horita, Z. (2016b). A review on high-pressure torsion (HPT) from 1935 to 1988. *Materials Science and Engineering A*, 652, 325–352. <https://doi.org/10.1016/j.msea.2015.11.074>
- Ghosh, A. K. (1988). U.S. Patent No. 4,721,537. Washington, DC: U.S. Patent and Trademark Office.
- Iwahashi, Y., Wang, J., Horita, Z., Nemoto, M., & Langdon, T. G. (1996). Principle of equal-channel angular pressing for the processing of ultra-fine grained materials. *Scripta Materialia*, 35(2), 143–146. [https://doi.org/10.1016/1359-6462\(96\)00107-8](https://doi.org/10.1016/1359-6462(96)00107-8)
- Jin, Y., Xi, C., Xue, P., Zhang, C., Wang, S., & Luo, J. (2020). Constitutive model and microstructure evolution finite element simulation of multidirectional forging for gh4169 superalloy. *Metals*, 10(12), 1–11. <https://doi.org/10.3390/met10121695>
- Kundu, A., Kapoor, R., Tewari, R., & Chakravarty, J. K. (2008). Severe plastic deformation of copper using multiple compression in a channel die. *Scripta Materialia*, 58(3). <https://doi.org/10.1016/j.scriptamat.2007.09.046>
- Lee, D. J., Lee, Y., Kim, H.-K., Kwon, Y.-N., Kim, H. S., & Yoon, E. Y. (2016). Analyses of sever plastic deformation behavior of hot isostatic pressed ni-base superalloy during high pressure torsion process. *Transactions of Materials Processing*, 25(4), 254–260. <https://doi.org/10.5228/kstp.2016.25.4.254>
- Manjunath, G. A., Shivakumar, S., Fernandez, R., Nikhil, R., & Sharath, P. C. (2021). A review on effect of multi-directional forging/multi-axial forging on mechanical and microstructural properties of aluminum alloy. *Materials Today: Proceedings*, 47, 2565–2569. <https://doi.org/10.1016/j.matpr.2021.05.056>
- Miura, H., Yu, G., & Yang, X. (2011). Multi-directional forging of AZ61Mg alloy under decreasing temperature conditions and improvement of its mechanical properties. *Materials Science and Engineering A*. <https://doi.org/10.1016/j.msea.2011.05.050>
- Nalkıran, S., & Şahbaz, M. (2023). Effects of the multi-directional forging at different deformation ratios on the mechanical properties of aa5083 aluminum alloy. *Proceedings of 27th International Scientific Conference MECHANIKA 2023*,

- 176–178.
- Öğüt, S., Kaya, H., & Kentli, A. (2021). Comparison of the effect of equal channel angular pressing, expansion equal channel angular pressing, and hybrid equal channel angular pressing on mechanical properties of az31 mg alloy. *Journal of Materials Engineering and Performance*, 1–13. <https://doi.org/10.1007/s11665-021-06430-8>
- Rezaee-Bazzaz, A., & Ahmadian, S. (2012). Modeling of mechanical behavior of ultra-fine grained aluminum produced by multiple compressions in a channel die. *Materials and Design*, 34. <https://doi.org/10.1016/j.matdes.2011.08.013>
- Şahbaz, M., Kaya, H., Kentli, A., Uçar, M., Öğüt, S., & Özbeyaz, K. (2019a). Experimental comparison of al5083 alloy subjected to annealing and equal-channel angular pressing. *International Journal of Computational and Experimental Science and Engineering*, 5(1), 52–55. <https://doi.org/10.22399/IJCESEN.394542>
- Şahbaz, M., Kaya, H., Kentli, A., Uçar, M., Öğüt, S., & Özbeyaz, K. (2019b). Analytical and numerical analysis comparison of equal channel angular pressing for Al5083 alloy. *Advanced Science, Engineering and Medicine*, 11(11), 1100–1103. <https://doi.org/10.1166/ase.2019.2461>
- Satheesh Kumar, S. S., Priyasudha, K., Rao, M. S., & Raghu, T. (2016). Deformation homogeneity, mechanical behaviour and strain hardening characteristics of titanium severe plastically deformed by cyclic channel die compression method. *Materials and Design*, 101. <https://doi.org/10.1016/j.matdes.2016.04.004>
- Segal, V. (2018). Review: Modes and processes of severe plastic deformation (SPD). In *Materials* (Vol. 11, Issue 7). Preprints. <https://doi.org/10.3390/ma11071175>
- Segal, V. M. (1977). The method of material preparation for subsequent working. *Patent of the USSR*, 575892, 330.
- Segal, V. M., Reznikov, V. I., Drobyshevskii, A. E., & Kopylov, V. I. (1981). Plastic metal working by simple shear. | plasticheskaya obrabotka metallov prostym sdvigom. *Izvestia Akademii Nauk SSSR. Metally*, 1.
- Sharath, P. C. (2021). Multi directional forging: An advanced deforming technique for severe plastic deformation. In *Advanced Welding and Deforming*. <https://doi.org/10.1016/B978-0-12-822049-8.00017-7>
- Stemler, P. M. A., Flausino, P. C. A., Pereira, P. H. R., de Faria, C. G., Almeida, N. G. S., Aguilar, M. T. P., & Cetlin, P. R. (2019). Mechanical behavior and microstructures of aluminum in the Multi-Axial Compression (MAC) with and without specimen re-machining. *Materials Letters*, 237. <https://doi.org/10.1016/j.matlet.2018.11.081>
- Valiev, R. Z., Murashkin, M., & Sabirov, I. (2014). A nanostructural design to produce high-strength Al alloys with enhanced electrical conductivity. *Scripta Materialia*, 76, 13–16. <https://doi.org/10.1016/j.scriptamat.2013.12.002>
- Valiev, Ruslan Z., & Langdon, T. G. (2006). Principles of equal-channel angular pressing as a processing tool for grain refinement. *Progress in Materials Science*, 51(7), 881–981. <https://doi.org/10.1016/j.pmatsci.2006.02.003>
- Valiev, Ruslan Z., Zhilyaev, A. P., & Langdon, T. G. (2013). Bulk nanostructured materials: Fundamentals and applications. In *Bulk Nanostructured Materials: Fundamentals and Applications*. Wiley-TMS. <https://doi.org/10.1002/9781118742679>
- Wang, M., Wang, J., Liu, W., Ma, Y., Liu, D., Guo, L., Huang, L., & Huang, B. (2017). Experimental and finite element analysis of flow behavior of 2a14 aluminum alloy during multi-directional forging. *International Journal of Engineering Research and Science*, 3(10). <https://doi.org/10.25125/engineering-journal-ijoeer>

oct-2017-1

Xia, X., Chen, Q., Zhao, Z., Ma, M., Li, X., & Zhang, K. (2015). Microstructure, texture and mechanical properties of coarse-grained Mg-Gd-Y-Nd-Zr alloy processed by multidirectional forging. *Journal of Alloys and Compounds*, 623, 62–68. <https://doi.org/10.1016/j.jallcom.2014.10.084>

Zhang, X., Xu, J., He, W., & Jia, J. (2024). Effect of multidirectional forging and aging treatment on wear properties of ZK61 alloy. *materials*, 17(2). <https://doi.org/10.3390/ma17020523>

About The Authors

Mehmet ŞAHBAZ, PhD is an Assistant Professor of Mechanical Engineering at Karamanoğlu Mehmetbey University in Karaman, Türkiye. He has master's and PhD degrees in Mechanical Engineering from Marmara University. His main areas of interest are SPD methods, mechanical behavior of materials, metallurgy, heat treatments and FEA.

E-mail: mehmetshbaz1@gmail.com, **ORCID:** 0000-0001-6379-8345

Similarity Index

The similarity index obtained from the plagiarism software for this book chapter is 15%.

CHAPTER 9***Wear Performance of Ex-situ NbC and In-situ Al₄C₃ Reinforced A356 Matrix Hybrid Composites at High Temperatures******Doğan ŞİMŞEK****National Defence University, Türkiye****İjlal ŞİMŞEK****National Defence University, Türkiye***To Cite This Chapter:**

Simsek, D. & Simsek, I. (2024). Wear Performance of Ex-situ NbC and In-situ Al₄C₃ Reinforced A356 Matrix Hybrid Composites at High Temperatures. In H. Gokmese, S. Bulbul, & Y. Uzun (Eds.), *Current Studies in Materials Science and Engineering* (pp. 128-144). ISRES Publishing.

Introduction

Compared to metals and its alloys, aluminum matrix composites (AMCs) have a higher strength and better wear resistance, which makes them useful in specialized application areas. For many years, many studies have been conducted by many researchers, especially on the wear resistance of AMCs under dry sliding conditions (Ipek, 2015; Tan et al., 2021). Ceramic particles (such as SiC, Al₂O₃, TiC, and B₄C) are used as reinforcement in AMCs to limit the quantity of plastic deformation in the matrix (Baskaran et al., 2014; Soy et al., 2015). In addition to these reinforcing materials, the use of various ceramic particle elements with different properties in the matrix expands the range of particle-reinforced composite materials. Among the reinforcing materials, NbC (Niobium Carbide) is a reinforcing material with 7.78 g/cm³ density, high hardness (2400 HV), high elasticity module (338.5 GPa), high melting point (3490 °C), high thermal conductivity (27 Wm⁻¹K⁻¹) and low linear expansion coefficient (6.5×10⁻⁶K⁻¹) (Travessa et al., 2017; Souto et al., 2018; García et al., 2019). NbC has a face-centered cubic structure whose lattice parameters are a=b=c=0.447 nm. They can form semi-compatible or compatible interfaces with the α-Al matrix (Lemine et al., 2022). The improvement of the matrix-reinforcement binding force and decrease in interfacial energy are benefits of creating such surfaces (semi-compatible or compatible interfaces) between the matrix and reinforcement (Demirskyi et al., 2019; Bian et al., 2021). In addition, NbC plays an important role in reducing grain size, increasing hardness, and improving resistance against oxidation (Dai et al., 2022).

It is known that in the improvement of hardness and mechanical properties in

AMCs, the production method is also effective as well as the reinforcement phase. AMCs are produced by solid, liquid, and semi-solid methods (Özyürek et al. 2012; Aksöz et al., 2014). Among these methods, high-energy ball milling, which is a solid-state manufacturing method, is seen as a good method for producing AMC. High-energy ball milling/alloying is a powder processing method that involves deformation, fracture, and cold welding of powders by repeated collisions of a ball. The application of this rather simplistic technique in the production of advanced materials was first successfully carried out in a study conducted by Benjamin (1970) in the late 1960s. In that study, it was revealed that mechanical alloying (MA) should be used in cases where the usual distribution of oxide particles in liquid metal is not possible. The mechanical alloying process begins with the use of mechanical force as a result of the repeated collision of high-energy balls, continues with cold welding of powders, excessive deformation occurs under the influence of repeated collision in the following stage, and the process is completed with fracture in the final stage. The fracture mechanism of the particles varies based on the particle size and the structure of the particles being milled. The plastic deformation increasing before the particle fracture leads to a dramatic increase in the stresses on the powder particle and then causes an excessive dislocation flow. At the later stage, the synthesis of a new chemical compound and fracture occurs (Sopicka-Lizer, 2010). Simsek and Ozyurek (2020) reported that they successfully produced different amounts of ZrO_2 -reinforced AMCs with an A356-Gr matrix by using a mechanochemical reaction method. In another study, Simsek (2019) produced Al-Graphite/ B_4C hybrid composites by the mechanical alloying method and examined their wear behavior. Simsek reported as the reinforcement amount in the matrix increased, weight loss decreased. Akcamli et al. (2022) investigated the wear and corrosion resistance of the composites. The study used the MA method to produce a composite by adding different amounts of graphene to the Al10Si matrix. They reported that the best wear resistance was in the composite containing high graphene and mechanically alloyed for 4 hours. Similarly, Rajaram et al. (2020) examined the wear behavior of Al-Si alloy and Al-Si-Graphite composites at room and high temperatures. They stated that wear rates decreased as temperature increased. In addition, they reported that the presence of graphite in composites provides better wear resistance for all these temperatures.

AMCs constitute an important material group of the automotive and aircraft industry due to the superior properties they provide. They have an important area of use, from pistons and connecting rods in internal combustion engines to braking systems of automobiles and airplanes (Rajaram et al., 2010). Reaching high temperatures, especially in service conditions, limits the use of Al alloys. In Al alloys, these limitations can be extended by the use of particle-reinforced composites. Therefore, in this study, 2% graphite was added to the matrix material (A356 alloy). Composite materials with an A356 (Al-Si-Mg) alloy matrix, in-situ Al_4C_3 , and varying amounts of ex-situ NbC reinforcement were produced using the high-energy ball milling method, a common technique in the automotive industry. Moreover, produced composites explore the influence of temperature variations on the wear characteristics and mechanisms, provide information on how the amount of reinforcement affects wear resistance. This research contributes valuable insights into the complex interplay between temperature, reinforcement content, and wear performance in composite materials.

Materials and Method

In experimental studies, A356 alloy powder (20-63 μm) supplied from LPW-Technology

Ltd. was used as matrix material. In A356 alloy powder, 2% graphite was added by weight. In addition, four different amounts of NbC (3, 6, 9, and 12 wt.%) with an approximate powder size of $\leq 20 \mu\text{m}$ were added. Before being added to A356 alloy powder, graphite powders were milled for 60 minutes. The chemical composition of the produced AMC is given in Table 1.

Table 1.
Chemical Composition of Produced AMC Powders (wt.%)

Sample	A356	Graphite	NbC
Matrix	98	2	---
3NbC	95	2	3
6NbC	92	2	6
9NbC	89	2	9
12NbC	86	2	12

The process parameters used in the production and characterization studies of powders with the chemical composition presented in Table 1 are given in Table 2.

Table 2.
Process Parameters Used in AMC Production and Characterization Studies

High Energy Ball Milling Parameters		Sintering Parameters	
Mill Type	Planeter	Environment	10^{-6} mbar vacuum
Vial	Stainless steel	Temperature	550 °C
Filling rate	%50	Time	60 min
Ball Powder Ratio	10:1	Metallography processes	
Process control chemical (PCC)	%1 Stearic acid	Metallography	Standard (400-1200 mesh) sand, 1 μm diamond paste, polishing
Process Time	240 min	Etcher	Keller's solution
Process period	15 min MA, 10 min waiting	Etching time	40-45 sec
Forming Parameters		Characterization	
Forming type	Cold forming	Microstructure	Scanning electron microscope (Carl Zeiss Ultra Plus Gemini Fesem)
Forming pressure	750 MPa	Phase analysis	X-Ray Diffraction Spectrometer (Rigaku Ultima IV)
Press type	Single axis hydraulic press	Density measurement (3 different samples)	Archimets' principle
Sample dimensions	$\text{Ø}12 \times 7$ mm	Hardness measurement (3 different samples and 5 different measurements)	Shimadzu brand microhardness (HV2 10s)
Lubricant	Zinc stearate		

In the study, wear tests were fulfilled in two steps. The test parameters used in the first step of wear tests are given in Table 3. The weight loss and wear parameter results obtained in the first step were evaluated. In the second step, wear tests were made using the load that provided the lowest wear rate in the first step. Moreover, the second step of wear tests was used at four different temperatures (100, 180, 260, and 340°C). Wear tests were carried out by adding a heating module on the standard pin-on-disc type standard wear test device. All tests, of the heating module after reaching the operating temperature were performed. Wear tests were carried out with 3 samples from each group. The mean values of the obtained results were calculated. The worn surfaces of the samples were examined with SEM.

Table 3.
Parameters Used in First-Step Wear Tests

Wear Test Parameters	
Wear tester	Pin on disc wear
Wear standard	ASTM-G-99
Sliding speed	0.5 ms ⁻¹
Load	10N, 20N and 30N
Sliding distance	53 m, 72 m and 94 m
Operating temperature	Room temperature (20 °C)
Counter disc	3271 HMV spheroidal graphite cast iron

Results and Discussions

Microstructural Characterization

Microstructure SEM images of the produced AMCs are shown in Fig. 1 and EDS analysis results are given in Table 4.

Figure 1.
SEM Images of AMCs Different Amounts NbC Added A356+2Gr (a), 3%NbC (b), 6%NbC (c), 9%NbC (d) and 12%NbC (e)

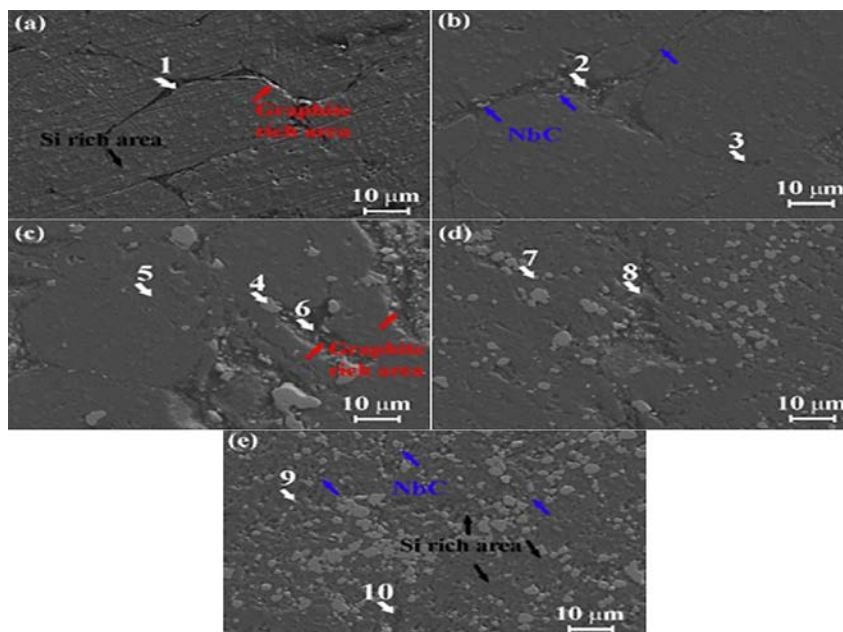


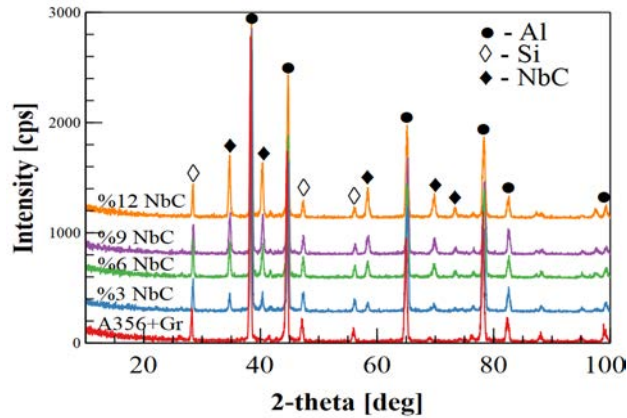
Table 4.*EDS Analysis Results of AMCs with Different Amounts of NbC Added (wt.%)*

Location	Al	Si	Mg	C	Nb	O
1	10.54	0.89	0.83	87.74	-----	-----
2	0.17	0.22	0.03	12.96	86.28	0.34
3	4.04	2.75	0.36	46.69	0.02	46.14
4	0.32	0.01	0.07	14.70	84.56	0.35
5	3.32	91.33	-----	5.33	0.09	0.13
6	6.74	0.77	0.02	82.59	4.60	5.29
7	0.38	-----	0.04	12.78	85.56	1.24
8	65.42	2.00	0.52	19.37	5.52	7.17
9	21.21	0.89	0.07	13.35	62.48	2.00
10	20.82	4.55	0.03	44.11	6.45	24.04

When the SEM images of AMCs to which different amounts of NbC were added are examined (Figure 1), it is observed that the structure of the produced composites consists of powder grains with a high sphericity ratio. In addition, it is observed that the graphite added to the alloy is concentrated at the grain boundaries. In the EDS analysis results given in Table 4, the high carbon rate at the grain boundaries (position 1) is clearly understood. The fact that the solubility of carbon in aluminum is low is due to the dense presence of graphite at the grain boundaries, which is added to the matrix as a solid lubricant (Choi et al., 2010).

It is observed that as the amount of reinforcement phase added in the matrix increases, it is distributed into the grains. However, it is observed that the reinforcement phase, whose size decreases, clusters at the grain boundaries in all composites. The clustering at the grain boundaries is clearly observed in AMC to which 3% NbC is added (Figure 1(b)). This clustering propensity results from the reinforcement phase's polarization as a result of the decrease in size caused by constant fracturing. In high-energy ball milling, the hard reinforcement phase is constantly fractured by the impact of high-energy balls, and its sizes are reduced. The hard reinforcement phase whose sizes are less than 1 μm is clustered by polarization. Similar results have been reported in some previous studies (Salimi et al, 2015; Sekar et al., 2018). The reinforcement phase (NbC) distributed into the grains is observed clearly with the increase in the amount of reinforcement phase in the produced AMCs. In the ductile-brittle alloying system, the relatively hard reinforcing phases are embedded in the matrix powder grains, which are ductile, in the first step of alloying. In the subsequent step, deformation hardening occurs, and in the continuing step, the powders undergo excessive deformation and fracture. As a result of the continuous repetition of these processes, a composite structure is obtained. It is observed that with the increasing reinforcement quantities in the matrix, the reinforcement phase is relatively homogeneously distributed in the structure. In addition, it is understood from the EDS results given in Table 4 (positions 3 and 10) that oxidation occurs in the structure of the produced composites, especially at the grain boundaries. During the milling process, constant collisions between high-energy balls and the milling chamber wall cause the formation of clean surfaces on powders. When removing powders from the mill, oxidation may occur due to the contact of these clean surfaces with the atmosphere (Simsek et al., 2019). The XRD analysis results of AMCs to which different amounts of NbC were added are given in Figure 2.

Figure 2.
XRD Results of AMCs with Different Amounts of NbC Added

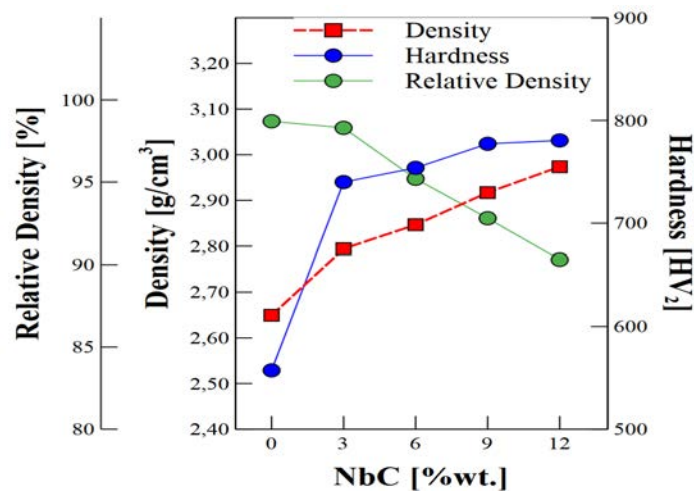


When the XRD results are examined, it is observed that there are Al and Si peaks in A356 alloy (Figure 2). It is observed that the NbC added to the matrix is at diffraction angles of (2θ) 34.7° (111), 40.38° (200), 58.36° (220), and 73.3° (311), respectively (PDF card no: 00-002-1031). As the amount of NbC added to the matrix increases, the densities of the peaks belonging to the reinforcement phase also increase in the same way. In addition, there is no apparent peak in the XRD results of the Al_4C_3 phase expected to occur in the structure. Similarly, peaks related to graphite added to the matrix could not be detected. The fact that the Gr added in the matrix is not visible in the XRD results can be explained by the low amount of %Gr added in the matrix. In a study conducted by Chu et al. (2001), it was reported that small graphite particles added to the alloy completely transformed within the structure, while large graphite particles remained as graphite in the structure. In addition, in the XRD results, it is observed that it contains the Al-Si and NbC phases. This shows that there is no reaction between the matrix and the NbC. In many studies, it is reported that the Al_4C_3 phase is formed as an interface in carbide-added composites (Kennedy et al., 2001; Bakshi et al., 2009).

Hardness and Density Results

The density and hardness results of AMCs added NbC are shown in Figure 3.

Figure 3.
Density and Hardness Results of AMCs Produced



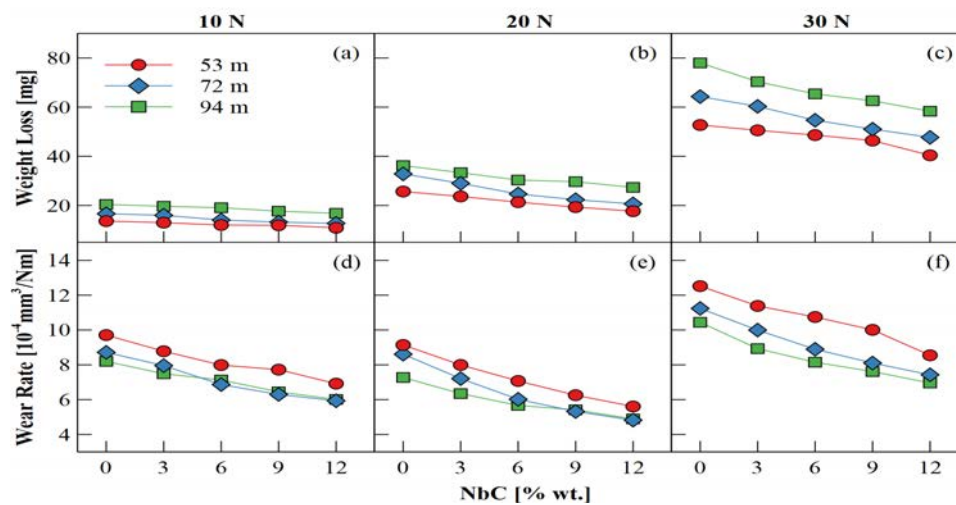
When Figure 3 (density results) is examined, it is observed that the density increases as the NbC amount in the matrix increases. Whereas the highest density was obtained as 2.97 g/cm^3 in AMC to which 12% NbC was added, the lowest density was obtained as 2.79 g/cm^3 in the matrix material. This increase in density is because the density of the NbC is high relative to the density of the A356 alloy. Similar results have been reported in the literature (Parvin et al., 2008; Efe et al., 2011) In addition, it is observed that the Relative Density (RD) decreases as the amount of NbC in the A356 (the matrix material) increases. One of the disadvantages of the method used is the inability to remove the porous structure in the produced parts. In the ball milling process, the powders undergo excessive deformation, and they fracture. As a result of the fracturing of the powders, roughness occurs on the powder surfaces. At the step of cold forming of powders, powders cannot be packed completely, and pores remain in the structure. This leads to a decrease in the RD of produced AMCs. Besides, deformation on matrix grains caused by increasing hard reinforcement particles in the matrix is another reason for the decrease in relative density. Results are similar to previous studies (Efe et al., 2011; Simsek and Ozyurek, 2020). Similarly, when Figure 3 (the hardness results) is examined, the hardness of the AMCs increases as increases the NbC amount in the matrix. The lowest hardness was procured as 557.27 HV matrix materials. If the highest hardness was procured as 674.8 HV in 12% NbC added AMC. The increase in hardness is due to the prevention of dislocation movements. Because NbC particles are harder against the matrix and prevent dislocation movements. In addition, the load on the matrix is transferred to the NbC phase, which leads to an increase in the AMCs' hardness and strength. (Satish Kumar et. al., 2019; Lemine et. al., 2022).

Wear Test Results At Room Temperature

The wear test results of NbC reinforcement AMCs, under different loads at room temperature are given in Fig. 4.

Figure 4.

Wear Test Results at Different Loads and at Room Temperature of NbC Reinforcement AMCs



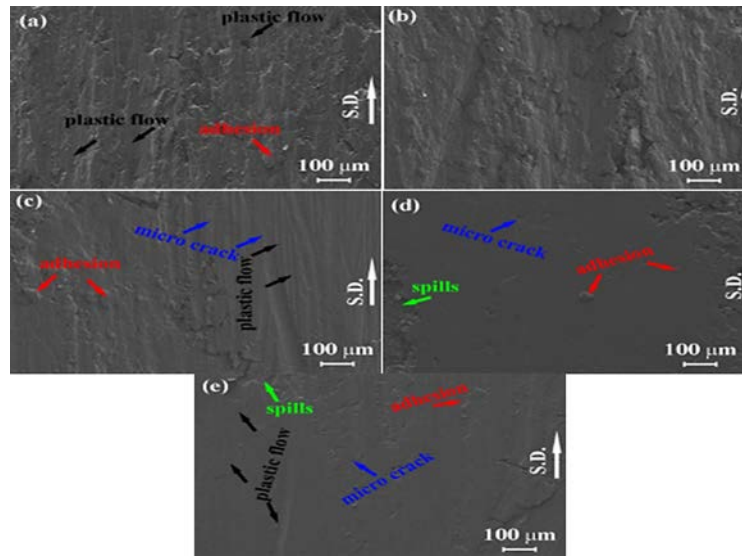
When wear test results are examined, it is observed that as load increases, weight loss also increases. The lowest weight loss was achieved under a load of 10 N. The increasing stresses on the wear surface of composites due to increasing load cause the

mechanical bonds between the matrix reinforcement to weaken. The fractures that occur due to this weakening increase weight loss (Sridhar et al., 2020). As increasing sliding distance in all loads is seen the weight loss increases. The micro-cracks occurring on the surface of composites at the beginning of the wear test (due to shear stresses) progress with increasing sliding distances and reach macro sizes. Cracks that reach macro sizes cause fractures and ruptures in the sample. The particles that break off from the composites during the wear test increase the weight loss. In a study, Basavarajappa et al. (2007) tried to determine the important wear parameters of metal matrix composites by using the Taguchi technique. According to their results, they reported the parameter that has the most physical and statistical effect on wear is the sliding distance. When the effect of the NbC amount in the weight loss graphs is examined, it is understood that the weight loss decreases of composites as the amount of NbC increases under all loads. It is determined that the lowest weight loss is in 12% NBC-added AMC in all loads. The obtained weight loss results and the expected hardness results support each other. Low weight loss is expected in materials with high hardness. This situation can be explained by the Archard equation. The results obtained are parallel to the results in the literature (Rajmohan et al., 2013; Çelik and Seçilmiş, 2017; Idrisi & Mourad, 2019). When the wear rates of AMCs which produced are investigated, it is observed that the lowest wear rate under all loads is in 12% NbC added composite (Figure 5 (c-d-e)). This reduction in wear rates can be associated with the porosity in the structure. Microchips formed in the course of wear keep in the pores of the structure, which causes a decrease in both weight loss and wear rate. Another condition that draws attention in the wear rate graphs is that the wear rate decreases as the sliding distance increases. This decrease in wear rates can be attributed to the hardness of the reinforcement phase as the dominant factor affecting the wear rate. It can also be attributed to the greater ability to load carrying of the reinforcing material and the between the NbC particles and the Al matrix, a strong interfacial bonding (Rajmohan et al., 2013). The worn surface SEM images at room temperature and 20N load of AMCs with different amounts of NbC added are given in Figure 5.

The worn surface SEM images observed that the traces of deformation occurring on the composite surface decrease as increases the amount of NbC in the matrix (Figure 5). Shedding is observed on the worn surfaces of AMC materials containing matrix (A356+2Gr) and 3% and 6% reinforcements. Plastic flow zones are observed on the surface of AMCs containing 9% and 12% reinforcement. In addition, micro-sized cracks that have not reached macro-size are observed on the surface of composites to which 9% and 12% NbC were added. The obtained results in Figure 3 and Figure 4, and the worn surface SEM images support each other. Hardness is one of the important parameters in determining the weight losses of materials (Kumar et al., 2010). Stresses occur on the composite's surface during wear. These stresses are intensified around the reinforcement particles and lead to the genesis of microcracks. In the later steps of the sliding, micro-cracks progress, and reach macro sizes by merging. Cracks reaching macro sizes cause shedding on the material surface (Simsek and Ozyurek, 2020). In tests made at room temperature, while it is seen that the dominant wear mechanism is the adhesive wear mechanism in AMCs containing matrix and low reinforcement amount, it is observed that the abrasive wear mechanism is active in AMCs containing a high amount of reinforcement.

Figure 5.

The Worn Surface SEM Images at Room Temperature and at 20 N Load of AMCs with Different Amounts NbC Added.

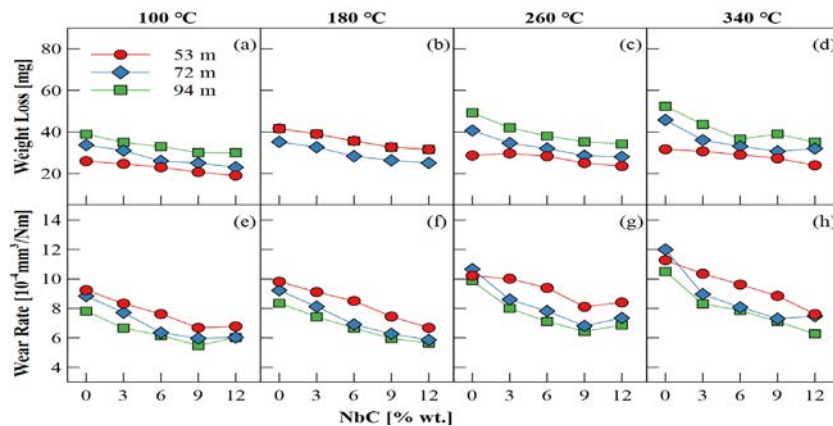


High Temperatures

Wear test results at high temperatures of AMCs, to which various NbC addition rates were used, under 20 N load are given in Fig. 6.

Figure 6.

Wear Test Results at High Temperature and under 20 N Load of AMCs Produced

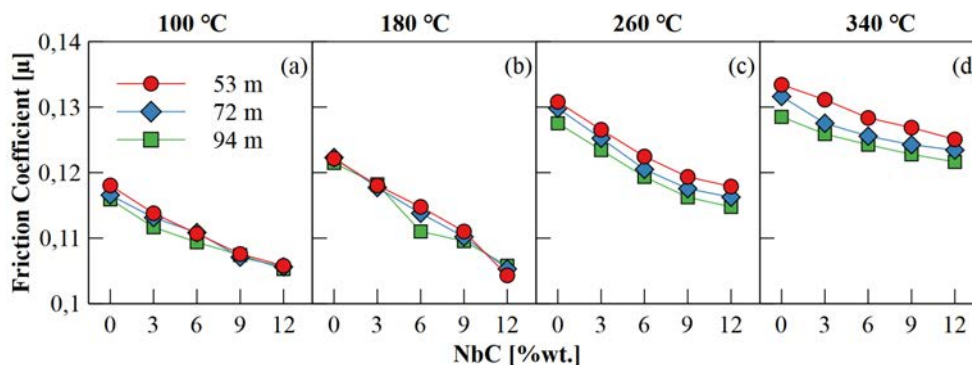


When weight loss results were examined, it occurred that weight loss (at all temperatures) decreased as the NbC increased in the matrix (Figure 6). The smallest loss in weight was achieved in the AMC material to which 12% NbC was added. Increased reinforcement in the matrix prevents dislocation movements in the matrix and increases the composite's resistance to plastic deformation (Uthayakumar et al, 2013). In addition, it is observed that weight losses increase as increases the operation temperature. The increase in weight loss can be attributed to the matrix softening with the operation temperature increasing. As the matrix (A356), which is the main element of the composite material, approaches the crystallization temperature, its ductility increases. This leads to the accumulation of stresses around the reinforcing particles (the effect of the load) during wear. Moreover, increasing the ductility of the matrix weakens and reduces the

strength of the bond between the matrix's with reinforcement. Because of this, it causes the creation of micro-cracks around the reinforcing particles. As temperature increases, an increase in weight loss occurs (Nemati et al., 2016; Simsek et al., 2022). Similarly, In the wear rate results is viewed that the wear rates also decrease as expected as the amount of NbC increases in the matrix. This reduction in wear rates can be associated with the hardness of the composite material. The fact that the weight loss and wear rate in general are low in materials with high hardness is a well-known phenomenon. However, it is observed that some of the results obtained do not meet this expectation. Examining the wear rate results, it is observed that at 100 °C and 260 °C temperatures (Figure 6(c and g)) and 94m sliding distance, the wear rates of 12% NbC-added composites increase compared to the 9% NbC-added composites. It can be said that these results may have been due to a coarse particle that snapped off while being worn. When the results of weight loss are examined in the same samples, it is observed that the decrease in weight loss is less than usual. During wear, several unexpected and uncontrollable situations may occur in the tribological system. For this reason, unexpected sudden weight losses and unexpected, unusual increases can be observed. Another noteworthy issue in the given wear rate results is that the wear rate results of the composite material to which 12% NbC was added are at approximate values in the final stage of sliding (94m) at all temperatures. The decrease in wear rates with increasing distance during the wear test can be explained by the protective effect of the oxide layer created on the composite surface. The lubricating effect of the oxide film layer formed on the sample surface and its relatively hard nature facilitate sliding. This leads to a decrease in the wear rate (Xiao et al., 2020; Tan et al., 2021). In addition, at high temperatures (260-340°C), a significant decrease is observed in wear rates. At low temperatures, the abrasive wear effect is reduced by the effect of the Al₂O₃ layer created on the wear surface of the matrix and the NbC phase. However, at high temperatures, it is easier for the oxide layer to form or fracture (due to the ductility effect). Therefore, the Al matrix is exposed to severe plastic deformation and wear. However, the wear particles formed as a result of severe plastic deformation without being able to move off from the tribological system. Therefore, the wear particles formed remain at the interface (between the pin-disk) under the influence of temperature and load. These wear particles remaining on the interface create a tribolayer on the sample surface as a result of crushing, oxidation, and re-bonding to the surface. This tribolayer leads to a decrease in both weight loss and wear rate (Mao et al., 2013; Şimşek et al., 2022). Friction coefficient results at high temperatures of AMCs, to which various NbC addition rates were used, under 20N load are given in Figure 7.

Figure 7.

Friction Coefficient Results at High Temperature and under 20 N Load of AMCs Produced

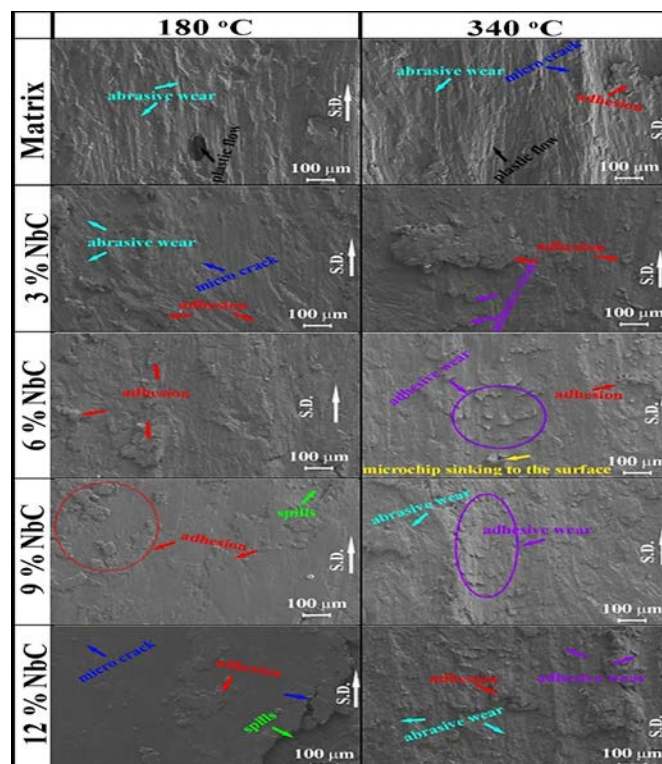


When Figure 7 is examined, it is observed that the friction coefficient decreases as the NbC quantity increases in the matrix. This decrease is associated with the hardness of the produced composite. The decrease of friction coefficient with high hardness is known. In addition, the increase in temperature leads to an increase in the friction coefficient. This increase in the friction coefficient is based on the fact that the recrystallization temperature is active at rising temperatures (Daoud et al., 2004; Zhu et al., 2012). During wear, an oxide layer is formed on the wear surface due to friction. This oxide layer, which is hard compared to the matrix, reduces the friction coefficient. However, increasing the ductility of the sample with increasing temperature causes the oxide film layer to fracture more easily due to stresses. A softer new contact surface is formed under the fractured oxide layer. This softer new contact surface increases the friction coefficient. (Raju et al., 2019; Ozyurek and Ciftci, 2011). Worn surface SEM images at 180 °C and 340 °C temperatures under 20N load of AMCs produced are given in Figure 8.

When the SEM images in Figure 8 are examined, wear marks parallel to the sliding surface can be seen. Moreover, up to AMC to which 6% NBC was added, it is observed that at both temperatures the wear marks are in different directions according to the direction of the sliding. The oxide layer formed on the sample surface under the influence of temperature and friction is broken due to the crack progression reaching macro sizes. While these relatively harder microchips move away from the tribological system, they create deep scratches on the surface, which is softer due to the influence of temperature. In addition, the hard oxide particles moving on the contact surface of the sample and the disk (softening of the sample surface under the influence of temperature) show different orientations. This leads to the formation of deep scratches on the wear surface, which are not parallel to the direction of sliding.

Figure 8.

Worn Surface SEM Images at 180 °C and 340 °C Temperatures under 20 N Load of AMCs Produced



In the worn surface images obtained at a temperature of 180 °C, it is observed that there is no abrasive wear effect on the surface of the AMCs to which 9% and 12% NbC were added. The abrasive wear mechanism is faced in abrasion tests performed at low temperatures (Lee et al., 2008). In these AMCs, it is observed that microchips formed during wear adhere to the sample surface. SEM images of the worn surface of 9% and 12% NBC-added AMCs confirm the wear rate and friction coefficient results. Hard oxide particles adhering to the worn surface again cause both friction and wear rate to decrease. The worn surfaces of all produced composites differ markedly based on the change in operating temperatures. It is clearly understood that the abrasive wear mechanism is active in the AMC, to which the matrix and 3% NbC reinforcement are added, at a temperature of 340°C. As the reinforcement content increases (6-12%), traces of deformation in the form of foliation are observed on the surface. It is observed that as a result of the increased amount of reinforcement, the adhesive wear mechanism is also active in addition to the abrasive wear mechanism. On the other hand, plastic flow zones formed are clearly visible on worn surfaces obtained by abrasion tests performed at room temperature (Figure 5), while it is observed that plastic flow zones disappear at high temperatures (180°C and 340°C). In a previous study, it was noted that at high temperatures, the plastic flow zones formed during sliding disappeared. It was stated that this was due to the backflow tendency of the matrix whose ductility increased due to gaps at the edges of the plastic flow zones (Nemati et al., 2016). In addition, because the microchips separated from the sample due to increasing operating temperatures adhere to the surface again under the influence of temperature and load, the occurred plastic flow zones are not seen. Microchips adhering/embedding to the sample surface can be clearly seen on the worn surface SEM images (Figure 8). In addition, the weakening of the mechanical bond between the matrix and the reinforcement due to increasing temperatures leads to the formation of deep deformation on the worn surface of the AMC (Tan et al., 2021).

Conclusions

In this study, the wear performance of AMCs produced by the high-energy ball milling method through adding different amounts of NbC to the A356+2%Gr matrix was examined at different temperatures. It was observed that in AMCs with low reinforcement content, the reinforcement phase (NbC) decreased to nano sizes and the reinforcement phase tended to cluster at grain boundaries. It was also observed that with the increase in the amount of reinforcement phase in the matrix, the reinforcement phase remained in micron sizes, and it was distributed homogeneously in the matrix. It was determined that the hardness of the AMC increased as the amount of NBC increased in the matrix. Compared to the matrix, the increase in hardness was achieved by about 21% in AMC to which 12% NbC was added. As the amount of reinforcement increased, the density of the produced AMC also increased. On the contrary, the relative density of the produced AMC decreased as the amount of reinforcement increased. In wear tests performed at room temperature and under different loads (the first step of the study), it was observed that as the amount of reinforcement in the matrix increased, weight loss increased under all loads. In terms of wear rates, the lowest wear rate was achieved under the load of 20 N. In the wear tests done at room temperature, it was found that the wear mechanism was abrasive. In the wear tests done at different operating temperatures under a load of 20 N in the second step of the study, it was observed that weight loss increased as the temperature increased. In terms of wear rate results, the lowest wear rate was obtained

at a temperature of 180 °C in AMC to which 12% NbC was added. It was seen that deformation occurred in the form of foliation on the wear surfaces of AMCs due to the increasing temperature. In addition, it was observed that the adhesive wear mechanism was activated as well as the abrasive wear mechanism due to the increasing temperature.

References

- Akçamlı, N., Şenyurt, B., Gökçe, H. & Ağaoğulları, D. (2022), “Powder metallurgical fabrication of graphene reinforced near-eutectic Al-Si matrix composites: Microstructural, mechanical and electrochemical characterization”, *Engineering Science and Technology, an International Journal*, 31, 101052, doi:10.1016/j.jestch.2021.08.009.
- Aksöz, S., Bican, O., Çalın, R., & Bostan, B. (2014), “Effect of T7 heat treatment on the dry sliding friction and wear properties of the SiC-reinforced AA 2014 aluminium matrix composites produced by vacuum infiltration”, *Proceedings of the Institution of Mechanical Engineers, Part J*, 228(3), 312-319, doi:10.1177/1350650113506570.
- Bakshi, S.R., Keshri, A.K., Singh, V., Seal, S. & Agarwal, A. (2009), “Interface in carbon nanotube reinforced aluminum silicon composites: Thermodynamic analysis and experimental verification”, *Journal of Alloys and Compounds*, 481(1-2), 207-213, doi:10.1016/j.jallcom.2009.03.055.
- Basavarajappa, S., Chandramohan, G. & Davim, J.P. (2007), “Application of Taguchi techniques to study dry sliding wear behaviour of metal matrix composites”, *Materials & Design*, 28(4), 1393-1398, doi:10.1016/j.matdes.2006.01.006.
- Baskaran, S., Anandkrishnan, V.A. & Duraiselvam, M. (2014), “Investigations on dry sliding wear behavior of in situ casted AA7075-TiC metal matrix composites by using Taguchi technique”, *Materials & Design*, 60, 184-192, doi:10.1016/j.matdes.2014.03.074.
- Benjamin, J.S. (1970), “Dispersion strengthened superalloys by mechanical alloying”, *Metallurgical Transactions*, 1, 2943-2951, doi:10.1007/BF03037835.
- Bian, Y., Ni, J., Wang, C., Zhen, J., Hao, H., Kong, X., Chen, H., Li, J., Li, X., Z. Jia, Luo, W. & Chen, Z. (2021), “Microstructure and wear characteristics of in-situ micro/nanoscale niobium carbide reinforced copper composites fabricated through powder metallurgy”, *Materials Characterization*, 172, 110847, doi:10.1016/j.matchar.2020.1108470.
- Choi, H.J., Shin, J.H. & Bae, D.H. (2010), “Self-assembled network structures in Al/C60 composites”, *Carbon*, 48(13), pp. 3700-3707, doi:10.1016/j.carbon.2010.06.013.
- Chu, H.S., Liu, K.S. & Yeh, J.W. (2001), “Damping behavior of in situ Al-(graphite, Al₄C₃) composites produced by reciprocating extrusion”, *Journal of Materials Research*, 16(5), 1372-1380, doi:10.1557/JMR.2001.0192.
- Çelik, Y.H. & Seçilmiş, K. (2017), “Investigation of wear behaviours of Al matrix composites reinforced with different B₄C rate produced by powder metallurgy method”, *Advanced Powder Technology*, 28(9), 2218-2224, doi: 10.1016/j.appt.2017.06.002.
- Dai, W., Yue, B., Chang, S., Bai, H., & Liu B., (2022), “Mechanical properties and

- microstructural characteristics of WC-bronze-based impregnated diamond composite reinforced by nano-NbC”, *Tribology International*, 174, 107777, doi:10.1016/j.triboint.2022.107777.
- Daoud, A., Abou-Elkhair, M.T. & Rohatgi, P. (2004), “Wear and friction behavior of near eutectic Al-Si+ZrO₂ or WC particle composites”, *Composites Science and Technology*, 64(7-8), 1029-1040, doi:10.1016/j.compscitech.2003.09.020.
- Demirskyi, D., Borodianska, H., Suzuki, T.S., Sakka, Y., Yoshimi, K. & Vasylykiv, O. (2019), “High-temperature flexural strength performance of ternary high-entropy carbide consolidated via spark plasma sintering of TaC, ZrC and NbC”, *Scripta Materialia*, 164, 12-16, doi:10.1016/j.scriptamat.2019.01.024.
- Efe, G.C., Yener, T., Altinsoy, I., İpek, M., Zeytin, S. & Bindal, C. (2011), “The effect of sintering temperature on some properties of Cu-SiC composite”, *Journal of Alloys and Compounds*, 509(20), 6036-6042, doi:10.1016/j.jallcom.2011.02.170.
- García, J., Ciprés, V.C., Blomqvist, A. & Kaplan, B. (2019), “Cemented carbide microstructures: a review”, *International Journal of Refractory Metals and Hard Materials*, 80, 40-68, doi:10.1016/j.ijrmhm.2018.12.004.
- Idrisi, A.H. & Mourad, A.H.I. (2019), “Wear performance analysis of aluminum matrix composites and optimization of process parameters using statistical techniques”, *Metallurgical and Materials Transactions A: Physical Metallurgy and Materials Science*, 50, 5395-5409, doi: 0.1007/s11661-019-05446-z.
- Ipek, R. (2005), “Adhesive wear behaviour of B₄C and SiC reinforced 4147 Al matrix composites (Al/B₄C-Al/SiC)”, *Journal of Materials Processing Technology*, 162, 71-75, doi:10.1016/j.jmatprotec.2005.02.207.
- Kennedy, A.R., Weston, D.P. & Jones, M.I. (2001), “Reaction in Al-TiC metal matrix composites”, *Materials Science and Engineering: A*, 316(1-2), 32-38, doi:10.1016/S0921-5093(01)01228-X.
- Kumar, S., Sarma, V.S. and Murty, B.S. (2010), “High temperature wear behavior of Al-4Cu-TiB₂ in situ composites”, *Wear*, 268(11-12), 1266-1274, doi:10.1016/j.wear.2010.01.022.
- Lee, J.M., Kang, S.B. & Han, J. (2008), “Dry sliding wear of MAO-coated A356/20 vol.% SiCp composites in the temperature range 25-180 °C”, *Wear*, 264(1-2), 75-85, doi:10.1016/j.wear.2007.01.044.
- Lemine, A.S., Fayyaz, O., Yusuf, M., Shakoor, R.A., Ahmad, Z., Bhadra, J. & Al-Thani, N.J. (2022), “Microstructure and mechanical properties of aluminum matrix composites with bimodal-sized hybrid NbC-B₄C reinforcements”, *Materials Today Communications*, 33, 104512, doi:10.1016/j.mtcomm.2022.104512.
- Mao, Y.S., Wang, L., Chen, K.M., Wang, S.Q. & Cui, X.H. (2013), “Tribo-layer and its role in dry sliding wear of Ti-6Al-4V alloy,” *Wear*, 297(1-2), 1032-1039, doi:10.1016/j.wear.2012.11.063.
- Nemati, N., Emamy, M., Penkov, O.V., Kim, J. & Kim, D.E. (2016), “Mechanical and high temperature wear properties of extruded Al composite reinforced with Al₁₃Fe₄ CMA nanoparticles,” *Materials & Design*, 90, 532-544, doi:10.1016/j.matdes.2015.11.001.

- Ozyurek, D. & Ciftci, I. (2011), "An investigation into the wear behaviour of TiB₂ particle reinforced aluminium composites produced by mechanical alloying", *Science and Engineering of Composite Materials*, Vol. 18(1-2), 5-12, doi:10.1515/secm.2011.003.
- Özyürek, D., Yıldırım, M., & Çiftçi, İ. (2012), "The tribological properties of A356-SiCp metal-matrix composites fabricated by thixomoulding technique", *Science and Engineering of Composite Materials*, 19(4)351-356, doi:10.1515/secm-2012-0012.
- Parvin, N., Assadifard, R., Safarzadeh, P., Sheibani, S. & Marashi, P. (2008), "Preparation and mechanical properties of SiC-reinforced Al6061 composite by mechanical alloying", *Materials Science and Engineering: A*, 492(1-2), 134-140, doi:10.1016/j.msea.2008.05.004.
- Rajaram, G., Kumaran, S., Rao, T.S. & Kamaraj, M. (2010), "Studies on high temperature wear and its mechanism of Al-Si/graphite composite under dry sliding conditions", *Tribology International*, 43(11), 2152-2158, doi:10.1016/j.triboint.2010.06.004.
- Rajmohan, T., Palanikumar, K. & Ranganathan, S. (2013), "Evaluation of mechanical and wear properties of hybrid aluminium matrix composites", *Transactions of Nonferrous Metals Society of China*, 23(9), 2509-2517, doi: 10.1016/S1003-6326(13)62762-4.
- Raju, R.S.S., Panigrahi, M.K., Ganguly, R.I. & Rao, G.S. (2019), "Tribological behaviour of al-1100-coconut shell ash (CSA) composite at elevated temperature", *Tribology International*, 129, 55-66, doi:10.1016/j.triboint.2018.08.011.
- Salimi, A., Borhani, E. & Emadoddin, E. (2015), "Evaluation of mechanical properties and structure of 1100-Al reinforced with ZrO₂ nano-particles via accumulatively roll-bonded", *Procedia Materials Science*, 11, 67-73, doi:10.1016/j.mspro.2015.11.094.
- Satish Kumar, T., Suganya Priyadharshini, G., Shalini, S., Krishna Kumar, K., & Subramanian, R. (2019), "Characterization of NbC-reinforced AA7075 alloy composites produced using friction stir processing", *Transactions of the Indian Institute of Metals*, 72, 1593-1596, doi:10.1007/s12666-019-01566-7.
- Sekar, K., Jayachandra, G. & Aravindan, S. (2018), "Mechanical and welding properties of A6082-SiC-ZrO₂ hybrid composite fabricated by stir and squeeze casting," *Materials Today: Proceedings*, 5, (9), 20268-20277, doi:10.1016/j.matpr.2018.06.398.
- Simsek, D. & Ozyurek, D. (2020), "The wear performance at high temperatures of ZrO₂-reinforced aluminum matrix composites produced by mechanochemical reaction method", *Journal of Tribology*, 142(10), 101701, doi:10.1115/1.4046857.
- Simsek, D., Ozyurek, D. & Salman, S. (2022), "Effect of TiC content on wear performance of A356 matrix composites at different temperatures," *Powder Metallurgy and Metal Ceramics*, Vol. 60(11-12), 706-716, doi:10.1007/s11106-022-00282-0.
- Simsek, D., Simsek, İ. & Ozyurek, D. (2019), "Production and characterization of Al-SiC composites by mechanical milling", *Bitlis Eren University Journal of Science and Technology*, 8(1), 227-233, doi:10.17798/bitlisfen.441420.

- Sopicka-Lizer, M. (Ed.). *High-energy ball milling: mechanochemical processing of nanopowders*, Elsevier, (2010). ISBN: 978-1-84569-531-6. doi:10.1016/B978-1-84569-531-6.50017-3.
- Souto, M.V.M., Araujo, C.P.B.D., Lima, M.J.S., Borges, F.M.M., Gomes, U.U. & Souza, C.P.D. (2018), "Synthesis and characterization of niobium carbide with copper addition obtained via gas-solid reaction", *Materials Research*, 21(3), 1108, doi:10.1590/1980-5373-MR-2016-1108.
- Soy, U., Ficici, F. & Demir, A. (2012), "Evaluation of the Taguchi method for wear behavior of Al/SiC/B₄C composites", *Journal of Composite Materials*, 46(7), 851-859, doi:10.1177/0021998311410510.
- Sridhar, H.S., Sanman, S., Prasad, T.B. & Chandra, B.T., (2020), "Effect of reinforcement and applied load on three-body dry sand abrasive wear behavior of A356 bottom ash metal matrix composites", *Materials Today: Proceedings*, 26, 2814-2816, doi:10.1016/j.matpr.2020.02.586.
- Şimşek, D., Özyürek, D. & Salman, S. (2022). "Wear behaviors at different temperatures of ZrO₂ reinforced A356 matrix composites produced by mechanical alloying method", *Industrial Lubrication and Tribology*, 74(5), 463-471, doi:10.1108/ILT-10-2021-0416.
- Şimşek, İ. (2019), "The effect of B₄C amount on wear behaviors of Al-Graphite/B₄C hybrid composites produced by mechanical alloying", *Journal of Boron*, 4(2), 100-106, doi:10.30728/boron.556707.
- Tan, H., Sun, Q., Chen, W., Zhu, S., Cheng, J. & Yang, J. (2021), "Tribological performance and wear mechanisms of a high-temperature wear-resistant Al-Si/SiAlON composite", *Tribology International*, 164, 107227, doi:10.1016/j.triboint.2021.107227.
- Travessa, D.N., Silva, M.J. & Cardoso K.R. (2017), "Niobium carbide-reinforced Al matrix composites produced by high-energy ball milling", *Metallurgical and Materials Transactions B*, 48, 1754-1762, doi:10.1007/s11663-017-0959-z.
- Uthayakumar, M., Aravindan, S. & Rajkumar, K. (2013), "Wear performance of Al-SiC-B₄C hybrid composites under dry sliding conditions", *Materials & Design*, 47, 456-464, doi:10.1016/j.matdes.2012.11.059.
- Xiao, J.K., Xiao, S.X., Chen, J. & Zhang, C. (2020), "Wear mechanism of Cu-based brake pad for high-speed train braking at speed of 380 km/h," *Tribology International*, 150, 106357, doi:10.1016/j.triboint.2020.106357.
- Zhu, H., Jar, C., Song, J., Zhao, J., Li, J. & Xie, Z. (2012), "High temperature dry sliding friction and wear behavior of aluminum matrix composites (Al₃Zr+α-Al₂O₃)/Al", *Tribology International*, 48, 78-86, doi:10.1016/j.triboint.2011.11.011.

About The Authors

Doğan ŞİMŞEK, is an Associate Professor at National Defence University Army NCO Vocational HE School, Department of Automotive Technology. He holds a PhD in Manufacturing Engineering from Karabuk University. His main areas of interest are material design, behaviors, composite materials, and internal combustion engines.

E-mail: dsimsek@msu.edu.tr, **ORCID:** 0000-0001-8339-9704.

İjlal ŞİMŞEK, is an Associate Professor at National Defence University Army NCO Vocational HE School, Department of Mechatronics Technology. She holds a PhD in Manufacturing Engineering from Karabuk University. Her main areas of interest are material design, and behaviors, manufacturing technologies.

E-mail: isimsek@msu.edu.tr, **ORCID:** 0000-0001-6542-8567.

Similarity Index

The similarity index obtained from the plagiarism software for this book chapter is 12%.

CHAPTER 10

Microstructure Analysis of Particle Reinforced Aluminum Matrix Composites Produced by Powder Metallurgy Using Image Processing Method

Nuri ATİK

National Defence University, Türkiye

Yusuf KARABACAK

National Defence University, Türkiye

İjlal ŞİMŞEK

National Defence University, Türkiye

Doğan ŞİMŞEK

National Defence University, Türkiye

To Cite This Chapter:

Atik, N., Karabacak, Y., Simsek, I. & Simsek, D. (2024). Microstructure Analysis of Particle Reinforced Aluminum Matrix Composites Produced by Powder Metallurgy Using Image Processing Method. In H. Gokmese, S. Bulbul, & Y. Uzun (Eds.), *Current Studies in Materials Science and Engineering* (pp. 145-156). ISRES Publishing.

Introduction

Alloys and casting metals are materials that offer both great performance and cost advantages. In contrast to casting metals, Metal Matrix Composites (MMCs) are more costly but provide better performance (Mortensen & Llorca, 2010). Some basic facts are what motivate the adoption of this technology despite its expense and certain difficulties. Firstly, overcoming the base material's strength limitations is made possible by the composite approach to material design. Secondly, it is the sole method that permits adding necessary components to some key metals, including oxides, nitrides, or carbides. Given that carbon, nitrogen, and oxygen are soluble in molten iron, carbides, nitrides, and oxides are rarely used to reinforce iron. In contrast, aluminum, copper, and magnesium do not have solubility for carbon. Therefore, composite structures at the core of carbide layers are formed for these metals. The same principle applies to oxides and nitrides as well. Thirdly, some phases, especially ceramics in finely divided form, exhibit

excellent properties. Particularly, ceramic particles in the micron size range can provide much higher strength than cast ceramics. Taking advantage of this on a macroscopic scale involves exceeding the strength limit of the alloy in the initial approach by adding finely divided non-metallic phases into the metal matrix (MMC). Many studies have reported an increase in strength in Metal Matrix Composite (MMC) compared to the matrix (Prajul Raj et al., 2023; Salur et al., 2021; Şimşek et al., 2020) .

However, the production methods for particulate-reinforced metal matrix composite (MMC) significantly impact material properties. Issues such as the particle size of reinforcement, wetting problems between the matrix and reinforcement, the formation of a porous structure, and agglomeration of the reinforcement phase are known to be associated with production methods. MMCs can be produced via solid (powder metallurgy), semi-solid (thixoforming), and liquid (infiltration) techniques. Because of its many benefits, powder metallurgy (PM) is the method most frequently used in the manufacturing of MMC, according to Prabhu et al. (2006) AMCs (Aluminum Matrix Composites) can be produced via a variety of techniques: semi-solid (thixoforming) (Lu et al., 2023; Özyürek et al., 2012), solid (powder metallurgy) (Fazlul Rahman et al., 2023), and liquid (infiltration) (Aksöz et al., 2014). According to Prabhu et al. (2006), powder metallurgy (PM) is more frequently used in the manufacturing of AMC because of its many benefits. The main benefit of the PM method with AMCs is its capacity to accomplish a uniform distribution of the reinforcement material within the matrix. Despite these advantages, there are also disadvantages to the PM method. The most well-known disadvantage of this technology is the powder packing problem. Powders undergo extreme deformation during the alloying process, which raises surface roughness. The compaction process results in the creation of non-sliding pores between the particles. This contributes even more to the resulting alloys' lower density (Yavuzer et al., 2019).

The more creative and data-driven approaches are quickly replacing the centuries-old traditional methods in the field of materials science and metallurgy today. These developments in material characterization and analysis are the result of the integration of artificial intelligence algorithms and image processing techniques (Xu et al., 2023). It is uncommon to use image analysis to assess the microstructure of particle-reinforced composite materials. Scanning electron microscopy (SEM) image processing can be difficult, but machine learning techniques make it easier (Čalkovský et al., 2021; Choudhary et al., 2022).

Particle-reinforced AMC microstructure analyses rely on a variety of analyses in addition to expert knowledge. SEM (Scanning Electron Microscopy) image size and quality are directly impacted by the expertise of the user. However, the identification of phases in the microstructure can be a time-consuming and challenging process with traditional methods. Therefore, different Deep Learning (DL) methods have been observed to be used in various studies in the literature. Madsen et al. (2018), developed a deep learning-based algorithm resilient to microscope parameters and noise for identifying the structure in Transmission Electron Microscope (TEM) images. They highlighted that the algorithm, trained with their developed simulation, demonstrated a high capacity for making reliable predictions on experimental images. Additionally, Ragone et al. (2020) suggested a modeling approach against deep learning for the real-time detection of atomic column heights in experimental high-resolution transmission electron microscopy (HRTEM) images of gold nanoparticles of different dimensions. According to their search, the modeling strategy created using their recommendations lays the groundwork for quick or instantaneous nanoparticle analysis and offers a framework for growing the

field of nanoscience's applications. Furthermore, Ziatdinov et al. (2017), recommended a technique that extracts the coordinates of each type of atom in the image using a neural network, and then uses that information to identify various fault types. They claimed that this deep learning-based approach, which is scalable and reminiscent of human operator logic, may bring about a significant change in the extraction and analysis of information from raw experimental data.

The most representative model of deep learning's single-stage object detection is the You Only Look Once (YOLO) series, which aims to quickly and precisely identify and categorize objects (Bochkovskiy et al., 2020). The first versions of the YOLO series, known as YOLO v1, had issues with inaccurate detection and poor target placement. The network's structure was altered to include high-resolution classifiers, group normalization, anchor boxes, and other modifications to enhance performance, especially in terms of detection speed. However, the Yolo v2 model is unable to achieve the necessary performance in terms of detecting overlapping targets.

The developed YOLOv3 significantly enhanced the network's performance by incorporating processes like multi-scale feature fusion, residual structures, an anchor selection mechanism, classification techniques, and more steps that widely expanded the network's overall capability (Kahler et al., 2023). To be sure, YOLO v4 is a useful tool for object detection applications because of its fast and precise target identification in higher-quality photos. Xu et al. (2023) showcased a model based on the network architecture of YOLO v4. They claimed that by identifying surface images of the component they pressed with low extrusion using the additive manufacturing technique, the model could accurately locate flaws and provide effective control performance.

In this study, a particle-reinforced aluminum matrix composite material was created using powder metallurgy's mechanical alloying process. The goal of the study was to determine the pore features and particle reinforcement by analyzing SEM (Scanning Electron Microscopy) images using the YOLO (You Only Look Once) v4 algorithm. This work provides a materials science methodology to evaluate microstructural properties more accurately and quickly by utilizing deep learning techniques.

Materials and Methods

Material Production and Characterization

In this study, approximately $\leq 63 \mu\text{m}$ particle size A356 alloy powder was mixed with 12% by weight of NbC. The powder mixtures, prepared by weight, were mechanically alloyed in a planetary ball mill. To avoid the powders overheating, the mechanical alloying process was completed in eight cycles totaling 240 minutes. Each cycle consisted of 30 minutes of alloying followed by 10 minutes of rest. The alloying process was conducted using a stainless-steel grinding cell with 8mm stainless steel balls. The parameters employed were a 10:1 powder-to-ball ratio, 50% filling ratio, and a milling speed of 300 rpm. As a processing control agent, 1% stearic acid was used. After the mechanical alloying process, the prepared composite powders were cold-formed using a uniaxial hydraulic press under 700 MPa pressure, resulting in cylindrical specimens with dimensions of $\text{\O}12 \times 7 \text{ mm}$. The cold-formed raw samples were sintered at 550 °C for 1 hour with a heating rate of 5 °C/min under a vacuum atmosphere of 10^{-6} mbar. Following the sintering process, the samples cooled down to room temperature at their own cooling rate, completing the sintering procedure. Post-sintering, the prepared samples underwent standard metallographic procedures and were etched with Keller's solution for 40–45 seconds. The etched AMC samples were examined in microstructure

analyses using a Carl Zeiss Ultra Plus Gemini scanning electron microscope + energy-dispersive spectroscopy (SEM+EDS). The SEM images used in the study were obtained from 10 different AMC samples produced under identical conditions, capturing images from various regions of each sample.

YOLO v4: The Fundamental Principles and Operating Mechanism

A useful tool for many different object detection applications is YOLO v4. This algorithm is well known for its capacity to recognize objects in images, and it offers a significant benefit for material analysis. YOLO v4 is perfect for complicated tasks like microstructure analysis because it can detect objects quickly and accurately (Xu et al., 2023).

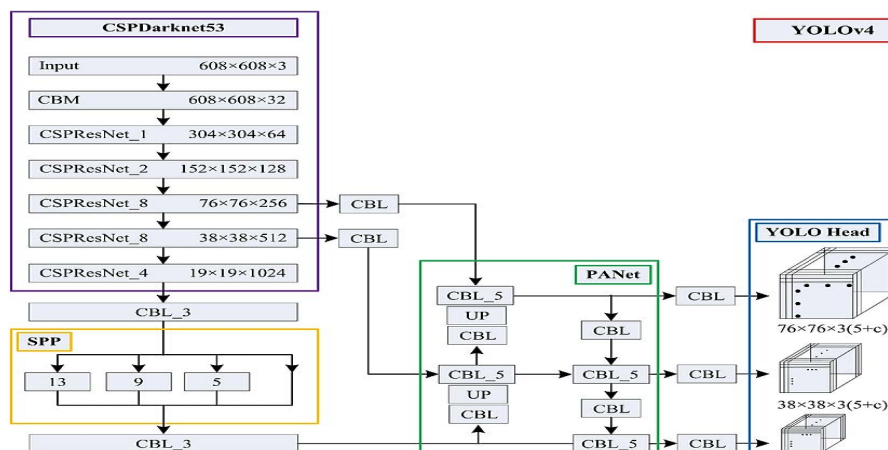
YOLO v4 offers several significant benefits:

- Quick Detection: YOLO v4 classifies and recognizes objects with speed.
- Multiple Object Detection: It can recognize several objects at once.
- Broad Applicability: Versatile enough to be employed in a range of settings.
- High Accuracy: Provides exact results while operating at a low error rate.

Opportunities for additional development still exist, and problems like difficult objectives and poor target detection persist. Bochkovskiy et al.'s (2020) YOLO v4 model substantially addresses the drawbacks of the YOLO v3 model. Three fundamental parts make up the YOLO network: the “Backbone,” “Neck,” and “Head.” The “Backbone” convolutional neural network collects and produces image features at different granularities. The “Neck” is a collection of network layers that integrate and mix image features. YOLO v4 is employed to send image features to the prediction layer and combine feature data from maps of various dimensions. (Anwar et al., 2021; Li et al., 2023).

The component known as the “Head” in a network predicts image features, creates bounding boxes, and predicts categories. YOLO v4 utilizes CSPDarknet53 for the Backbone, SPP (Spatial Pyramid Pooling) + PANet (Path Aggregation Network) for the Neck, and “YOLO Head” for the Head, which remains consistent with YOLO v3. The network structure of YOLO v4 is shown in Figure 1. (Chen et al., 2021).

Figure 1.
YOLO v4 Structure



During network optimization, YOLO v4 selects CSPDarknet53 with CSP as the Backbone to suppress unnecessary gradient information. The CSP module used in YOLO v4, compared to the Darknet53 used in YOLO v3, can integrate all gradient changes into the feature map to reduce computation and parameter requirements while maintaining accuracy. In the Backbone section of YOLO v4, the Mish activation function is used to allow better input penetration, enabling the system to perform the recognition task of Si, NbC, and space with higher efficiency and cost-effectiveness, applying less strain on resources (Chen et al., 2021).

In the Neck section of YOLO v4, the SPP (Spatial Pyramid Pooling) module is utilized as an additional module, while the PANet (Path Aggregation Network) serves as a feature fusion module. The SPP module can significantly expand the receptive field, separate crucial contextual features, enhance global and local accuracy in complex environments, and improve detection efficiency in fruit recognition. As observed in previous studies, the PANet module addresses the deficiency of unidirectional feature fusion in Feature Pyramid Networks (FPN). It achieves improvement by adding bottom-up feature fusion and enhancing feature extraction capabilities. Due to the random distribution of the items to be identified in the photos, there is always some overlap and collision, which makes it common for approaches like YOLO v3 to be overlooked and misidentify elements in such circumstances. However, by merging photos during training through random scaling, cropping, and alignment, YOLO v4 can more successfully handle this problem. This methodology has the potential to generate heterogeneous backdrops, fortify the network, and improve element detection in demanding contexts. The technique of mosaic data augmentation is employed to accomplish this. (Anwar et al., 2021).

Object Detection Network Training and Result Analysis

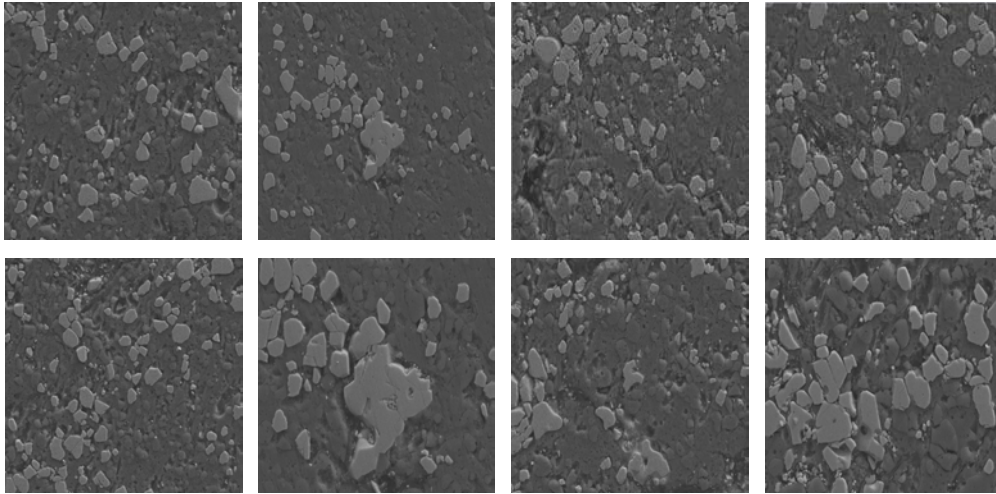
Experimental Work Platform

Google Colab was utilized for model training due to its access to better processors and memory resources. On the other hand, for other tasks such as image data processing, a computer with an AMD Ryzen 5 5500U, Radeon Graphics, 2100 MHz, 6 cores, and 12 logical processors was used. The Python programming language, under Microsoft Windows 11 Pro, within Jupyter Notebook in Anaconda, was employed for all the software programs in this article.

Used Datasets and Their Characteristics

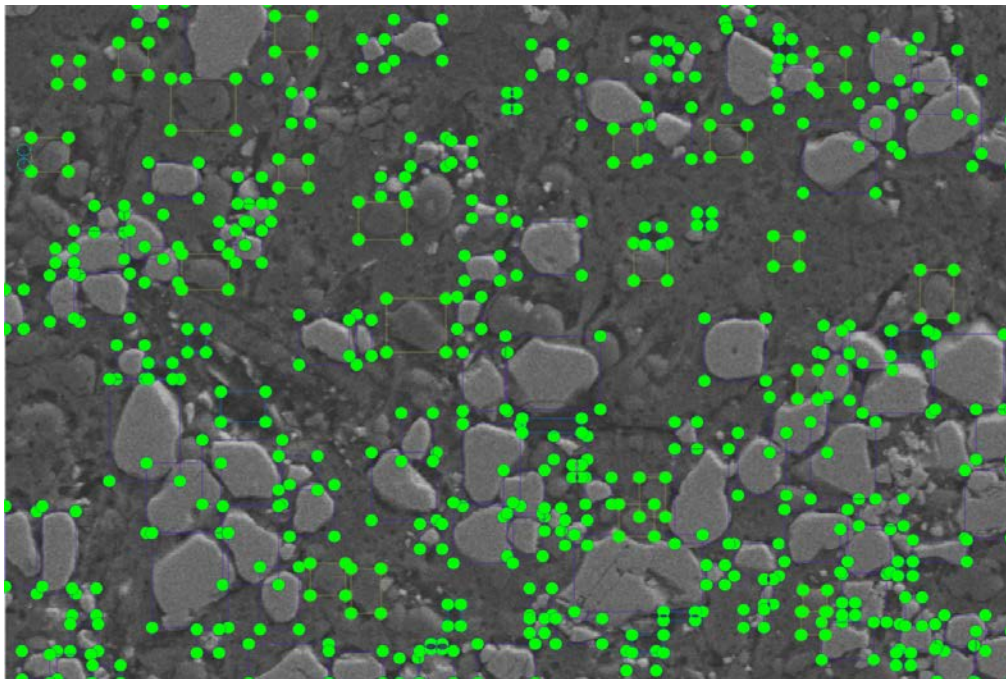
A total of 25 SEM images were used to train the system. In these 25 images, 3129 labeling operations were applied.

Figure 2.
SEM Images



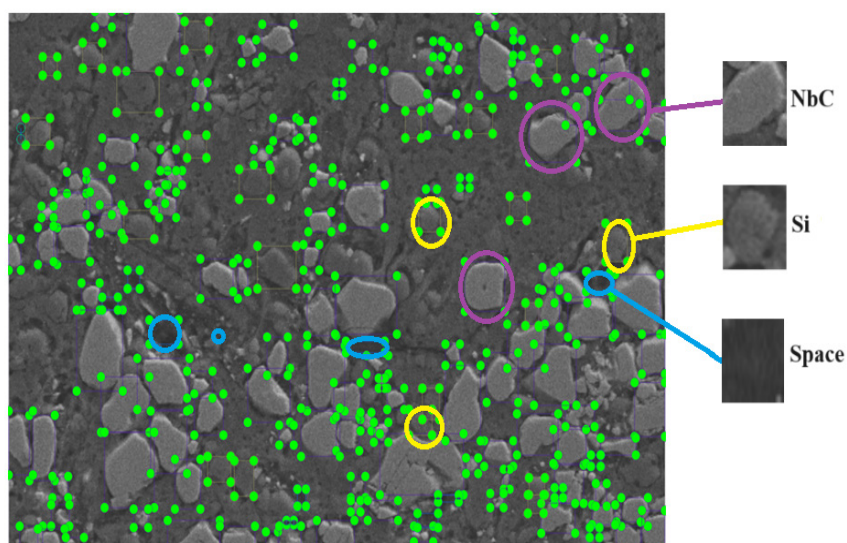
Some of the SEM photographs used in Figure 4 are shown.

Figure 3.
A SEM Image With Labeling Operations Performed



Purple- NbC, Yellow- Si, Blue- Space

Figure 4.
Close-up of NbC, Si and Space



In Figure 5, the annotations made on a SEM image used for training are shown. Here, purple boxes are used for “NbC,” yellow boxes for “Si,” and blue boxes for space.

Figure 5.
An Example Coordinates of A Label (The numbers of image: Width, Height, X, Y)

0.677344 0.658333 0.510938 0.187500

Training Method

Google Colab was used to train the model. Firstly, the obtained images and created label files were transferred to Google Colab. Subsequently, the created training algorithm was executed, and the trained files were downloaded to the local computer. Then, algorithmic work on this file continued on the local computer.

Algorithm Evaluation Metrics

Test time (T), Precision (P), Recall (R), Average Precision (AP), and F1 score metrics were utilized to evaluate the algorithm’s performance in this study. Precision is known as the percentage of true positive samples among all the positive samples predicted by the model. Recall is the ratio of true positive samples correctly predicted by the model to all true positive samples. Precision and recall typically have a negative relationship, where one rises while the other falls. A P-R curve can be plotted to see how they distribute. AP can be used as a comprehensive evaluation index to balance the effects of precision and recall and assess a model more comprehensively. (Chen et al., 2023; Ho et al., 2020).

A higher value indicates that the model performs better. The area under the P-R curve is indicated by the AP value. The F1 score, considering both precision and recall of the classification model, is the harmonized average of precision and recall. The applied calculation formula is as follows (Jiang et al., 2023; Li et al., 2021).

$$P = \frac{TP}{TP + FP} \times 100\% \quad (1)$$

$$R = \frac{TP}{TP + FN} \times 100\% \quad (2)$$

$$AP = \int_0^1 P(R) dR \quad (3)$$

$$F1Score = \frac{2xPxR}{P + R} \times 100\% \quad (4)$$

TP: The number of actual positive samples that produced the expected positive results.

FP: The proportion of real negative samples with anticipated positive results.

FN: Actual negative sample count with unfavorable prediction outcomes.

Detection time was evaluated using image detection and frame rate (FPS - Frames Per Second). As shown in Eq. (5), the average detection time per image is calculated by dividing the total detection time by the number of detections. As demonstrated in Eq. (6), the frame rate is denoted as FPS. The shorter the time spent on a single image, the larger the FPS result, indicating a faster detection speed of the neural network model (Li et al., 2021; Li et al., 2023).

$$Time = \frac{Total\ Time}{Test\ Interval} \quad (5)$$

$$FPS = \frac{1}{Time} \quad (6)$$

Results and Discussion

The applied YOLO v4 model yielded a mAP@0.5 value of 64.5% and an FPS value of 15.77.

This study introduces a novel perspective for material analysis using the YOLO v4 algorithm and SEM images. The research results encompass significant advantages in the fields of materials science and metallurgy. (Pei et al., 2021).

Fast and precise material analysis: Material analysis performed with the YOLO v4 algorithm enables the rapid and detailed detection of Si, NbC, and spaces in SEM images. This can accelerate the analysis process and enhance the precision of the results. (Zheng et al., 2021).

Figure 6.
Detection Images

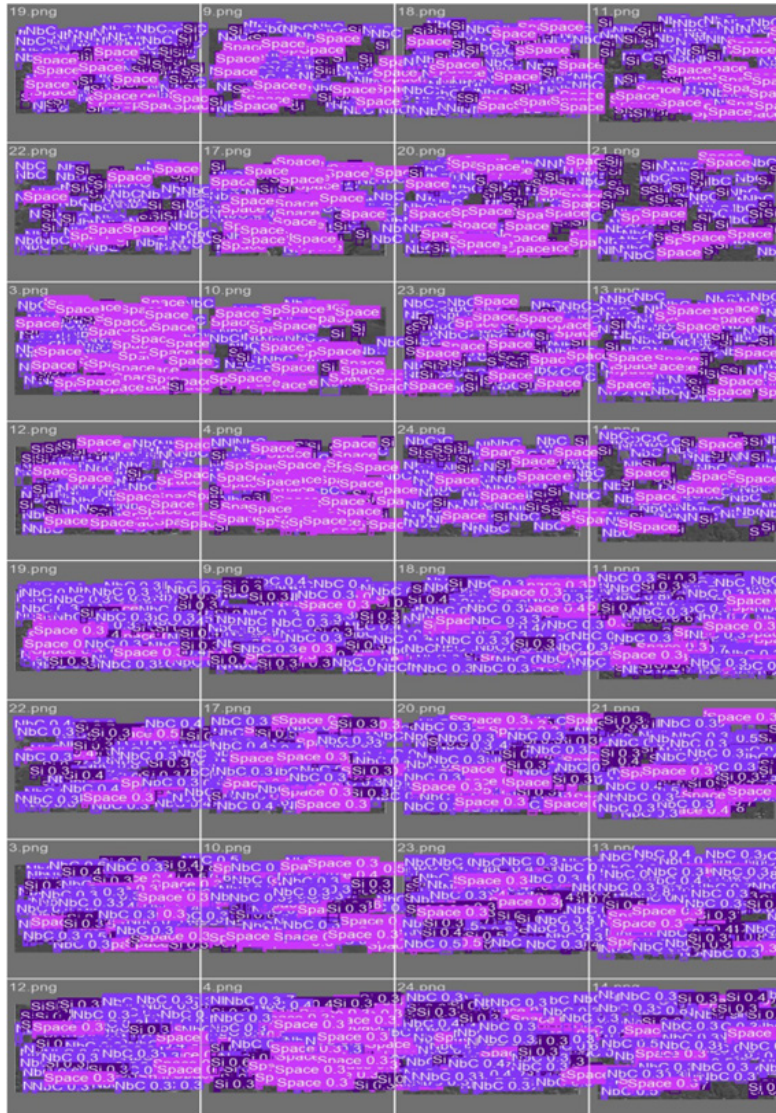
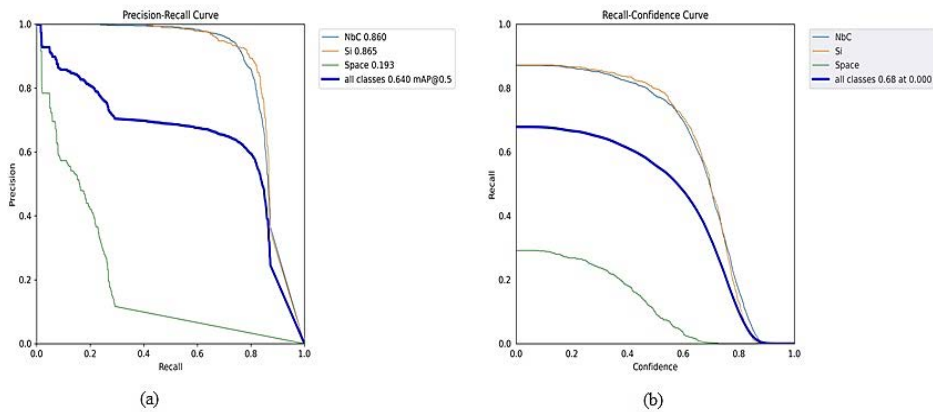


Figure 7.
(a) PR and (b) RC Graphics



Easy data processing and collection: The YOLO v4 algorithm can efficiently process large datasets and perform object detection rapidly. This facilitates working with large datasets for researchers. (Li et al., 2021).

Potential for materials engineering and design: This strategy opens up new avenues for material engineers to explore in terms of design. The identification of novel material structures and constituents can be sped up with high-precision material analysis. Regarding artificial intelligence and materials science integration this study shows how artificial intelligence methods can be incorporated into the engineering and materials science fields. There is room for future innovation and development with this feature.

These encouraging findings may signal the start of a new chapter in the study of material characterization and analysis. Advanced technologies, especially the YOLO v4 algorithm, can greatly enhance the efficiency and data-drivenness of materials science and engineering.

References

- Aksöz, S., Bican, O., Çalın, R., & Bostan, B. (2014). "Effect of T7 heat treatment on the dry sliding friction and wear properties of the SiC-reinforced AA 2014 aluminium matrix composites produced by vacuum infiltration", *Proceedings of the Institution of Mechanical Engineers, Part J: Journal of Engineering Tribology*, 228(3), 312-319, doi:10.1177/1350650113506570
- Anwar, N., Shen, Z., Wei, Q., Xiong, G., Ye, P., Li, Z., Lv, Y., & Zhao, H. (2021). "YOLOv4 based deep learning algorithm for defects detection and classification of rail surfaces", *IEEE International Intelligent Transportation Systems Conference (ITSC)*, 1616-1620, doi:10.1109/ITSC48978.2021.9565036
- Bochkovskiy, A., Wang, C.-Y., & Liao, H.-Y. M. (2020). "YOLOv4: Optimal Speed and Accuracy of Object Detection", *Preprint at arXiv*, doi:10.48550/arXiv.2004.10934
- Čalkovský, M., Müller, E., Meffert, M., Firman, N., Mayer, F., Wegener, M., & Gerthsen, D. (2021). "Comparison of segmentation algorithms for FIB-SEM tomography of porous polymers: Importance of image contrast for machine learning segmentation", *Materials Characterization*, 171, 110806, doi:10.1016/j.matchar.2020.110806
- Chen, F. X. R., Lin, C. Y., Siao, H. Y., Jian, C. Y., Yang, Y. C., & Lin, C. L. (2023). "Deep learning based atomic defect detection framework for two-dimensional materials", *Scientific Data*, 10(1), 91, doi:10.1038/s41597-023-02004-6
- Chen, Z., Huang, J., Xu, H., & Zhang, X. (2021). "Improved real time object detection method for remote sensing image based on YOLOv4", *Proceedings - 2021 International Conference on Computer Information Science and Artificial Intelligence, CISAI 2021*, 244-249, doi:10.1109/CISAI54367.2021.00053
- Choudhary, A. K., Jansche, A., Grubesa, T., Trier, F., Goll, D., Bernthaler, T., & Schneider, G. (2022). "Grain size analysis in permanent magnets from Kerr microscopy images using machine learning techniques", *Materials Characterization*, 186, 111790, doi:10.1016/j.matchar.2022.111790
- Rahman, F., Anburaj, J., & Chanakyan, C. (2023). "Optimization of squeeze casting process parameters on mechanical properties of SiCp reinforced LM25 composites through Taguchi technique", *Materials Research Express*, 10(7), 076515, doi:10.1088/2053-1591/ace75e
- Chao-Ching, H., Su, E., Li, P. C., Bolger, M. J., & Pan, H. N. (2020). "Machine vision and deep learning based rubber gasket defect detection", *Advances in Technology Innovation*, 5(2), 76, doi:10.46604/aiti.2020.4278

- Jiang, L., Yuan, B., Wang, Y., Ma, Y., Du, J., Wang, F., & Guo, J. (2023). "MA-YOLO: A method for detecting surface defects of aluminum profiles with attention guidance", *IEEE Access*, 11, 71269-71286, doi:10.1109/ACCESS.2023.3291598
- F. Kähler, A. C. K. Shetty and T. Schüppstuhl, "AI-based endpoint detection for surface defect removal on aircraft components", *2023 IEEE/SICE International Symposium on System Integration (SII)*, Atlanta, GA, USA, 2023, 1-6, doi:10.1109/SII55687.2023.10039239.
- Li, C., Cai, J., Qiu, S., & Liang, H. (2021). "Defects detection of steel based on YOLOv4", *Proceeding-2021 China Automation Congress, CAC 2021*, 5836-5839, doi:10.1109/CAC53003.2021.9728621
- Li, S., Guo, S., Han, Z., Kou, C., Huang, B., & Luan, M. (2023). "Aluminum surface defect detection method based on a lightweight YOLOv4 network", *Scientific Reports*, 13(1), 1-12, doi:10.1038/s41598-023-38085-x
- Lu, X., Hao, W., Kuang, S., Zhang, Y., Wu, M., & Zhao, Y. (2023). "High-strength, high-toughness SiCp reinforced Mg matrix composites manufactured by semisolid injection molding", *Journal of Materials Research and Technology*, 26, 4219-4228, doi: 10.1016/j.jmrt.2023.08.142
- Madsen, J., Liu, P., Kling, J., Wagner, J. B., Hansen, T. W., Winther, O., & Schiøtz, J. (2018). "A deep learning approach to identify local structures in atomic-resolution transmission electron microscopy images", *Advanced Theory and Simulations*, 1(8), 1-12, doi:10.1002/adts.201800037
- Mortensen, A., & Llorca, J. (2010). "Metal matrix composites", *Annual Review of Materials Research*, 40, 243-270, doi:10.1146/annurev-matsci-070909-104511
- Özyürek, D., Yildirim, M., & Çiftçi, I. (2012). "The tribological properties of A356-SiCp metalmatrix composites fabricated by thixomoulding technique", *Science and Engineering of Composite Materials*, 19(4), 351-356, doi:10.1515/secm-2012-0012
- Pei, Z., Rozman, K. A., Doğan, Ö. N., Wen, Y., Gao, N., Holm, E. A., Hawk, J. A., Alman, D. E., & Gao, M. C. (2021). "Machine-learning microstructure for inverse material design", *Advanced Science*, 8(23), 1-9, doi: 10.1002/advs.202101207
- Prabhu, B., Suryanarayana, C., An, L., & Vaidyanathan, R. (2006). "Synthesis and characterization of high volume fraction Al-Al₂O₃ nanocomposite powders by high-energy milling", *Materials Science and Engineering: A*, 425(1-2), 192-200, doi:10.1016/j.msea.2006.03.066
- Prajul Raj, P., Sridhar, R., Pugazhenthir, R., Anbuhezhiyan, G., & Ganesh, M. (2023). "Investigating the mechanical properties of tungsten carbide metal matrix composites with Al 6061", *Materials Today: Proceedings*, doi:10.1016/j.matpr.2023.03.605
- Ragone, M., Yurkiv, V., Song, B., Ramsubramanian, A., Shahbazian-Yassar, R., & Mashayek, F. (2020). "Atomic column heights detection in metallic nanoparticles using deep convolutional learning", *Computational Materials Science*, 180, 109722, doi:10.1016/j.commatsci.2020.109722
- Salur, E., Aslan, A., Kuntoğlu, M., & Acarer, M. (2021). "Effect of ball milling time on the structural characteristics and mechanical properties of nano-sized Y₂O₃ particle reinforced aluminum matrix composites produced by powder metallurgy route", *Advanced Powder Technology*, 32(10), 3826-3844, doi:10.1016/j.apt.2021.08.031

- Şimşek, İ., Şimşek, D., & Özyürek, D. (2020). “The effect of different sliding speeds on wear behavior of ZrO₂ reinforcement aluminium matrix composite materials”, *International Advanced Researches and Engineering Journal*, 4(1), 1-7, doi:10.35860/iarej.676152
- Xu, L., Zhang, X., Ma, F., Chang, G., Zhang, C., Li, J., Wang, S., & Huang, Y. (2023). “Detecting defects in fused deposition modeling based on improved YOLO v4”, *Materials Research Express*, 10(9), 095304, doi:10.1088/2053-1591/acf6f9
- Yavuzer, B., Özyürek, D., & Gürü, M. (2019). “The effect of milling time on microstructure and wear behaviours of AISI 304 stainless steel produced by powder metallurgy”, *Acta Physica Polonica A*, 135(4), 735-738, doi:10.12693/APhysPolA.135.735
- Zheng, L., Wang, X., Wang, Q., Wang, S., & Liu, X. (2021). “A fabric defect detection method based on improved YOLOv5”, *2021 7th International Conference on Computer and Communications, ICCCC 2021*, 620-624, doi:10.1109/ICCC54389.2021.9674548
- Ziatdinov, M., Dyck, O., Maksov, A., Li, X., Sang, X., Xiao, K., Unocic, R. R., Vasudevan, R., Jesse, S., & Kalinin, S. V. (2017). “Deep learning of atomically resolved scanning transmission electron microscopy images: chemical identification and tracking local transformations”, *ACS Nano*, 11(12), 12742-12752, doi:10.1021/acsnano.7b07504

About The Authors

Nuri ATİK, is a lecturer at National Defence University Army NCO Vocational HE School, Department of Mechatronics Technology. He holds a master’s degree in Weapon Systems Engineering from National Defence University. His main areas of interest are artificial intelligence, robotics and mechatronic system design.

E-mail: natik@msu.edu.tr, **ORCID:** 0000-0001-5203-3646.

Yusuf KARABACAK, is a lecturer at National Defence University Army NCO Vocational HE School, Department of Mechatronics Technology. He holds a PhD in Mechatronics Engineering from Selçuk University. His main areas of interest are mechatronic system design, control theory and applications and artificial intelligence.

E-mail: ykarabacak@msu.edu.tr, **ORCID:** 0000-0001-9864-7512.

İjlal ŞİMŞEK, is an Associate Professor at National Defence University Army NCO Vocational HE School, Department of Mechatronics Technology. She holds a PhD in Manufacturing Engineering from Karabuk University. Her main areas of interest are material design, and behaviors, manufacturing technologies.

E-mail: isimsek@msu.edu.tr, **ORCID:** 0000-0001-6542-8567

Doğan ŞİMŞEK, is an Associate Professor at National Defence University Army NCO Vocational HE School, Department of Automotive Technology. He holds a PhD in Manufacturing Engineering from Karabuk University. His main areas of interest are material design, and behaviors, composite materials, and internal combustion engines.

E-mail: dsimsek@msu.edu.tr, **ORCID:** 0000-0001-8339-9704

Similarity Index

The similarity index obtained from the plagiarism software for this book chapter is 14%.

CHAPTER 11***Investigation of Mechanical Behaviour of Crimp Effect on Fiber Reinforced Composite Materials******Hasan Hüseyin TAŞER****Istanbul Gelişim University, Türkiye****Mehmet KAYRICI****Necmettin Erbakan University, Türkiye***To Cite This Chapter:**

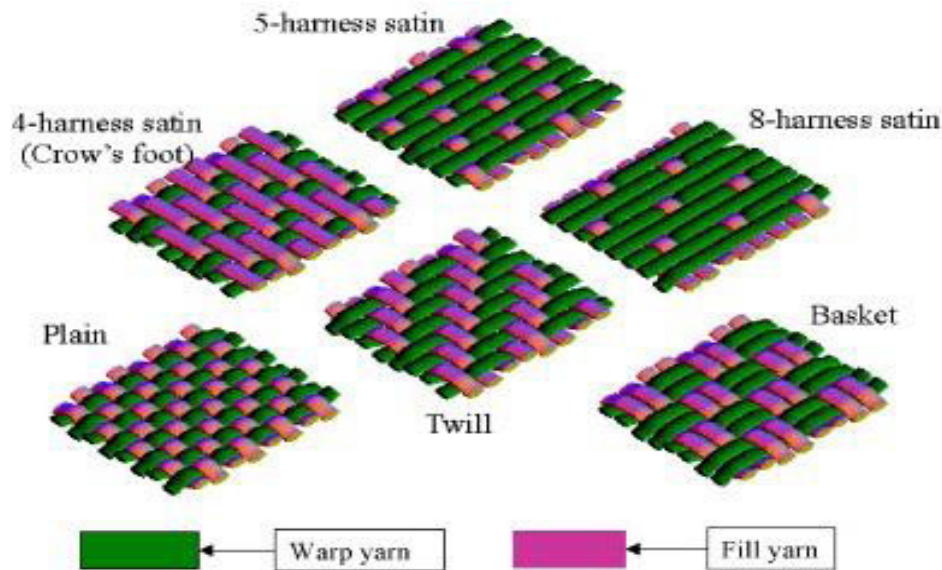
Taser, H. H. & Kayrici, M. (2024). Investigation of Mechanical Behaviour of Crimp Effect on Fiber Reinforced Composite Materials. Processing Method. In H. Gokmese, S. Bulbul, & Y. Uzun (Eds.), *Current Studies in Materials Science and Engineering* (pp. 157-168). ISRES Publishing.

Introduction

When woven fabrics are obtained, the yarns, i.e. fiber bundles, are brought perpendicular to each other on the looms. The transverse and longitudinal yarns of the fabric produced are named differently. The fiber bundles along the fabric are called “warp yarns”, and the fiber bundles that weave perpendicularly to these fiber bundles are called “weft yarns”. Warp fiber bundles are in the direction of the length of the fabric and weft fiber bundles are in the direction of the width of the fabric. The density formed by the interlacing of weft and warp fiber bundles can be controlled, which enables the formation of different woven fabrics. Woven fabrics such as plain, twill, and satin are produced according to the density of these fiber bundles. Due to the direction of the yarns and their intertwining, it also causes several problems. These problems are called fluctuation of fiber bundles, i.e. crimping. The crimping effect adversely affects the fabric mechanically. Since straight fibers take a more regular shape within each other, they are more durable and provide advantages in mechanical properties. Satin fabrics are less crimped. As a disadvantage of this situation, the integrity of the fabric decreases. This causes the fiber bundles to move easily when used. The gaps between adjacent yarns (also called inter-yarn spacing) are controlled by the amount of overlap (weave) given to the filling yarn after the warp yarns are interlaced. Both the geometry of the weave (or fabric fold) and the inter-yarn spacing affect the mechanical properties of the composite material. Simple looms produce wide and flat (plain) fabrics with two sets of yarns in the warp (0°) and weft (90°) directions. With specialized machines, it is also possible to produce triaxial weaves consisting of three sets of yarns intersecting and intertwining with each other at angles ranging from 30° to 60°. Woven fabrics are widely used as reinforcement in high-performance composite materials (Ramakrishna, 2004, p. 41).

Figure 1.

Various 2D mesh fabric structures (Ramakrishna, 2004, p. 41)

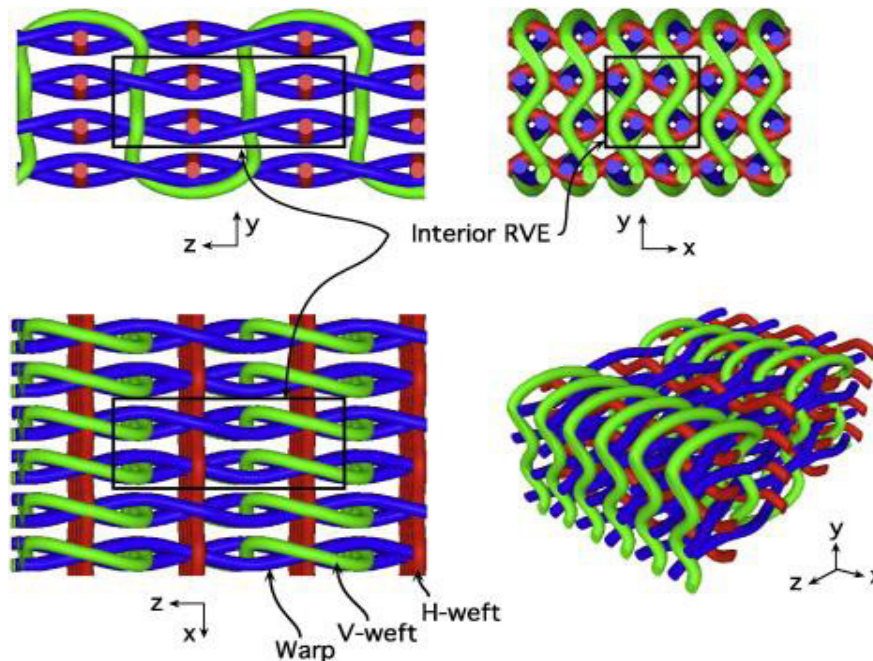


It is the fluctuation of the fibers that make up the so-called crimp yarn. It is a situation where a bundle of fibers forming the fabric deviates from a straight axis and follows a complex path or changes from regular to irregular. Crimp formation can occur naturally, mechanically, or chemically depending on the desired condition in the fiber. The crimp effect is also said for fiber bundles. It fluctuates or distorts due to the interweaving of the fabric. The crimp is defined algebraically as the number of waves divided by the unit length or the distance between the fibers as a result of loosening and flattening under a certain tension. In naturally formed fiber bundles, crimp, which occurs as a result of fiber growth, is an important factor affecting the strength, spinning ability, and processing performance of the fiber bundles. However, it increases its use by affecting its performance.

Crimp, which occurs as a result of the fluctuation of fiber bundles, is one of the most basic characteristics of natural and synthetic fibers, which are fiber types. The types of crimp found in fiber bundles are also described in this study. The functionality of fiber bundles and their effect on the properties of the final product are also described. Crimp is measured in terms of parameters of several characteristic properties such as length, angle, amplitude, length, index, and degree of crimp. The characteristic of the fold is designed in three dimensions for clarity. The mechanical properties of the folds occurring in the fiber bundles on the fabric are also explained (Maity, 2014).

Figure 2.

3D plain weave consisting of warp, horizontal (H-weft), and vertical weft (V-weft) (S. Maity, 2014).



The crimp formed in the fibers used in the textile industry is among the basic parameters that form the process capability and product quality of the fabrics. Cotton, one of the natural fiber bundles, has a crimp. Local textile materials designed for the processing of natural fibers are basically made by people with straight shapes and the ability to shape should be suitable for friction and cohesion (Bauer-Kurz, 2000, p. 36). These properties can be artificially regulated as an extra control. Thus, in the textile industry, the crimp in fiber bundles is mechanically loaded by the increase of fiber bundles, either naturally or during the processing of fibers, and triggers the undulation of other fiber bundles, so-called successive waves. For this purpose, the crimp in the fiber bundles is called the degree of deviation from the uniformity of the fibers. Fiber waviness is expressed as the difference between the length of the straightened fibers and the waviness of the crimp.

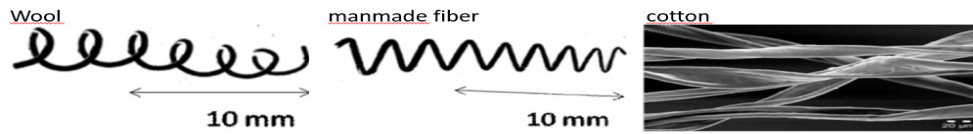
A crimp in a textile fiber strand is;

- Crimp in yarns
- Crimp in staple fiber
- It can be classified as a fold in the filaments.

Crimp in staple fibers is;

- Helical crimp (wool)
- Planner crimp (man-made fibers) and
- Folds (cotton).

The crimp in cotton fibers is a microscopic phenomenon, but the crimp in other fibers is macroscopic and visible to the naked eye.

Figure 3.*Types of crimp in staple fibers*

Glass fiber weaving is a type of glass fiber woven fabric produced according to the intended use for different purposes. Glass fiber weaving is a mixture of limestone, magnesium, foggy sand, aluminum, and acid substances used all over the world and produced from thin glass pieces. The alkalinity of these substances is low. Woven glass fiber has been used at the forefront of the composite material industry since the 1970s. They are products that are produced by twisting glass rovings untwisted and then twisted into continuous glass fiber and weaving textile yarns.

Glass fiber woven fabric is produced in different ways for different applications. It is compatible with vinyl ester, polyester, and epoxy. Resin impregnation is done before or after the fibers are placed on the mold. The weaving technique applied on a fabric affects that fabric. There are non-woven fabrics other than glass fiber woven fabrics. These are called nonwoven.

Glass Fiber Properties

The basic raw material for glass fiber production is none other than ordinary glass. However, while the actual glasses are composed of alkali and alkaline earth silicates and even complex mixtures containing borates and aluminates, those to be used in fiber production are mostly soda-lime silicates or borax silicates.

The ratio of additives varies according to the properties desired to be imparted to glass. Therefore, the chemical structure of glass fibers cannot be given precisely. However, it can be said that it consists of silicon dioxide and calcium carbonate. However, the proportions of sodium carbonate, aluminum hydroxide, magnesium oxide, and boric acid added for different purposes may vary.

Glass fiber types:

- A-Type Glass Fiber: Alkaline lime glasses with or without boron addition. Special types contain more than 0.8% alkali oxide compounds. They are produced with the use of soda lime silicate glasses where strength, stability, and good electrical resistance are not required as in type E glass fiber.
- C- Type Glass Fiber: It consists of calcium borosilicate glasses that provide chemical stability against corrosive acidic conditions. They have very good resistance to chemicals, both acids and alkalis.
- D- Type Glass Fiber: It consists of borosilicate glasses with a low dielectric constant for electrical applications.
- E- Type Glass Fiber: Aluminum borosilicate glasses containing less than 0.8% alkali oxide compounds. It is used in the reinforcement of synthetic fibers and where high strength and electrical resistance are required. Typical glasses, which have a wide range of uses, were originally developed for electrotechnical purposes. Today, however, they are also used in the reinforcement of synthetic

materials (especially in glass-reinforced plastics in the form of woven fabrics). Since they are resistant to acids, alkalis, and other chemicals, they are widely used in the chemical industry for the production of filters.

- ADVANTEX Type Glass Fiber: Type E glass fiber consists of calcium aluminosilicate glass, which provides many of the advantages of the ECR GLASS type at a fraction of the cost.
- ECR GLASS Type Glass Fiber: Consists of calcium aluminosilicate glass containing a maximum of 2% alkali. It consists of calcium aluminosilicate glass containing 2% alkali, designed for strength, electrical resistance, and acidic corrosion resistance.
- AR-GLASS Type Glass Fiber: A mixture of alkali zirconium silicates and alkali-resistant glasses is used.
- R Type Glass Fiber: It is the type formed by using calcium aluminosilicate glasses when acidic corrosion resistance and strength are required.
- S-2 Type Glass Fiber: S-2 type high strength glass fibers are fibers formed from high-temperature mixtures of aluminum silicates with finenesses ranging from 5-27 μm . Most of the silicate glass fibers are produced for the textile and composite industry.

In addition to these types, there are also M-type and Z-type glass fibers;

- M-type glass Fibers: Beryllium-containing glasses with high modulus of elasticity.
- Z-type glass Fibers: These are glass fibers used in the reinforcement of concrete and can be used together with cement.

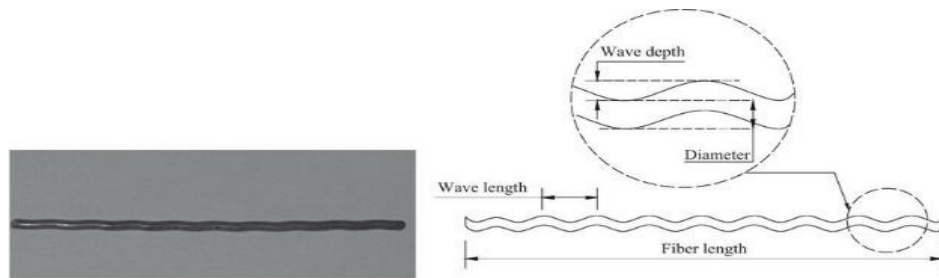
In fiber-reinforced composites, which are one of the composite types, the mechanical properties, which are characteristic features of the composites, are based on the arrangement of the fiber bundles by applying the stretching method. The elasticity of the fibers is controlled by pre-tensioning before the matrix element used is cured at a certain temperature. The first of the studies in this field starts with the result that a stronger structure is left by breaking the weak fibers by applying a pre-tensioning process before the fiber bundles are placed in the mold. It is foreseen to obtain a stronger structure with the breakage of weak bonds. In recent years, studies on the strength structures obtained by pre-breaking weak fibers have been increasing rapidly. The main advantage of fiber prestressing is to prevent cracks and delaminations in the final product due to weak bonds and to obtain stronger products. It is to prevent residual stresses that may occur in the fibers. Various pre-stretching techniques are also being investigated (Jayan et al., 2021).

With the development of technology, the use of reinforced fiber fabrics is rapidly increasing in industries such as automotive, aerospace, and textile. These developments cause the performance of the characteristic properties of advanced composite materials to increase. With the application of production techniques, mechanical properties are improved. As a result of these developments, the demand for these materials is increasing. The prevention of residual stresses that occur in the production of composite materials is among the main issues. These residual stresses are thought to occur during the production phase of composite materials. Residual stresses may occur due to reasons

such as inhomogeneous distribution of matrix materials within the structure, and physical defects during production. During phase change, residual stresses may occur during the transition from liquid to solid phase. To prevent these stresses in fiber fabrics, it is necessary to ensure that weak bonds are broken during production. With the process of breaking the weak bonds with pre-stretching, the fabrics will become mechanically advantageous (Khan et al., 2024).

The filament winding method, which is among the production techniques, can induce residual stresses in the production process of fiber bundles. It can also cause residual stresses that may occur in the final composite materials. It can cause incompatibility, voids, and residual stresses between the matrix material and fiber reinforcement. This is important for mechanical and thermal characterization. Residual stresses cause negative results in this case. It is a good method to improve the mechanical and thermal properties of reinforced composites with the prestressing process in the fibers without increasing their cross-section and weight by breaking the weak bonds. It provides further improvement of existing properties without additional cost in the final composite materials. Pre-stretching of reinforcing materials during the curing of matrix materials will increase the performance of the composite material as it will prevent residual stresses (Mostafa et al., 2017).

Figure 4
Crimped fiber



Residual stresses from tensile testing in composites will increase stresses and increase cracks in the matrices and reduce the strength of the material. These adverse effects may include the presence of matrix cracks, residual stresses, and fiber fluctuations. These adverse effects hurt the life of the final composite materials. It is necessary to minimize the negative effects. For this reason, a prestressing process can be applied. The volume fraction of the materials is also very important. It is necessary to pay attention to these ratios to ensure that the cost and materials are durable and can be utilized efficiently. Generally, approximately 60% fiber and 40% matrix material constitute fiber-reinforced composite materials. This ratio was determined in terms of cost and taking into account the previous studies. Improving the mechanical properties of composite materials will be of great benefit for many pending requirements of future applications. Therefore, efforts to improve the mechanical properties of composites are still ongoing, either through the development of materials used in the production of composites or through the improvement of related manufacturing techniques (Hui et al., 2021).

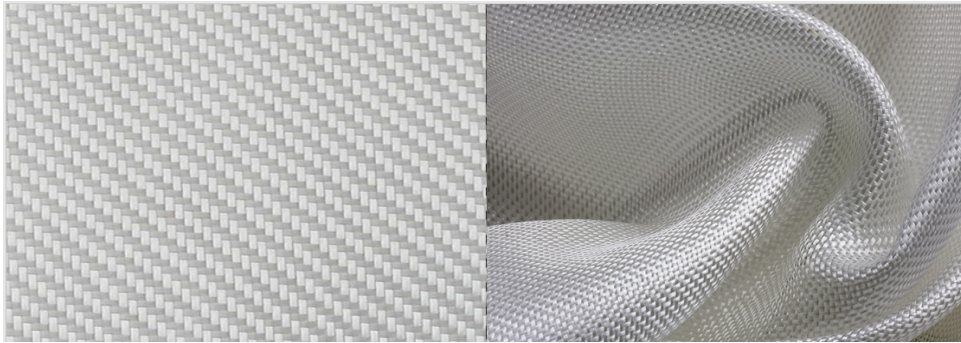
In this study, glass twill fabric was produced with and without prestressed PE reinforcement and compared in terms of mechanical properties. Mechanical tensile and three-point bending tests were carried out on the fabricated specimens.

Materials and Methods

Glass fiber fabric was used as a reinforcing element and polyethylene film was used as matrix material. PE films used as matrix material were placed between the fiber fabrics used as reinforcement elements. PE films soften under temperature and fill the pores of the fibers and increase the strength of the fibers by combining with the fiber fabric.

Figure 5.

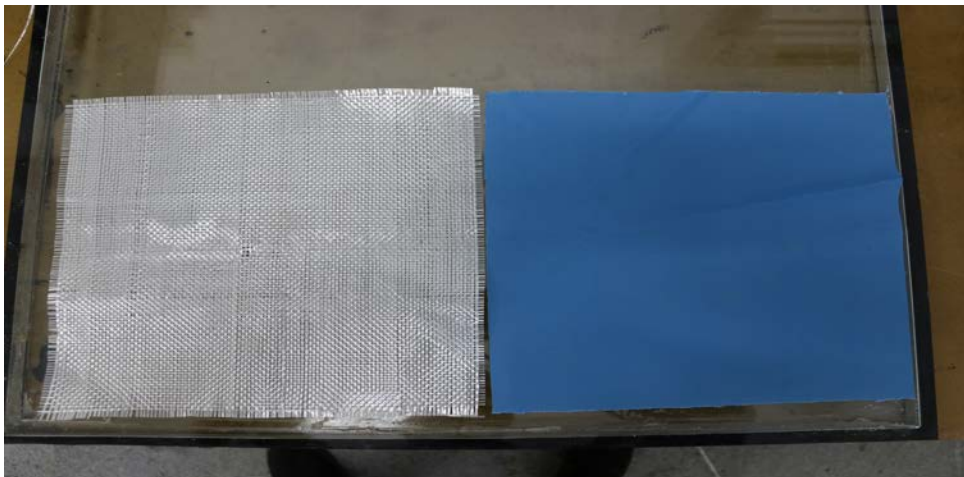
Glass fiber fabrics



The specimens were produced in two different ways: pre-stressed and non-prestressed. The non-prestressed specimens were produced on metal molds prepared in the design program and laser cut to precise dimensions. Glass fiber fabrics 290x290 mm and PE film as matrix material 240x240 mm were cut on frame molds.

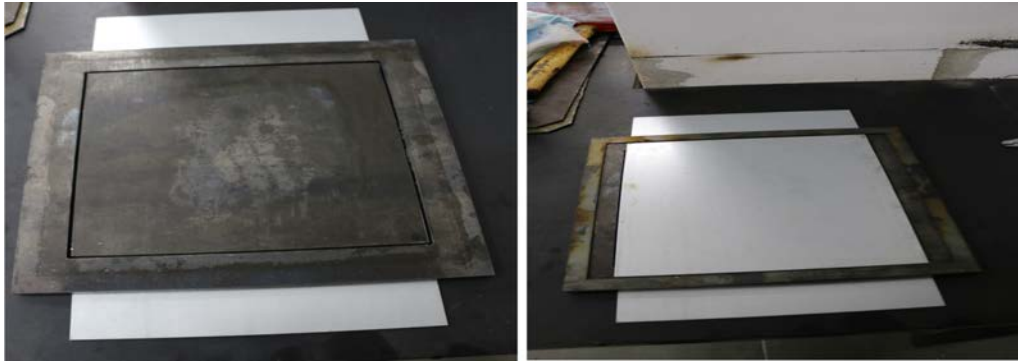
Figure 6.

Reinforcement and matrix elements



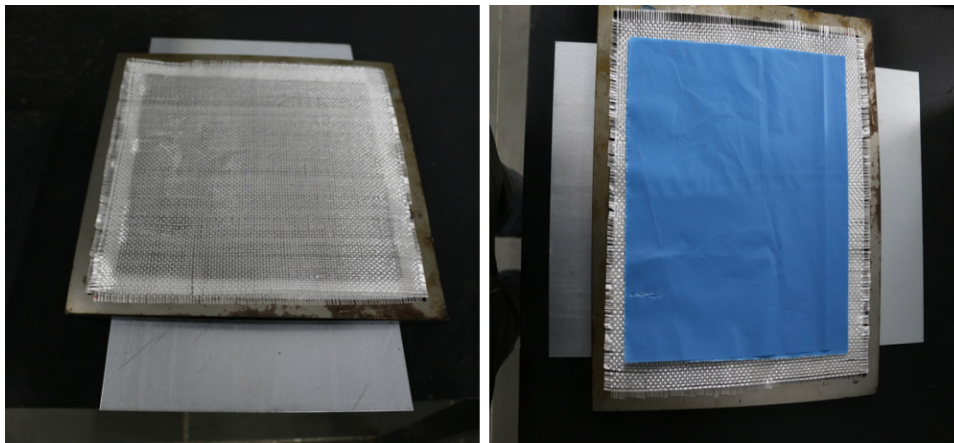
The cut samples were stacked on top of each other by paying attention to their volume fractions. Due to the density differences of fiber and matrix material, 10 layers of PE film were placed between 3 layers of glass fibers. The wall thickness of the produced samples is 1 mm and a layer of frame was placed on the fibers to prevent the film layer from overflowing.

Figure 7.
Sheet moulds



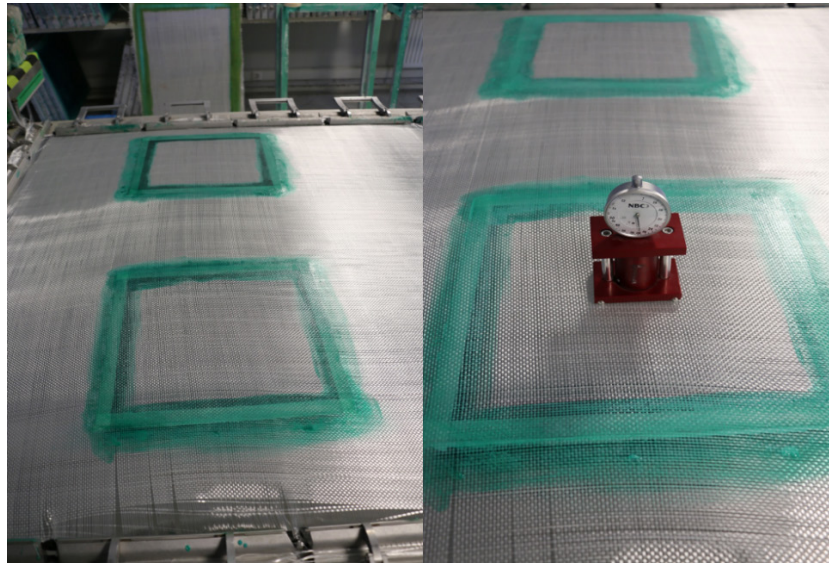
After fabrication, heat-resistant greaseproof paper was used to prevent easy removal of the specimens from the sheet frame and to prevent sticking. The specimens prepared without pre-tensioning were placed in a hydraulic press and cured under temperature and pressure. The temperature was gradually increased by paying attention to the melting temperature of the matrix material PE film and homogeneous distribution of the film layer in the fiber pores was ensured.

Figure 8.
Sample production



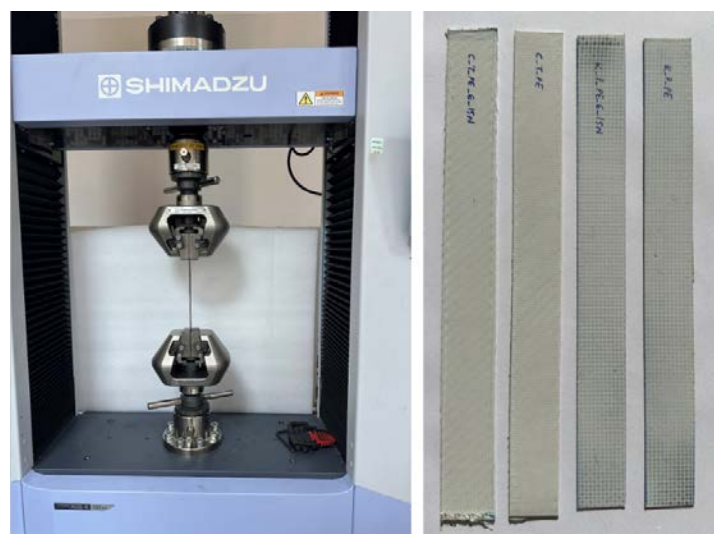
For the production of prestressed specimens, the fiber fabrics were stretched with double-sided tensioning according to the desired tensile force in the prestressing machine. The main purpose of pre-tensioning is to ensure that the weak yarns in the production stage of fiber fabrics are broken by the tension force and that the remaining parts remain more robust. After the fiber fabrics are pre-tensioned, they are glued to the frame with a special adhesive. PE films are placed on the glued fibers by the volume fraction and another layer of fiber fabric is laid. This cycle is repeated 3 times and the samples are prepared with stretched fabrics and PE films between them.

Figure 9.
Prestressing process



After the prestressing process is completed, the specimen is cured in a hydraulic press under a certain pressure and temperature. The temperature is gradually increased considering the melting temperature of the PE film. After the curing process is completed, the specimens are easily removed from the sheet frame with the help of a silicone mold release agent. The adhesive materials on the edges of the demoulded specimens are cut with guillotine shears. Specimens with dimensions of 150x150x1 mm were prepared for prestressed materials. Glass fiber specimens with dimensions of 250x25 mm for tensile test and 150x12,7 mm for flexure test were cut into 5 pieces each.

Figure 10.
Tensile test and specimens



Glass fiber fabrics were subjected to tensile tests with and without prestressing with 5 separate specimens of 250x25x1 mm dimensions. It was observed that the specimens generally started to break near the jaw parts.

Figure 11.
Damage on Specimens



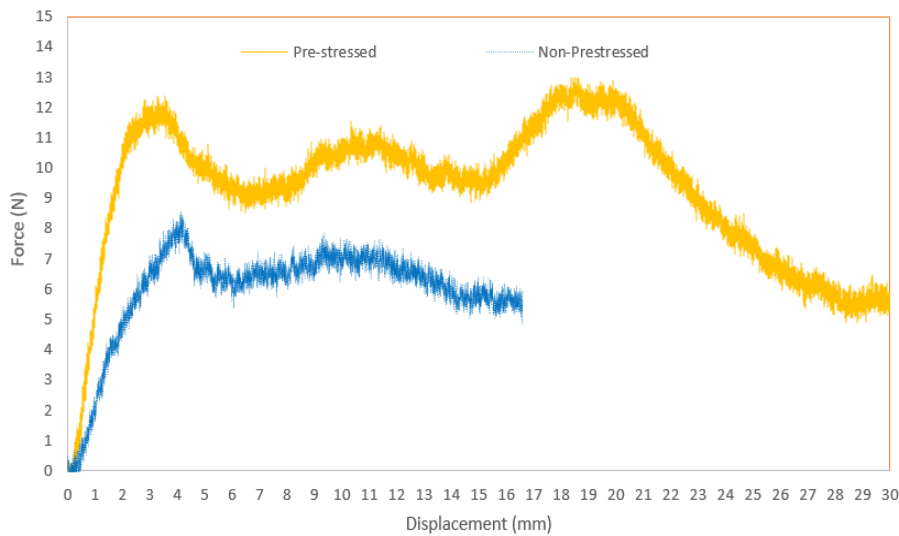
Prestressed and non-prestressed glass fiber fabrics were subjected to three-point bending tests, each with 5 separate specimens with dimensions of 150x12.7x1 mm.

Figure 12.
Flexure test and specimens



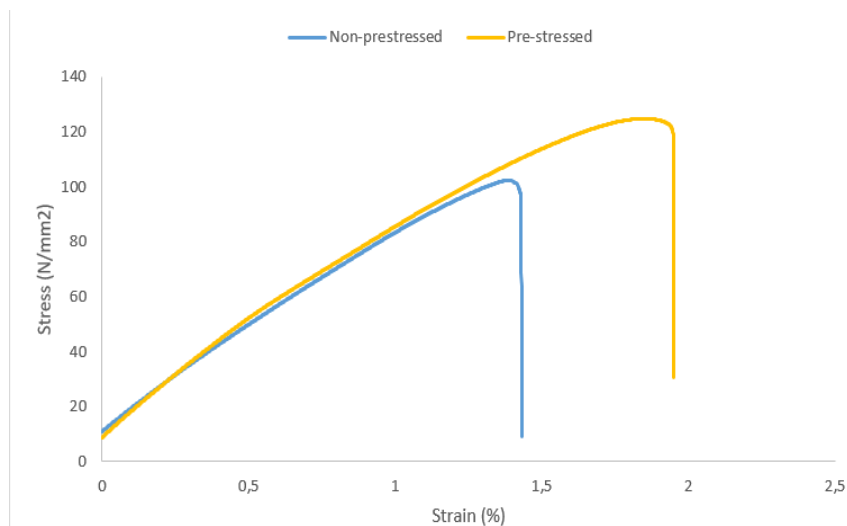
Since there is no stretching in the prestressed materials, the ability to move in the thermoplastic matrix is less, failing the pre-stressed specimens for the three-point bending test.

Figure 13.
3-point bending test graph



As a result of the stretching application, a 30% tensile strength increase and a 25% strain increase were achieved. fiber fabric reinforced polymers provide an advantage in this area. Despite stretching difficulties, these increases are very important. It contributes significantly to the literature.

Figure 14.
Tensile test graph



References

- Bauer-Kurz, I. (2000). Fiber crimp and crimp stability in nonwoven fabric processes. North Carolina State University.
- Hui, X., Xu, Y., & Zhang, W. (2021). An integrated modeling of the curing process and transverse tensile damage of unidirectional CFRP composites. *Composite Structures*, 263, 113681. <https://doi.org/10.1016/j.compstruct.2021.113681>
- Jayan, J. S., Appukuttan, S., Wilson, R., Joseph, K., George, G., & Oksman, K. (2021). An introduction to fiber reinforced composite materials. In *Fiber reinforced*

composites (pp. 1-24). Woodhead Publishing. <https://doi.org/10.1016/B978-0-12-821090-1.00025-9>

Khan, F., Hossain, N., Mim, J. J., Rahman, S. M., Iqbal, M. J., Billah, M., & Chowdhury, M. A. (2024). Advances of Composite Materials in Automobile Applications–A Review. *Journal of Engineering Research*. <https://doi.org/10.1016/j.jer.2024.02.017>

Maity, S. (2014). Characteristics and effects of fiber crimp in nonwoven structure. *Journal of the textile association*, 74(6), 360-366.

Mostafa, N. H., Ismarrubie, Z. N., Sapuan, S. M., & Sultan, M. T. H. (2017). fiber prestressed polymer-matrix composites: a review. *Journal of Composite Materials*, 51(1), 39-66. <https://doi.org/10.1177/0021998316637906>

Ramakrishna, S. (2004). *An introduction to biocomposites*. Imperial College Press.

About The Authors

Hasan Hüseyin TAŞER, MSc is a lecturer at İstanbul Gelişim University, Department of Hybrid and Electric Vehicles. He holds a master's degree in Mechanical Engineering from Necmettin Erbakan University in Konya, Türkiye. His main areas of interest are polymer materials, composite materials, nanocomposites, electric vehicles and battery materials.

E-mail: hhtaser@gelisim.edu.tr, **ORCID:** 0000-0001-5138-9085

Mehmet KAYRICI, PhD, is an Assistant Professor of Mechanical Engineering at Necmettin Erbakan University in Konya, Türkiye. He holds a PhD in Mechanical Engineering from Necmettin Erbakan University. His main areas of interest are polymer materials, composite materials and nanocomposites.

E-mail: mkayrici@erbakan.edu.tr, **ORCID:** 0000-0002-9778-2349

Similarity Index

The similarity index obtained from the plagiarism software for this book chapter is 6%.

CHAPTER 12***Metal Recovery with Calixarene******Ümmü ÖZGÜN****Necmettin Erbakan University, Türkiye****Muhammed İhsan ÖZGÜN****Necmettin Erbakan University, Türkiye***To Cite This Chapter:**

Ozgun, U. & Ozgun, M. I. (2024). Metal Recovery with Calixarene. In H. Gokmese, S. Bulbul, & Y. Uzun (Eds.), *Current Studies in Materials Science and Engineering* (pp. 169-180). ISRES Publishing.

Introduction

Metals are essential to modern society and the developed world (Wernick & Themelis, 1998). In recent years, with the development of industry and the increase in population, environmental pollution caused by heavy metals has increased significantly (Naaz & Pandey, 2010). Every year, many waste metals are discharged into nature from various industrial fields such as electronics, metallurgy, mining, metal processing, and electroplating. Metals produced as waste from various industrial fields are shown in Table 1 below (Jadhav & Hocheng, 2012).

Table 1*Waste Metals Released by Various Industries (Jadhav & Hocheng, 2012)*

Waste type	Metals in waste
Electronic	Cu, Sn, Zn, Au, Ni, Ag, Al
Fly Ash	Cu, Al, Zn, Cr, Ni, Pb
Petroleum Spent Catalyst	Ni, Mo, Co
Batteries	Ni, Ag, Cd
X-ray Films	Ag
Metal Finishing	Cr, Cu, Ni, Au, Zn, Cd, Ag

Since heavy metals are toxic and tend to accumulate in living organisms, it is vital to remove them from nature and wastewater. Therefore, it becomes a necessity in the industry to recover wastes as toxic or valuable components (González-Muñoz et al., 2006).

Nowadays, the recovery of metals is significant because recycling metals eliminates the pressure on nature. In addition, recovered metals contribute to the economy of countries. Moreover, decreasing ore reserves due to the increasing population necessitates the recovery of metals (Jadhav & Hocheng, 2012).

Metals are indispensable materials for industrial economies because they are used in many areas. Because metals are durable, they are widely used in rail systems, building

construction works, the automobile industry, battery technologies, the glass industry, and many other areas. They are also widely used in the electricity because they conduct heat and electricity. In addition, metals and their compounds are used as catalysts in chemical reactions. Metals are a material that will constantly be in demand thanks to their ability to be processed and recycled. Metal recovery is essential, considering the decrease in ore reserves in the Earth's crust. More efficient use of recovered products will increase economic development and reduce the search for ore (Williamson, 1997; Tilton, 2015; Williams et al., 1987).

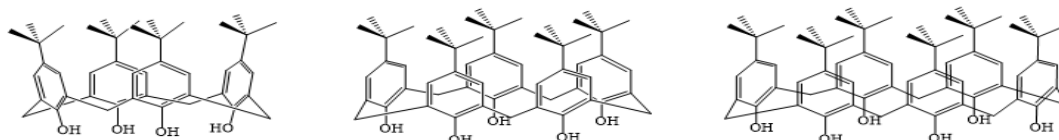
Alternatives related to utilitarian recovery are needed to minimize losses during metal processing. Technologies such as ionic liquid technology, bio-recovery, nano-biotechnology, and mechanochemical technology can be pragmatic methods (Ramachandran et al., 2016). Some techniques reported to be used to recover precious metals are; Techniques such as ion exchange, chemical precipitation, biosorption, adsorption, chelation, solvent extraction, and leaching (Firmansyah et al. 2018; Schreier & Edtmaier, 2003; Colpani et al., 2019; Golunski et al., 2002).

What is Calixarene?

Calixarenes are cylindrical supramolecules of phenolic groups linked together by methylene bridges (Gutsche, 1983). The word calix means cup or bucket. Large-volume calixarene compounds are named this way because they have a bucket-like structure (Figure 1).

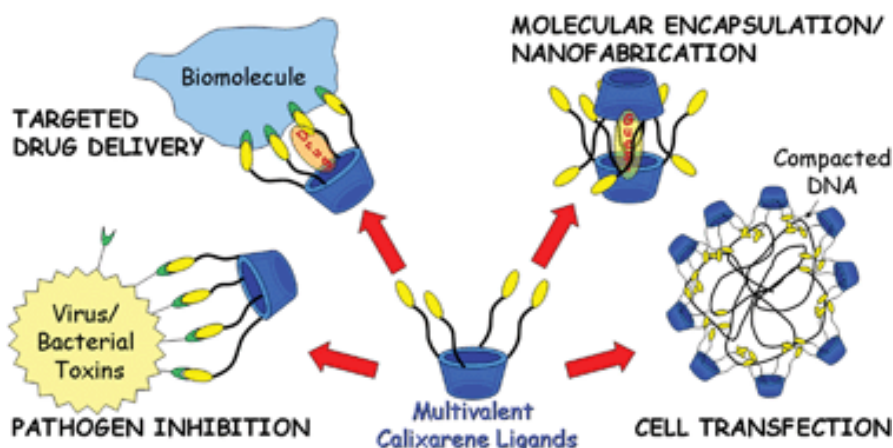
Figure 1

Structure of Calixarenes ($n = 4, 5, 6$)

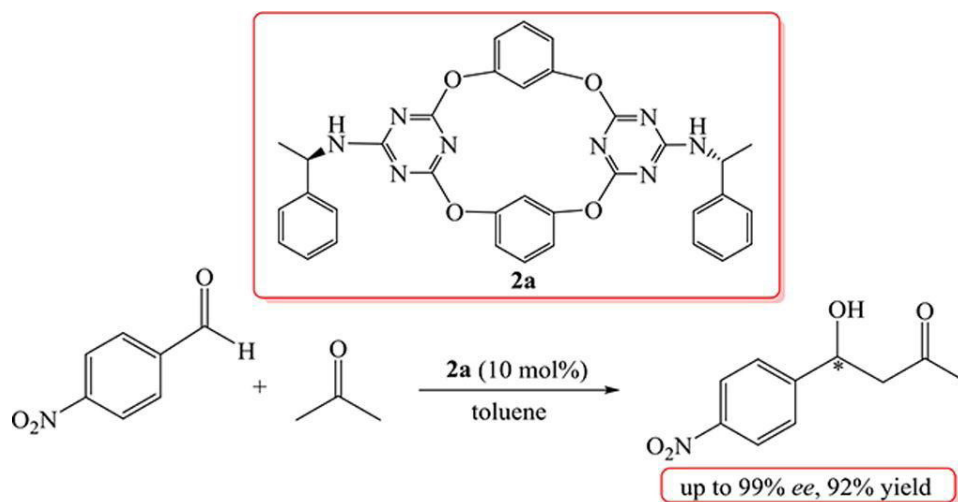


Calixarenes, a class of macrocyclic compounds, have been a significant part of scientific research since their discovery in the 20th century. With their unique ability to form complexes with both organic and inorganic structures, they have played a significant role in advancing our understanding of chemical interactions (Gutsche, 1989; Vicens & Böhmer, 1991). This adaptability is further enhanced by the ability to synthesize different derivatives in the laboratory. The properties of calixarenes are not static, but change as the structure attached to the molecule changes. This dynamic nature allows for the synthesis of specialized calixarenes for various applications (Vicens et al., 1994).

Calixarenes are widely used in chemistry, biology, and metallurgy. They are used in molecular separators, drug carriers, and biological sensors in biology (Figure 2; Baldini et al., 2007).

Figure 2*Use of Calixarene Ligands in Biology (Baldini et al., 2007)*

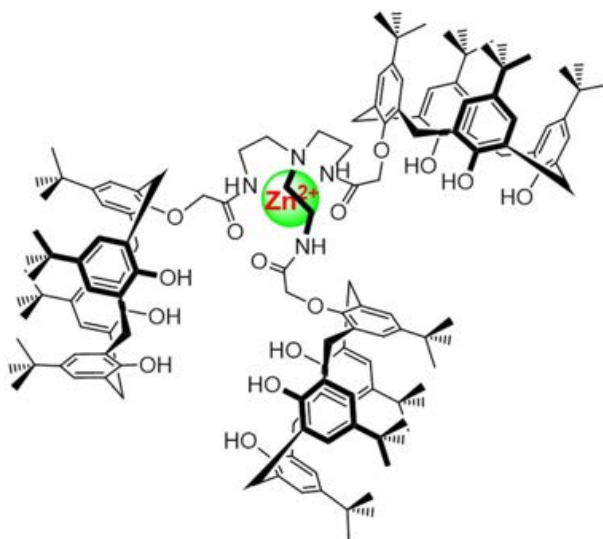
In chemistry, calixarenes are used for separation, chiral catalysts, molecular recognition, and catalysis. Calixarenes, which have hydrophobic cavities that can hold small molecules or ions, are also crucial for host-guest chemistry (Figure 3; Genc et al., 2019).

Figure 3*A Chiral Tetraoxacalix[2]arene[2]triazine-based Organocatalyst (Genc et al., 2019)*

In addition, calixarenes are also preferred in metallurgy due to their ability to selectively remove specific metal ions from a solution. Today, it is a molecule which attracts much attention in metal recovery. Thanks to its special chemical structure, calixarene provides high selectivity to metal ions and ensures their effective separation from the solution. Adding different functional groups to calixarenes upper and lower rims can provide metal recognition capabilities. In addition, since calixarenes have many derivatization possibilities, they are used as chemical sensors (Mlika et al., 1998; Mlika et al., 2020) and selective receptors (Figure 4, Othman et al., 2020).

Figure 4

A Calixarene-based Supramolecule Sensitive to Zn²⁺ (Othman et.al., 2020)



Synthesis of calixarenes

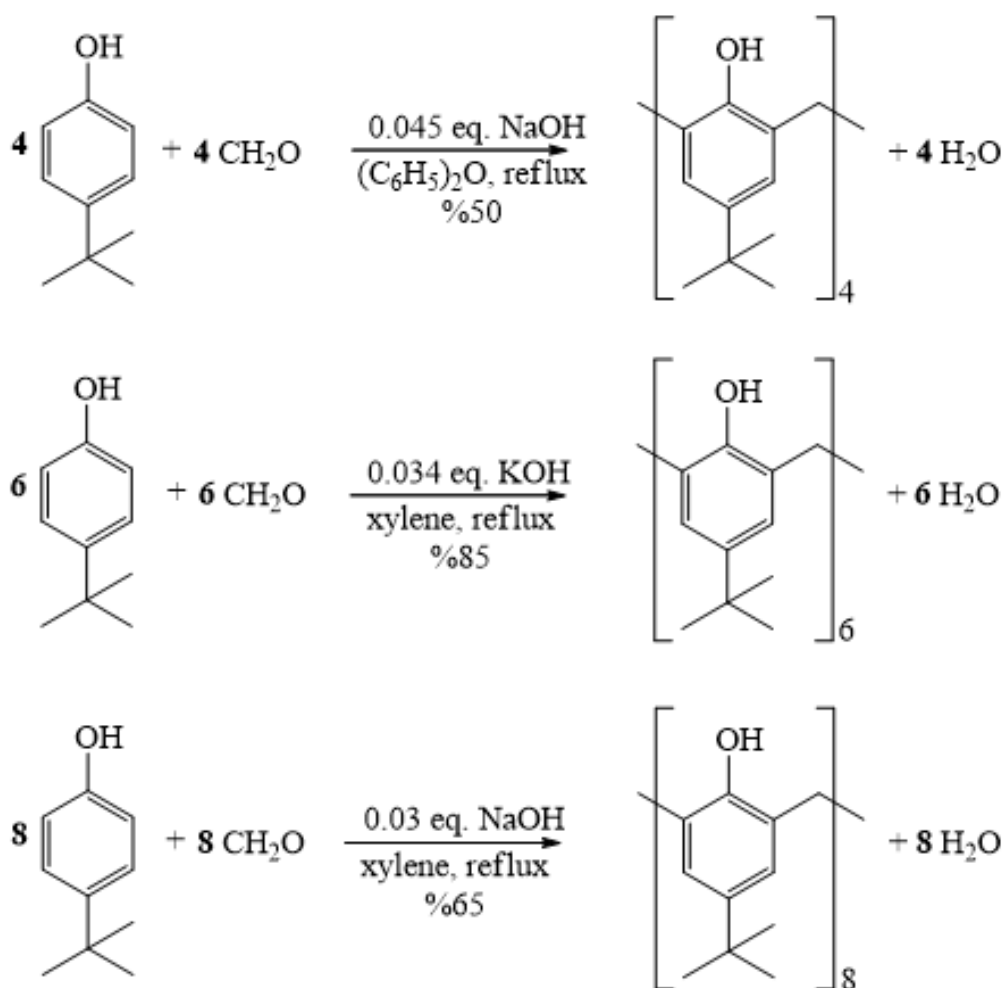
In calixarenes obtained by phenol-formaldehyde condensation, *p*-substituted phenols must be used. Otherwise, it has been shown that cross-linked polymers can be formed by bonding from both ortho and para positions (Gutsche, 1989). The synthesis of Calixarenes can be examined in two groups: acid-catalyzed and base-catalyzed.

Base-catalyzed one-step synthesis of calixarenes

Gutsche et al. (1983), have developed convenient procedures for the one-step synthesis of three primary cyclic oligomers, Calix [4], [6], and [8] arenes. By carefully controlling the reaction conditions, three major calixarene derivatives, Calix [4], [6], and [8] arenes, were synthesized in 50, 85, and 63% yield, respectively (Figure 5).

The research team encountered a significant challenge when the optimized conditions using *p*-*tert*-butylphenol resulted in the formation of mixed products that were difficult to separate when applied with other phenols. However, they overcame this obstacle by using *p*-*tert*-butylphenol as the most important starting material in calixarene synthesis.

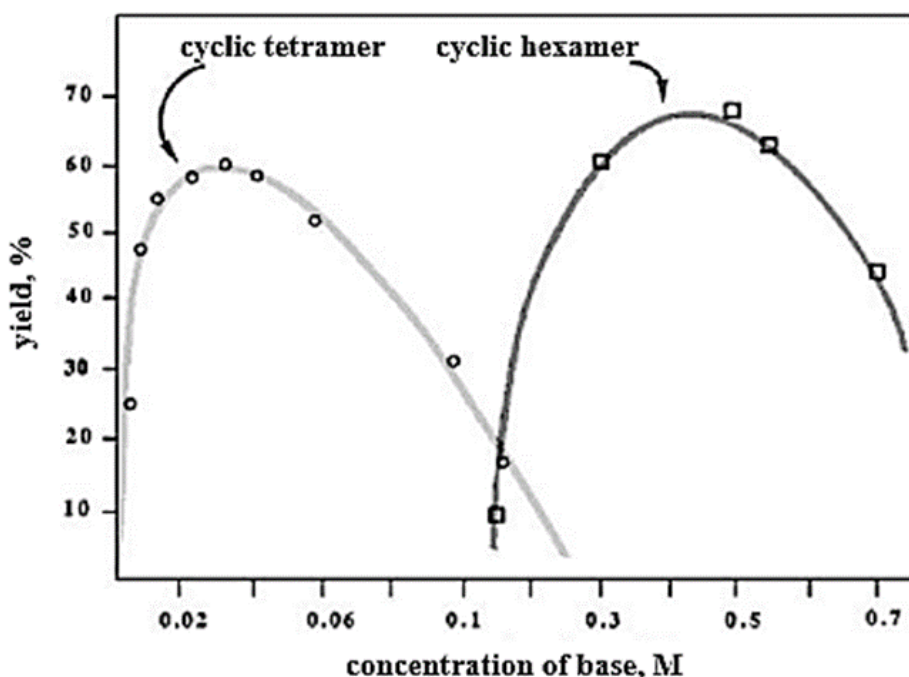
Figure 5
One-Step Synthesis of *p*-*tert*-butylcalix[*n*]arenes



The type and amount of base used in the base-catalyzed single-step synthesis of calixarenes and the solvent in which the reaction is carried out significantly affect the product and yield to be formed (Figure 6). It has been shown that LiOH and NaOH should be preferred for the synthesis of cyclic tetramers and octamers, and RbOH or CsOH cations should be preferred for the synthesis of cyclic hexamers according to the ion diameters of alkali metal hydroxides (Gutsche, 1988).

Figure 6

Effect of the Concentration of Base on the Formation of Cyclic Tetramer and Cyclic Hexamer (Gutsche, 1987)



Another factor that plays a role in the synthesis of calixarenes containing different numbers of aromatic rings is the solvent used. While a high-boiling-point apolar solvent such as diphenyl ether (bp. 220 °C) should be used for the cyclic tetramer, apolar solvents such as xylene (bp. 145 °C) with a low-boiling-point apolar solvent should be preferred for the cyclic hexamer and octamer.

Acid-catalyzed synthesis of Calixarene

Although linear oligomers were formed in very high yields when *p-tert*-butylphenol and formaldehyde were reacted under acidic conditions, cyclic oligomers were obtained in meager yields (Ludwig & Jr, 1986). However, calixarenes were synthesized in very high yields when *p-tert*-butylphenol and s-trioxane were reacted in chloroform with *p*-toluene sulfonic acid (Gutsche, 2001). In contrast to the reaction conditions in primary media, the reaction product obtained in acid-catalyzed media is a mixture of cyclic tetramer to large-ring calixarenes with $n > 8$. Therefore, the acid-catalyzed synthesis method is a preferred method for the isolation of large-ring calixarenes.

Methods of Metal Recovery with Calixarene

1. Adsorption

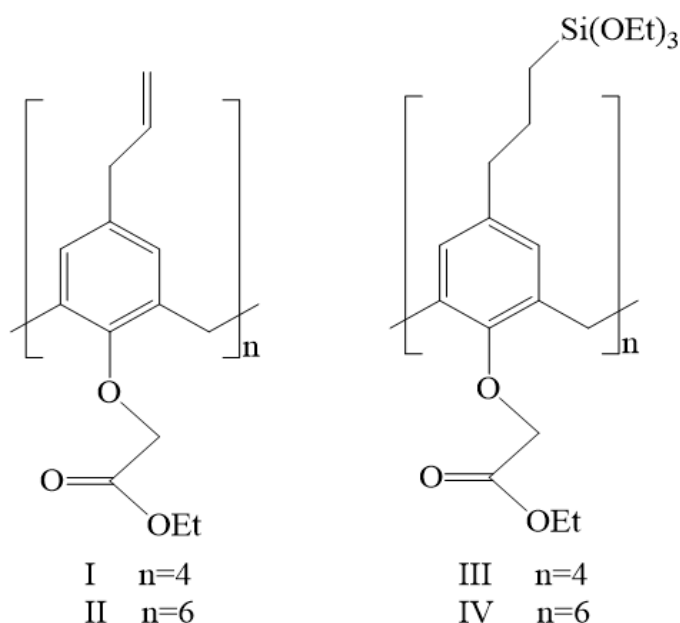
Calixarenes adsorb metal ions from the solution and separate them from the solution. This adsorption process is based on the interaction of the hydrophobic inner cavity and the outer surface of calixarene with metal ions. Calixarene-based adsorbent capable of metal adsorption was first reported by Shinkai et al. (1988). The first silica-supported calixarene containing adsorbent was reported by Glennon et al. (1993). They prepared triethoxy

silane carrying calixarene derivatives for the stationary phase in chromatography and used them to separate alkali metal ions. This calixarene-based silica gel was selective towards Na(I).

The effectiveness of calixarenes in metal ion separation was further underscored by Glennon et al. (1993) when preparing an adsorbent on octadecyl silica (ODS) using a hydroxamic acid derivative of calixarene. This adsorbent, an octadecyl silica-supported calixarene derivative, showed exceptional selectivity towards Fe(III) over other metal ions such as Mn(II), Cd(II), Pb(II), Co(II), Zn(II), Cu(II), Ni(II). The high affinity of the hydroxamic acid group for Fe (III) was a critical factor in the success of this adsorbent (Figure 7).

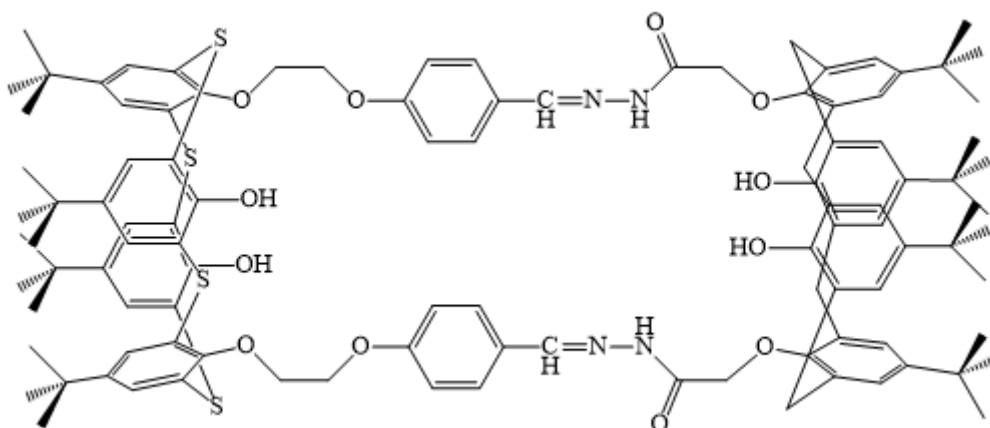
Figure 7

Structure of p-allylcalix[n]arene Ethyl Acetate and Triethoxy Silane p-n-propylcalix[n]arene Ethyl Acetate



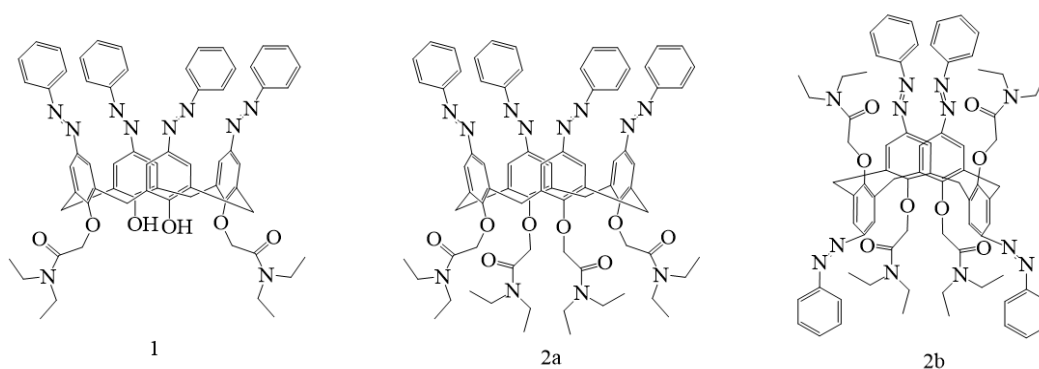
2. Extraction

Calixarenes extract metal ions from the solution by forming complexes in an organic solvent. This method allows metal ions to be collected in a concentrated form and separated from the solution. In this regard, Yang et al. (2006) have studied the complexation of metal cations with bis(calix[4]arene) derivatives. They synthesized bis-calix[4]arene, which consists of a calix[4]arene unit and a thiacalix[4]arene unit, as shown in Figure 8.

Figure 8*Bis-calix[4]arene Structure Used in Metal Ion Extraction*

The synthesized bis(calix[4]arene) derivative showed good extraction ability against soft and hard cations. This compound showed good extraction selectivity for cesium or potassium over sodium and silver over mercury. In the study, the complexation properties of tris(calix[4]arene) derivatives were also investigated, and they exhibited high extraction properties for hard metal cations.

In a pivotal study conducted by Dumazet-Bonnamour et al. (2005), various derivatives of calixarene were synthesized and their efficiency was probed by employing them in metal extraction, setting the stage for our current research.

Figure 9*Various Calixarene Derivatives Used for Extraction*

Calixarene-based tetra-amide derivative molecule 2a (cone conformation) is the most efficient molecule for the extraction of K^+ (75%), Ca^{2+} (48%), and Na^+ (51%) ions. In the experiments, the extraction efficiencies of molecule 2b (1,3-alternate conformation) were similar to 2a; in the extractions made with 2b, 52% for K^+ and 42% for Ca^{2+} were obtained. However, small percentages, such as 4%, were obtained for Na^+ and Mn^{2+} .

In the experiments with molecule number 1, a di-amide derivative, it was observed that it extracted the same metals as 2a and 2b, but the yield was significantly different. This difference in extraction yield is thought to be influenced by the number of amides on the calixarene (Figure 9, Dumazet-Bonnamour et. al., 2005).

3. Ion exchange resin

Pesticides, heavy metals, dyes, and chemicals pollute our environment and water and seriously harm human health. To protect our environment and human health, water treatment is carried out using ion exchange resins. Calixarenes are essential in molecular discrimination and selective ions due to guest-host interactions. Because of their ring-shaped structure, calixarenes are compounds that recognize and bind ions. Calixarene-based ion exchange resins capture and retain metal ions in solution through mutual ion exchange. These resins provide high selectivity and efficiency in metal recovery.

The advantages of calixarene-based ion exchange resins include high selectivity, chemical and thermal stability, reusability, and effective retention of ions. These properties make such resins widely used in various industrial and research applications such as water treatment and metal recovery (Jumina & Kurniawan, 2022).

Three methods are used to prepare calixarene-based ion exchange resins. These are:

1. Addition of calixarene to commercially available resins
2. Polymerization of calixarene
3. Preparation of calixarene derivatives by cross-linking reaction

Several ion exchange resins have been prepared using these techniques. These resins have shown successful selectivity in removing heavy metal ions.

Applications of Calixarenes in Metal Recovery

Calixarenes have a wide range of applications in recovering and recycling metals. Their unique flexibility, molecular structure, and derivatization capabilities make them essential tools in industrial and environmental areas. Some of the application areas are mentioned below.

1. Environmental cleaning

It effectively removes polluting metal ions such as mercury, cadmium, and lead from soil and water resources.

2. Hydrometallurgy

Calixarenes are widely used in metal recovery, processing, and mining. They are particularly effective in recovering rare earth elements such as cobalt, nickel, and copper.

3. Mining and industrial waste management

Calixarenes can be used to recover and treat metal ions in wastewater from mining activities. Thus, industrial waste can be recycled or disposed of safely, reducing its environmental impact.

4. Electronic waste recycling

Calixarenes can be used to recover valuable metals in electronic waste. They can separate and recover valuable metals, especially from old computers, mobile phones, and other electronic devices.

5. Water treatment

Calixarenes can be used to treat polluted water, remove heavy metal ions from water

resources, and improve drinking water quality.

6. Catalysts

Calixarenes can also be used as catalysts. By effectively binding specific ions in chemical reactions, they can increase the rate of some reactions.

7. Analytical chemistry

Calixarene can be used as a selective sensor to analyze and determine metal ions. This allows for the sensitive and accurate determination of metal ions in laboratory studies.

References

- Baldini, L., Casnati, A., Sansone, F., & Ungaro, R. (2007). Calixarene-based multivalent ligands. *Chem. Soc. Rev.*, 36(2), 254–266. doi:10.1039/b603082n
- Colpani, G. L., Dal’Toé, A. T. O., Zanetti, M., Zeferino, R. C. F., Silva, L. L., de Mello, J. M. M., & Fiori, M. A. (2018). Photocatalytic adsorbents nanoparticles. In *Advanced Sorption Process Applications*. IntechOpen. <https://doi.org/10.5772/intechopen.79954>.
- Dumazet-Bonnamour, I., Halouani, H., Oueslati, F., & Lamartine, R. (2005). Calixarenes for metal cations extraction. *Comptes Rendus Chimie*, 8(5), 881-891.
- Firmansyah M. L., Kubota F. & Goto M. (2018). Solvent extraction of Pt (IV), Pd (II), and Rh (III) with the ionic liquid trioctyl (dodecyl) phosphonium chloride. *Journal of Chemical Technology & Biotechnology*, 93 (6), 1714–1721.
- Genc, H. N., Ozgun, U., & Sirit, A. (2019). Chiral tetraoxacalix [2] arene [2] triazine-based organocatalysts for Enantioselective Aldol reactions. *Tetrahedron letters*, 60(27), 1763-1768.
- Glennon, J.D., O’Connor, K., Srijaranai, S., Manley, K., Harris, S.J., McKerverey, M.A. (1993). Enhanced chromatographic selectivity for Na⁺ ions on a calixarene-bonded silica phase. *Anal. Lett.* 26(1), 153–162.
- Golunski S., Rajaram R., Hodge N., Hutchings G. J. & Kiely C. J. (2002). Low-temperature redox activity in co-precipitated catalysts: a comparison between gold and platinum-group metals. *Catalysis Today* 72 (1–2), 107–113.
- González-Muñoz, M., Rodríguez, M., Luquea, S. & Álvarez, J. (2006). Recovery of heavy metals from metal industry waste waters by chemical precipitation and nanofiltration. *Desalination*, 200, 742-744.
- Gutsche, C. D. (1983). Calixarenes. *Acc. Chem. Res.*, 16, 161-170.
- Gutsche, C. D. (1989) Topics in calixarene chemistry. *J. Inclusion Phenom.*, 7, 61-72.
- Gutsche, C. D. (2001). Synthesis of calixarenes and thiacalixarenes. In *Calixarenes 2001* (pp. 1-25). Dordrecht: Springer Netherlands.
- Gutsche, C. D. and Nam, K. C., 1988, Calixarenes, 22. Synthesis, properties, and metal complexation of aminocalixarenes, *J. Am. Chem. Soc.*, 110, 6153-6162.
- Jadhav, U.U. & Hocheng H. (2012). A review of recovery of metals from industrial waste. *Journal of Achievements of Materials and Manufacturing Engineering*, 54(2), 159-167.
- Jumina, & Kurniawan, Y. S. (2022). Supramolecular Ion-Exchange Resins Based on

- Calixarene Derivatives for Pollutant Removal from Aquatic Environmental Samples. *Inorganic-Organic Composites for Water and Wastewater Treatment: Volume 2*, 161-200.
- Ludwig, F. J. & Jr, A. G. B. (1986). Reversed-phase liquid chromatographic separation of p-tert-butylphenol-formaldehyde linear and cyclic oligomers. *Anal. Chem.*, 58, 2069–2072.
- Mlika, R., Dumazet, I., Ouada, H. B., Jaffrezic-Renault, N., Lamartine, R., Gamoudi, M., & Guillaud, G. (2000). Cu²⁺-ISFET type microsensors based on thermally evaporated p-tert-butylcalix [9 and 11] arene thin films. *Sensors and Actuators B: Chemical*, 62(1), 8-12.
- Mlika, R., Ouada, H. B., Jaffrezic-Renault, N., Dumazet, I., Lamartine, R., Gamoudi, M., & Guillaud, G. (1998). Study of ion-selective evaporated calixarene film used as a sensitive layer on ISFET sensors. *Sensors and Actuators B: Chemical*, 47(1-3), 43-47.
- Naaz, S., & Pandey, S. N. (2010). Effects of industrial waste water on heavy metal accumulation, growth and biochemical responses of lettuce (*Lactuca sativa* L.). *Journal of Environmental Biology*, 31(3), 273. https://jeb.co.in/journal_issues/201005_may10/paper_06.pdf
- Othman, A. B., Mellah, B., Abidi, R., Kim, J. S., Kim, Y., & Vicens, J. (2020). Complexing properties of pyrenyl-appended calix [4] arenes towards lanthanides and transition metal cations. *Journal of Inclusion Phenomena and Macrocyclic Chemistry*, 97, 187-194.
- Ramachandran S., Ganesh P. S., Sivasubramanian V. & Kumar B. G. P. (2016). Current developments in mass production of microalgae for industrial applications. In: *Environmental Sustainability Using Green Technologies*. CRC Press, 185–210.
- Schreier G. & Edtmaier C. (2003). Separation of Ir, Pd and Rh from secondary Pt scrap by precipitation and calcination. *Hydrometallurgy* 68 (1–3), 69–75.
- Shinkai, S., Kawaguchi, H., Manabe, O. (1988). Selective adsorption of UO₂²⁺ to a polymer resin immobilizing calixarene-based uranophiles. *J. Polym. Sci. C* 26, 391–396.
- Tilton, J. E. (2015). *World metal demand: trends and prospects*. Routledge.
- Vicens, J. & Böhmer, V. (1991). *Calixarenes: A versatile class of macrocyclic compounds*, Kluwer Academic Publishers, Dordrecht, Boston, London.
- Vicens, J., Asfari, Z. & Harrowfield, J. M. (1994) *Calixarenes 50 thanniversary commemorative issue*, Kluwer Academic Publishers, 213-218.
- Wernick, I. & Themelis, N.J. (1998). Recycling Metals for the Environment. *Annual Reviews Energy and Environment*, 23, 465-497. <https://doi.org/10.1146/annurev.energy.23.1.465>
- Williams R.H., Larson E.D. & Ross M.H. (1987). Materials, affluence, and industrial energy use. *Annu. Rev. Energy Environ.* 12, 99–144.
- Williamson D. (1997). Into the next millennium: the long bull market in metals and minerals. *Min. Eng.* 49(6), 61–64.
- Yang, F. F., Zhao, X., Huang, C. Y., Guo, H. Y., Zheng, S. N., & Peng, Q. (2006). Synthesis and complexation properties of novel biscalixarene composed of calix [4] arene and thiacalix [4] arene subunits. *Chinese Chemical Letters*, 17(8), 1029.

About The Authors

Ümmü ÖZGÜN, PhD, is a postdoctoral researcher at the central laboratory (BITAM) of Necmettin Erbakan University in Konya, Türkiye. She holds a PhD in Organic Chemistry from Necmettin Erbakan University. Her main areas of interest are supramolecular chemistry, natural compounds chemistry, pheromone chemistry, chromatography, design and use of chiral catalysts.

E-mail: ummu.vural@gmail.com, **ORCID:** 0000-0002-5682-3001.

Muhammed İhsan ÖZGÜN, is a research assistant of Metallurgy and Materials Engineering at Necmettin Erbakan University in Konya, Türkiye. He holds a PhD in Mechanical Engineering at Necmettin Erbakan University. His main areas of interest are material characterization, metal casting, recycling of metals.

E-mail: miozgun@erbakan.edu.tr, **ORCID:** 0000-0003-0048-3439.

Similarity Index

The similarity index obtained from the plagiarism software for this book chapter is 12%.

CHAPTER 13

4E Analyses of the Power Plants

Dilek Nur ÖZEN

Necmettin Erbakan University, Türkiye

To Cite This Chapter:

Ozen, D. N. (2024). 4E Analyses of the Power Plants. In H. Gokmese, S. Bulbul, & Y. Uzun (Eds.), *Current Studies in Materials Science and Engineering* (pp. 181-194). ISRES Publishing.

Introduction

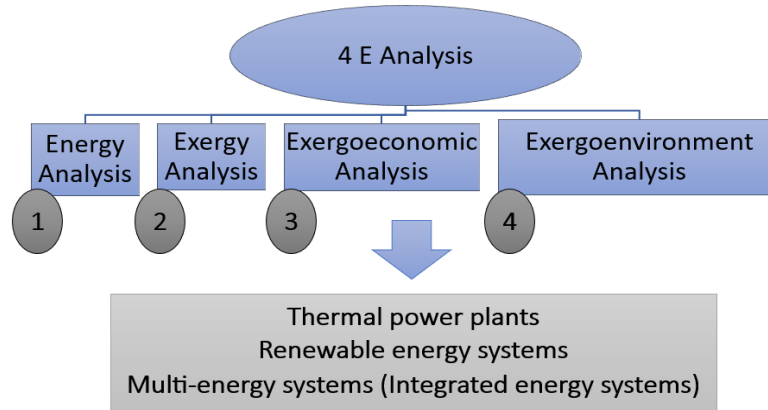
Energy is the potential to perform work, and according to the 1st law of thermodynamics, energy cannot be created or destroyed; it can only be conserved in terms of quantity. In this regard, the first law of thermodynamics deals only with quantity. The fundamental purpose of thermodynamics is to convert low-quality energy into high-quality energy. The 2nd law of thermodynamics emphasizes the quality of energy and measures the potential for converting energy into work. Power plants are energy plants that can convert thermal energy into power. In this section, information is provided about 4E analyses (Energy, Exergy, Exergo-economic, Exergo-environmental) for the design and improvement of power plants, and a case study is presented without numerical values. This section aims to demonstrate, alongside 4E analyses in power plant design, illustrating the plant's performance and its environmental impacts.

4E Analyses

Energy analysis alone is not sufficient to improve the design of thermal power plants, renewable energy plants, and integrated energy plants and to find optimum operating conditions. The exergy of the elements that make up the plant, which is the energy availability area, and the cost of the exergy should be evaluated together with the cost of the plant elements. The relationship of the plant with its environment should also be taken into account for a detailed analysis. From this perspective, 4E analysis, which includes energy, exergy, exergo-economic, and exergo-environmental analyses, is an approach that evaluates the quantity, quality, and environmental impact of energy. In this section, information about 4E analyses is provided (Figure 1).

Figure 1.

4E Analysis Sequential Order for Proposed Generation Plants (Tahir Et Al., 2021)



Energy Analysis

Energy analysis is a fundamental thermodynamic analysis. It provides a general understanding of the plant's performance but does not offer detailed guidance to the decision-makers. This is because energy analysis examines energy as a whole and does not take its usability into account. In the energy analysis of energy plants, when writing governing equations, plant elements are typically defined as control volumes operating under steady-state conditions. Energy analysis has been conducted based on the general energy and mass conservation equations provided below.

$$\sum \dot{m}_{in} - \sum \dot{m}_{out} = 0 \quad (1)$$

$$\dot{Q} - \dot{W} = \sum (\dot{m}h)_{out} - \sum (\dot{m}h)_{in} \quad (2)$$

Energy analysis involves performance criteria that indicate the plant's performance, namely the net power output and the first law efficiency. Efficiency typically compares the desired output to the input energy expended for the purpose. In energy plants, thermal efficiency is provided with equation (3).

$$\eta_{system} = \frac{\dot{W}_{net}}{\dot{Q}_{in}} \quad (3)$$

Here, \dot{Q}_{in} is determined by the lower heating value (LHV) of the fuel if the thermal energy required for the power plant is obtained through the combustion of a fuel. The LHV of the fuel is the thermal energy value obtained by the complete combustion of the fuel and its cooling to ambient temperature.

$$\dot{Q}_{in} = \dot{m}_{fuel} LHV \quad (4)$$

In power plants, net power is determined by subtracting the consumed power from the generated power. Net power is also referred to as useful power in the literature.

$$\dot{W}_{net} = \dot{W}_T - \dot{W}_{P \text{ or } C, \text{ both or either}} \quad (5)$$

Here, \dot{W}_T , \dot{W}_P , and \dot{W}_C represent the turbine, pump, and compressor powers, respectively.

Exergy Analysis

Exergy analysis, unlike energy analysis, provides the opportunity to evaluate the plant's performance by considering the availability of energy. Exergy is the maximum work potential that can be obtained from a reversible state change. In this case, exergy destruction is the lost work potential. Exergy analysis helps identify the plant element with the highest exergy destruction, and the focus is on improving this plant element.

The exergy rate of a stream is determined with equation (6) (Wang et al., 2016).

$$\dot{Ex} = \dot{Ex}^{PH} + \dot{Ex}^{CH} + \dot{Ex}^{KN} + \dot{Ex}^{PT} \quad (6)$$

Here, \dot{Ex}^{CH} , \dot{Ex}^{PH} , \dot{Ex}^{PT} and \dot{Ex}^{KN} respectively represent the chemical, physical, potential, and kinetic exergy rates. Typically, in power plants, potential and kinetic exergy changes are ignored as they are considered to be small. For unit mass, kinetic and potential exergies are determined with equations (7 and 8):

$$ex^{KN} = \frac{1}{2}v^2 \quad (7)$$

$$ex^{PT} = gz \quad (8)$$

Chemical exergy is also not considered in power plants when there is no chemical reaction. The chemical exergy can be calculated according to Bejan (Bejan, 1988)

$$ex^{CH} = (\mu_i^* - \mu_{0,i})y_i \quad (9)$$

Here, y_i , μ_i^* and $\mu_{0,i}$ respectively represent the mole fraction of element "i", the chemical potential of element "i" in the mixture at the restricted dead state, and the chemical potential of element "i" at the dead state. For detailed information about recommended chemical exergy equations for various fuels, Stepanov's study (1994) can be used as a reference.

In this section of the case study, only physical exergy is considered due to the absence of a chemical reaction. Physical exergy is determined with equation (10) (Zhang et al., 2021).

$$ex^{PH} = h - h_0 - T_0(s - s_0) \quad (10)$$

Physical exergy is the sum of thermal and mechanical exergies. Therefore, physical exergy is also referred to as thermomechanical exergy. Thermal and physical exergies are determined with equations (11 and 12) (Gundersen, 2009).

$$ex^T = h(T, P) - h(T_0, P) - T_0[s(T, P) - s(T_0, P)] \quad (11)$$

$$ex^M = h(T_0, P) - h(T_0, P_0) - T_0 [s(T_0, P) - s(T_0, P_0)] \quad (12)$$

Here, “ex” represents exergy per unit mass. The methods used to determine the exergy destruction rate $\left(\dot{Ex}_{D,k}\right)$ in plant elements are the “Input-Output” concept and the “Fuel-Product” concept. The “Fuel-Product” concept is preferred in this study because it is organized based on the exergy given to the plant according to the purpose of the plant and to achieve that purpose (Wang et al., 2016).

$$\dot{Ex}_{D,k} = \dot{Ex}_{f,k} - \dot{Ex}_{p,k} \quad (13)$$

Here, $\dot{Ex}_{f,k}$ is the fuel exergy, which is the exergy provided to the plant element according to its purpose. $\dot{Ex}_{p,k}$ is the product exergy, representing the exergy gained from the fuel exergy in line with the plant’s purpose. Fuel exergy is a term widely accepted in exergy terminology. However, the term “fuel” often confuses as it is generally defined in plants where combustion reactions occur. For this reason, in most studies in the literature, the term “feed exergy” is used instead of “fuel exergy” to avoid ambiguity.

$\dot{Ex}_{D,k}$ value of the “k” plant element can also be calculated according to the input and output exergy rates (Nami et al., 2017).

$$\dot{Ex}_{Q,k} + \dot{m}_{i,k} ex_{i,k} = \dot{Ex}_{W,k} + \dot{m}_{o,k} ex_{o,k} + \dot{Ex}_{D,k} \quad (14)$$

In exergy analysis, performance criteria can be given as the exergy efficiency of the overall plant (η_{plant}), the exergy efficiency of each plant element (ε_k), and the exergy destruction ratio for each plant element ($Y_{D,k}$).

$Y_{D,k}$ is the ratio of the $\dot{Ex}_{D,k}$ value of a plant element to the total exergy destruction rate of the overall plant. The $Y_{D,k}$ value is determined with equation (15) (Anvari et al., 2015).

$$Y_{D,k} = \frac{\dot{Ex}_{D,k}}{\dot{Ex}_{D,t}} \quad (15)$$

The ε_k value is provided by dividing the $\dot{Ex}_{P,k}$ value by the $\dot{Ex}_{F,k}$ value (Anvari et al., 2015).

$$\varepsilon_k = \frac{\dot{Ex}_{P,k}}{\dot{Ex}_{F,k}} \quad (16)$$

There is no single definition in the literature for the exergy efficiency of the plant that carries a unique meaning. When the literature is examined, it will be seen that exergy efficiency is defined either based on the incoming and outgoing exergies or based on the purpose and the exergy that needs to be supplied to the plant for that purpose. According to this explanation, the first exergy efficiency is defined as the input-output efficiency. The second exergy efficiency is defined as the consumed-produced efficiency. The input-output efficiency is calculated with the following equation (Marmolejo-Correa & Gundersen, 2012):

$$\eta_{plant} = \frac{\sum Exergy Output}{\sum Exergy Input} = 1 - \frac{\sum Exergy Destroyed}{\sum Exergy Input} \quad (17)$$

There are five different definitions for the consumed-produced efficiency in the literature, and the equations corresponding to these definitions are provided below (Marmolejo-Correa & Gundersen, 2012):

Eq. (18) was defined by Grassmann (1950):

$$\eta_{plant} = \frac{Useful Exergy Output}{Useful Exergy Input} \quad (18)$$

Eq. (19) was defined by Szargut et al. (1988):

$$\eta_{plant} = \frac{Exergy of Useful Products}{Feeding Exergy} \quad (19)$$

Eq. (20) was defined by Baehr (1968) (Baehr, 1988) and Kotas (Kotas, 1995):

$$\eta_{plant} = \frac{Desired Output}{Necessary Input} \quad (20)$$

Eq. (21) was defined by Tsatsaronis (1993) and Bejan et al. (Bejan et al., 1996):

$$\eta_{plant} = \frac{Exergy of Products}{Exergy of Fuel} \quad (21)$$

Eq. (22) was defined by Brodyansky et al. (1994):

$$\eta_{plant} = \frac{Exergy out - Transit Exergy}{Exergy in - Transit Exergy} \quad (22)$$

Exergo-economic Analysis

The exergy flow has a cost. Therefore, it is necessary to evaluate the relationship between the cost of exergy destruction and the plant investment cost. Exergo-economic analysis is an analysis that combines exergy analysis with cost analysis. Exergo-economic analysis contributes to the improvement of the plant by determining the source, magnitude,

and location of thermodynamic inefficiency. Modified Productive Structure Analysis (MOPSA), Last in First out (LIFO) and, Specific Exergy Costing (SPECOC) are the most popular methods used in exergo-economic analysis (Tahir et al., 2021). The SPECOC method has been preferred in this section for the case study.

Specific Exergy Costing (SPECOC)

In the SPECOC method, exergy rates entering and exiting the plant are costed as fuel and product exergies. Costing of plant elements is done according to operating conditions.

In the SPECOC method, cost balance equations are written for each plant element. When writing cost balance equations, the entering and exiting exergy rates to and from the plant element are costed with the unit exergy flow cost. In this case, for the equations to be solvable, the number of equations must be equal to the number of exergy flows. To achieve this equality, auxiliary equations are written in the SPECOC method according to the fuel and product rules.

The general cost equation used in the SPECOC method is provided below (Lazzaretto & Tsatsaronis, 2006).

$$\sum \dot{C}_{o,k} + \dot{C}_{w,k} = \dot{C}_{q,k} + \sum \dot{C}_{i,k} + \dot{Z}_k \quad (23)$$

$\dot{C}_{o,k}$, $\dot{C}_{w,k}$, $\dot{C}_{i,k}$, and $\dot{C}_{q,k}$ represent, respectively, the exergy cost rate leaving the “k” plant element, the cost of work (expressed according to the sign convention), the cost rate of exergy entering the “k” plant element, and the cost of heat (expressed according to the sign convention). These parameters are determined with equations (24-27) (Hou et al., 2018).

$$\dot{C}_{o,k} = c_o \dot{E}_{o,k} \quad (24)$$

$$\dot{C}_{w,k} = c_w \dot{W}_k \quad (25)$$

$$\dot{C}_{i,k} = c_i \dot{E}_{i,k} \quad (26)$$

$$\dot{C}_{q,k} = c_q \dot{Q}_k \quad (27)$$

Where “c” is the cost per unit of each exergy stream; The cost of the plant element includes investment, maintenance, and repair costs. The cost rate of the “k” element (\dot{Z}_k) is defined as (Hou et al., 2018):

$$\dot{Z}_k = \frac{Z_k \cdot CRF \cdot \varphi}{(N \cdot 3600)} \quad (28)$$

where Z_k is the purchase cost of the “k” element; N refers to the annual number of operating hours; φ is the maintenance factor; CRF is the capital recovery factor, which

is given as (Akbari & Mahmoudi, 2014) :

$$CRF = \frac{i_r (1+i_r)^n}{((1+i_r)^n - 1)} \quad (29)$$

i_r is the interest rate and n is the number of useful years of operation.

In the SPECO method, auxiliary equations are written according to the fuel (F rule) and product (P rule) rules. Thus, the number of equations is equalized with the number of unknowns. The fuel and product rules are applied based on the definitions of fuel and product exergies.

In exergo-economic analysis, the performance criteria, which play an important role in evaluating the analysis results, are described below:

The mean unit fuel cost of the “k” plant element ($c_{f,k}$) is determined by dividing the fuel cost rate ($\dot{C}_{f,k}$) of the “k” plant element by $\dot{E}x_{f,k}$ value (Hou et al., 2018).

$$c_{f,k} = \frac{\dot{C}_{f,k}}{\dot{E}x_{f,k}} \quad (30)$$

The mean unit product cost of the “k” plant element ($c_{p,k}$) is determined by dividing the product cost rate ($\dot{C}_{p,k}$) of the “k” plant element by the $\dot{E}x_{p,k}$

$$c_{p,k} = \frac{\dot{C}_{p,k}}{\dot{E}x_{p,k}} \quad (31)$$

The mean unit product cost of the overall plant ($c_{p,tot}$) is the sum of \dot{Z}_k and \dot{C}_f values of the elements that make up the plant, divided by $\dot{E}x_p$ value (Hou et al., 2018)

$$c_{p,tot} = \frac{\sum_{i=1}^{n_k} \dot{Z}_k + \sum_{i=1}^{n_f} \dot{C}_{f,i}}{\sum_{i=1}^{n_p} \dot{E}x_{p,i}} \quad (32)$$

Exergy destruction cost rate ($\dot{C}_{D,k}$) can be calculated in two ways. $\dot{C}_{D,k}$ value can be provided based on $c_{p,k}$ or $c_{f,k}$ value. In this section, it was preferred to find the $\dot{C}_{D,k}$ value according to $c_{f,k}$ the value of the case study (Hou et al., 2018).

$$\dot{C}_{D,k} = c_{f,k} \dot{E}x_{D,k} \quad (33)$$

The exergo-economic factor (f_k) is an evaluation criterion used to compare $\dot{C}_{D,k}$ and \dot{Z}_k values (Hou et al., 2018).

$$f_k = \frac{\dot{Z}_k}{\dot{Z}_k + \dot{C}_{D,k}} \quad (34)$$

Exergo-environmental Analysis

Exergo-environmental analysis is an approach that combines exergy analysis with environmental impact assessment to evaluate the environmental impact of energy systems. Traditional environmental analysis focuses on emissions and pollutants. Exergo-environmental analysis, unlike traditional environmental analysis, considers both the quantity and quality of energy flows within the system.

The main purpose of exergo-environmental analysis is to measure the environmental impact of energy systems by evaluating the exergy destruction associated with various processes and components. This methodology provides a more comprehensive understanding of the environmental impacts of energy conversion processes compared to traditional methods.

By taking exergy destruction into account, exergo-environmental analysis can identify inefficiencies and areas for improvement in energy facilities and lead to the development of more sustainable and environmentally friendly technologies. It also allows different energy conversion alternatives to be compared according to their environmental impacts, helping decision-makers choose the most appropriate options to reduce environmental impacts.

The governing equations used in exergo-environmental analysis are presented below (Meyer et al., 2009):

$$\dot{B}_{in,k} + \dot{Y}_k + \dot{B}_k^{PF} = \dot{B}_{out,k} \quad (35)$$

$$\dot{B}_k = \dot{E}x_k \cdot b_k \quad (36)$$

$$\dot{Y}_k = \dot{Y}_k^{CO} + \dot{Y}_k^{OM} + \dot{Y}_k^{DI} \quad (37)$$

where $\dot{B}_{in,k}$ and $\dot{B}_{out,k}$ are the environmental impact rate of the output exergy rate and input exergy rate of the element “k”, \dot{Y}_k is the environmental impact of the element “k”, \dot{B}_k^{PF} is the environmental impact rate of pollutants, b_k is the specific environmental impact rate, \dot{Y}_k^{CO} , \dot{Y}_k^{OM} and \dot{Y}_k^{DI} are the environmental impact rates generated during the component creation, operation, and maintenance (Qi et al., 2024).

The exergo-environmental factor whose equation is given below can be evaluated as the performance criterion for exergo-environmental analysis (Meyer et al., 2009).

$$f_{b,k} = \frac{\dot{Y}_k}{\dot{Y}_k + \dot{B}_{D,k}} \quad (38)$$

Where $\dot{B}_{D,k}$ is the exergy destruction environmental impact rate (Qi et al., 2024).

Case Study

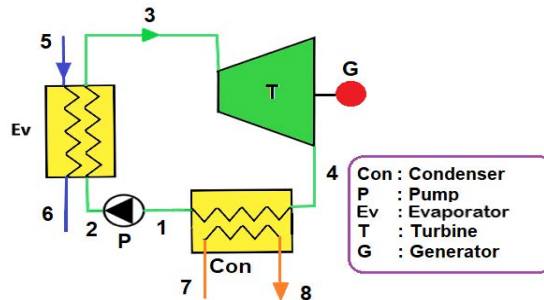
In this section, an Organic Rankine cycle (ORC) is proposed, and the equations required for the 4E analyses of this cycle are given.

Description of the Proposed Plant

The ORC is a thermodynamic cycle that uses refrigerant as the operating fluid and converts the received thermal energy into power. The operating principle of the ORC, whose schematic view is provided in Figure 2, is as follows. The turbine plays a leading role in the ORC. The condenser, pump, and evaporator are plant elements that prepare the operating fluid for the turbine inlet and ensure the continuity of the cycle. In the condenser, the heat of the steam is rejected after the turbine outlet, and then the steam enters the pump, where its pressure is raised to the turbine inlet pressure. Thermal energy is supplied to the operating fluid in the evaporator. This is the operating principle of the cycle.

Figure 2.

Schematic of Proposed Plant



Assumptions of the Proposed Plant

A mathematical model has been developed for the proposed plant's 4E analyses. The mathematical model consists of energy conservation, exergy, cost, and environmental balance equations. The following assumptions have been made in solving the mathematical model of the plant:

- Plant elements work under steady-state situations.
- Changes in potential and kinetic energy in plant elements have been neglected.
- Heat and pressure losses in plant elements and the connecting lines between them have been neglected.
- The steam at the condenser outlet is considered as saturated liquid.

Simulation Conditions of the Proposed Plant

To design an energy plant, it is necessary to determine the design input values for the plant initially. In this stage, the more limited the input values the designer accepts, except for a certain output, the more flexible the mathematical model will be. In Table 1, the parameters of the simulation conditions accepted for the proposed plant are provided without numerical values.

Table 1.

Simulation Conditions of The Proposed Plant

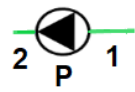
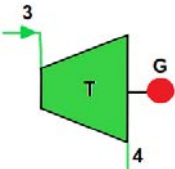
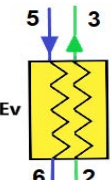
Parameter	Symbol
Ambient temperature	T_0 [K]
Ambient pressure	P_0 [kPa]
Turbine isentropic efficiency	η_T [%]
Pump isentropic efficiency	η_P [%]
Pressure rate	P_{R-ORC} [-]
Superheat temperature	T_{st-ORC} [°C]
Condenser outlet temperature	T_1 [°C]
Thermal source temperature	T_5 [°C]
Coolant input temperature.	T_7 [°C]
Coolant mass rate.	$\dot{m}_{coolant}$ [°C]
Net power	\dot{W}_{net} [kW]

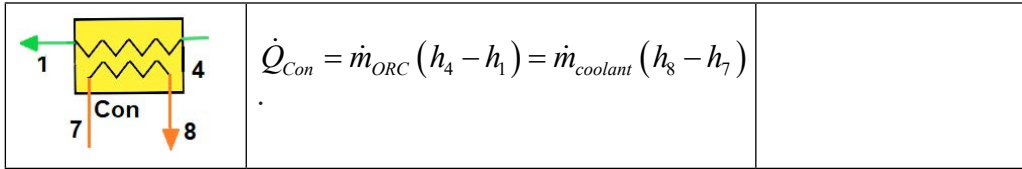
Energy Analysis

The energy conservation equations for each plant element are given in Table 2.

Table 2.

Energy Equations for the Elements of The Plant

Element	Energy Balance Equation	
	$\dot{W}_P = \dot{m}_{ORC} (h_2 - h_1)$	$\eta_P = \frac{(h_{2s} - h_1)}{(h_2 - h_1)}$
	$\dot{W}_T = \dot{m}_{ORC} (h_3 - h_4)$	$\eta_T = \frac{(h_3 - h_4)}{(h_3 - h_{4s})}$
	$\dot{Q}_{Eva} = \dot{m}_{ORC} (h_3 - h_2) = \dot{m}_{source} (h_5 - h_6)$	



Exergy Analysis

For a better understanding of the expressions, fuel, and product exergies for each element of the case study, RC, is given in Table 3.

Table 3.
Fuel And Product Exergies of All Elements

Element	$\dot{E}x_{F,k}$ Equations	$\dot{E}x_{P,k}$ Equations	$\dot{E}x_{D,k}$ Equations
P	\dot{W}_P	$\dot{E}x_2 - \dot{E}x_1$	$\dot{E}x_{D,P} = \dot{W}_P - (\dot{E}x_2 - \dot{E}x_1)$
T	$\dot{E}x_3 - \dot{E}x_4$	\dot{W}_T	$\dot{E}x_{D,T} = (\dot{E}x_3 - \dot{E}x_4) - \dot{W}_T$
Eva	$\dot{E}x_5 - \dot{E}x_6$	$\dot{E}x_3 - \dot{E}x_2$	$\dot{E}x_{D,Eva} = (\dot{E}x_5 - \dot{E}x_6) - (\dot{E}x_3 - \dot{E}x_2)$
Con	$\dot{E}x_4 - \dot{E}x_1$	$\dot{E}x_8 - \dot{E}x_7$	$\dot{E}x_{D,Con} = (\dot{E}x_4 - \dot{E}x_1) - (\dot{E}x_8 - \dot{E}x_7)$

Exergo-economic Analysis

The equations of \dot{Z}_k values for each plant element are given in Table 4.

Table 4.
 Z_k Values of the Elements of The Plant

Element	Z_k equations
P (Cao et al., 2017)	$3540.\dot{W}^{0.71}$
T (Cao et al., 2017)	$\frac{479.34\dot{m}}{(0.92 - \eta_T)} \ln\left(\frac{P_i}{P_o}\right) [1 + \exp(0.036T_i - 54.4)]$
Eva, Con (Cao et al., 2017)	$30000 + 750.A^{0.81}$

The cost equations for each plant element are provided in Table 5.

Table 5.
The Cost Equations for All Elements

Element	Exergy Cost Balance Equations	
P	$\dot{C}_1 + \dot{C}_{WP} + \dot{Z}_P = \dot{C}_2$	$c_{WP} = c_{WT}$ (Assumption)
T	$\dot{C}_3 + \dot{Z}_T = \dot{C}_4 + \dot{C}_{WT}$	$c_3 = c_4$ (F Rule)
Eva	$\dot{C}_5 + \dot{C}_2 + \dot{Z}_{Eva} = \dot{C}_3 + \dot{C}_6$	$c_5 = c_6$ (F Rule)
Con	$\dot{C}_4 + \dot{C}_7 + \dot{Z}_{Con} = \dot{C}_1 + \dot{C}_8$	$c_1 = c_4$ (F Rule)

Exergo-environmental Analysis

The exergo-environmental equations for each plant element are provided in Table 6.

Table 6.
The Exergo-environmental and Auxiliary Equations for All Elements

Element	Exergy Cost Balance Equations	
P	$\dot{B}_1 + \dot{B}_{WP} + \dot{Y}_P = \dot{B}_2$	$b_{WP} = b_{WT}$
T	$\dot{B}_3 + \dot{Y}_T = \dot{B}_4 + \dot{B}_{WT}$	$b_3 = b_4$
Eva	$\dot{B}_5 + \dot{B}_2 + \dot{Y}_{Eva} = \dot{B}_3 + \dot{B}_6$	$b_5 = b_6$
Con	$\dot{B}_4 + \dot{B}_7 + \dot{Y}_{Con} = \dot{B}_1 + \dot{B}_8$	$b_1 = b_4$

References

- Akbari, A. D. & Mahmoudi, S. M. S. (2014). Thermoeconomic analysis & optimization of the combined supercritical CO₂ (carbon dioxide) recompression Brayton/organic Rankine cycle. *Energy*, 78, 501–512. <https://doi.org/10.1016/j.energy.2014.10.037>
- Anvari, S., Khoshbakhti Saray, R. & Bahlouli, K. (2015). Conventional and advanced exergetic and exergoeconomic analyses applied to a tri-generation cycle for heat, cold and power production. *Energy*, 91, 925–939. <https://doi.org/10.1016/j.energy.2015.08.108>
- Baehr, V. H. D. (1968). Towards a definition of exergy efficiency: a systematic study. *Brennstoff-Wärme-Kraft*, 20(5), 197–244.
- Baehr, V. H. D. (1988). Problems with exergy? Towards a definition of efficiencies under the consideration of the 2nd law of thermodynamics. *Brennstoff-Wärme-Kraft*, 40(11), 450–457.
- Bejan, A. (1988). *Advanced Engineering Thermodynamics*. Wiley.
- Bejan, A., Tsatsaronis, G. & Moran, M. (1996). *Thermal design & optimization* (1st ed.). John Wiley & Sons.
- Brodyansky, V. M., Sorin, M. V & Le Goff, P. (1994). *The efficiency of industrial processes: exergy analysis and optimization* (Elsevier).

- Cao, Y., Ren, J., Sang, Y. & Dai, Y. (2017). Thermodynamic analysis and optimization of a gas turbine and cascade CO₂ combined cycle. *Energy Conversion and Management*, 144, 193–204. <https://doi.org/10.1016/j.enconman.2017.04.066>
- Grassmann, P. (1950). Towards a general definition of efficiencies. *Chemie Ingenieur Technik*, 22(4), 77–80.
- Gundersen, T. (2009). The concept of exergy and energy quality.
- Hou, S., Zhou, Y., Yu, L., Zhang, F., Cao, S. & Wu, Y. (2018). Optimization of a novel cogeneration system including a gas turbine, a supercritical CO₂ recompression cycle, a steam power cycle and an organic Rankine cycle. *Energy Conversion and Management*, 172, 457–471. <https://doi.org/10.1016/j.enconman.2018.07.042>
- Kotas, T. J. (1995). *The exergy method of thermal plant analysis* (2nd ed). Krieger Publishing.
- Lazzaretto, A. & Tsatsaronis, G. (2006). SPECO: A systematic and general methodology for calculating efficiencies and costs in thermal systems. *Energy*, 31(8–9), 1257–1289. <https://doi.org/10.1016/j.energy.2005.03.011>
- Marmolejo-Correa, D. & Gundersen, T. (2012). A comparison of exergy efficiency definitions with focus on low temperature processes. *Energy*, 44(1), 477–489. <https://doi.org/10.1016/j.energy.2012.06.001>
- Meyer, L., Tsatsaronis, G., Buchgeister, J. & Schebek, L. (2009). Exergoenvironmental analysis for evaluation of the environmental impact of energy conversion systems. *Energy*, 34(1), 75–89. <https://doi.org/10.1016/j.energy.2008.07.018>
- Nami, H., Nemati, A. & Jabbari Fard, F. (2017). Conventional and advanced exergy analyses of a geothermal driven dual fluid organic Rankine cycle (ORC). *Applied Thermal Engineering*, 122, 59–70. <https://doi.org/10.1016/j.applthermaleng.2017.05.011>
- Qi, X., Yang, C., Huang, M., Ma, Z., Hnydiuk-Stefan, A., Feng, K., Siarry, P., Królczyk, G. & Li, Z. (2024). Conventional and advanced exergy-exergoeconomic-exergoenvironmental analyses of an organic Rankine cycle integrated with solar and biomass energy sources. *Energy*, 288. <https://doi.org/10.1016/j.energy.2023.129657>
- Stepanov, V. S. (1994). *Chemical energies and exergies of fuels*.
- Szargut, J., Morris, D. R. & Steward, F. R. (1988). *Exergy analysis of thermal, chemical, and metallurgical processes*. Hemisphere Publishing Corporation.
- Tahir, M. F., Haoyong, C. & Guangze, H. (2021). A comprehensive review of 4E analysis of thermal power plants, intermittent renewable energy and integrated energy systems. In *Energy Reports* (Vol. 7, pp. 3517–3534). Elsevier Ltd. <https://doi.org/10.1016/j.egy.2021.06.006>
- Tsatsaronis, G. (1993). Thermoeconomic analysis and optimization of energy systems. *Progress in Energy and Combustion Science*, 19(3), 227–257.
- Wang, Z., Xiong, W., Ting, D. S. K., Carriveau, R. & Wang, Z. (2016). Conventional and advanced exergy analyses of an underwater compressed air energy storage system. *Applied Energy*, 180, 810–822. <https://doi.org/10.1016/j.apenergy.2016.08.014>
- Zhang, Y., Yao, E. & Wang, T. (2021). Comparative analysis of compressed carbon dioxide energy storage system and compressed air energy storage system under low-temperature conditions based on conventional and advanced exergy methods. *Journal of Energy Storage*, 35. <https://doi.org/10.1016/j.est.2021.102274>

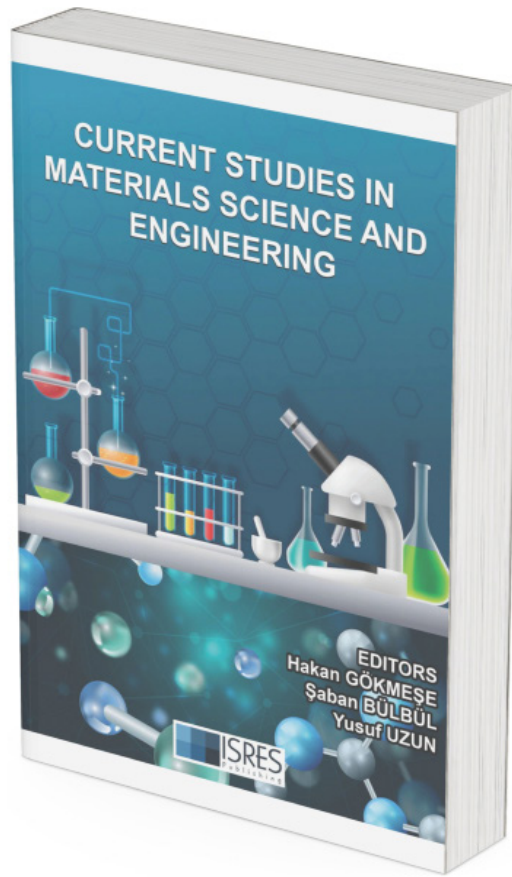
About The Authors

Dilek Nur ÖZEN, PhD is an Associate Professor of Mechanical Engineering at Necmettin Erbakan University in Konya, Türkiye. She holds a PhD in Mechanical Engineering from Selcuk University. Her main areas of interest are exergy and exergo-economic analyses of energy plants.

E-mail: dnozen@erbakan.edu.tr, **ORCID:** 0000-0002-8622-4990

Similarity Index

The similarity index obtained from the plagiarism software for this book chapter is 25%.



Current Studies in Materials Science and Engineering is published from the selected papers invited by the editors.

This edition includes 13 sections on materials and engineering used in today's technology. At least two international reviewers review all submissions.

The purpose of the book is to provide the readers with the opportunity of reading scholarly refereed publication in the fields of materials and engineering.

Current Studies in Materials Science and Engineering is published by ISRES Publishing.